# An Investigation to Enhance Stratification in Solar Domestic Hot Water Tanks Using Photovoltaic Power

By

Araf Othman Taher

Submitted in partial fulfillment of the requirements

for the degree of Doctor of Philosophy

at

Dalhousie University

Halifax, Nova Scotia

August 2019

*I dedicate this work to*

*My dear father Othman, My dear mother Fathia*

*My dear wife Khadiga, and my children Fathia, Othman,*

*and Mabruka and my son-in-law Ibrahim,*

*My dear brothers and sisters*

*My beloved granddaughter Jenan,*

*My University in Tobruk, and beloved country, Libya.*

Table of contents

# List of Tables

# List of Figures

# Abstract

Improved energy conservation methods and awareness of these methods in the industrial sector, along with the decreasing cost of photovoltaic (PV) technology, implicates PV-water heating system designs as economically sustainable alternatives to traditional methods for domestic hot water systems (DHWS). The proper design for an electric resistance immersion heater element in a thermo-syphon side-arm storage tank using PV power heating has not yet been determined. This research is an experimental investigation to evaluate the proper design of a thermo-syphon side-arm storage tank using PV-heating, with longitudinally perforated manifolds that work with standard Canadian domestic solar hot water tanks under different climate conditions in Halifax, Nova Scotia.

The evaluation of the performance of the hot water inlet devices was based on the assessments of flow visualization, temperature distributions inside the storage tank, degrees of stratification (DOS), availability, availability ratio, energy delivery, entropy ratio, merit factor and internal entropy generation. The most effective hot water inlet device is the one which has a high DOS, availability change, merit factor, energy delivery, and average availability ratio. Furthermore, it has a low entropy ratio and a low internal entropy generation.

The results of this testing indicated that using a four-port manifold in which the port diameter increases gradually from small at the bottom to large at the top is a workable solution to enhance stratification. Also, the four-port manifold has the highest degree of stratification, and a high change rate for the temperature of the top tank layers and responded earlier in the day than the traditional design for most of the experimental tests. This means the four-port manifold has the ability to enhance stratification. Furthermore, we found that it is difficult to use entropy ratios to determine the ability of hot water inlet devices to enhance stratification, because the entropy difference values were too small. Moreover, the normalized entropy ratio and internal entropy generation results were both greater than one, which are an unrealistic value. Due to this issue we cannot recognize these two parameters in our evaluations.

# List of Symbols Used

| | |
|---|---|
| A | Availability, J |
| A | Cross section area, $m^2$ |
| AC | Alternating current |
| ave | Average |
| BOS | Balance of solar PV system |
| BZ | Bottom zone |
| c | Specific heat, J/kg. K |
| D | Diameter, m |
| DC | Direct current |
| del | Delivered water |
| DOS | Degree of stratification |
| E | Energy of the node, J |
| Exp | Experiment |
| g | Acceleration of gravity, m/sec |
| H | Height, m |
| h | Thickness, m |
| h | Specific enthalpy, J/kg |
| hL | head loss in the pipe, m |
| i | Layer number |
| Int | Initial |
| $K_L$ | Losses coefficient |
| L | Length, m |
| LCB | Linear current booster |
| M | Manifold |
| Mix | Mixed tank |
| M | Mix number |
| m | Mass, kg |
| mean | Mean tank temperature, ˚C |
| $\dot{m}$ | mass flowrate, kg/sec |
| MF | Merit factors |
| n | |
| P | Pressure, pa |
| PVDHW | Photovoltaic domestic hot water |
| P | Power, W |
| Pr | Prandtl number |
| $Q_{start}$ | Heat stored at the beginning of the test, J |
| $Q_{End}$ | Heat stored at the end of the test, J |
| q | Rate of heat transfer, W |
| R | Resistance, ohm |
| $R_{EG}$ | Internal entropy generation |
| Re | Reynolds number |
| RPM | Rigid porous manifold |
| real | Experimental tank |

| | |
|---|---|
| S | Side-arm |
| S | Entropy, J/kg K |
| s | Specific entropy, J/kg K |
| SBCD | Sintered bronze conical diffuser |
| str | Stratified tank |
| STS | Solar thermal system |
| STC | Standard test conditions |
| SDHW | Solar domestic hot water |
| T | Tank |
| T | Temperature, ˚C |
| TCSS | Thermocouple on stain steel probe |
| TCC | Thermocouple on copper probe |
| TES | Thermal energy storage |
| TZ | Top zone |
| $u_m$ | Mean velocity, $m^2$ |
| V | Volume, $m^3$ |
| V | Voltage, V |
| VDC | Volts Direct Current |
| w | Water |
| y | Vertical coordinate, m |
| $\eta_{str}$ | Stratification efficiency |
| ε | Exergy of stored liquid, J |
| 0 | Dead state temperature |
| ΔH | Change of the height (m). |
| ΔP | Differential pressure |
| ΔT | Differential temperature |
| ρ | Density, $kg/m^3$ |
| $\int_{Darcy}$ | Darcy friction factor |
| ν | Kinematic viscosity, $m^2/sec$ |

# Acknowledgments

I would like to express my gratitude to Allah who has given me the power to complete this research study.

My gratitude to my supervisor Dr. Peter Allen for his academic guidance, and support during this work. It was truly a pleasure to study under his supervision and learn from him.

Many thanks to the other members of the supervisory committee, Dr. V. Ismet Ugursal and Dr. M El-Hawary, for their valuable advice and suggestions regarding the preparation of this thesis. I would also like to thank the staff of the Mechanical Engineering for their laboratory assistance.

My appreciation to my father, my mother, my beloved children, brothers and sisters for their support and encouragement throughout my graduate studies at Dalhousie University. A word of appreciation is due to my wife: thank you for your patience and encouraging words during some difficult times

I am also grateful for the funding provided by Thermo Dynamic Ltd and ASPIRE program to carry out the experimental setup.

My gratitude goes to the Libyan Ministry of Education for my scholarship and the financial support. Also, I would like to acknowledge the funding and support from the Nova Scotia Graduate Scholarship through the Faculty of Graduate Study at Dalhousie University.

# Chapter 1: Introduction

## 1.1. Renewable Energy

The recent widespread industrialization of the developing world and subsequent rapid increase in fossil fuel consumption have resulted in a disproportionate amount of gas emissions as well as a looming threat of insufficient fossil fuel supplies[1]. Both of these issues are contributing to current global energy problems related to pollution from burning fossil fuels and potential power shortfalls [1]. The industrial revolution in developing countries, transportation and energy emissions all lead to an increase in greenhouse gases emissions. As a result, the surface temperature of the earth has increased and will causes climate change, increasing sea water salinity and flood or drought [52].

Nevertheless, energy continues to play a large role in our daily lives, which means we are now looking for power sources which can augment or even replace fossil fuels. One of the main alternative sources is renewable energy [1]. Records show that the global power generating capacity for renewable energy in 2017 accounted for 70% of net additions. However, carbon dioxide emissions also rose by 1.4%, after remaining at a constant level for three years. Lower fossil fuel prices, strong economic development, and weakening energy efficiency efforts were the three main factors causing the increases in the levels of carbon emissions. On the other hand, approximately 178 gigawatts were added globally to levels of renewable power generation capacity, which was the largest yearly increase on record. The totals for coal, natural gas and nuclear power combined would be less than the new solar photovoltaic (PV) generating capacity alone [36].

In light of the broad range of environmental problems being caused by the use of fossil fuels, many countries are advancing the use of renewable energy to support their electrical grid networks. In fact, renewable energy is mainly being developed in direct response to the negative side effects of fossil fuels and the dangers of nuclear power plants [36]. Of the renewable energy sources the greatest potential is PV solar power. This form of "clean" energy could satisfy the expanding power demands in many places in the world. Despite some issues related to utilizing PV solar power for solar thermal applications (such as, for instance, that this technology requires a large roof space on buildings), it is considered an important solution for reducing the output of greenhouse gas emissions, as well as for eliminating nuclear industrial disasters, increasing stability, and providing energy to remote regions [15].

## 1.2. Solar Photovoltaic (PV)

In 2016, an estimated 18.2% of global total final energy consumption was attributed to the use of renewable energy, and by 2017, the number of countries with renewable energy targets and support policies had notably increased [36]. As can be seen in the Figure (1-1), there were double the number of solar PV installations compared to wind power installations in 2017. In fact, due in large part to strong growth in China, solar PV has become the top source of new power-producing capacity over the past year, expanding worldwide capacity to around 402 GWDC. In 2017 alone, solar PV represented almost 55% of newly installed renewable power capacity [36].

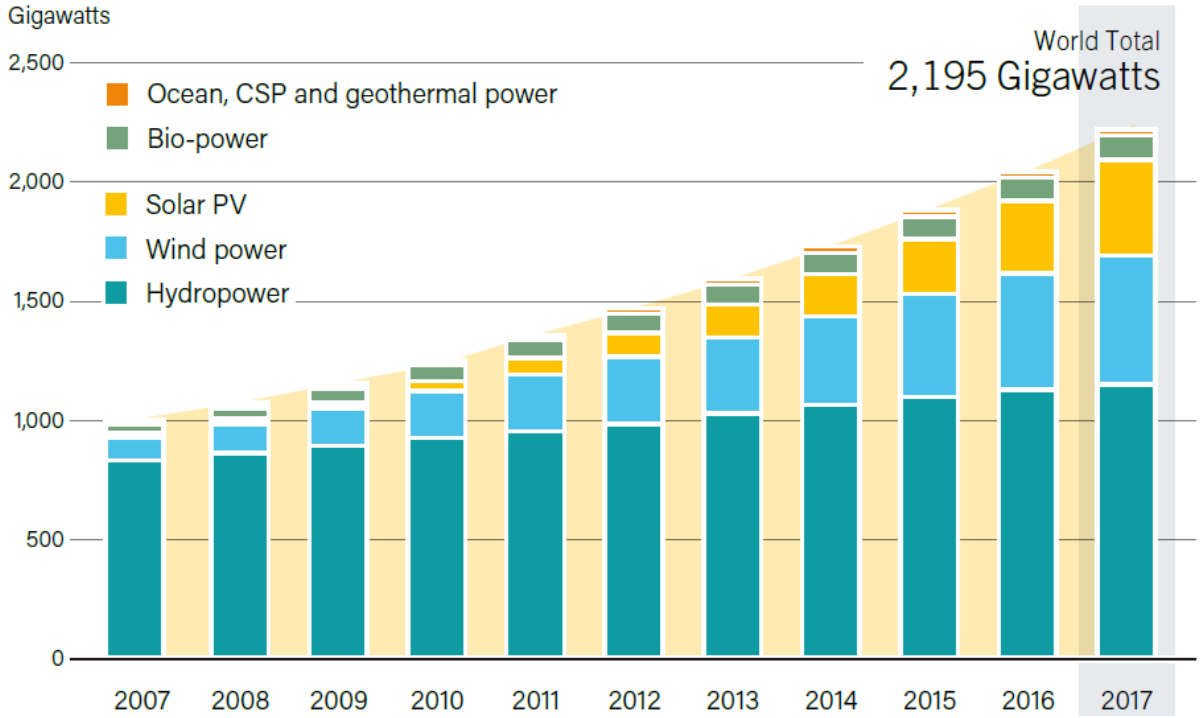


Figure 1-1 Global renewable power capacity for 2007-2017, adapted from [36].

As shown in Figure (1-2), the cost of PV power 10 to 100 kWp has declined, while the cost of electricity from PV is competitive with other solar thermal applications and conventional power [15]. Photovoltaic water heaters offer the promise of being less expensive within the next several years and may approach a point that is economically applicable for residential structures. To that end, commercial companies continue to explore the feasibility of a PV domestic hot water (PVDHW) system.

Improved energy conservation methods in the industrial sector, along with the decreasing costs of PV technology, are rendering PV water heating system designs an economically sustainable alternative to traditional methods.

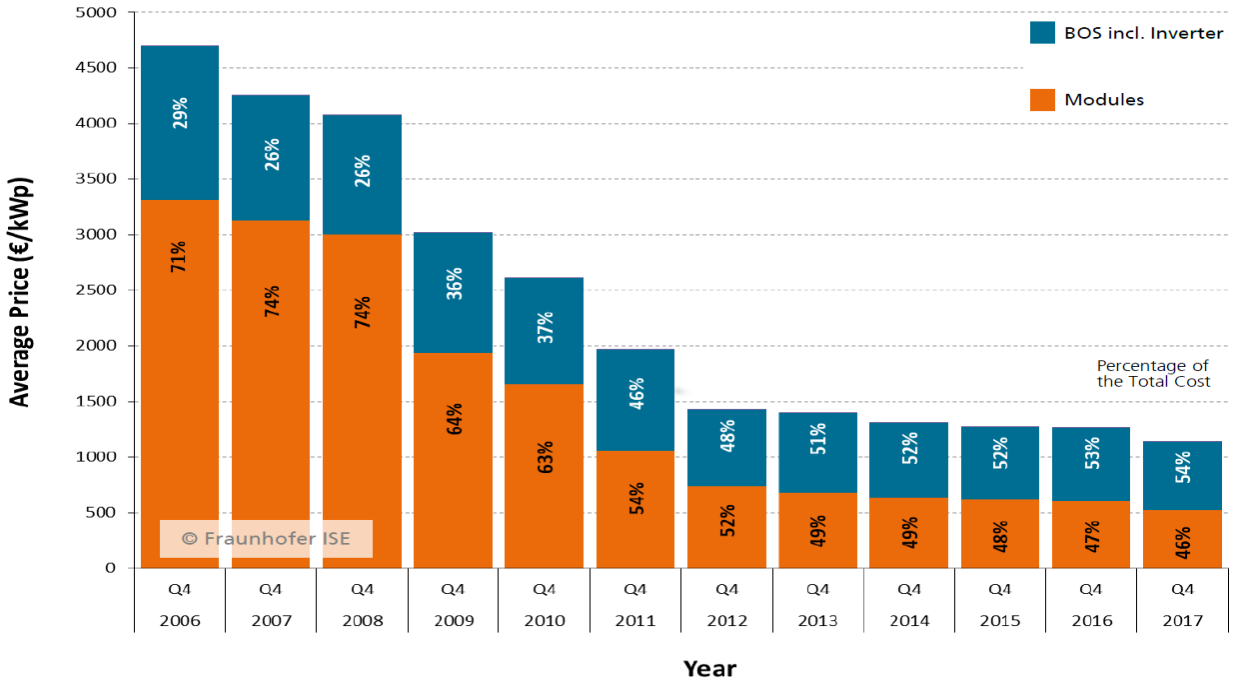


Figure 1-2 Historical price development for 10 to 100 kWp roof-top solar PV system, adapted from [15].

## 1.3. Thermal Energy Storage

Thermal energy storage (TES) is a system which stores thermal energy through the cooling or heating of a storage medium. The stored energy can be accessed at a later time, either for cooling or heating purposes, or for generating energy [13]. TES systems are currently mostly used in buildings and industrial processes. However, due to climate vagaries, the methods used to store renewable energy must accord with the environment to ensure the application of efficient, practical, and sustainable techniques [13].

In general, when used in conjunction with PV systems, TES systems are able to help balance energy demands as well as provide an energy supply on a daily, weekly and seasonal basis when there is low or no solar radiation. TES does not just control the demand and supply patterns to sustain energy, but also boosts the performance and thermal reliability of the system. In other words, it can increase the overall efficiency of the energy system by, for example, matching energy

supply and demand or exploiting the variable production of renewable energy sources. Peak demand can also be reduced with TES systems [40].

Figure (1-3) shows the categories of thermal energy storage for solar energy. Sensible heat storage with a water medium, which is the most inexpensive choice, is based on heating or cooling a liquid or solid storage medium to store thermal energy. Latent heat storage uses phase-change materials, while thermo-chemical storage uses chemical reactions to store as well as release thermal energy. Latent heat storage and thermo-chemical storage systems are relatively expensive compared to sensible heat storage, but low energy density of sensible heat storage requires large volumes to function properly. In order to discharge thermal energy at a constant temperature, sensible heat storage systems must be suitably designed [8].

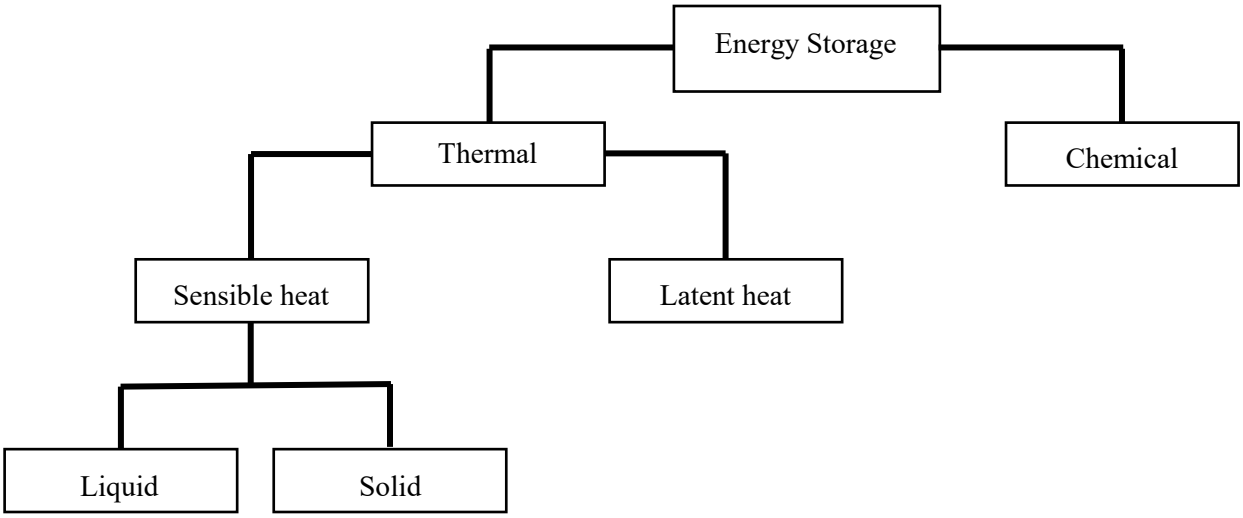


Figure 1-3 Categories of energy storage.

Solar domestic storage tanks should have a large tank capacity rather than relying on an electrical or gas storage tank to cover the shortage cause by fluctuations in solar radiation energy. Thermally stratified tanks provide a higher quality of energy to the load and can produce more heat than fully

mixed tanks [9]. Improving the design of solar tanks, side-arm heaters, and manifolds will enhance thermal stratification inside solar domestic hot water tanks, which will then lead to increasing the energy availability, allowing users to access hot water at any time of the day [2].

## 1.4. Thermal Stratification

Thermal stratification in a solar hot water tank has the effect of decreasing the amount of auxiliary energy consumption so that the energy storage efficiency for the whole system may be increased [2]. If the cold water is allowed to be mixed with the hot water in the solar domestic hot water tank, the supplied temperature to the load is lowered, and the quality of energy is degraded. However, the proper design for enhancing the thermal stratification inside a side-arm storage tank using PV has not yet been determined. Most of the factors that cause mixing inside solar domestic hot water tanks are known, but research is required both to clarify the important issues and develop devices that enhance stratification [21]. Furthermore, thermal energy storage is one of the main components in a solar domestic hot water (SDHW) system. Designing an effective thermal storage tank for these systems is essential for meeting the heating demands when the supply and the exhaust of energy cannot be kept in balance [13]. For this reason, thermal energy storage has become an important area of research toward enhancing the performance of SDHW systems.

# Chapter 2: Objective

Designing and constructing an effective thermal storage tank for an SDHW system is essential for meeting the heating demands when the supply and exhaust of energy cannot be kept in balance [13]. A thermally stratified tank provides a better quality of energy to the load and can produce more heat than fully mixed tanks. The objectives of the present research study are as follows:

- To devise methods to enhance thermal stratification in a PV water heater and to develop experimental and analytical methods to determine the relative effectiveness of the thermo-syphon side-arm with three hot water inlet devices using a PV power heater under different climate conditions in Halifax, Nova Scotia, Canada.
- To use the flow visualization pattern, which is one of the most appropriate assessments for checking the hot water flow pattern inside a tank.
- To operate, test, and compare the thermal performance of the side-arm heater with the three inlet hot water devices in order to choose which one best enhanced stratification. An effective hot water inlet device is one which delivers the water heated by the side-arm heater to the tank at the level where the temperature of the water in the tank matches the temperature of the heated water, thereby enhancing stratification.

## 2.1. Contributions of the Present Research Work

- Enhanced stratification in the SDHW system using PV power will contribute to the industry by providing important information on the ability and effectiveness of using photovoltaics to provide low-grade heat.
- The application of the side-arm heater significantly improves the design and operational factors that deal with stratification in solar domestic hot water tanks. Thermal stratification decreases the operational periods of auxiliary energy supply, thus increasing the energy storage efficiency of the entire system.

# Chapter 3: Literature Review

## 3.1. Thermal Stratification

Thermal stratification plays an important role in hot water storage systems. For example, it increases the collector efficiency and the storage of useful energy, which comes about by having access to the higher temperature at the top of the tank where water is drawn for use [38]. Thermal stratification occurs within a thermal storage tank as a result of temperature gradients and buoyancy effects during heat supply. These effects produce a thermocline region that separates the hot and cold water in the tank. Researchers have found that energy storage efficiency and overall system efficiency may be increased by utilizing fully stratified water tanks [22]. These types of tanks are classified into two types: direct heating source and indirect heating mode. For indirect heating, water can be easily kept in thermal stratification due to natural convection, but energy efficiency will be decreased due to insufficient heat transfer [13].

Maintaining thermal stratification in a storage tank requires that mixing be inhibited. Mixing depends on the design of the tank and the operational conditions. For example, forced convection mixing is due to the momentum of the fluid streams entering the storage tank and depends on the flow rate of the entering stream and the design of the inlet. Natural convection can also cause mixing when the fluid entering the storage tank is colder than the surrounding fluid [11].

Thermal stratification within the tank has been studied intensively since the 1970s. A number of factors enhance the degree of stratification inside a storage tank, and there are also several factors contributing to destratification inside the tank. How closely a practical tank can approach the ideal tank is still an open question, and the proper design to enhance stratification in a storage tank still

needs further experimental and theoretical investigation. The following sections provide a brief review of research that has been conducted on thermal stratification in storage tanks [22].

In their experimental study on thermally stratified hot water storage tanks, Lavan and Thompson [28] looked for a method that would remove hot water from a storage tank and add cold water while maintaining steep thermoclines. They also investigated the effects of several geometric and dynamic parameters on thermal stratification, mass flow rate, length-to-diameter ratio, and inlet and outlet temperature differences. The researchers discovered that, for greatest efficiency, the inlet port should be as close as possible to the tank bottom and the flow should be toward the wall side. The outlet port at the top of the tank was found to be much less crucial and had only a slight effect on performance. Furthermore, Lavan and Thompson [28] concluded that efficiency should increase with increasing L/D ratio, inlet and outlet port diameter, and temperature differences between 11.1 ℃ and 27.8 ℃. The data were experimentally correlated to predict efficiency in terms of the Reynolds number, the tank Grashof number, and the tank length-to-diameter ratio. In their conclusion, the researchers suggested that stratification would be best maintained in tanks with walls made of plastic, concrete, or other material characterized by low thermal conductivity [28].

Miller [31] investigated the influence of heat transfer from the wall via conduction on a stratified storage hot water. He tested two laboratory tanks: one made of aluminum and the other of glass [31]. The main objective of this work was to determine the effect of wall conductivity and wall thickness on the thermocline by using numerical methods. Miller [31] found that the aluminum wall material generated convection currents in the water and achieved average temperatures in the tank faster than the water. However, this caused convection currents, which then destroyed the stratification of the thermocline at a much faster rate than anticipated. The destratification was not as significant if the temperature variance in the hot storage tank was small or the thermal energy

was directly used. In the glass tank, a uniform temperature was obtained and most of the thermocline degradation was due to poor insulation. Miller [31] concluded that the destratification in the tanks was affected by higher Rayleigh numbers, increased wall thickness, and a decrease in aspect ratio. Finally, Miller [31] suggested that natural convection effects must be considered in the calculation of the heat transfer across the thermocline.

Loehrke, Holzer, Gari and Sharp [30] performed studies to preserve stratification in liquid thermal storage tanks by using different manifold designs subjected to variable inlet temperature conditions. They constructed and tested two types of vertical porous manifolds: a rigid porous manifold (RPM) and a flexible porous manifold. The flexible manifold was supported by a vertical rod to keep it vertical. The research team [30] concluded that if the incoming fluid density differs from the local tank density at the entry point, vertical momentum is imparted to this supply fluid. Under ideal conditions, this depends on supply fluid temperature, flow rate and tank temperature profile, the supply fluid rises or falls in the perforated manifold, maintaining a pressure balance with the tank fluid until it reaches the level at which the manifold density matches that of the surrounding tank fluid. It then flows into the tank [30].

Additionally, Loehrke et al. [30] found that much better stratification was achieved with a vertical pipe, and that uniform distribution is obtained with less mixing when the flow is introduced through a cross manifold suspended just below the water surface. Finally, they inferred that the cross-section area of this flexible cylinder can vary in response to pressure differences between the tank and the manifold fluids. This action tends to prevent inflow and outflow through the porous wall until the level of equal densities is reached [30].

In 1979, Sliwinski [44] studied the degree of thermal stratification in thermal energy storage tanks. The objective of this research was to experimentally determine the inlet and outlet conditions which are most suitable for enhancing stratification during the charging stage. Sliwinski [44] found that the thermocline observed at the storage inlet for the Richardson number was as low as 0.244. Below this value, the boundary region is observed until the Richardson number is less than 0.002, at which point the tank is completely mixed. Furthermore, Sliwinski [44] found that the stratification was a function of the Richardson and Peclet numbers; hence, at small values of inverse Peclet numbers, the degree of stratification is sensitive to variation in the Richardson numbers. On the contrary, where values of Peclet numbers increase, the degree of stratification is insensitive to the variation in Richardson numbers [44].

In 1982, Gari and Loehrke [17] provided the basis for the design of number of manifolds for enhancing stratification in liquid storage tanks. Many researchers found that one of the causes of destratification occurs when the incoming fluid from the collectors is cooler than the water stored at the top of the tank. Under this condition, liquid introduced at the top of the tank will flow downward, mixing with the surrounding fluid, until some equilibrium level is reached. Accordingly, they designed a perforated manifold to inhibit mixing between the manifold and tank fluids until the level at which the density of the two fluids match is reached. Such a manifold may be described as controlling buoyant jets that will not destroy stratification in the tank [17].

In the investigations, a number of inlet chambers ranging in diameter from 2.5 cm to 10 cm were built and tested [17]. The theory was obtained through experiments conducted in a 2.3 $m^3$ steel tank with a water depth of 2 m. The manifold for this tank was constructed with a 10 cm diameter PVC pipe and perforated at a diameter of 2.5 cm. The researchers inferred that the manifold holes size should be less than D/4 for the rigid porous section to inhibit shear-induced turbulent mixing.

The rigid manifolds with hole diameters from D/4 to D/8 showed little influence of hole size on performance. Moreover, they found that the manifold pressure can be changed by varying either the cross-section area or the frictional characteristics of the manifold [17].

Jaluria and Gupta [24] examined the decay of thermal stratification with time in the absence of any external convective flow that might cause mixing in the storage tank. The decay of the stratification with time is caused by heat transfer to the environment. The decay of the surface temperature is dependent on the initial temperature distribution and on the energy loss. The experimental arrangement consisted of water contained in two Plexiglas tanks. The researchers found that the buoyancy-induced mixing which occurs maintains the upper layers as isothermal and gives rise to horizontal temperature homogeneity in the water body. The decrease in the surface temperature is accompanied with an increase in the temperature in the bottom layers, followed by a decrease in temperature throughout the water body at the later stages. The researchers concluded that these characteristics made the stratified medium a better energy storage system compared to the isothermal case [24].

In 1987, Shyu and Hsieh [43] studied the unsteady natural convection in enclosures with a stratified medium by using a numerical solution. Three cases involving enclosure walls were studied: one wall without insulation on it; one wall with outside insulation, and one wall with inside insulation. The researchers [43] found that heat can be transferred from the hot medium to the cold via the heat-conducting wall, and that this mechanism destroys thermal stratification. Their computational results indicated the superiority of placing the insulation inside to maintain the thermal stratification in the medium. They also found that the outside insulation accelerated the stratification decay more than the other insulation. When placing the insulation over the inside surface, not only is the heat loss to the ambient air reduced but the thermal stratification is also

maintained more effectively. Therefore, they concluded that the system is highly recommended for solar thermal applications [43].

Zurigat, Liche, and Ghajar [50] studied turbulent mixing correlations for a thermocline thermal storage tank. The turbulent mixing during charge and discharge cycles is the major contributor to the loss of thermodynamic availability of storage energy. Based on the obtained correlations, Zurigat et al. [50] concluded that the inlet geometry starts to influence thermal stratification in a thermocline thermal storage tank for Richardson numbers less than 3.6.

In 1988, Spaulding [45] developed a device that can deliver water entering a storage tank to an elevation where the incoming water and the tank water match in temperature. The manifold in the experiment had holes positioned at its higher and lower ends. However, the researchers [45] changed the design of the stratifier without reducing the performance. Specifically, they used a three-part device instead of a single porous inlet device. The findings from this strategy indicated that there was a decrease in the plume entrainment, and that the inlet device can generate thermal stratification within a SDHW tank [45].

In 1989, Holland and Lightstone [21] performed an analytical investigation to review low-flow stratified tank solar water heating systems. They found that the performance of stratified solar hot water systems can be improved by more than 38% if one compares them to systems having a high flow rate and a fully mixed tank. Also, the researchers [21] successfully decreased the costs of copper pipe by replacing it with low-cost easy-to-install nylon tubing and using the thermo-syphon principle instead of a side pump. In addition, they indicated that the momentum of the water jet entering the tank produces a mixing that is usually localized to a small horizontal region near the inlet port. Under certain conditions this region may extend to include much of the tank. Such a

mixing region can be identified by the relationship between the vertical distance between the inlet and outlet port (L) and the mixing region height (L*). The height relationship denoted by (L*/L) is less than 0.05 when the Richardson number is greater than 0.5; however, for smaller Richardson numbers, the value of the dimensionless height relation rises sharply. The researchers also found that good stratification was not achieved at a Richardson number as high as 4.7, since the incoming flow was not laminar [21].

In the same research study, Holland and Lighthouse [21] investigated the plume entrainment in solar domestic hot water tanks. This entrainment mixes the water, thus destroying ideal stratification. Plume entrainment will often occur in low-flow systems at mid-afternoon when the availability of solar energy has decreased. As a result, water entering the tank top will be cooler than the water at the top of the tank, producing a downward flowing plume [21].

Several researchers have proposed methods to eliminate plume entrainment. The first suggestion was that a light flexible hose can be connected to the tank inlet. However, the researchers [6] noticed that the flexible hose manifold still had some problems which can arise if air bubbles attach to the hose. The second suggestion involved a vertical permeable manifold connected to the inlet port [28, 30, and 45]. By proper design of the hydraulic resistance inside the manifold, the water can be made to travel directly to the correct level within the manifold and then out the permeable walls. Finally, the effect of conductive walls on a charging tank was also investigated. The researchers [31] found that, in this case, the walls will tend toward achieving average temperature in the tank faster than the water, which causes convection currents that destroy stratification. Their investigations discovered that stratification in aluminum tanks degraded ten times faster than that in glass tanks. In addition, their computational results showed that the tank configuration which best maintained the stratification was inside an insulated tank. Interestingly, their investigation

revealed that the axial conduction in the wall does not play an important role in the heat transfer processes, which made the tank without insulation maintain stratification better than a tank with outside insulation [43].

In [51], Ghajar and Zurigat devised a computer code and determined numerically the influence of inlet geometries on thermal stratification in a thermal storage tank. From the results of this experiment, they inferred that the effect of inlet geometry is negligible for Richardson numbers above 10 [51].

In [39], Rosen and Hooper's objective was to develop models for temperature distribution in vertically stratified thermal storages, which are sufficiently accurate for use in engineering design and analysis, and sufficiently simple that they are convenient to use and provide useful physical insights into the systems. The researchers [39] showed that the advantage of exergy methods in evaluating thermodynamic advantages of thermal storages is not being utilized because some engineers see the procedures as too complex. Responding to this issue, the authors [39] presented approximations that would reduce the difficulty of the analysis.

Davidson [11] devised a coefficient to characterize mixing in solar water storage tanks. A new dimensionless coefficient to quantify mixing in storage tanks was based on height-weighted energy, or moment of energy. The researcher [11] calculated the new energy index to quantify mixing in storage tanks from the vertical profile. The upper and lower bounding values of this moment of energy were determined theoretically over any thermal test history by assuming perfect stratification and complete mixing, respectively. The Mix number incorporating these theoretical values is 1 for complete mixed tank and 0 for an ideally stratified tank. This dimensionless

coefficient gave a realistic assessment of the effectiveness of tank designs in enhancing thermal stratification. The vertical moment of energy in a solar storage tank is defined as:

$$M = \int_0^H ydE$$

$$E_i = \rho_i . cp_i . V_i . T_i$$

where $y_i$ is the distance measured from the bottom of the tank to the center of the node i, $V_i$ is the volume ($m^3$), and the energy of the node i is:

The Mix number is given by: $\text{Mix number} = \frac{M_{Str} - M_{real}}{M_{Str} - M_{mixed}}$

$M_{Str}$ and $M_{mix}$ represent the largest and smallest values of the moment of energy, respectively [11].

Al-Najem and Al-Refaee [4] showed that eddy conductivity factor caused by hydrodynamic disturbances at the inlet and outlet ports of storage tank plays an important role in the performance of thermal stratification. In fact, it represents the most significant item in the performance of thermal stratified storage. A proper design of the inlet and outlet diffusers helps to reduce the hydrodynamic disturbance, which is directly responsible for destroying the thermocline layers. In addition, the researchers [4] found that the turbulent mixing factor caused by the mixing process is strongly affected by the Reynolds and Richardson numbers and flow inlet geometry. Finally, they concluded that the warm water which enters from the top would easily enhance stratification, but cold water would mix the temperature inside the tank [4].

In 1998, Eames and Norton [14] studied the effect of tank geometry on thermally stratified sensible heat storage in hot water tanks. They performed 32 experimental tests, with the inlet temperature ranging between 11 and 52°C, fluid inlet velocities in the range of 25-90 mm/s, and various

permutations of inlet and outlet port locations. The researchers [14] found that when subject to low velocity inlet jets in square or circular diameter, the storage tank cross-sectional geometries had only a slight impact on the stratification development. The store charging was performed more efficiently for tall aspect ratios than shorter ones. Moreover, the thermocline degraded due to convective mixing resulting from both heat loss from and conduction within the store walls. The researchers [14] revealed that a single inlet port with variable inlet temperature led to destratification, and that the solution to this problem was having a range of inlet ports at different heights. This set-up would allow the inlet fluid to enter the storage tank at the height at which the resident store fluid temperature most closely matches the inlet fluid temperature [14].

Hahne and Chen [18] performed a numerical study for the flow and heat transfer characteristics of a cylindrical hot water store. They found that storage efficiency increases with increasing Richardson and Peclet numbers [18].

In [37], Rosengarten, Morrison and Behnia studied a method for characterizing and evaluating the performance of hot water storage systems in terms of their temperature distribution. They concluded that the change in exergy from the stratified state to the delivery state depends on the storage energy and the stratification, and that if only the first law of thermodynamics is used, it is not possible to distinguish a stratified tank from a mixed tank. In addition, they found that exergy and stratification efficiency, as well as energy, should be used to ascertain the performance of such heat exchangers. For this reason, incorporation of a second law analysis allows different temperature distributions to be quantified in the terms of available energy and makes an excellent tool for the design and analysis of a hot water storage system. Rosengarten et al. [37] then derived the following equation, which enables the exergy to be calculated as a function of the delivery temperature and environmental temperature:

$$\varepsilon = mc\left[T_{del} - T_{mean} - \frac{T_0}{H}\int_0^H \ln\left(T_{del}/T_{(y)}\right) dy\right]$$

Furthermore, they concluded that exergy is highly dependent on the temperature used in the above equation [37]. Due to this issue, when using exergy to evaluate and compare thermal storage devices, consistent definitions of the temperature were required. An arbitrary choice of the dead state temperature, without physical justification, can cause confusion and misleading comparisons. The researchers [37] thus used the water inlet temperature as the dead state temperature in their non-dimensional exergy term to calculate the stratification efficiency. The non-dimension exergy efficiency can be written as:

$$\eta_{Str} = \frac{\varepsilon}{mc(T_{del} - T_{mean})} = 1 - \frac{T_0}{H(T_{del} - T_{mean})}\int_0^H \ln\left(T_{del}/T_{(y)}\right) dy$$

where $\eta_{Str}$ is stratification efficiency, $\varepsilon$ is exergy of stored liquid (J., c : Specific heat, J/kg.℃.), $T_0$ is dead state temperature ˚C, m is mass kg, $T_{del}$ is temperature at which water is delivered in ˚C, $T_{mean}$ is mean tank water temperature in ˚C. H : Tank height, m, y is the vertical coordinate inside tank m.

In [38], Rosen performed an assessment of the thermodynamic performance of cold thermal storage systems using exergy and energy analyses. Several cases were considered, including some storage which is homogeneous and others which undergo phase changes. The researcher [38] determined that exergy analysis offers a more realistic and precise assessments of the efficiency and performance of cold thermal storage systems. In addition, Rosen [38] found that the potential usefulness of exergy analysis in addressing and solving cold thermal storage problems is significant. The exergy or availability can be obtained by using the following equation:

$$A = m \sum_{i=1}^{n} (h_i - h_o) - T_o(s_i - s_o)$$

here A is availability, $h_i$ is specific enthalpy of the layer (kJ/kg), $h_o$ is dead state specific enthalpy (kJ/kg), $T_0$ is dead state temperature (˚C ), m is mass of the tank in kg, $s_i$ is specific entropy of the layer (kJ/kg), and $s_o$ is dead state specific entropy (kJ/kg) [38].

Knudsen [27] studied the effect of different solar tank designs and volumes as well as different hot water consumption patterns on thermal performance. In addition, he studied how the thermal performance is influenced by mixing in the solar tank during draw-offs. Knudsen [27] concluded that a mixing rate of 40% during draw-offs caused a greater decrease in the thermal performance of spiral tank systems than in the thermal performance of mantle tank systems. Furthermore, as stated by Andersen and Furbo [6], a half-ball baffle plate positioned above the cold-water inlet port inside the storage tank can improve the thermal performance of the system during the mixing draw-offs.

Zachar, Farkas and Szlivka [49] performed a numerical analysis to evaluate the effect of plate sizes located opposite to the inlet port in order to increase the thermal stratification inside a storage tank. In the study, the inlet and outlet are located centrally at the top and bottom region of the tank. After investigating the flow of cold water into the top of storage tank, the researchers [49] inferred the following three points. First, a larger plate diameter should be placed to preserve stratification with high inlet flow rates. Second, due to the high inlet flow rate, the flow should be diverted away from the center of the tank and forced towards the wall to take advantage of the continuity law. Finally, the size of the plate diameter does not significantly increase the thermal stratification in cases when the hotter water is charged at the top and the colder inflow is charged into the bottom of the tank [49].

Shah and Furbo [41] performed theoretical and experimental analyses of water jets entering a solar storage tank. Three inlet designs were investigated as shown in Figure (3-1): a raw pipe, a pipe with a small hemispherical baffle plate, and a pipe with a large flat baffle plate. With the three inlets, nine draw-off tests with different inlet flow rates were carried out and the temperature stratification in the tank was measured during the draw-offs. The researchers [41] applied the first and second laws of thermodynamics to characterize the inlets' influence on the thermal conditions and thus the deliverable energy in the tank. The results showed how the entropy and exergy changes in the storage during the draw-offs were influenced by the Richardson number, the volume draw-off and the initial tank conditions. The researchers [41] then concluded that the poor inlet design reduced the energy quality, that the inlet pipe with the plate had the most deliverable energy, and that the inlet row pipe had the least deliverable energy.

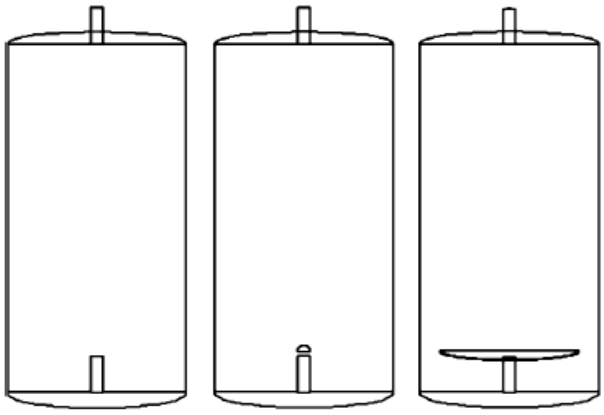

Figure 3-1 Model outline of the tank with the three different main water inlets (Shah and Furbo (2003))

In 2004, Outtrim [34] studied immersed thermosiphon heat exchangers for SDHW systems. The objective of this research was to experimentally check different heat exchangers under normal operating conditions for Halifax Nova Scotia, Canada. The researcher [34] calculated the availability by using the first and second laws of thermodynamic efficiency for each component

by changing the hot water inlet geometry and hydraulic resistance. In the experiment, it was found that reducing the water flow rate enhanced the level of stratification and that the availability was affected by the degree of stratification and the average tank temperature. Conversely, plume entrainment decreased the level of stratification at the end of the experimental tests [34].

In [25], Jordan and Furbo compared two different marketed inlet designs – one connected to a small curved plate placed above the inlet tube, and the other one connected to a much larger flat plate. The cold domestic water in the experiment entered the stores in a vertical direction from the bottom of the tanks. Jordan et al. [25] found that the thermal stratification inside the two tanks exhibited different rates of dependence on the flow rate, the draw-off volume, and the initial temperature in the storage tank.

In 2005, Shah and Furbo [42] performed five experiments with flow rates from 2 L/min to 10 L/min. The stratifier was designed as a main tube with three unobstructed and flaps at the openings. The flaps were made of soft material, which allowed them to open and close depending on the temperature and pressure conditions inside and outside the pipe. In conducting their tests, the researchers [42] obtained two major findings. First, the non-return valve reduced the unwanted flow going into the stratifier at the lowest opening, and second, the stratifier was most efficient for flow rates between 5 L/min and 8 L/min. The researchers [42] suggested that, because the volume flow rate was less than 5 l/min, further development of these stratifier designs was warranted.

Knudsen, Morrison, Behnia and Furbo [26] studied a vertical mantle heat exchanger with a lower mantle inlet position as shown in Figure (3-2). The flow structure was assessed for both high and warm inlet temperature flows and for a mixed and stratified inner tank and mantle. “High” refers to the inlet temperature being higher than the core tank temperature at the top of the mantle,

and “warm” indicates the inlet temperature between the core tank temperature at the top and bottom of the mantle. Knudsen et al. [26] concluded from their research findings that a vertical mantle heat exchanger is able to promote stratification in the inner tank even when the mantle inlet temperature is lower than the tank temperature at the input level of the mantle.

Figure 3-2 Glass mantle tank (Knudsen, et al. (2005))

In 2005, Dahagan, Hosni and Hoda [10] performed an experimental investigation of the thermal behavior of a vertical solar tank, using energy and exergy analyses. In this study, the experimentation was done on a realistic operation condition and load pattern. The researchers [10] found that the thermal stratification degraded from night until morning, as the heat supply is ineffective and the demand for hot water increases. The degradation of thermal stratification is due to the diffusion of heat from the top hot water layers to the bottom cold region and axial heat conduction through tank’s wall [10].

Andersen, Furbo and Fan [6] investigated the performance of fabric stratification pipes during heating and cooling tests and then compared them to the performance of a rigid stratification pipe with non-return valves. The researchers [6] found that the main improvement in using a non-rigid pipe as a stratification inlet pipe is that the fabric pipe can enlarge or contract, leading to an equalization of the pressure in the pipe at all water levels of the tank. Andersen et al. [6] assumed that by using two fabric layers (with a distance of about 10 mm between each fabric layer) instead of using one fabric layer, laminar flow could develop between the two layers. They also assumed that the unwanted horizontal heat transfer would reduced [6].

However, they discovered that when the distance between the fabric layers was too small, the flow became turbulent and a larger amount of heat was transferred [6]. Conversely, the test findings indicated that a larger fabric pipe diameter results in a larger surface area of the pipe, which then increases the heat transfer between the inlet stratification pipe and the tank [6]. The researchers also concluded that with two layers of fabric, the temperature at the top of the tank increased and the temperature at the bottom decreased in comparison to tests performed on one-layer fabric stratification pipe. Moreover, the stratification with the rigid stratification pipe and non-return valves was very close to the perfectly stratified profile because the horizontal heat transfer through the wall of the rigid pipe is much lower than the horizontal heat transfer through the fabric wall [6].

In 2007, Panthalookaran, Heidemann and Muller-Steinhagen [35] formulated a new analysis that was based on the first and second laws of thermodynamics. In their experiments, the researchers [35] restricted themselves to the characterization of stratified thermal energy stores (TES), in view of its application to the design analysis of hot water seasonal heat stores. The basic approach of the Rosen and Dincer [38] methods was to evaluate the difference or the ratio between

the exergy contents of a stratified and a fully-mixed thermal energy storage tank. In both cases, the exergy of the stratified TES was evaluated using an equivalent temperature whose definition depends on the energy levels in the real system. In addition, Rosen et al. [38] defined an equivalent temperature as the moment of energy or the Mix number definition. They evaluated the thermal performance of a thermal storage tank by using the dimensionless internal entropy generation relationship, such that:

$$R_{EG} = \frac{\Delta s_{real} - \Delta s_{Str}}{\Delta s_{mixed} - \Delta s_{Str}}$$

where $R_{EG}$ : Internal entropy generation [38].

Altuntop, Tekin, Ozceyhan and Gunes [3] analyzed solar energy storage tank designs involving various obstacle geometries, such as cylindrical, semi-cylindrical and conic. These geometries are considered to minimize the mixing of hot and cold water so that water may be supplied at high temperatures. Real geometrical dimensions for typical solar applications and realistic boundary conditions were also used. The researchers [3] assumed that the flow rate of the hot water drawn from the tank would be equal to the rate of the cold water entering the tank from the main line (note that the cold water velocity from the main line is 1 m/s). Altuntop et al. [3] concluded that placing an obstacle in the tank provides better thermal stratification compared to storage without an obstacle.

Furthermore, the researchers [3] found that the obstacle types with a gap in the center appear to have better thermal stratification than those with a gap near the tank wall. Thus, with a 30-min duration, obstacle number D (as shown in Figure 3-3) provides the best thermal stratification in the tank among all the other obstacles and can supply hot water at higher temperatures. Moreover,

the results of the study indicated that, for obstacles A, B, and D, thermal stratification increases with increasing obstacle distance from the bottom of the hot water storage tank.

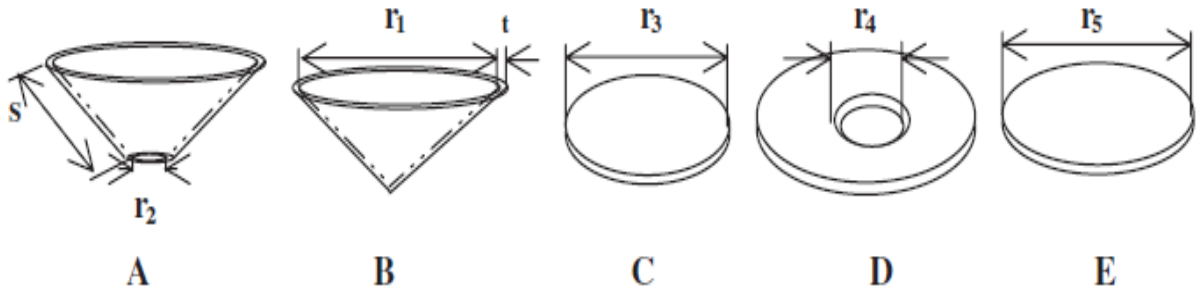


Figure 3-3 Various obstacle geometries to enhance stratification inside the solar tank. (Altuntop, et al. (2005))

From a theoretical point of view, Haller, Cruickshank, Streicher, Harrison, Andersen and Furbo [19] examined a variety of proposed methods for characterizing thermal stratification in energy storage systems. Their work focused on methods that can be used to determine the ability of a storage to promote and maintain stratification during charging, storing and discharging. Their aim was to represent this ability with a single numerical value in terms of a stratification efficiency for a given experiment or under given boundary conditions [19].

Han [22] performed a survey of thermal stratification within the water storage tank, summarizing earlier research on how the parameter impacts stratification. Some details from this investigation can be found in Table (3-1).

Table 3-1 Previous Research on Influence of Dimensionless Numbers on Thermal Stratification

| Author | Year | Parameter Consideration | Conclusions | Stratification |
|---|---|---|---|---|
| Zurigat et al. | 1990 | Richardson number | $Ri < 3.6$ | Inlet geometry has great influence on stratification |
| Ghajar and Zurigat | 1991 | Richardson number | $Ri > 10$ | Inlet effect can be neglected |
| Yoo and Pak; Al-Nimr | 1993 | Peclet number | At high Peclet | Stratification less apparent |
| Cai and Stewart; Son | 1993 | Archimedean and Reynolds numbers | $Ar > 5$ and $Re < 1000$ | Cold fluid will not extensively mix with warmer fluid |
| Van Berkel et al. | 1999 | Richardson number | $Ri > 10 - 20$ | Clear mixing appearing |
| Ramsayer | 2001 | Richardson number | $Ri > 0.2$ | Mean temperature gradient is not influenced by inlet flow |
| Stewart and William | 2001 | Froude and Reynolds numbers | $Re > 6000$ | Does not result in a significant thermocline |
| Brown and Lai | 2004 | Richardson number | $Ri > 0.615$ | Stratification is observed |

In 2011, a study conducted by Alsagheer [2] developed and designed perforated manifolds that work with standard Canadian solar domestic hot water system. These were evaluated under different climate conditions. The purpose of the perforated manifold is to inhibit mixing between the manifold and tank. The manifold may be described as controlling buoyant jets so as not to destroy stratification in the tank. The results showed that stratification can be enhanced by using a perforated manifold increasing gradually from small at the bottom to large diameter at the top as shown in Figure (3-4), and that high stored exergy can be obtained under different operational conditions. However, the experiment did not approve the theoretical calculation, which states that the gradual increasing of the hole diameters from the bottom to the top should reduce unwanted flow and enhance the performance of the manifold [2].

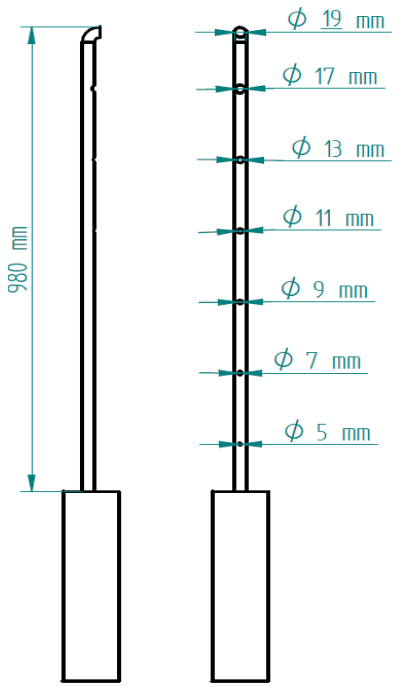


Figure 3-4 Perforated manifold increases gradually from small at the bottom to large diameter at the top

Marí, Gasque, Gutiérrez, Colomer, Ibáñez, and Altozano [16] examined the effect of two water inlet devices in a hot water storage tank during a thermal charge process of thermal stratification. Two water inlet devices, a sintered bronze conical diffuser (SBCD) and a conventional inlet elbow (E) were examined at three different flow rates. Marí et al. [16] determined that greater thermal stratification was achieved using the inlet SBCD for the three flow rates. The researchers also noted that, in the case of the elbow, the loss of thermal stratification was largely influenced by the flow [16].

In brief, most of the factors that cause mixing inside solar domestic hot water tanks are known, but research is required to clarify the important issues and develop devices that enhance stratification [21]. The stratification would be best maintained in tanks with walls made of plastic, or other material characterized by low thermal conductivity [28], and the destratification occurs when the incoming fluid from the collectors is cooler than the water stored at the top of the tank

[17]. The poor inlet pipe design reduced the energy quality [41]. Furthermore, the stratification can be enhanced by using a perforated manifold increasing gradually from small diameter at the bottom to large diameter at the top [2]. The methods currently used to evaluation of thermal stratification may be categorized as: Those based on the general dimensionless numbers of heat transfer and fluid dynamics, on the first law of thermodynamics, on the second law of thermodynamics. The combination of first law and second law makes an excellent tool for design of how hot water tank [37]. The researchers determined that a vertical mantle heat exchanger is able to promote stratification in the inner tank even when the mantle inlet temperature is lower than the tank temperature at the input level of the mantle [26]. In considering the literature findings presented in this review, we can see that most of the factors that cause destratification inside solar domestic hot water tanks are known. However, further research is required both to clarify the important issues experimentally and to develop other devices that enhance thermal stratification in solar tanks using a side-arm heater. Considering the literature findings presented in this review, we can see that most of the factors that cause destratification inside solar domestic hot water tanks are known. However, further research is required both to clarify the important issues experimentally and to develop other devices that enhance thermal stratification in solar tanks using a side-arm heater.

### 3.2. Photovoltaic Water Heating System

Nowadays, the cost of photovoltaic (PV) power has declined and the cost of electricity from PV is competitive with other solar thermal applications and conventional power. Photovoltaic water heaters offer the promise of being less expensive within the next several years and may soon approach a point where they are economically feasible for domestic and commercial applications as photovoltaic domestic hot water systems (PVDHW) [15].

The use of a PVDHW system has many advantages over a solar thermal system (STS). For instance, the pipe work and heat exchanger are eliminated in a PVDHW and there are no moving parts to wear out or break down. As well, there is no fluid leakage problem, freezing of fluids, or failure of pumps. Also, PV system installation is much easier than STS and can reduce heat loss and improve heat transfer efficiency. As shown in Figure (3-5), PVDHW systems have electric resistance heaters rather than a heat exchanger. This difference means that there is no limit to the temperature of water that can be produced. In addition (and most importantly), since the system is creating electricity, there is no waste of energy and the excess power can easily be routed to a useful application. Although PV power is currently more expensive than existing solar thermal systems, PV water heating systems are anticipated to become less expensive than solar thermal systems in the near future [12].

In 1994, Brian P. Dougherty and A. Hunter Fanney of the National Institute of Standards and Technology in Gaithersburg, USA, patented the photovoltaic water heating system (PVWHS) [12]. The PVWHS is an unconventional thermal solar domestic hot water system which consists of a PV array connected to several resistive heating elements within a water storage tank. The array produces electrical power during periods of solar irradiation, and this power is immediately dissipated in the resistive elements. The system, which incorporates a microprocessor controller to select the appropriate combination of resistors, causes the PV array to operate near its maximum power point during solar irradiation fluctuations. The controller sequentially connects six resistive elements to the array in parallel as irradiation increases based on predetermined irradiance level switch points. Over time, the resulting controller performance indexes to maximum possible energy output from the array.

Dougherty et al. [12] installed and monitored the performance of the PV solar hot water system at the Great Smoky Mountains National Park in September, 1996. The system was then monitored until early in 2000 [12]. Dougherty et al. [12] believed that once the price of PVs declined, the solar PV hot water systems would capture the majority of the renewable water heating market. However, more work was needed to be done.

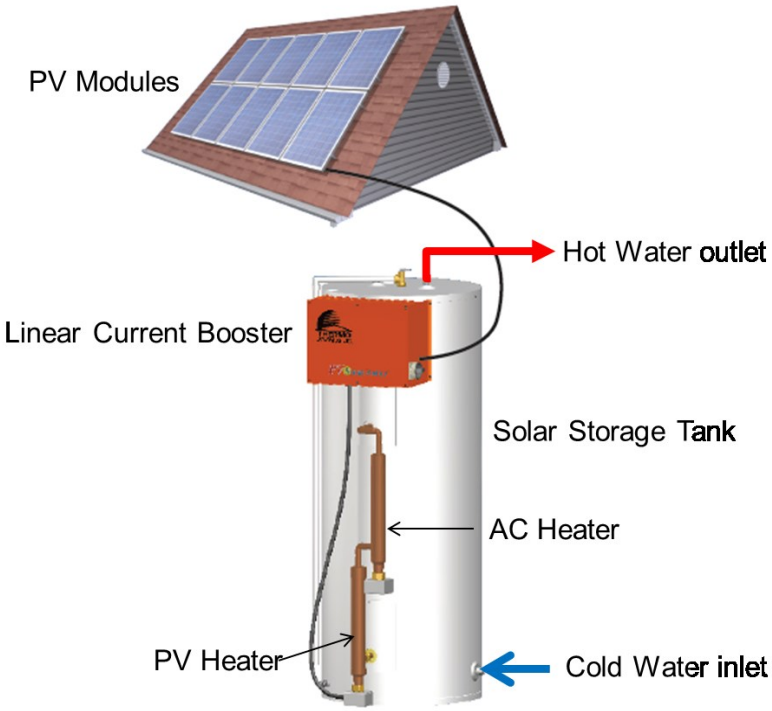


Figure 3-5 Solar photovoltaic hot water system.

As shown in Figure (3-5), the system requires neither a battery for energy storage nor an inverter to convert the direct current to the alternating current. Instead, the direct current power is supplied by solar panels. Power from the solar panels is distributed to a linear current booster which is designed to keep the panel voltage at a constant value for peak power. The power supplied by the PV array is fed to an electric resistance immersion heater element connected to the domestic hot water tank. One of the heating elements is hardwired to the PV array, while the other heaters are

connected when needed, using mechanical relays. The decision regarding which elements to connect to at any given time depend solely on the solar irradiance supply signal to a microprocessor-based controller. The main advantages of a PVHWS that uses parallel connected heating elements are that you decrease the size of the PV array and yet achieve the same or greater power output. This is compared to having just one heating element permanently connected to the PV array, which could capture around 66.5 % of the maximum possible array power output over the full irradiance range [7].

In 2009, Thomasson [48] made a microprocessor program to monitor water usage and adjust power to heater elements to provide hot water according to usage. Around the same time, Newman and Newman [33] applied for a patent for a PV water heating system that matches the load resistance of the resistance heating element to the power that is available from the PV solar array. This is done in order to maximize energy transferred to the water in the storage tank [33]. Lichtenberger [29] applied for a patent for a solar powered fluid heater system to work in a novel solar power system with a PV. This includes a novel resistance heating element, water heater adaptor, and energy conversion control, the latter which incorporates microprocessor control with improved efficiency and safety.

In short, although we have not yet arrived at the point where the renewable water heating market is dominated by PV hot water systems, energy conservation and awareness have improved over the past few decades and the cost of PV technology has decreased. Furthermore, while there are some new ideas that use the PVWHS, the literature presently contains no research on the sidearm heater principle in the PVWHS. Therefore, the proper design of an electric resistance immersion heater element in thermo-syphon side-arm storage tank using PV power heating has not yet been determined.

# Chapter 4: Experimental Set-up and Procedure

## 4.1. Experimental Apparatus

An experimental set-up was constructed to investigate stratification in a solar domestic hot water (SDHW) tank heated by photovoltaic (PV) power under various climate conditions. The tests were conducted at the solar thermal laboratory in the Mechanical Engineering department of Dalhousie University, Halifax, Canada. The experimental set-up consists of PV modules, a linear current booster, a water storage tank, a side-arm heater with dye injection system, instrumentation, and a data acquisition system. The experimental components are shown in Figure (4-1).

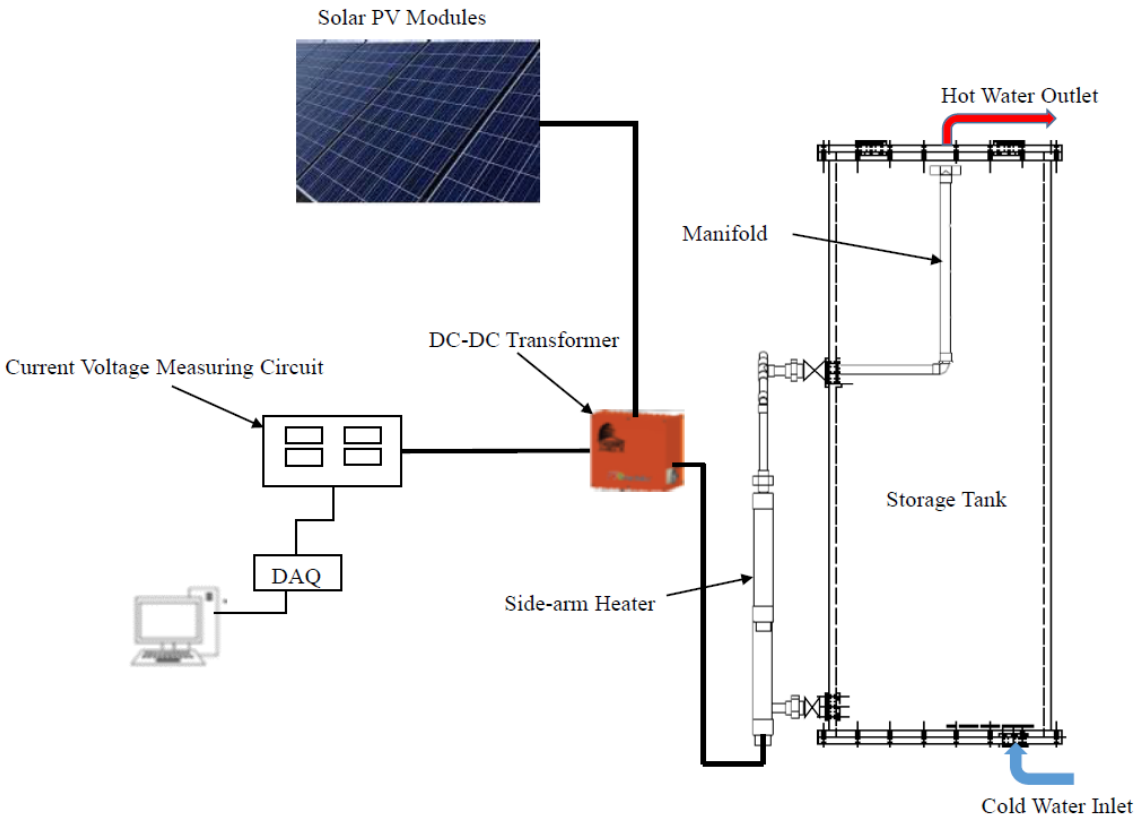


Figure 4-1 Experimental set-up of solar PV domestic hot water system

### 4.1.1. PV Modules

The PV array consists of 10 modules. Two rows of modules in parallel with five modules in series in each row were mounted on the roof of the solar thermal laboratory to power the SDHW system. The modules are sloped at a $45^0$ angle and positioned at true south. Each module has a nominal power output of 235 watts under standard test conditions (STC), the specifications for which are shown in Appendix D. The actual power is subject to change at different air temperature and solar radiation values. A decrease in ambient air temperature or an increase in solar radiation will cause an increase in PV power. A PV water heating system requires neither a battery for energy storage nor an inverter to convert the direct current to alternating current. The direct current power supplied by the ten PV modules is supplied to a linear current booster, which is designed to keep the voltage of the modules at a constant value for peak power. The power supplied by the PV array is fed to an electric resistance immersion heater element in a thermo-syphon side-arm connected to side entry ports on the domestic hot water tank.

### 4.1.2. Linear Current Booster

A linear current booster (LCB) is a DC-DC current transformer, as shown in Appendix C. Power from the PV is distributed to the LCB, which is designed to keep the voltage of the modules in this case, the voltage of the PV array is maintained at 150 VDC. At lower solar radiation, the LCB takes the low output current from the PV modules and steps it up to provide the high current to start the heating element.

### 4.1.3. Water Storage Tank

A 370-litre rectangular acrylic (Plexiglas) hot water storage tank insulated with 51 mm of removable insulation was used for this research (for dimensions, see Appendix E). The tank was reconstructed to accommodate the side-arm thermosiphon heater. The tank was equipped with an

air vent to remove the air from the top of the tank. This air vent acts as a safety valve to maintain static pressure at the top of the tank so that it does not go above atmospheric pressure. The walls are made of 12.7 mm clear acrylic and reinforced with steel angle and threaded rod. A 15 cm x 15 cm diffuser plate was placed above the inlet mains cold water supply port at the bottom of storage tank to preserve stratification with high inlet flow rates. Twenty-two thermocouples were installed in two probes located at two corners of the tank to measure the temperatures at different layers from the bottom to the top, inside the tank. The SDHW storage tank has an inlet to the mains supply cold water at the bottom and an exit for the delivery of hot water at the top. To decrease heat losses, the all-Plexiglas tank side is insulated with a polyisocyanurate foam board with a thickness of 51mm and an RSI 2.9 K/W.

### 4.1.4. Side-arm Heater

A side-arm heater draws cold water from the bottom of the tank and delivers hot water at the top by means of natural convection, eliminating the need for a pump. The hot water rises through a manifold until it reaches the level where the density matches that of the surrounding tank water, at which point it flows into the tank. This promotes stratification within the system. The side-arm heater connected with the injection system was manufactured by Thermo-Dynamic Ltd as shown in Figure (4-2) and has been modified to accommodate the injection system at the Renewable Energy Lab (the dimensions are given in Appendix E). A dye-color injection system was used to visualize the delivery of hot water flow patterns in the tank.

An additional AC heater was connected to the side-arm heater. The purpose of the auxiliary heating element is to ensure an adequate hot water supply when the availability of solar energy has decreased or during instances of low water temperature. The side-arm heater is constructed of copper pipe. It has two unions: one at the top of the AC heater housing, and the other at the bottom

of the PV heater housing. This arrangement simplifies the side-arm assembly of the domestic hot water tank if maintenance on the heater element needs to be performed. Additionally, polyethylene insulation was placed around the side-arm and all connected pipe line to decrease heat losses (RSI 0.4 K/W).

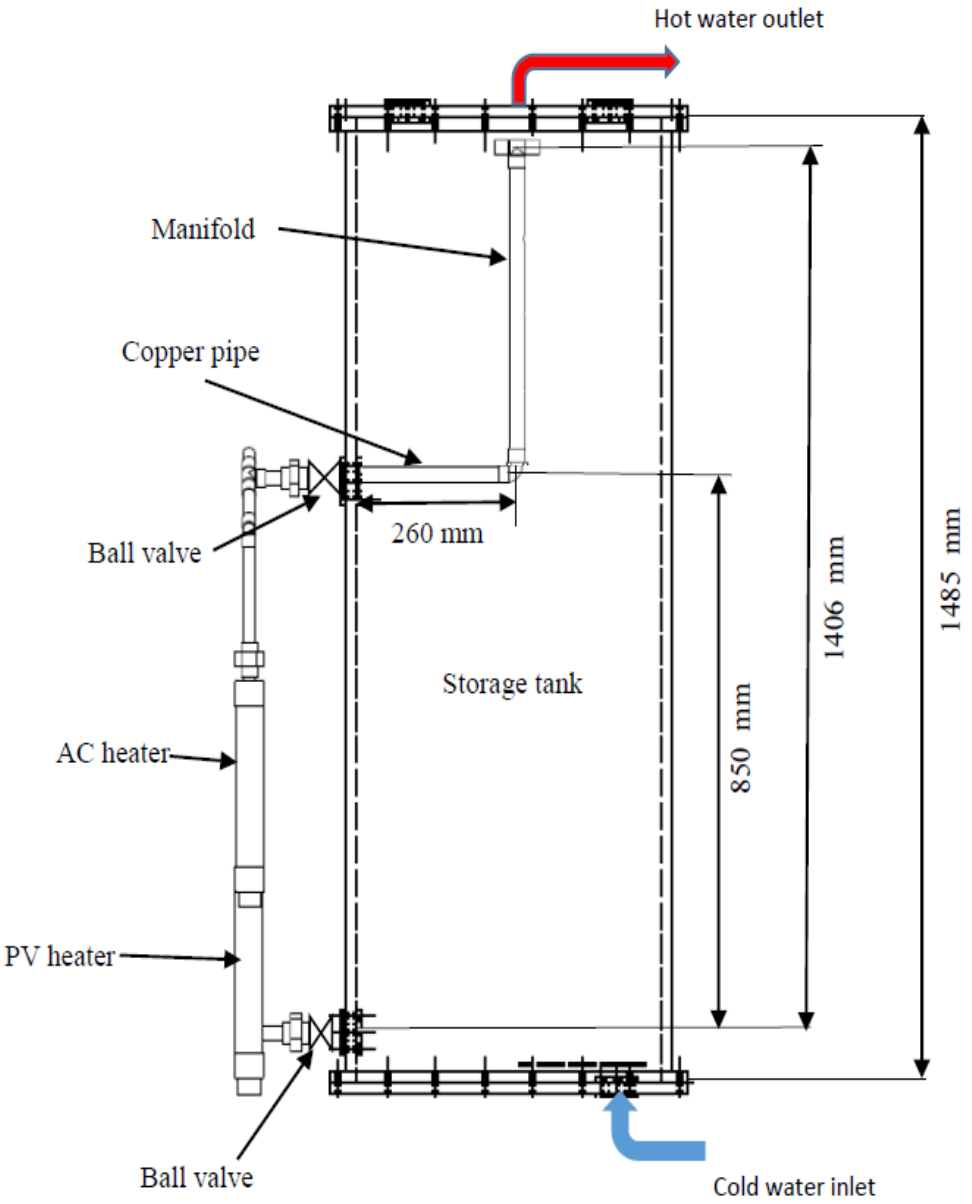


Figure 4-2 Side-arm heater connected with a manifold.

The heating element used in the side-arm heater is shown in Appendix C. The PV heater specifications are 9000 W at 240 V, the resistance of the heater is given by:

$$R = \frac{V^2}{P} = 6.4\Omega.$$

The ten PV modules can produce 2350 watt at full sun, at 150 VDC. The PV current is given by:

$$I = \frac{P}{V} = 15.7\ A$$

The voltage across the heater at full sun is given by:

$$V = (P \,.\, R)^{0.5} = 123\ V$$

The AC heater specifications are 1500 W at 120 V, and 9.6 Ω. Further, the side-arm heater has 1-inch N.P.S. threading that allows the heater element to be easily screwed into and out of the side-arm. Detailed drawings and specifications of the side-arm heater components can be found in Appendix E.

### 4.1.5. Hot Water Inlet Devices

The results of several research investigations show that a one-port hot water distributor placed at the top of a domestic hot water tank reduces stratification and leads to decreased energy equality [2, 17, 21 and 34]. The present research proposes a novel hot water inlet device that eliminates plume entrainment and enhances thermal stratification in a storage tank. Due to fluctuations in solar radiation, water delivered from the side-arm heater sometimes has a lower temperature than the water at the top of a domestic hot water tank, creating a downward flowing plume. This plume will pass through the hot water in the solar water tank, causing destratification. The solution to this problem can be achieved by a manifold having inlet ports at different heights. The purpose of the perforated manifold is to deliver the water heated by the side-arm heater to the tank at the level where the temperature of the water in the tank matches the temperature of the heated water.

According to the experimental work of ALsagheer [2] and other researchers mentioned in the literature review, a copper manifold with four ports that increase gradually from a small port diameter to a large port diameter is a workable solution. In this work, a copper tube with only one port at the top and a copper diffuser which increases from ¾ to 1½ in were designed and constructed at the Renewable Energy Laboratory at Dalhousie University. Each manifold was operated under variable input power and then evaluated under actual conditions in Halifax, Canada. The aim was to identify a side-arm heater with hot water inlet devices that enhance the thermal stratification in an SDHW tank system.

In the experiments, the manifolds and conventional hot water distributors were installed and removed from a large port at the top of the hot water tank to decrease the shutdown time (more specifics dimensions are shown in Appendix E). The assessment of the performance of the side-arm heater system with the inlet hot water distributor was based on the evaluation of the availability and the entropy of the experimental SDHW tank with the availability and the entropy of the fully mixed and perfect stratified SDHW tanks. The exergy or availability of the experimental tank was evaluated according to the measured temperature in different thermocouple positions in the SDHW tank. The most efficient hot water distributor is the one resulting in higher availability and merit factor, and lower internal entropy generation and entropy ratios.

Flow visualization tests were also conducted to evaluate the performance of the hot water inlet devices in enhancing and maintaining thermal stratification in an SDHW tank. The tests of the side-arm heater with the following hot water distributor were started under reasonable and realistic conditions for cold and hot tank temperatures.

#### 4.1.5.1. One-port Manifold

The one-port hot water distributor was one of the conventional designs as shown in Figure (4-3). It consisted of a copper tube (Type M) with a nominal inner diameter of 20.5 mm (¾ in) and an outer diameter of 22 mm (7/8 in). Connected to the outlet pipe of the side-arm heater, it delivered the heated water through a T-connection at the top of the storage tank.

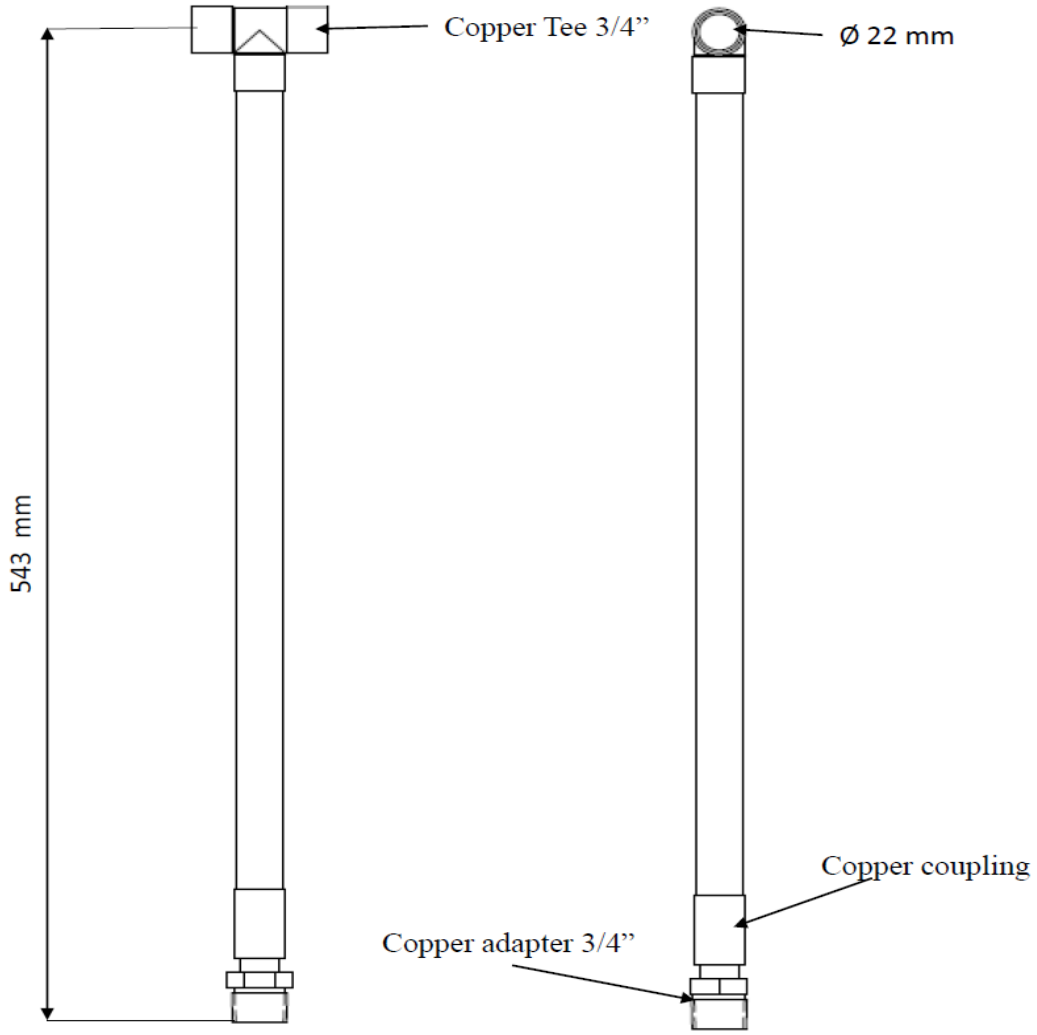


Figure 4-3 One-port manifold.

#### 4.1.5.2. Diffuser

The hot water distributor diffuser was another one of the conventional designs consisting of a copper diffuser as shown in Figure (4-4). The inlet copper diffuser was increased from 20.5 mm (¾ in) to 41 mm (1½ in) to reduce the inlet velocity of the hot water flow rate. The inlet copper diffuser was connected to the outlet pipe line of the side-arm heater and delivered the heated water at the middle of the storage tank.

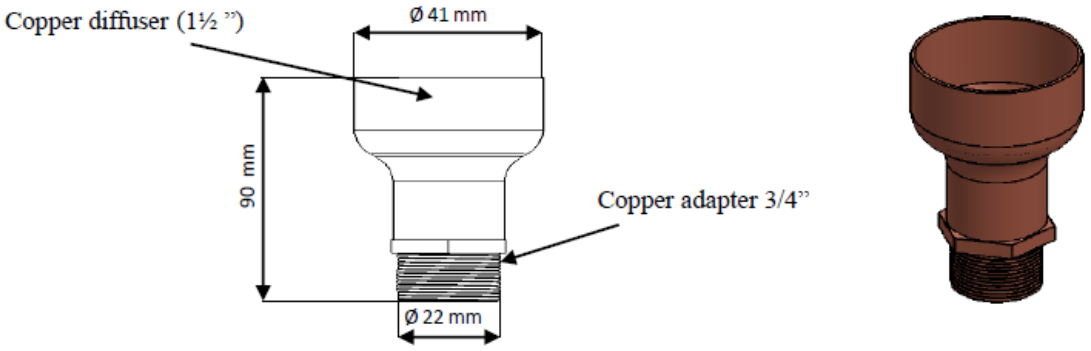


Figure 4-4 Hot water inlet diffuser

#### 4.1.5.3. Four-port Manifold

In an endeavor to enhance thermal stratification in a solar domestic hot water tank, a copper manifold with four ports which increased gradually in size from a small to a large diameter was designed and tested. The supply hot water from the side-arm heater rose or fell in the four-port manifold, maintaining pressure difference with the surrounding tank hot water until it reached the level at which the water density matched that of the surrounding tank hot water. At this point, the water flowed into the tank. The size of the ports of the four-port manifold increased gradually from

a small to a large diameter at the top in order to avoid inflow and outflow through the ports until the level was reached at which the density of the two fluids matched.

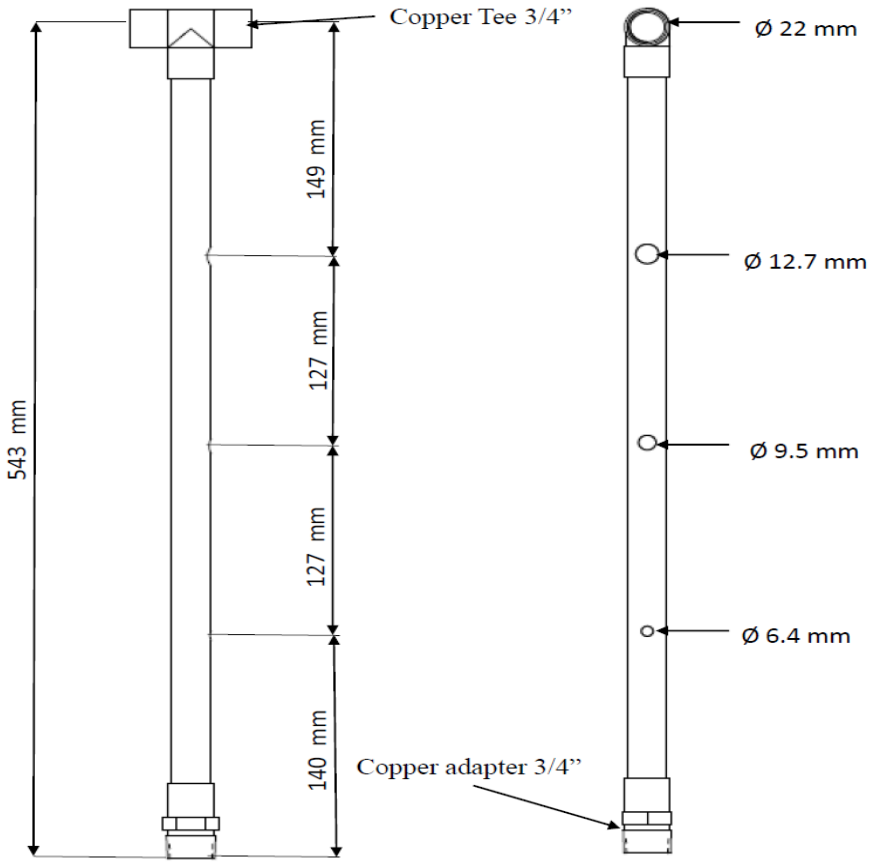


Figure 4-5 Four-port manifold.

This manifold enhances thermal stratification in the tank by controlling buoyant jets. The four-port hot water distributor was designed and constructed at the lab and consists of a copper tube (Type M) with a nominal inner diameter of 19 mm (¾ in) and an outer diameter of 22 mm (7/8 in) as shown in Figure (4-5). The distance between the top of the tank and the center of the highest outlet port is 20 mm. The diameter of the ports increases gradually from the bottom to the top, specifically from 6.4 mm to 9.5 mm to 12.7 mm to 20.6 mm. The hot water enters the manifold through the bottom. The four-port inlet distributor has a built-in thermocouple in front of each port to measure the temperature of the hot water inlet.

### 4.1.6. Instrumentation

Instrumentation is the science and technology of complete measurement systems. Using instrumentation, physical quantities are measured so as to obtain data which can be transmitted to recording and display devices. Between the transducer and the recording or display device, the signal normally requires some form of processing. In any general measurement system, the sensing element or transducer converts variations in the measured quantity into corresponding electrical signals. In order to make the electrical output from the transducer suitable for instrumentation purposes, signal conditioning is usually required. Many transducers give a very small electrical output which must be amplified before it can be used to operate an indicator or recorder.

#### 4.1.6.1. Current Voltage Measuring Circuit

The measuring circuit was constructed in the Renewable Energy Lab, as shown in Figure (4-6). It is a circuit consisting of resistors and was constructed to measure the voltage and current on both sides of the linear current booster. The voltage and current of the PV module are higher than the maximum values that can be measured by LabVIEW, which is a system engineering software. The PV voltage was measured using a voltage divider on the input to bring the value within LabVIEW range. By choosing the appropriate resistor values, the voltage was decreased to a level within range of the LabVIEW program, as follows:

$$V_{Out} = \frac{R_1}{(R_1 + R_2)} V_{IN}$$

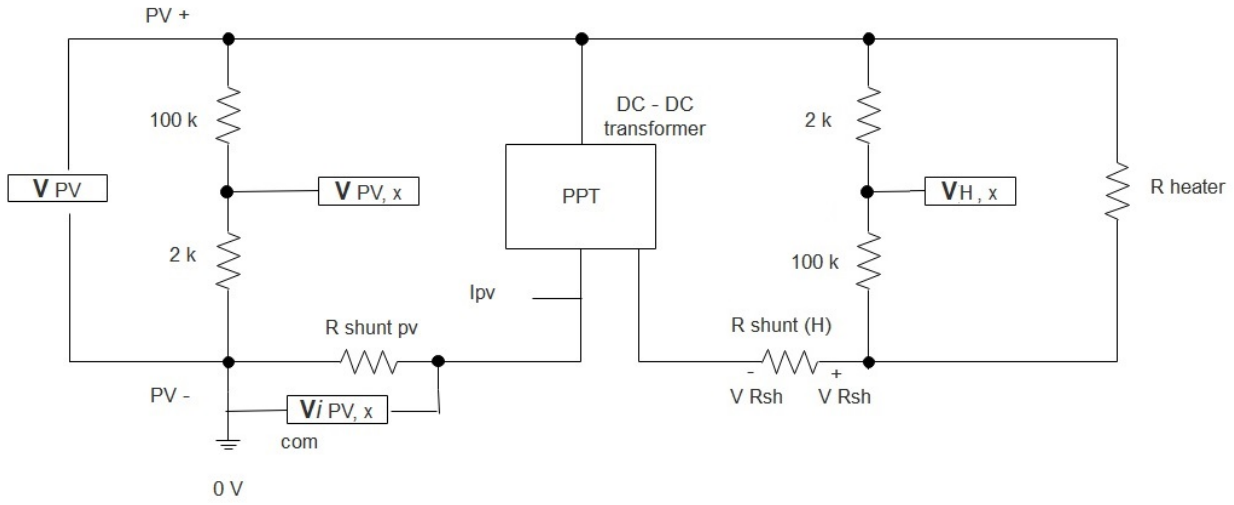


Figure 4-6 Current voltage measuring circuit.

The resistance had to be relatively high to limit the amount of current that would flow through the resistors. The PV current flowing from the LCB was measured by connecting a current resistor in series. This approach was not suitable to monitor and measure the current using LabVIEW. To increase the current signal to make it measureable by LabVIEW, a differential amplifier was used to amplify the voltage across the resistors to a suitable resolution. The PV power was not measured directly; instead, the PV module power was calculated as the product of the voltage and the current.

#### 4.1.6.2. Thermocouples

Thirty-two temperature measurements were made using T-type thermocouples, as shown in Figure (4-7). T-type thermocouples were preferred for their relative low cost and simplicity; they also do not require a current source and have a suitable temperature range for this experimental set-up. To record the temperature profile, 22 thermocouples were inserted in each tank in two probes located at two corners of the tank at 135 mm intervals from the top to the bottom. Twelve of the thermocouples were installed in a stainless steel probe, while the other ten were installed in a

copper probe. In addition, temperature measurements were recorded at the inlets and outlets of the PV and AC side-arm heaters, at each port in the manifold, mains supply water, and water delivery or hot water outlet. At the Renewable Energy Lab, accuracy tests were conducted on the T-type thermocouples used in the experimental set-up at both ice point and boiling point temperatures. The tests were within the specified accuracy range ($\pm 0.5$ ℃).

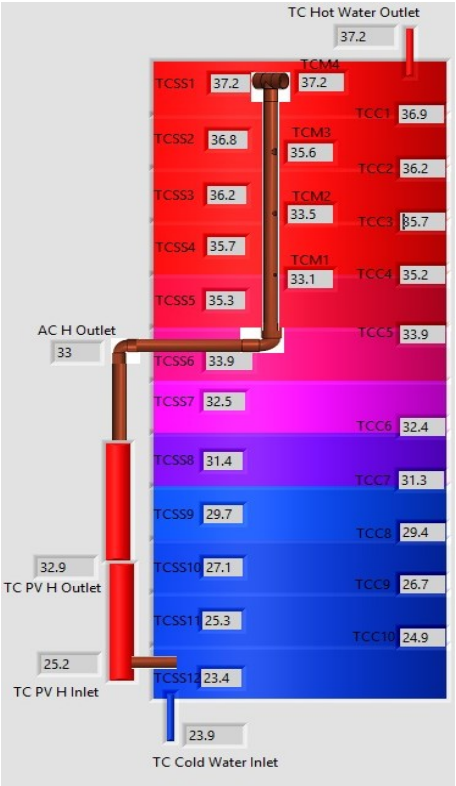


Figure 4-7 Solar storage tank showing location of the thermocouples.

#### 4.1.6.3. Data Acquisition System

All of the T-type thermocouples were connected to a National Instruments 16-channel thermocouple Compact DAQ module (NI9213). The voltage and current on both sides of the LCB were connected to a DAQ module (NI9209). All measurements were monitored and recorded every minute during the test. National Instrument's LabVIEW was used to interface the device to the computer. The VI program and block diagram can be seen in Figures (4-8) and (4-9).

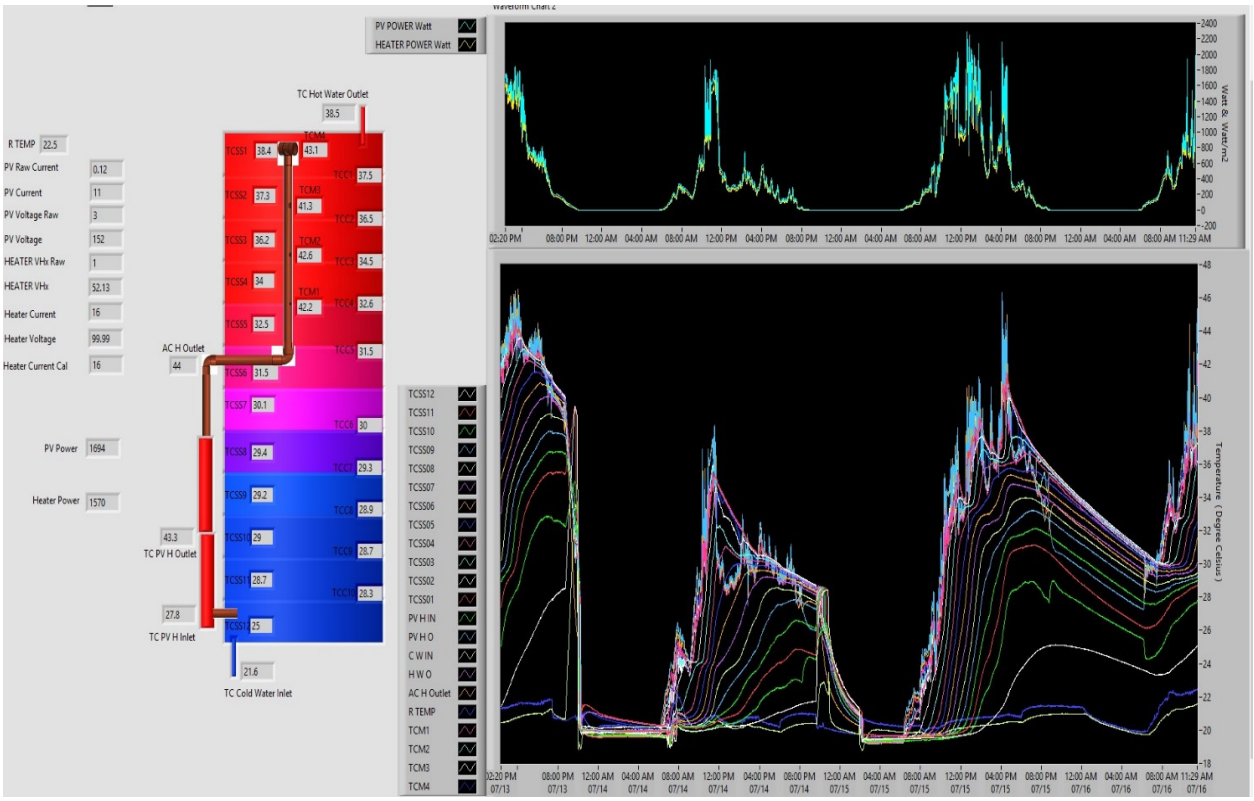


Figure 4-8 VI programs.

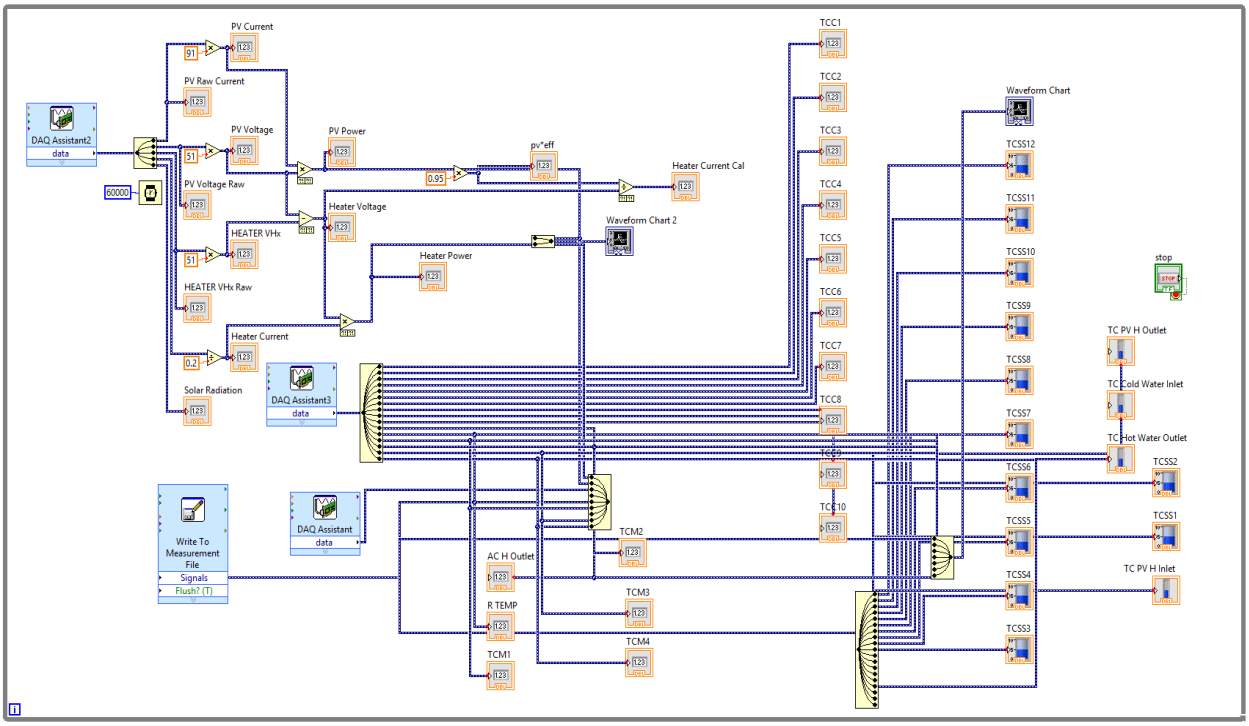


Figure 4-9 Block diagram.

## 4.2. Experimental Procedure

The experiments for this research were conducted at the Renewable Energy Laboratory at Dalhousie University. The experimental work was done to identify a side-arm heater, connected with various types of hot water distributor devices, that enhances thermal stratification in an SDHW system tank. To evaluate the thermal performance and stratification of this system, the following test procedure was used.

### 4.2.1. PV Variable Solar Power

The test of the side-arm heater with the manifolds was started under realistic conditions of cold and hot tank temperatures and under actual weather conditions in Halifax, Canada. The tests were conducted daily for eight hours during the months of June, July, August, September and October of 2018. The manifolds and conventional hot water distributors were installed and removed from a small manhole at the top of the domestic hot water tank. The test of the side-arm heater with the manifolds was started under practical and realistic cold and hot tank temperature conditions.

- Cold tank temperature test: Prior to starting the test, the SDHW tank were fully discharged, which took approximately 90 minutes. Then, before refilling the tanks, the mains supply water was discharged to the drain for approximately 15 to 25 minutes to drain the warm water inside the piping within the building and to get the actual mains water supply temperature. The tank took approximately 30 minutes to refill. Once filled with water, the SDHW tank and side-arm were drained for 5 minutes to remove any air bubbles which may prevent natural convection and cause inaccurate data in the experimental results. The cold water temperature ranged between 16 and 21˚C, depending on the time of year the experiment was conducted.

- Hot tank temperature test: Instead of discharging the hot water inside the storage tank, we used the hot water which had been heated on the day prior to the next experimental test.

All measurements were monitored and recorded in one-minute intervals during the test. National Instruments' LabVIEW created an Excel file for each experimental test for data analysis. In addition, temperature data, PV power was displayed on the computer's monitor screen to support the operator with fast instantaneous control. The assessment of the performance of the side-arm heater system with the hot water distributor devices was evaluated according to the measured temperature in different thermocouple positions in the SDHW tank recorded in the Excel sheet.

### 4.2.2. Flow Visualization

We obtained a flow visualization of hot water flow patterns inside the tank using the AC and PV heater elements during the dye injection. The power delivered to the AC electric heater was 1500 watts, which simulated PV solar power input on an average sunny day. The flow visualization experiments were intended to demonstrate that the manifold with four ports increases gradually from a small to a large diameter, which may eliminate the plume entrainment inside the storage tank and enhance stratification. The insulation was removed from half of one side of the Plexiglas tank in order to visualize the flow pattern. The following two tests procedure were conducted:

First, the storage tank was charged with cold water from the mains supply. We then switched on the AC electrical heater element until a steady heat added inside the manifold was established. A color dye was injected through the injection system, as shown in Figure (4-10), with the incoming hot water inside the manifold. The hot water flow pattern inside the tank was video recorded and analyzed when the ink started entering the tank.

Second, the storage tank initial average hot water temperature was 50˚C. We discharged 100 liters of hot water in order to simulate actual hot water consumption on a daily basis and replaced it with

cold water from the mains supply. After replacing 100 liters of hot water in the storage tank, we let it set for at least 15 minutes to reach quasi-equilibrium. Then, an AC electrical heating element was switched on until a steady temperature inside the manifold was established. A color dye was injected through the injection system with the incoming hot water inside the manifold. The hot water flow pattern inside the tank was video recorded and analyzed when the ink began to enter the storage tank.

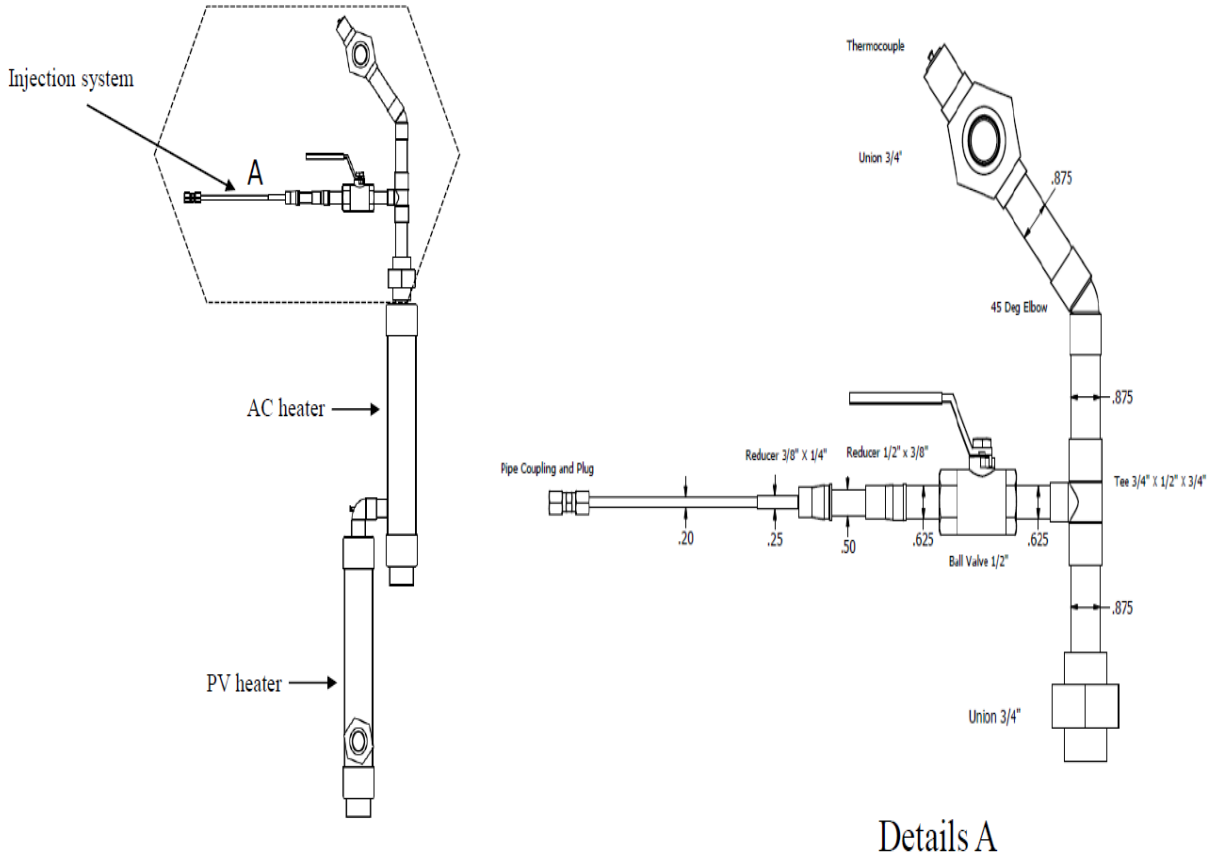


Figure 4-10 Side-arm heater connected with dye color injection system.

# Chapter 5: Theoretical Background

## Buoyancy Induced Flows

Buoyancy induced flow is achieved by a net hydrostatic pressure difference between the SDHW tank and side-arm PV and AC heater, causing a buoyancy force-driven flow [2, 46]. The static pressure is affected by the density, whereas the shear pressure is affected by the water flow rate and viscosity. The net hydrostatic pressure difference between the SDHW tank and side-arm PV and AC heater connected with the manifold, as shown in Figure (5-1) at the bottom of the SDHW tank, was calculated according to Eq. (5-1):

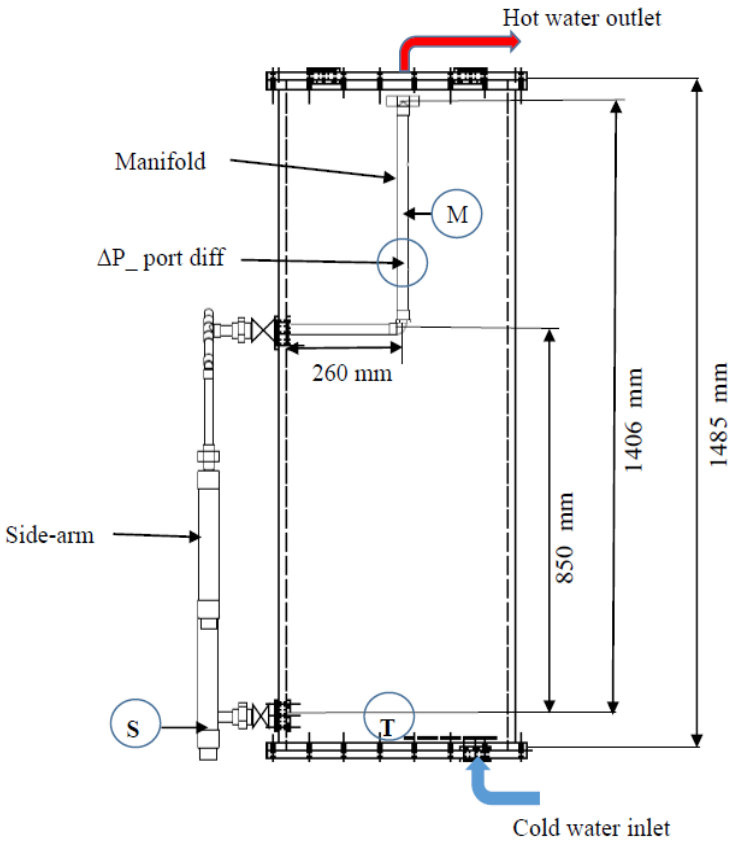


Figure 5-1 Pressure evaluating position in storage tank and side-arm heater connected with a manifold.

$$\Delta P_{\text{NET Hydrostatic}} = (\sum_{i=1}^{12} P_T) - P_S - P_M \qquad (5-1)$$

$$\Delta P_{\text{NET Hydrostatic}} = \sum_{i=1}^{12}(h_i\ \rho_i\ g)_{\text{Tank}} - (h\ \rho\ g)_{\text{PV Heater}} - (h\ \rho\ g)_{\text{AC Heater}} - (h\ \rho\ g)_{\text{Manifold}}$$

where:

$\Delta P \rightarrow$ the differential pressure at the bottom of the tank $(Pa)$.

$P_T \rightarrow$ pressure at the bottom of the tank $(Pa)$.

$P_S \rightarrow$ pressure at the bottom of the side-arm heater $(Pa)$.

$P_M \rightarrow$ pressure at the bottom of the manifold $(Pa)$.

$h_i \rightarrow$ thickness of the layer $(m)$.

$i \rightarrow$ number of the layer.

$g \rightarrow$ acceleration of gravity $\left(\frac{m}{s^2}\right)$.

$\rho \rightarrow$ density of the water inside the tank and the side-arm heater ($kg/m^3$).

For example, Figure (5-2) shows a net hydrostatic pressure difference between the SDHW tank and the side-arm PV and AC heater connected to the manifold during the low PV average power test and hot tank conditions. The average difference in the pressure from 9 a.m. to 6 p.m. was approximately 17 Pa.

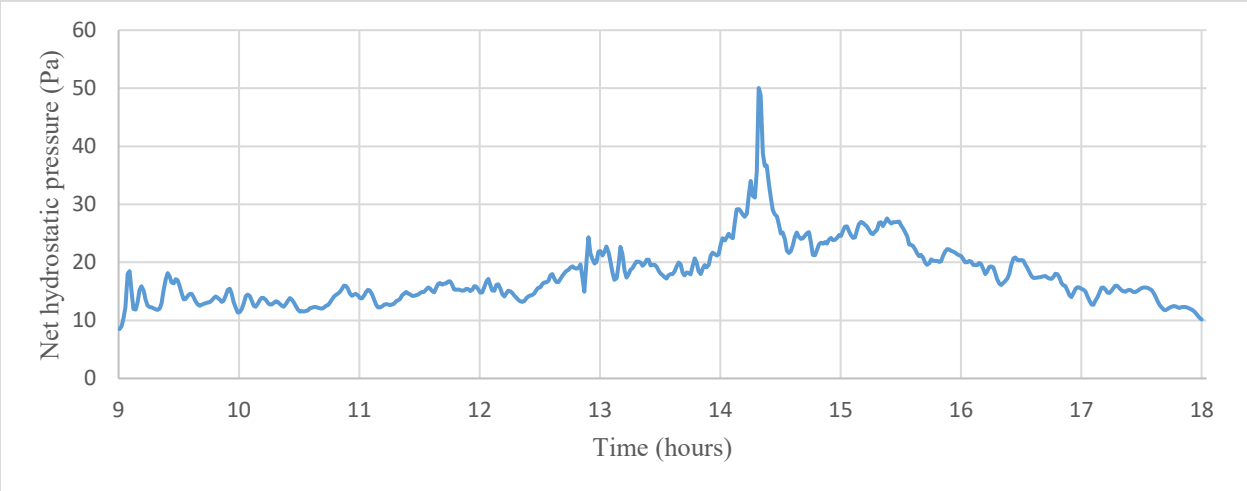


Figure 5-2 Net hydrostatic pressure difference using one-port hot water inlet device

For example, Figure (5-3), shows the PV heater power plots, and the inlet and outlet temperature from the PV heater during the low PV average power test and hot tank conditions from 9 a.m. to 6 p.m. on Sep 19th. The hot water flow rate responded similarly to the PV power heater, i.e., the higher the PV heater power to the side-arm heater element, the greater the hot water flow rate. The water flow rate passing through the side-arm heater was calculated by using Equation (5-5), and inlet and outlet temperature measurement from Figure (5-3), supposing that heat loss from the side-arm heater was insignificant. The average flow rate of hot water through the manifold during this test was 0.43 L/min (0.007 kg/sec).

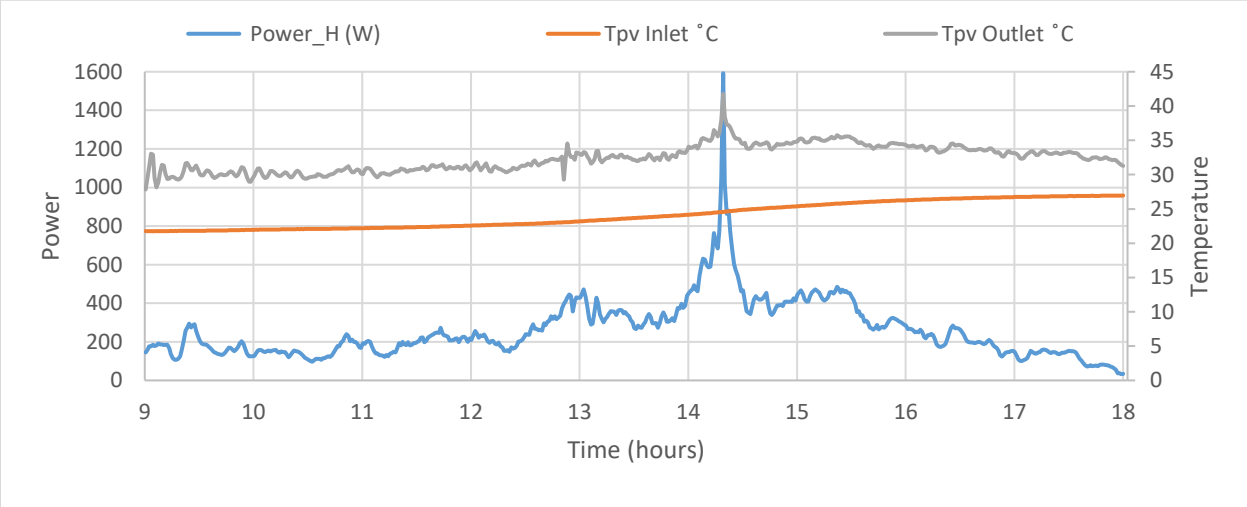


Figure 5-3 Heater power and side-arm PV heater inlet and outlet water temperature

**Losses in the Side-arm Heater, Pipes, and Fittings**:

Losses in fittings are dependent on the geometry-related loss coefficient, $K_L$, and the velocity of the fluid flow, $u_m$. The pressure drop at sudden expansion and contraction, entrance, valves, elbow, tee, and exit losses were calculated according to Eq. (5-2):

$$\Delta P = K_L \frac{\rho}{2} u_m^2 \qquad (5-2)$$

The shear pressure losses in the side-arm heater and inside the manifold were calculated using the Darcy-Weisbach equation for fully developed steady incompressible pipe flow, as expressed in Eq. (5-3):

$$\Delta P_{\text{Shear pressure}} = \int_{\text{Darcy}} \frac{L}{D}\ \rho\ \frac{{u_m}^2}{2} \qquad (5-3)$$

where $\int_{\text{Darcy}}$ indicates the Darcy friction factor, L refers to the length of the pipes, D represents the diameter of the pipes, and $u_m$ the hot water means velocity inside the pipes and side-arm heater. The Darcy $(\int_{\text{Darcy}})$ is a theoretical equation that predicts the frictional energy loss in a pipe based on the velocity of the fluid and the resistance due to friction [46].

The head loss, hL in the manifold was calculated using the Darcy friction factor for a fully developed steady incompressible pipe flow:

$$hL_{\text{Manifold}} = \int_{\text{Darcy}} \frac{L}{D}\ \frac{{u_m}^2}{2g}$$

The pressure drop inside the side-arm heater and pipes was calculated using Eq. (4-4), as follows:

$$\Delta P = hL\,.\,g.\,\rho \qquad (5-4)$$

The amount of heat transferred from the PV heater to the cold water passing through the side-arm heater is normally calculated by using Eq. (5-5), supposing that heat loss from the side-arm heater is insignificant:

$$q = \dot{m}_{\text{Side}_{\text{arm}}\text{Heater}}\ .\ Cp_{\text{PV}_{\text{Heater}}}.\ \Delta T_{\text{PV}_{\text{Heater}}} \qquad (5-5)$$

$q \rightarrow$ the rate of heat transfer $(W)$.

$\dot{m} \rightarrow$ the mass flowrate inside the side-arm heater $\left(\frac{kg}{s}\right)$.

$Cp \rightarrow$ water-specific heat inside the side-arm heater $\left(\frac{kJ}{kg.K}\right)$.

$\Delta T \rightarrow$ PV heater temperature difference(K).

The pressure drop in pipes is a function of the Reynolds number, and the flow of hot water inside the side-arm heater is considered laminar flow if the value of the Reynolds number is less than 2,300. Here, the hot water flow rate was calculated according to Equation (5-6). The Reynolds ranges inside the side-arm heater were from 1,000 to 2,000, which is considered laminar flow.

The Reynolds number is given by Eq. (5-6):

$$\text{Reynold\#}_{\text{Manifold}} = \frac{\text{Di}_{\text{Manifold}}\ \text{u}_{\text{m}_{\text{Manifold}}}}{\nu} \qquad (5-6)$$

The mean velocity inside the side-arm heater and manifold is calculated by using Eq. (5-7):

$$\text{u}_{\text{m}_{\text{Heater}}} = \frac{\dot{\text{m}}_{\text{Side}_{\text{arm}}\text{Heater}}}{\rho_{\text{PV\_Heater}}(\text{Ac}_{\text{Heater}} - \text{Ac}_{\text{Dht}})} \qquad (5-7)$$

where $\text{D}_{\text{ht}} \rightarrow$ element heater outer diameter ( m ).

$$\text{u}_{\text{m}_{\text{Manifold}}} = \frac{\dot{\text{m}}_{\text{Side}_{\text{arm}}\text{Manifold}}}{\rho_{\text{PV}_{\text{Manifold}}}\ \text{A}_{\text{Pipe}}} \qquad (5-8)$$

$$\text{Frication Factor}\int_{\text{Darcy}} = \frac{64}{\text{Reynold\#}_{\text{Manifold}}} \qquad (5-9)$$

The differential pressure as shown in Figure (4-2), was calculated using Eq. (5-10), as follows:

$$\Delta\text{P}_{\text{Port Differential Pressure}} = \Delta\text{P}_{\text{NET Hydrostatic Pressure}} - \Delta\text{P}_{\text{Pressuer Losses}} \qquad (5-10)$$

$$\Delta\text{P}_{\text{Port Differential}} = \text{K}_{\text{L}}\frac{\rho\,.\,\text{u}^2}{2} = \text{K}_{\text{L}}\frac{\dot{\text{m}}_{\text{w}}{}^2}{2\,\rho\left(\pi\,\frac{\text{D}^2}{4}\right)^2} \qquad (5-11)$$

$\dot{\text{m}}_w \rightarrow$ the heated water flow rate inside the side-arm heater (kg/s).

$\text{K}_{\text{L}} = 1$

For example, the difference between the hydrostatic pressure and pressure losses when using a one port manifold during the low PV average power test and hot tank conditions were calculated using equation (5-10),and (5-11).As seen in Figure (5-4) the average port differential pressure from 9 a.m. to 6 p.m. during this test was approximately 5 Pa.

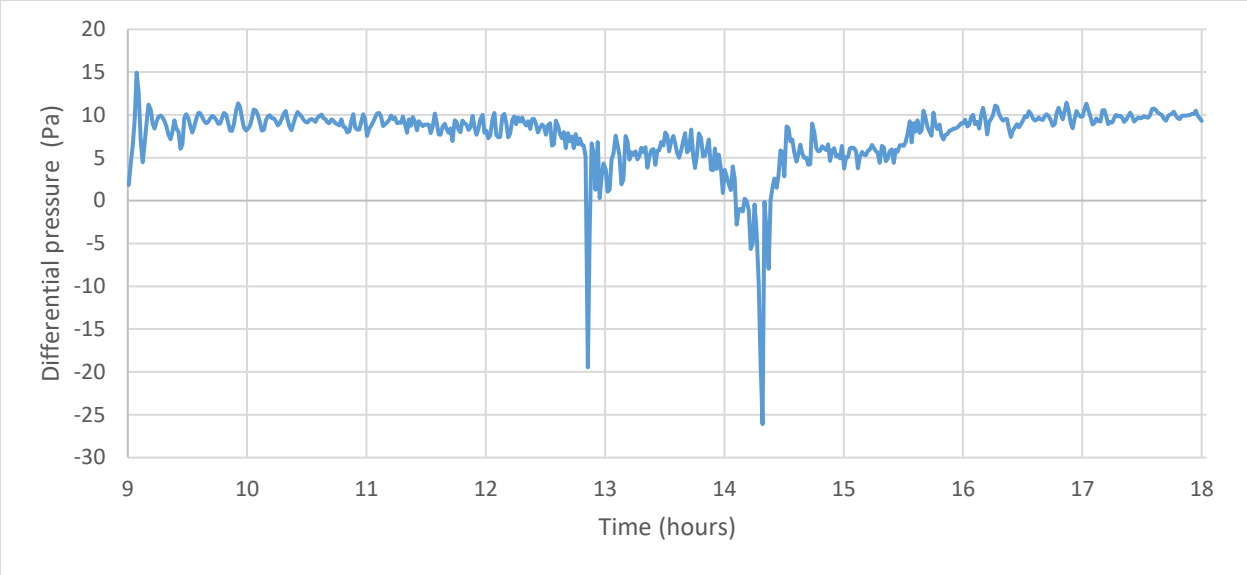


Figure 5-4 Differential pressure using one-port hot water inlet device.

The supply of hot water from the side-arm heater rose or fell in the four-port manifold, maintaining a pressure difference with the surrounding hot water in the tank until it reached the level at which the water density matched that of the surrounding water. At this point, the water flowed into the tank. Because the four-port manifold increases gradually from a small to a large diameter at the top the inflow and outflow through the ports could be avoided until the level was reached at which the density of the two fluids matched.

Based on the experimental data from a one port manifold as shown in table (5-1), a set of equations was used to calculate the lower port diameter to improve stratification and to prevent cold water being sucked from the lower ports of the manifold at the middle of tank. This cold water would have mixed with hot water delivered from the side-arm heater inside the manifold, which would lead to decreases in the quality of the hot water at the top of the tank and a pressure differential between the tank and the sidearm.

According to Alsagheer [2] the design guidelines for manifolds for a SDHW system are as follows:

- Calculate the average density of the water in the storage tank by measuring temperature at each of the twelve layers.
- Calculate the average density of the hot water inside the side-arm heater and the manifold by measuring temperature of the water at the inlet and outlet of the side-arm heater, and at the top of the one port manifold.
- Calculate the water flow rate passing through the side-arm heater by using Equation (5-5), supposing that heat loss from the side-arm heater is insignificant.
- Calculate the pressure drop through the side-arm heater, manifold, and pipe fitting by using equations (5-2) and (5-3).
- Calculate the net hydrostatic pressure, and the pressure difference between the hot water inside the side-arm heater connected with the manifold and the cold water in the storage tank using Equations (5-1) and (5-10).
- The number of ports in the manifold and the length of the manifold depends on tank dimensions and the required volume of the hot water in each layer.
- Calculate the lower port diameter required to prevent cold water from being sucked from the tank to the manifold using Equation (5-11).

Table (5-1) shows some examples of the data used to calculate the lower ports diameter during variable PV power under cold tank and hot tank conditions. In addition, the table shows the side-arm heater PV inlet and outlet temperature, the PV power, the tank average temperature, and the manifold outlet temperature. The calculations of lower port diameters, and the pressure differential

between the manifold and the tank were determined according to the difference in densities. As shown in table (5-1) the diameters of the lower ports were calculated for all tests based on the above parameters. The hot water flow rate inside the side-arm heater was in the range of 0.3 – 1.3 L/min, and the available pressure to drive the flow through the hole in the manifold was in the range of 0.9 Pa to 16 Pa. Using the differential pressure results in equation (5-11), the required lower port diameter was in the range of 6.5 mm to 22 mm. This result explains why lower port diameter of the four-port manifold in our design is 6.35 mm to prevent cold water suck from the lower ports of the manifold at the middle of tank. Anything smaller than 6.35 mm may cause too much flow resistance and then the water cannot leave the manifold at the prober level.

Table 5-1 Calculations of Lower Port Diameters to Prevent Cold Water from Being Sucked.

| PV Power | Side- arm PV heater Temperature | | Tank Conditions | Manifold Temperature | Tank Average Temperature | Water flow rate | Total Loss | Net Hydrostratic pressure | Differential pressure | Lower Port diameter |
|---|---|---|---|---|---|---|---|---|---|---|
| | inlet | outlet | | outlet | | | | | | |
| watt | ˚C | ˚C | | ˚C | ˚C | LPM | Pa | Pa | Pa | mm |
| 240 | 22 | 34 | Hot | 34 | 32 | 0.3 | 3.2 | 14 | 10.9 | 6.5 |
| 235 | 43 | 56 | Hot | 55 | 54 | 0.3 | 2.7 | 12 | 9.3 | 6.5 |
| 549 | 20 | 34 | Cold | 30 | 26 | 0.6 | 11.7 | 28 | 16 | 8.1 |
| 329 | 15 | 21 | Cold | 21 | 15 | 0.7 | 20.1 | 24 | 3.7 | 13.5 |
| 396 | 43 | 56 | Hot | 57 | 54 | 0.5 | 7.8 | 19 | 11.2 | 8.1 |
| 902 | 29 | 42 | Hot | 42 | 36 | 1.0 | 34.3 | 35 | 0.9 | 22.2 |
| 1449 | 20 | 38 | Cold | 30 | 22 | 1.2 | 49.7 | 51 | 1.2 | 22.3 |
| 1384 | 26 | 44 | Hot | 44 | 35 | 1.1 | 45.7 | 48 | 2.7 | 18.0 |
| 1938 | 15 | 37 | Cold | 36 | 20 | 1.3 | 63.0 | 66 | 3.4 | 18.3 |
| 1661 | 32 | 52 | Hot | 52 | 43 | 1.2 | 53.7 | 56 | 2.7 | 18.6 |

## 5.1. Thermal Performance

The stratification of a solar domestic hot water tank using a side-arm PV heater was evaluated by calculating the thermal performance of a storage tank in terms of storage stratification. The tests were conducted on a nominal outer diameter 22.22 mm (3/4 in) copper tube with one port at the top of the tank, a 22.2 to 40.9 mm (3/4 in to 1.5 in) diameter diffuser, and a nominal outer diameter 22.22 mm (3/4 in) copper tube with four ports increasing gradually from a small dimeter to a large one. The objectives of these experimental works were to operate each hot water inlet devices connected with the side-arm heater under variable input power and to evaluate them under actual conditions in Halifax, Nova Scotia, Canada, in order to identify a side-arm heater with a hot water inlet device that enhances thermal stratification. The designed hot water inlet devices are shown in Figure (5-5).

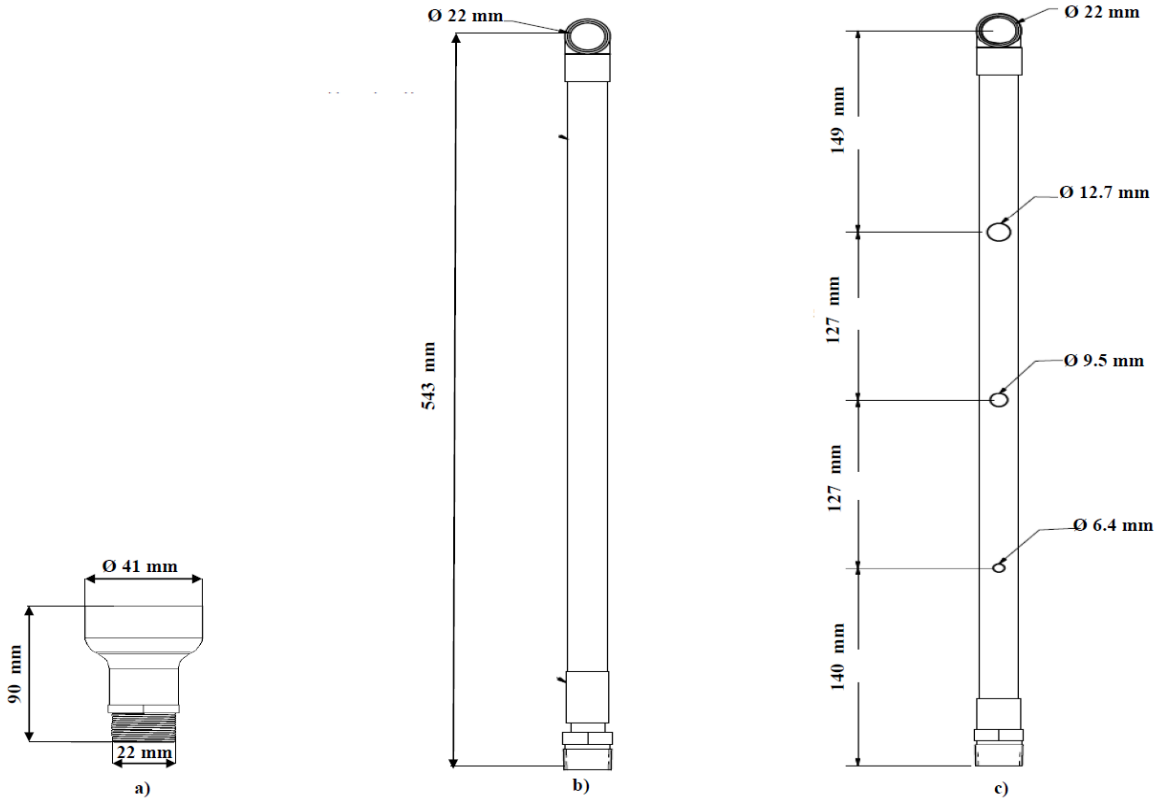


Figure 5-5 Hot water devices configurations: a) diffuser, b) one-port tube, c) four-port manifold.

The weather conditions in Halifax during the testing period were classified into three categories:

1. Mostly cloudy and raining day (low average PV heater power "< 500 W").
2. Partly cloudy day (medium average PV heater power "500-900 W").
3. Mostly sunny day (high average PV heater power "> 900 W").

The tests of the side-arm heater with various hot water inlet devices were undertaken with cold and hot tank temperatures. In cold tank conditions, the water from the storage tank was drained prior to the test and the tank refilled with the mains water supply. The experimental tests were conducted from June to October 2018. Throughout this time, the mains water supply temperatures changed from 16 to 21˚C. The difference between the water temperature at the top and the bottom of the storage tank before starting the test was in the range 1-3˚C. The hot tank conditions are due to the water in the storage tank being heated on the day prior to the new test. The average hot water temperature in the storage tank before starting the test was in the range of 28-36˚C.

### 5.1.1. Evaluation of Hot Water Inlet Device Performance

The assessment of the performance of the side-arm heater system with the three hot water inlet devices was based on the evaluation of the availability and the entropy of the experimental SDHW tank with the availability and the entropy of a fully mixed and perfectly stratified SDHW tank. The exergy or availability of the experimental tank was evaluated according to the position of the thermocouples in the SDHW tank, as shown in Figure (5-6). The most efficient side-arm heater with inlet hot water device is the one resulting in higher availability, energy delivery, merit factor, and high degree of stratification. Furthermore, the tank should have lower entropy ratios and internal entropy generation [2].

There are three main ways to evaluate the thermal stratification of thermal energy storages: those based on the general dimensionless numbers of heat transfer and fluid dynamics, those based on

the first law of thermodynamics, and those based on the second law of thermodynamics. Rosen and Hooper (1992) have shown that if only the first law of thermodynamics is used, it is not possible to distinguish a stratified tank from a mixed tank [39]. The combination of energy, exergy and stratification efficiency makes an excellent tool for the design and analysis of a hot water storage system. In this research, exergy analysis was used to evaluate the findings. Thermal stratification doesn't care whether the source of heat from a PV or a wall outlet.

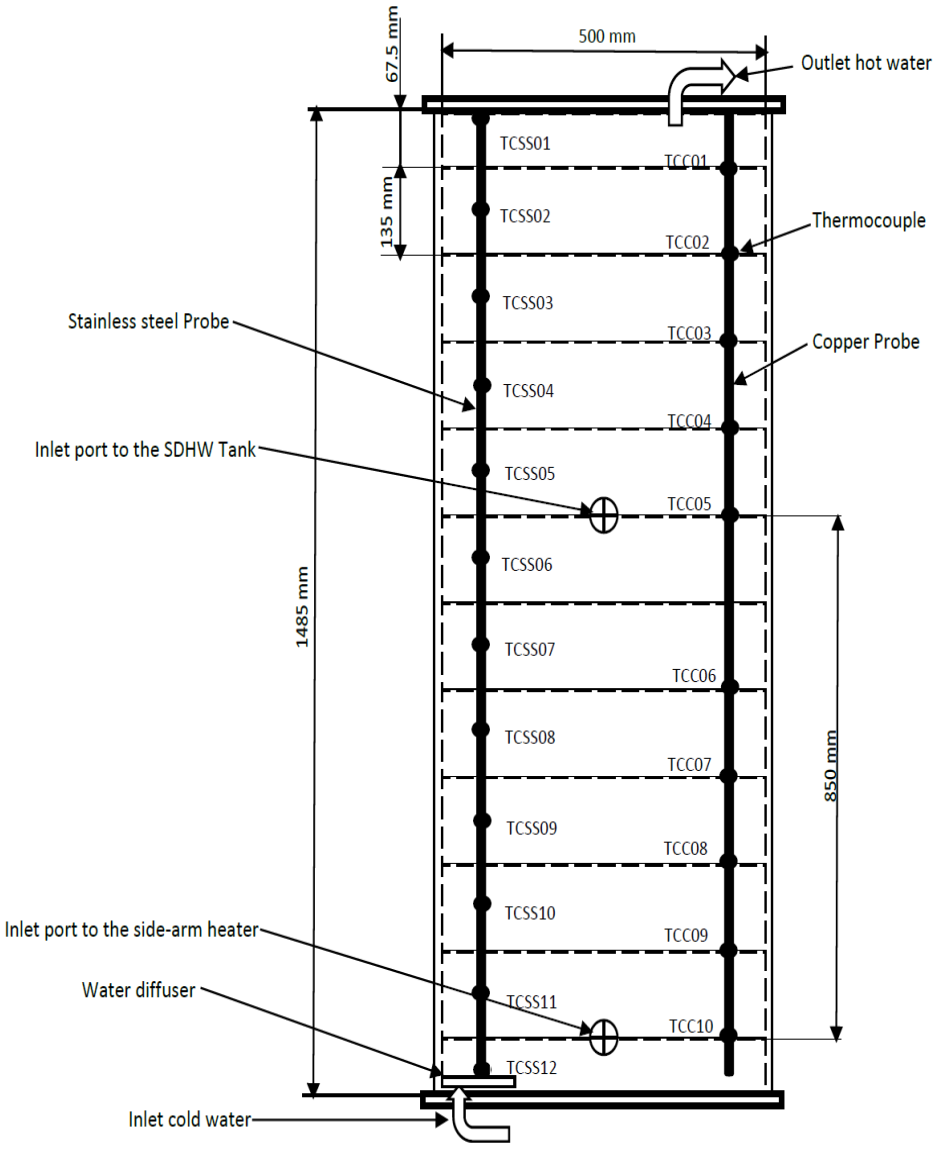


Figure 5-6 Diagram showing Plexiglas tank and location of thermocouple inside the tank

**Degree of Stratification (DOS)**

The DOS approach is one of the assessment methods that is used to evaluate the stratification within the tank. Sliwinski [44] defined DOS as the change in temperature between layers with regards to the change of the height between layers in the storage tank. The DOS calculated according to Equation (5-12). A more efficient way of comparing the two tested strategies is by looking at the difference between the slopes of the lines in the thermocline region of the elevation curves.

$$\mathrm{DOS} = \sum_{i=1}^{12} \frac{\Delta T}{\Delta H} \qquad (5-12)$$

Where

$\Delta T$ → change in temperature between layer (˚C).

$\Delta H$ → change of the height (m).

i → number of the layer.

To calculate the degree of stratification in the SDHW tank, the rate of change in temperature per the change in the difference between the layers was determined for all levels. As no precise rules could be found regarding the exact gradient to use for a stratified tank, 5°C/m was chosen as the cut-off measure. Thus, any DOS of less than 5°C/m between two layers was not considered during the evaluation. The sum of DOS of all layers was then taken for each period. The Larger the number of the sum, the higher the quality of stratification [44]. The average value of DOS was determined using only those values that were greater than 1/10 of the maximum DOS for each period [45].

For more clarification as shown in Figure (5-7) there are three main factors which affect the thermal performance parameter. First, in considering the degree of stratification or temperature

differences between layers inside a storage tank, the degree of stratification is directly proportional to the availability and inversely proportional to the entropy. The second factor which affects the thermal performance parameter is that the dead state temperature is inversely proportional to the availability and directly proportional to the entropy. The third factor is that the tank average temperature is directly proportional to the availability and inversely proportional to the entropy. The effect of temperature difference between layers, dead state temperature, and tank average temperature is shown in Figure (5-7).

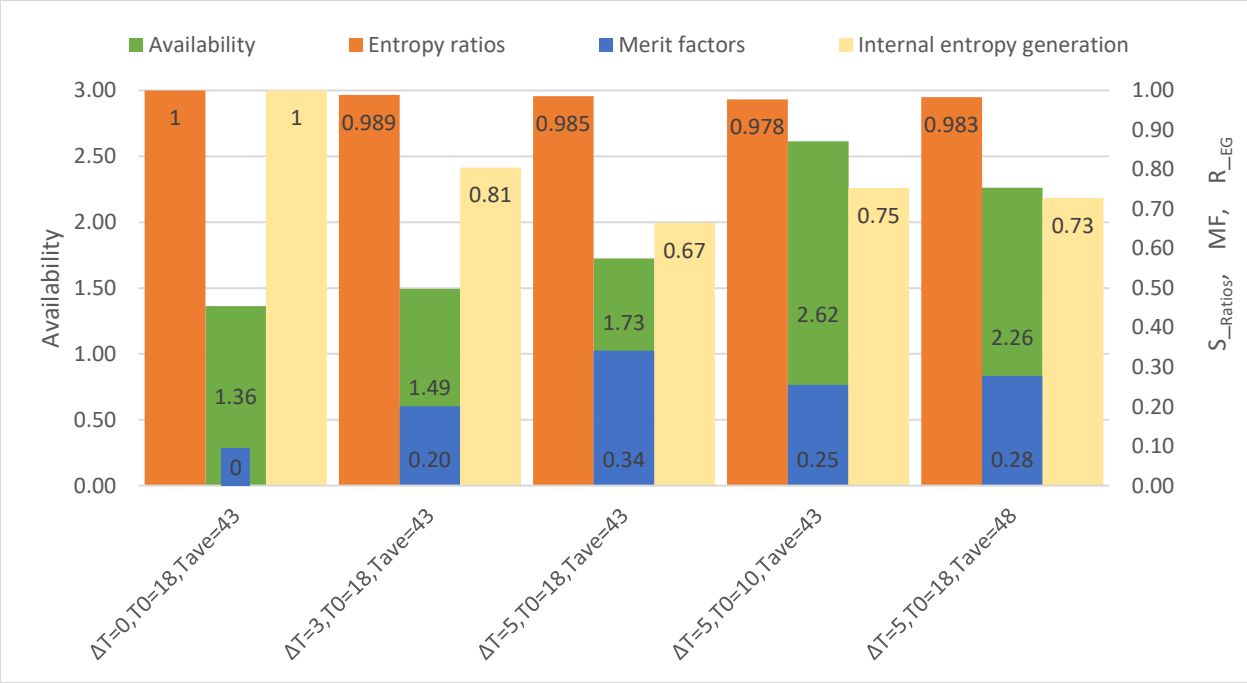


Figure 5-7 Effect of temperature difference, dead state, and tank average temperature.

For example, to simulate the experimental tank the availability, merit factor, entropy ratios, and internal entropy generation were assessed in a commercially available solar domestic hot water tank with a volume of 270 L as shown in Figure (5-7). The tank was divided into ten layers. To simulate the performance of SDHW Tank the following parameters were used: as the difference of degree of stratification 0, 3 and 5, dead state temperatures of 10 and 18°C, and average tank

temperatures of 43 and 48°C. We evaluate the experimental SDHW Tank based on the comparison of its availability and the entropy with those of a fully mixed and a perfectly stratified SDHW tank.

As shown in Figure (5-7), if the degree of stratification between layers increases from 0 to 5 the availability will increase from 1.36 to 1.73 MJ, and the merit factors will increase from 0 to 0.34. On the other hand, the entropy ratios will decrease from 1-0.985 and the internal entropy generation will decrease from 1-0.67. If the dead state temperature increases from 10 to 18°C the availability will decrease from 2.62-1.73 MJ, and internal entropy generation will decrease from 0.75- 0.67. However, the entropy ratios will increase from 0.987-0.985, and the merit factors will increase from 0.25 to 0.34. If the average tank temperature increases from 43 to 48°C the availability will increase from 1.73-2.26 MJ, and the internal entropy generation increases from 0.67-0.73. On the other hand, the merit factor decreases from 0.34-0.28 and entropy ratios decreases from 0.985-0.983.

In short, it is clear from Figure (5-7) that the changing of DOS, using availability, entropy, merit factor, and internal entropy generation parameters assessment were giving results in the same behavior. However, the changing of dead state temperature, and average tank temperature using, the internal entropy generation parameters were producing infrequent results.

**Availability**

Availability is a thermodynamic quantity that represents the maximum reversible work that can be obtained from a closed system when it comes into equilibrium with a reference state [32]. If we allow the cold water to mix with the hot water in the storage tank, this will lead to a decrease in the availability and ultimately in a decrease in the delivery of hot water temperature to consumers. The availability was calculated using Eq. (5-13).

$$A = \sum_{i=1}^{n} m_i[(h_i - h_o) - T_o(s_i - s_o)] \qquad (5-13)$$

where:

A: Availability of energy in the tank (MJ).

m: Mass of water, kg.

$i$: Layer number.

$h_i$: Enthalpy of the layer, kJ/kg.

$h_0$: Enthalpy evaluated at environmental temperature, kJ/kg.

$T_0$: Environmental temperature, K.

$s_i$: Entropy of the layer, kJ/kg ·K.

$s_0$: Entropy evaluated at environmental temperature, kJ/kg ·K.

According to Hermansson [20], selection of the environmental temperature or dead state temperature is a critical parameter for a good evaluation, because without reasonable grounds, this parameter may give wrong evaluations. Several researchers [2, 34, and 37] have discussed the choice of the dead state temperature. In the present research, the dead state temperature represents the state in which energy is not valuable to the user of the SDHW system. For an SDHW system, the dead state temperature should be the mains water supply temperature or the temperature at the bottom of the SDHW tank for cold tank conditions.

The mains water supply temperature was selected as the dead state temperature because if the water temperature is equal to the main water supply temperature, there is no useful energy for the SDHW system user.

**Process to Evaluate the Thermal Performance of Hot Water Inlet Devices**

In assessing the level of stratification, we can compare the experimental tank to a theoretical tank with ideal stratification. Shah and Furbo [41] presented the concept of an ideal stratified tank in their study. In this work, the perfectly stratified tank consists of two isothermal volume regions, as shown in Figure (5-8). The bottom zone was set at the environmental temperature, which is the mains water supply temperature, while the top zone was set at the maximum temperature at the top of the experimental tank at the end of the test [41]. We assumed that the bottom part of the perfectly stratified storage tank had the dead state temperature to evaluate the designed hot water inlet devices. Based on this assumption, we calculated the thermal performance, availability and entropy of each designed manifold as the end of each test.

The heat addition to the tank, $Q_{Added}$, was calculated with respect to the energy contained in the tank both at the beginning of the experimental test and at the end. It was determined using Eq. (5-14), as follows:

$$Q_{Added} = Q_{End} - Q_{Start} \qquad (5-14)$$

$Q_{Start}$ : Heat stored at the beginning of the test, MJ.

$Q_{End}$ : Heat stored at the end of the test, MJ.

$$Q = m_{water}\, C_{P_{ave}}\, T_{Tank\,ave} \qquad (5-15)$$

The mass of hot water in the perfectly stratified tank was calculated according to Eq. (5-16): the energy content of the perfect tank and the experimental tank was based on mains water temperature.

$$Energy_{perfect} = Energy_{Experimental}$$

$$m_{Top}\, C_{P\_Top}\,(T_{Top} - T_0) + m_{Bottom}\, C_{P\_Bottom}\,(T_{Bottom} - T_0) = m_{tank}\, C_{P\_ave}(T_{ave} - T_0) \qquad (5-16)$$

According to Shah and Furbo [41]: $T_{Bottom} = T_0$

$$m_{Hot\,water} = \frac{m_{tank}\, C_{P\_ave}(T_{ave} - T_0)}{(C_{P_{Top}}.\, T_{Top} - C_{P_0}.\, T_0)}$$

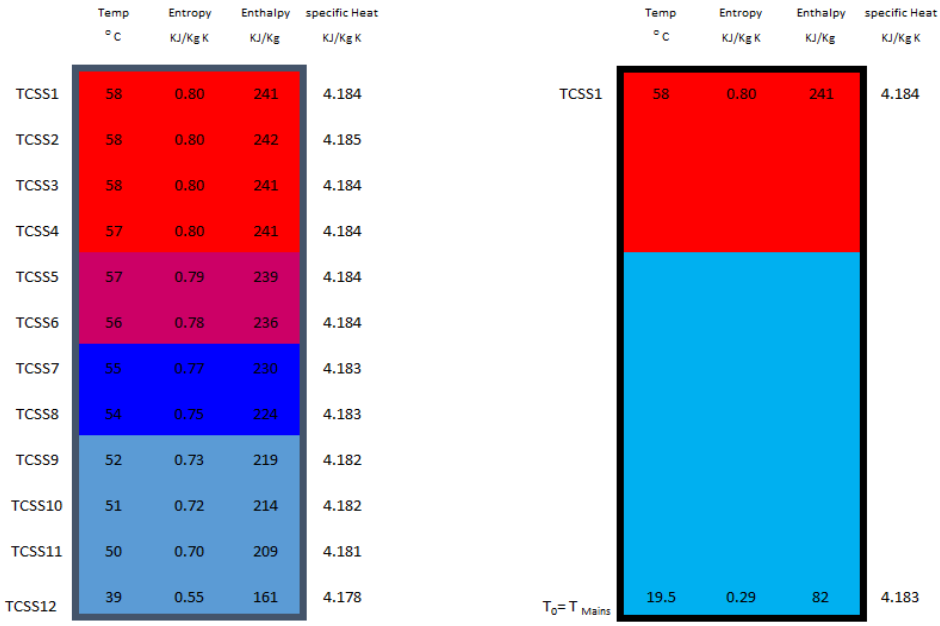


Figure 5-8 Solar domestic hot water tank configurations: a) experimental tank, b) perfect tank.

Perfect availability at both the top and bottom of the tank was calculated based on the ideal mass of hot water equation, which considered the initial energy, the dead state properties, and the top layer properties of the final actual tank. Equation (5-17) was used to calculate perfect availability, as follows:

$$A_{\text{Perfect tank}} = ([\{h_{B\,Z} - h_o\} - T_o\{s_{BZ} - s_o\}]m_{C\,w} + [\{h_{T\,Z} - h_o\} - T_o\{s_{TZ} - s_o\}]m_{H\,w}) \qquad (5-17)$$

The availability of the fully mixed tank was calculated using the average temperature of the actual tank. The availability of the actual tank was then calculated using the temperature of each thermal layer.

$$A_{\text{Mixed tank}} = m_{\text{Total}}[(h_{\text{ave}} - h_o) - T_o(s_{\text{ave}} - s_o)]$$

**Availability Ratios**

Alsagheer [2] evaluated the most efficient hot water inlet device is the one which has the highest average availability ratio. Hence, the availability ratios were calculated according to Eq. (5-18):

$$A_{\text{Ratio}} = \frac{A_{\text{Final Actual}} - A_{\text{Int}}}{Q_{\text{ADDED}}} \qquad (5-18)$$

**Entropy**

The entropy of the fully mixed tank was calculated using the average temperature of the actual tank, and the entropy of the actual tank was calculated using the temperature of each thermal layer. The perfectly stratified tank consists of two isothermal volume regions, which is the same as the availability calculation principle. At the end of the test, the bottom zone was set at the environmental temperature (i.e., the mains water supply temperature), while the top zone was set at the maximum temperature at the top of experimental tank. The total entropy of the perfect SDHW tank was the entropy of the perfect of top zone plus the entropy of the perfect bottom zone. The perfect entropy was calculated according to Eq. (5-19), as follows:

$$S_{\text{stratified tank}} = S_{B\,Z}\,\text{mass}_{C\,W} + S_{T\,Z}\,\text{mass}_{H\,W} \qquad (5-19)$$

- Merit factors

Alsagheer [2] evaluated the merit factors of the solar storage tank by using a dimensionless relationship as shown in equation (5-20). This basic approach was used to calculate the difference in the entropy of the perfect tank and the entropy of the experimental tank. The result is then divided by the difference of the entropy of a perfect tank and the fully mixed tank. Hence, when the entropy of the experimental tank equals the entropy of the perfect tank the merit factor will be highest.

$$\text{Merit Factor} = 1 - \frac{S_{\text{PER}} - S_{\text{FINAL ACTUAL}}}{S_{\text{PER}} - S_{\text{MIXED}}} \qquad (5-20)$$

- Entropy Ratios (S)

Shah and Furbo [41] evaluated the solar storage tank stratification according to equation (5-21), which is the entropy difference between the entropy of dead state temperature and the perfect stratified tank divided by the entropy difference of the entropy of dead state temperature and the actual tank.

$$\text{Entropy ratios} = \frac{S_0 - S_{\text{perfect}}}{S_0 - S_{\text{Exper}}} \qquad (5-21)$$

- Internal Entropy Generation "$R_{EG}$"

A comparison between the thermal performances of the manifolds in terms of internal entropy generation ratios was conducted using the entropy ratios. The internal entropy generation ratios were defined by Panthalookaran et al. [35], who calculated the difference in the entropy change of the experimental tank to the entropy change of the ideal stratified tank, and then divided the result by the difference of the entropy change of a fully mixed tank and the ideal stratified tank. To calculate this ratio, the difference of the entropy change of the mixed tank should be larger than the entropy of the experimental tank, and the entropy of the experimental tank must be larger than the ideal stratified tank. The internal entropy generation was calculated according to Eq. (5-22):

$$\mathrm{R_{EG}} = \frac{(\Delta \mathrm{S_{EXP}} - \Delta \mathrm{S_{ideal\ str}})}{(\Delta \mathrm{S_{Mix}} - \Delta \mathrm{S_{ideal\ str}})} \qquad (5-22)$$

The entropy difference was calculated according to Eq. (5-23):

$$\Delta \mathrm{S_{Perf}} = \left(\mathrm{Cp_{12}}\ \ln\frac{\mathrm{T_{12}}}{\mathrm{T_0}}\right)\mathrm{Mass_{B\,Z}} + \left(\mathrm{Cp_1}\ \ln\frac{\mathrm{T_1}}{\mathrm{T_0}}\right)\mathrm{Mass_{T\,Z}} \qquad (5-23)$$

The most efficient hot water inlet device is the one which has the lowest entropy ratio and lowest internal entropy generation. In general, the perfectly stratified tank has higher availability and lower entropy than the actual tank. Hence, the most effective hot water inlet device should have a higher average of availability ratios and a lower internal entropy generation ratio than the other devices.

**Delivery Energy**

The first basis for comparing the three different system configurations was on delivered energy. The ideal system configuration would exhibit the largest amount of delivered energy, as this would reduce the amount of auxiliary energy input required to meet the set-point temperature [9]. Cruickshank evaluated the delivery energy according to Eq. (5-24), as follows:

$$\text{Delivery energy} = m_i \left[ \sum_{i=1}^{3} Cp_i T_i - 3Cp_0 T_0 \right] \qquad (5-24)$$

where:

m: Mass of water, kg. $i$: Layer number, $i \rightarrow$ number of the layer, $Cp_{water} \rightarrow$ specific heat of the water (kJ/kg.K), $T_i \rightarrow$ temperature of the top three layers at which the water is delivered (˚C ), $T_0$ dead state temperature ( ˚C )

To make a good evaluation a normalization was performed. Normalization is to bring all the PV power values, dead state temperatures for a cold tank, and average tank temperatures for hot tank conditions to an equal level for comparison. For example, as shown in the table (5-1) the energy delivery experimental results for the 1.5-inch diffuser, four-port manifold and one-port tube during the high PV average power and cold tank conditions were 9.02, 9.48 and 10.13 MJ, respectively. The sequences as shown in the table; first step is to normalize average PV power, and the second step is to normalize the dead state temperature. The normalization final results for the 1.5-inch diffuser, four-port manifold and one-port tube were 9.3, 11.8 and 9.4 MJ, respectively.

Table 5-2 Normalization of energy delivery for the three hot water inlet devices under high PV power and cold tank condition

| | 1.5 in Diffuser | Four-port | One-port |
|---|---|---|---|
| Energy delivery Experimental value (MJ) | 9.02 | 9.48 | 10.13 |
| PV average power (W) | 1079 | 1115 | 1206 |
| 1ST step normalize average PV power | $9.02 * \frac{1115}{1079} = 9.3$ | $9.48 * \frac{1115}{1115} = 9.48$ | $10.13 * \frac{1115}{1206} = 9.36$ |
| Dead state temperature (˚C ) | 20 | 16 | 20 |
| 2nd step normalize dead state temperature | $9.3 * \frac{20}{20} = 9.3$ | $9.48 * \frac{20}{16} = 11.85$ | $9.36 * \frac{20}{20} = 9.36$ |
| Energy delivery normalization results (MJ) | 9.3 | 11.8 | 9.4 |

All thermodynamics properties such as density, entropy, specific heat and enthalpy were calculated by using the regression equations, as shown in Appendix B.

# Chapter 6: Results and Discussion

In this chapter, the experimental results from the variable PV power tests are presented, analyzed and discussed. The output data from the LabVIEW data acquisition were analyzed using a Microsoft Excel worksheet. The experimental results have been organized into graphs and bar charts for discussion and comparison. The evaluation of the performance of the manifolds was based on the assessment of flow visualization, temperature distributions inside the storage tank, degree of stratification (DOS), availability, availability ratio, energy delivery, entropy ratio, merit factor and internal entropy generation. The most effective hot water inlet device is deemed to be the one that has a high DOS, availability change, merit factor, energy delivery, and average availability ratios. Furthermore, the most effective inlet should have a low entropy ratio and a low internal entropy generation.

Sixty-two experiments were executed on the side-arm PV water heater with the three types of hot water inlet devices. Most of the experiments were performed from sunrise to sunset. However, the comparisons among the chosen experiments were performed between 9 a.m. and 6 p.m. The time from sunrise to 9 a.m. and the time from 6 p.m. to sunset was not included in the comparison because we did not see any hot water flow rate from the bottom of the tank to the top of the tank during those time periods. Moreover, the heater power was typically less than 100 watts during those times.

As a sample of the experimental results, the graphs and tables in this section of the discussion are chosen from a low average PV heater power for cold and hot tank conditions, while the other graphs are chosen from medium and high average power, as shown in Appendix A.

## 6.1. Cold Tank Condition Tests

### 6.1.1. Power and Hot Water Flow Rate

Figure (6-1) shows the PV heater power plots from 9 a.m. to 6 p.m. during the low average heat power tests and cold tank conditions on June 25th, October 2nd, and August 22nd. In these tests, a 1.5-inch diffuser, four-port manifold and one-port copper tube are used. The PV average heater power for the 1.5-inch diffuser, four-port manifold and one-port tube were 199, 240 and 272 watts, respectively. The experiment showed readings of highly variable PV power heater caused by light clouds or by a high-rise building which obstructed the sun. The solar PV power readings also experienced sudden drops due to the sun passing by the high-rise building as shown in Figure (6-1a) from 16 to 17:20. These effects are not expected to have any significant changes on the results.

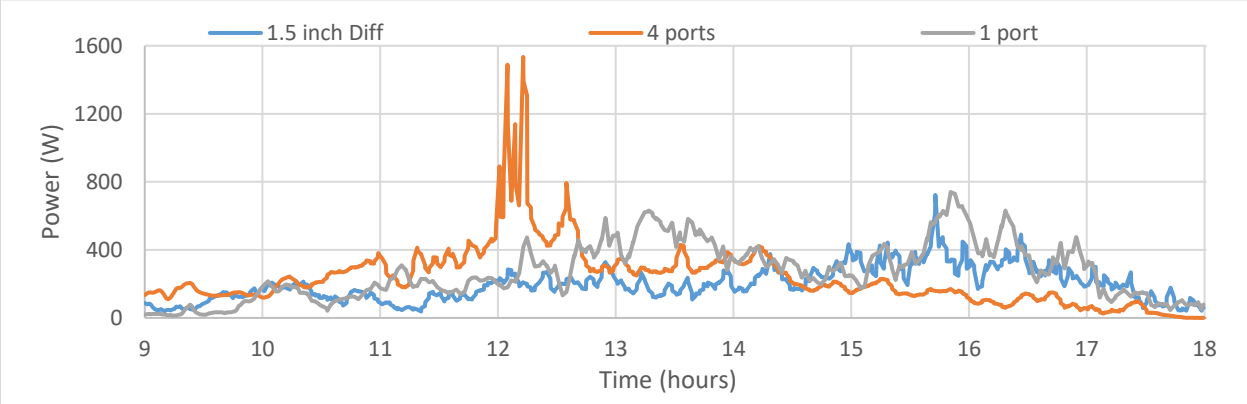


Figure (6-1) Low PV power heater during three hot water inlet device tests for cold tank conditions.

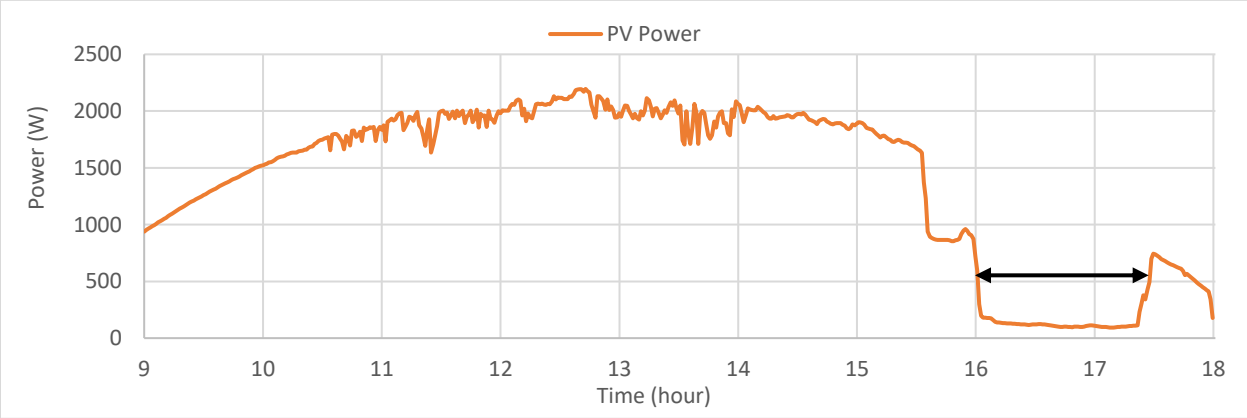


Figure (6-1a) High PV power for four-port hot water inlet device tests for cold tank conditions.

Figure (6-2) shows the hot water flow rate through the side-arm heater with each hot water delivery device over the test period during the low average PV heat power experiments and cold tank conditions. The hot water flow rate responds similarly to the PV power heater, i.e., the higher the PV heater power to the side-arm heater element, the greater the hot water flow rate. The force that drives the hot water flow rate in our experiment is due to density differences between the water in the tank and the water in the side-arm heater and manifold outlet tube. High degrees of stratification (DOS) were found to be caused by very low circulation rates [2, 4, 17, and 34].

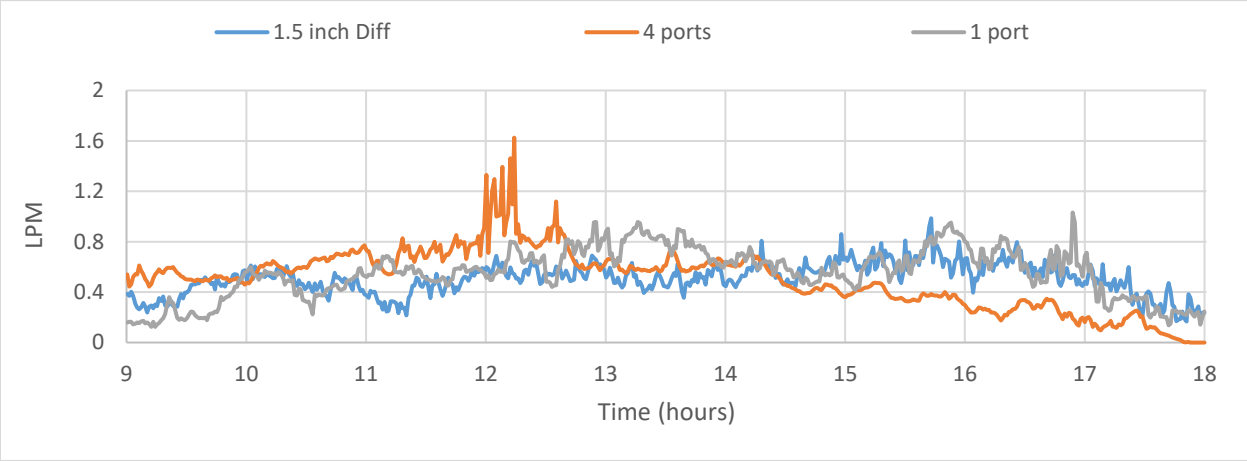


Figure 6-2 Hot water flow rate inside the side-arm heater under low PV power and cold tank conditions.

Figure (6-3) shows the average PV heater power and dead-state temperature for low average PV power and cold tank condition tests.

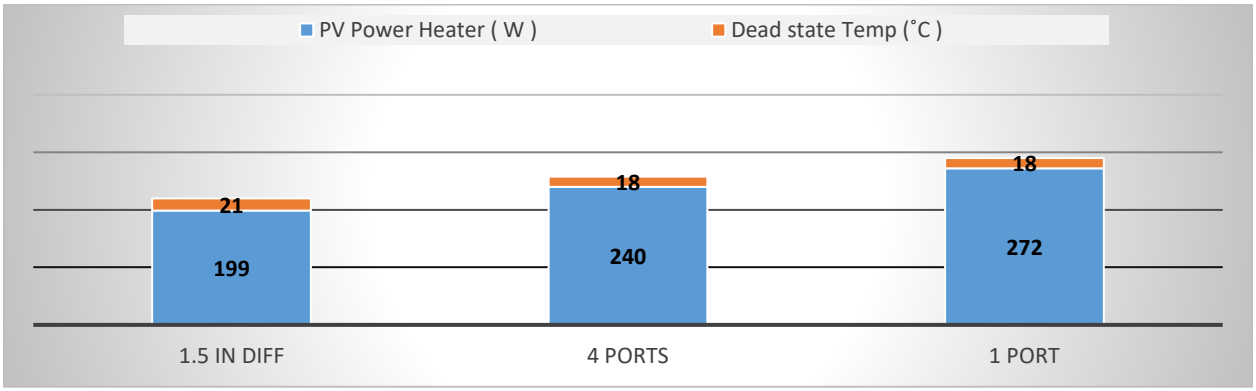


Figure 6-3 Low average PV power and cold tank condition tests.

### 6.1.2. Temperature

The assessment of water temperature inside a domestic hot water tank gives the best indication of stratification levels [2, 22, 34, and 44]. Stratification is desirable in thermal energy storage, as it resolves the issue of not being able to draw hot water off the top of the tank early in the day, compared to a uniform tank temperature. Figure 6-4, 6-5, and 6-6 shows a plot of the tank temperature and side-arm heater with three inlet hot water devices. The temperature of the water inside the tank was assumed to be represented by the temperature recorded by the twelve thermocouples. During stand-by conditions or when no heat has been added to the storage tank, the top hot water layers in the storage tank sink the heat, thus heating the bottom cold water layers. From this process, each layer reaches the temperature of the adjacent layer above it due to conduction between the stratified layers.

Figure (6-4) shows the temperature distribution in a cold SDHW tank using a 1.5-inch diffuser. The test started at 9 a.m. and ended at 6 p.m. and the data were taken at one-minute intervals. TCSS1 represents the top temperature of the SDHW tank, while TCSS12 represents the bottom temperature of the tank. At the beginning of the cold tank temperature experiment, the tank layer temperatures were approximately uniform. The difference between temperatures at the top and the bottom of the tank was 1.5˚C: the temperature at the bottom of the tank was 21˚C and the temperature at the top was 22.5˚C.

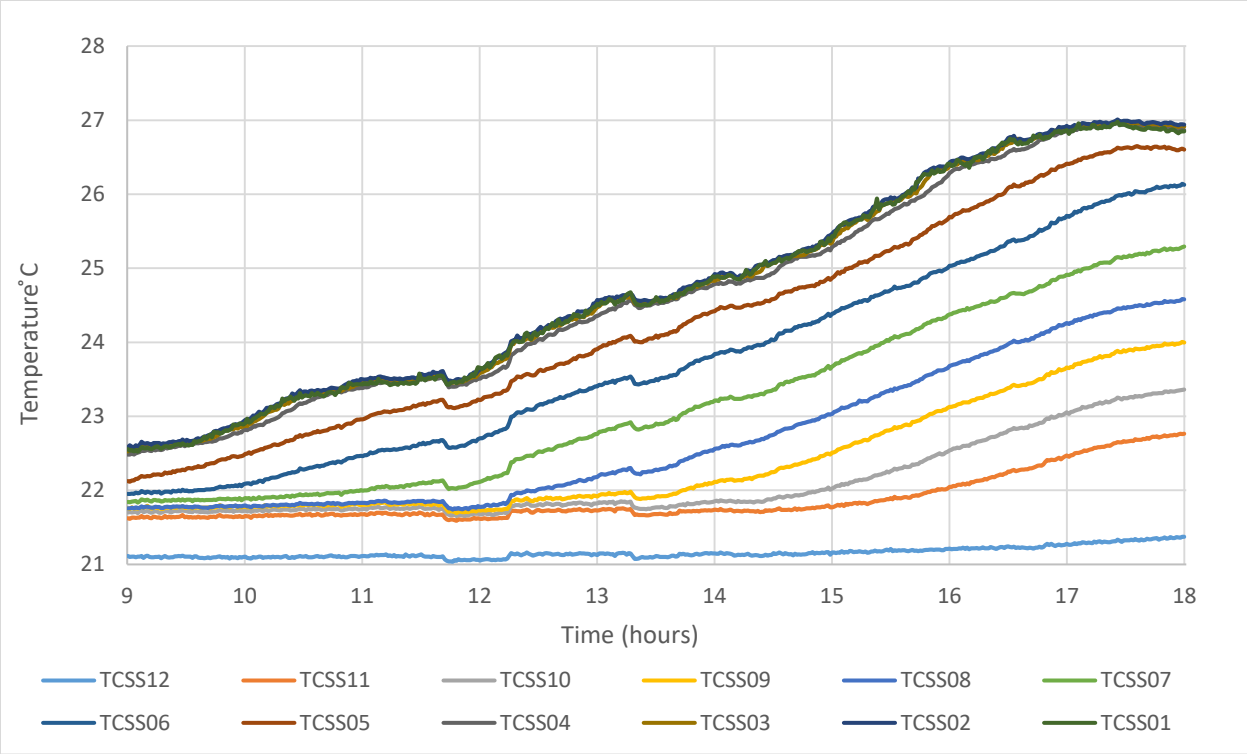


Figure 6-4 Graph showing 1.5-inch diffuser inlet device, low average PV power, and cold tank conditions.

The Figure (6-4) shows that the four top layers had the same temperatures from the beginning to the end of the test and that the temperature change rate for the top layer was quite slow. The top of the tank reached its highest temperature of 27˚C at the end of the test, with the difference in the top layer temperature at the beginning and the end of the experiment being 5.5˚C. As shown in Table (6-1), the top tank temperature change rate between the highest temperature and the start-up temperature of the top layer was 0.7˚C/h. The change rate of the temperature was very slow, and this led to a decrease in the availability and energy delivery. In such a case, the consumer would not be able to access hot water early in the morning.

Table 6-1 Temperature Change Rate of the three tank Top Layers for Low PV power and Cold Tank Condition

| 1.5-inch Diffuser | 4 Ports | 1 Port |
|---|---|---|
| ˚C/h | ˚C/h | ˚C/h |
| 0.7 | 2.8 | 1.8 |

Figure (6-5) shows the temperature distribution in cold SDHW tanks using a four-port manifold. The cold water is drawn through the PV heater from the bottom of the tank and the hot water is delivered at a different level at the top of the tank. The four-port manifold has been designed to inhibit mixing between the manifold and tank fluids until the level is reached at which the density of the two fluids matches. The four ports increase in diameter gradually to decrease the amount of cold water being drawn into the manifold from the middle of the tank and delivered to the top or to prevent a decrease in the side-arm heater outlet temperature. At the beginning of the cold tank temperature test, the temperatures of the tank layers were approximately uniform at 19˚C across all levels. The temperature at the bottom of the tank was 18.5˚C and the temperature at the top tank was 20˚C.

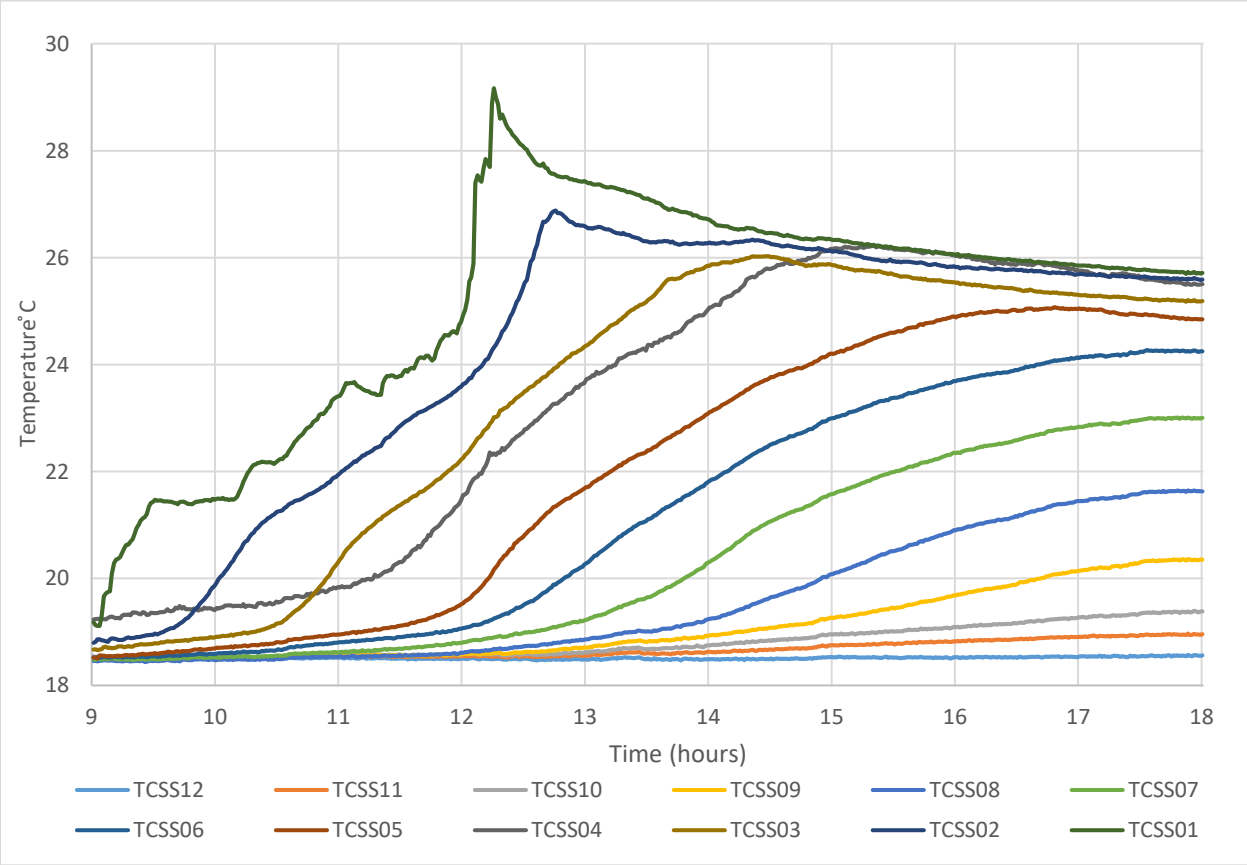


Figure 6-5 Graph showing four-port manifold inlet device, low average PV power, and cold tank conditions.

According to Figure (6-5), as the heater power increased, the temperatures at the top of the tank started to increase and reached a high of 29˚C at 12 p.m., which was nearly the same as the side-arm outlet water temperature. The top temperature change rate between the highest temperature and the top layer start-up temperature was 2.9˚C/h. The second layer of the thermocouple reading had a half-hour delay and the third layer thermocouple reading had a one-hour delay, with respect to the thermocouple in the top layer. The top four thermocouple readings had a higher rate of temperature change than the bottom layer thermocouple readings.

As can be seen in the graph, there was a rapid rise in temperature at the top of the tank as soon as the solar radiation increased early in the morning. Moreover, when the solar radiation decreased after 2 p.m., the top two layers had a slight decrease in temperature but remained constant after that, whereas the middle layer temperatures started to increase gradually. This shows that the four-port manifold strategy responded earlier in the day than the traditional design. The four-port hot water inlet devices delivered the water heated by the side-arm heater to the tank at the level where the temperature of the water in the tank matches the temperature of the heated water. Thus, this strategy enhanced the stratification and allowed the consumer to use hot water early in the morning. As energy is added to the SDHW tank through the four-port inlet manifold design, there is constantly a high degree of stratification and energy delivery to the consumer.

Figure (6-6) shows the temperature distribution in a cold SDHW tank using a copper tube with one port at the top, which will draw the cold water from the bottom of the tank and deliver hot water to the top of tank. At the beginning of the cold tank temperature test, the tank layer temperatures were approximately uniform: the temperature at the bottom of the tank was 18˚C and the temperature at the top tank was 20˚C. The tank's highest temperature (29˚C) occurred at 4 p.m.

As shown in Table (6-1), the top temperature change rate between the highest temperature and the top layer start-up temperature was 1.8˚C/h. The graph shows that any change in the PV power heater were reflected in the top layer temperature. At 1:30 p.m., the top temperature started to decrease due to a decline in solar radiation. Subsequent decreases in the PV heater power supplying the tank caused plume entrainment mixing. Plume entertainment is often the result of decreases in the amount of solar energy radiation, which leads to a downward flowing plume due to the water entering the top of the tank being cooler than the water at the top layers of the tank [2]. Because of this action, a decline in the temperature of the top layers of the tank occurs, which leads to decreases in the quality of the hot water.

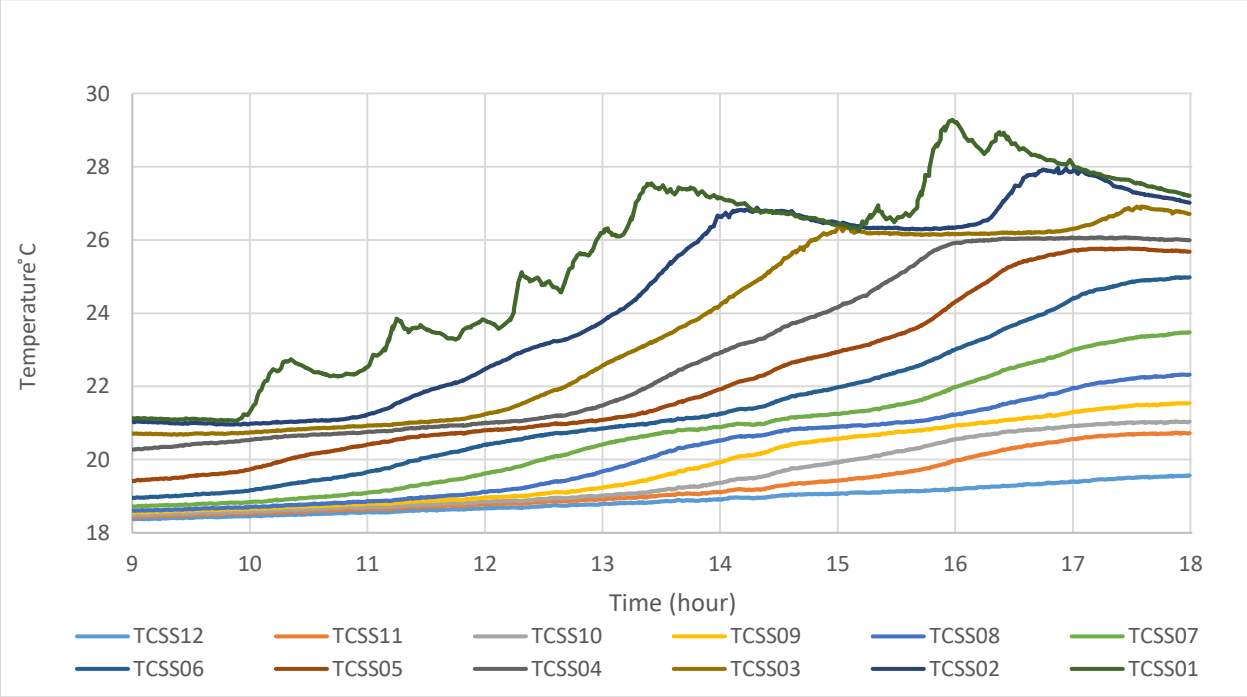


Figure 6-6 Graph showing one-port copper tube inlet device, low average PV power, and cold tank conditions.

From Figure (6-6), we can see that the solar energy increased the temperature at the top of the tank. However, as the solar energy decreased, the temperatures at the top of the tank also decreased. When the delivered hot water was cold compared to the water at the top of the tank, the cold water

sank downward to meet the matched water temperature at a lower layer. On its way down, the water mixed with warmer water at the upper and middle layers, cooling them down. This process decreases the availability of hot water in the storage tank. A copper tube pipe with one port at the top would have decreased the stratification and had an impact on the delivery of hot water to consumers.

### 6.1.3. Degree of Stratification (DOS)

Figure (6-7) shows the degree of stratification (DOS) for the three different hot water inlet devices inside the storage tank. The four-port manifold had the highest DOS values in the morning, reaching 55 by 14:00. The DOS for the four-port manifold started decreasing after 14:00, and decreased slightly until the end of the test. In addition, the graph shows that the 1.5-inch diffuser remained constant at low DOS throughout the beginning of the testing time, reaching a maximum value of 20 at the end of the experiment. The one-port tube also had an increase in the DOS from 9 to 40 by 14:00, reaching the highest value of 82 at 16:00. However, between 16:00 and the end of the test, the one-port tube showed a sharp decrease to a value of 45.

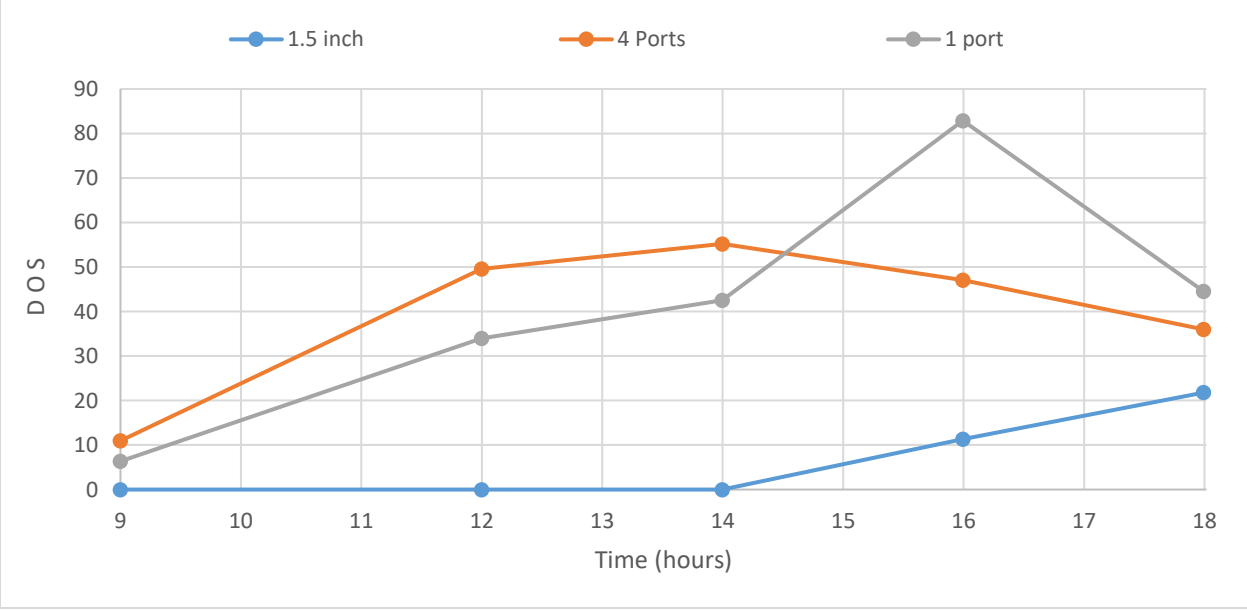


Figure 6-7 Degree of stratification of three hot water inlet devices, low average PV power, and cold tank conditions.

To calculate the degree of stratification in the SDHW tank, the rate of change in temperature per the change in the difference between the layers was determined for all levels. The maximum value of DOS was then taken for each period. An average value of DOS was determined using only those values that were greater than 1/10 of the maximum DOS for each period [45]. Figure (6-8) shows the average DOS of the three hot water inlet devices inside the storage tank. The four-port manifold had the highest average DOS from start-up until mid-day, followed by a slight decline and relative stability from 14:00 until the end of the test. The one-port tube also had an increase in average DOS up to 11 at 12:00, reaching the highest average value of 14 between 14:00 and 16:00. However, between 16:00 and the end of the test, the one-port tube showed a sharp decrease to a value of 7.

The graph (6-8) shows that the 1.5-inch diffuser remained constant at low average DOS throughout the beginning of the testing time, reaching a maximum value of 7 at the end of the experiment. The four-port manifold has the highest DOS in the tank early in the morning and a constant level throughout the rest of the test. Hence, this type of manifold will enhance stratification throughout the tank, leading to an increase in energy levels.

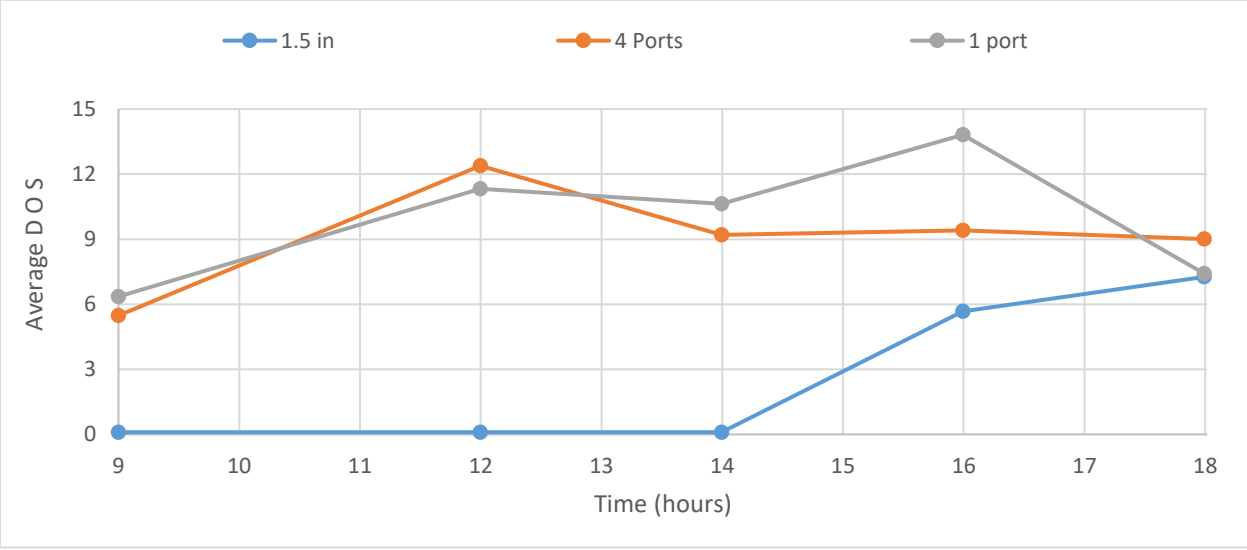


Figure 6-8 Average DOS of three inlet devices, low average PV power, and cold tank conditions.

Figure (6-9) shows the temperature distribution in a cold SDHW tank using a 1.5-inch diffuser inlet device. The temperature curves on each graph represent the tank water temperature distribution at each level at start-up, midday, 2 p.m., 4 p.m., and system shutdown. At the start-up of the cold tank experiment, the tank temperature was approximately uniform. The increase in temperature at the top of the tank was quite slow, to which we attributed the outlet of the hot water being injected into the middle of the storage tank, where it was distributed to warm up the top five layers. The difference in the top tank temperature at the beginning of the test and at midday was only 0.7°C. The 1.5-inch device did little to enhance the stratification within the tank.

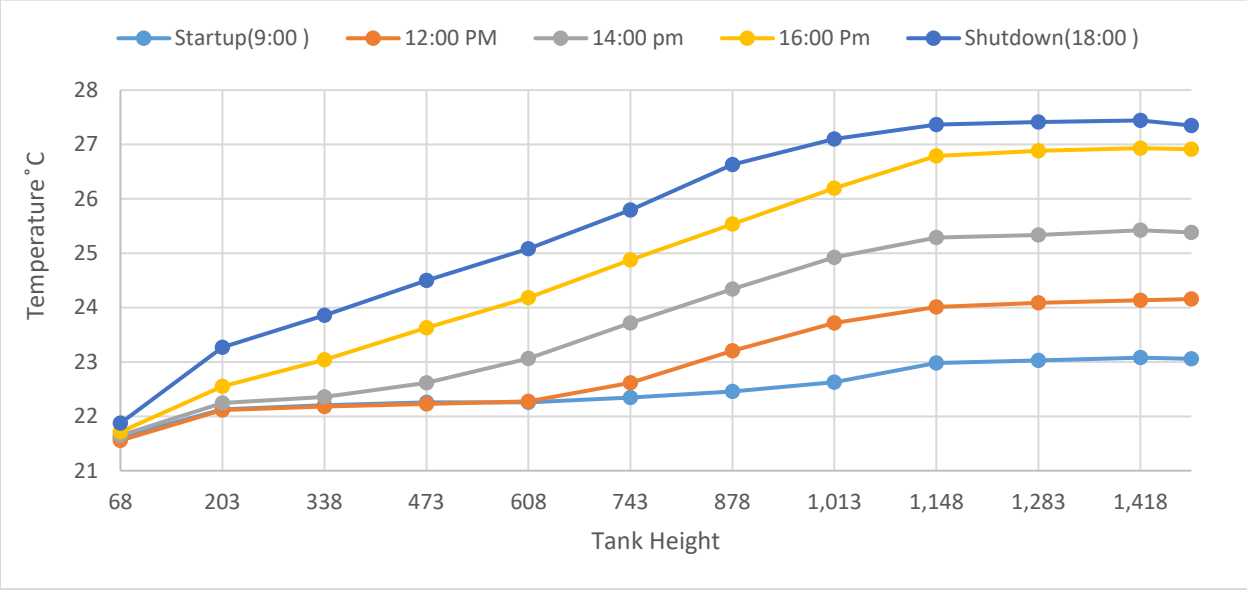


Figure 6-9 Graph showing 1.5-inch diffuser inlet device, low average PV power, and cold tank conditions.

Figure (6-10) shows the temperature distribution in a cold SDHW tank using a four-port manifold inlet device. At the start-up of the cold tank test, the tank temperature was approximately uniform. The water temperature at the top of the tank rose sharply early in the morning to 25 – 26°C and remained at this temperature until shutdown. The difference in the temperature at the top of the tank between 9 a.m. and 12 p.m. was 6°C, which was the highest value among the inlet devices.

However, when a decrease in solar energy power occurred, there was no significant change in the temperature at the top layer of the storage tank.

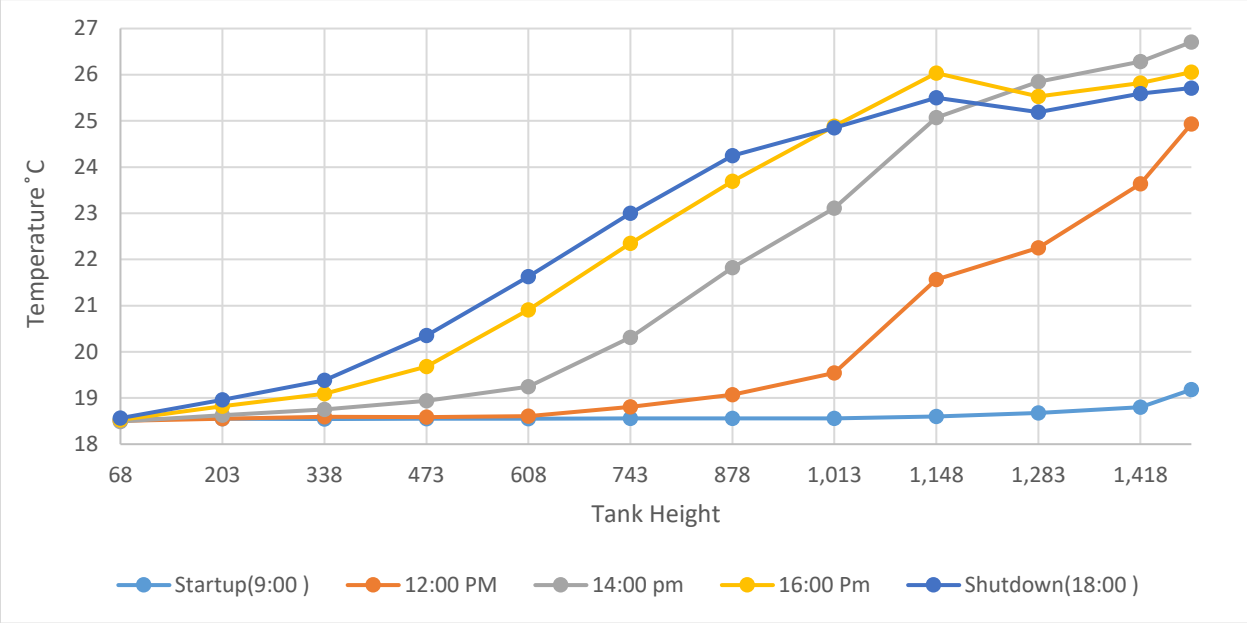


Figure 6-10 Graph showing four-port manifold inlet device, low average PV power, and cold tank conditions.

Figure (6-11) shows the temperature distribution in a cold SDHW tank using a one-port tube inlet device. At the start-up curve of the cold tank condition test, the tank layer temperature was approximately uniform. The difference in the temperature at the top of the tank between 9 a.m. and 12 p.m. was 3°C, which indicates that the hot water discharged from the PV power heater was distributed to the top seven layers. We observed that there was a cycle of temperature changes, where the temperature kept rising and falling from 12 p.m. to the end of the test. This cyclical change shows that the temperature at the top of the tank is affected directly by fluctuations in solar radiation energy. The one-port inlet device did not maintain the same level of temperature at the top of the tank throughout the experiment, which would negatively affect energy delivery to consumers.

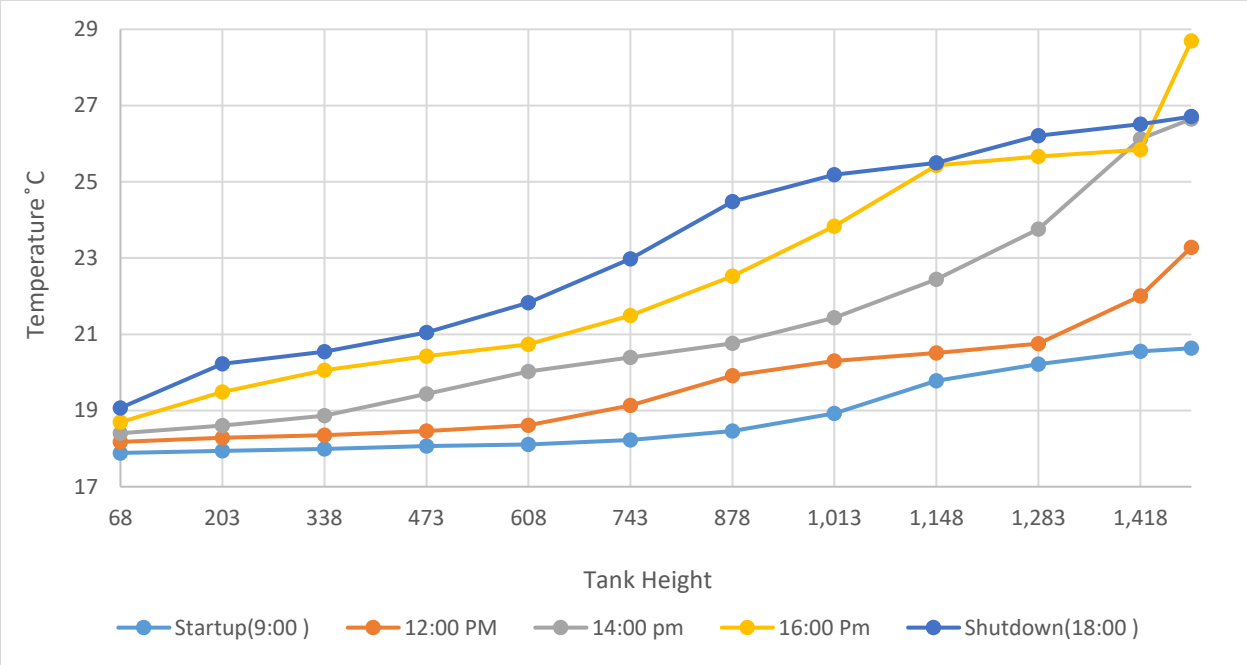


Figure 6-11 Graph showing one-port copper tub inlet device, low average PV power, and cold tank conditions.

### 6.1.4. Availability and Availability Ratio

In this section, availability and availability ratios are analyzed and discussed for cold tank condition tests using 1.5-inch, four-port and one-port inlet devices. An important variable for the availability of stored tank energy and one which could have a substantial effect on the outcomes is the dead-state temperature. For this study, the dead-state temperature was taken as the water temperature of the cold mains supply. The level of stratification, the mean tank temperature, and the dead-state temperature are the three main factors affecting changes in stored availability.

Figure (6-12) shows the availability over time in a cold SDHW tank using the three aforementioned hot water inlet devices. Figure (6-13) shows changes in availability, average PV heater power, and main supply water temperature for the same domestic hot water tanks using the three hot water inlet devices. This value of availability is dependent on the average PV power heater and the main supply water temperature for the cold tank. In Figure (6-13), we can see that the availability of the one-port tube at the top of the tank was the highest at 0.15 MJ, with the four-port manifold coming

in slightly lower at 0.13 MJ. However, the heater power for the one-port was 272 watts, while for the four-port manifold, it was 240 watts. This shows that whenever there was an increase in the PV power and a decrease in main water supply temperatures, availability will increase. Furthermore, when we normalized the PV average power and the dead-state temperature, we obtained the same availability change for the four-port manifold as for the one-port tube. Thus, after normalizing the power and the dead-state temperature, the availability change for the 1.5 diffuser, four-port manifold and one-port tube was 0.09, 0.13 and 0.13 MJ, respectively.

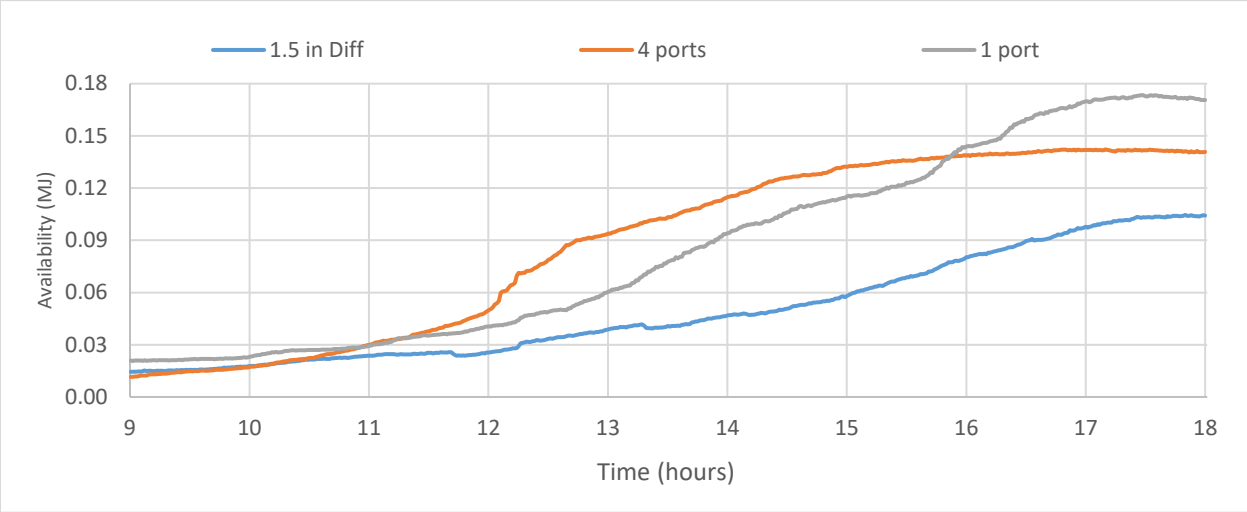


Figure 6-12 Availability change for three inlet devices in low average PV power and cold tank conditions.

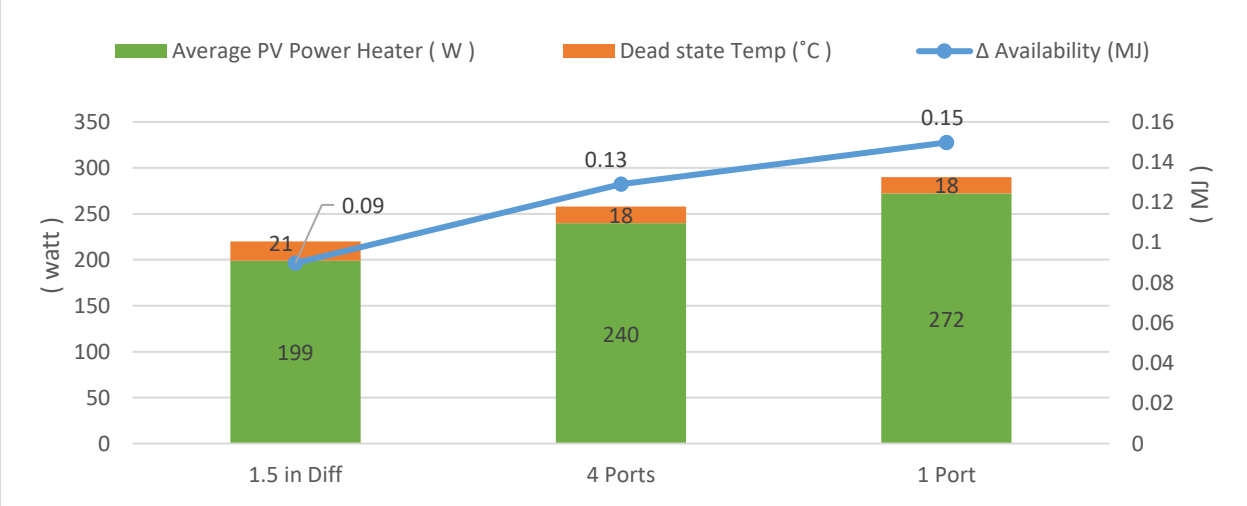


Figure 6-13 Availability change for three hot water inlet devices in cold tank conditions.

Figure (6-14) shows the availability ratio from 9 a.m. to 6 p.m. The availability ratios for the four-port manifold rapidly increased early in the morning. Moreover, the curve for the four-port manifold was consistently the highest value from the beginning to the end of the tests compared to the curve for other traditional devices. However, although the availability ratios for the four-port manifold were more or less constant from 1 p.m. to 4 p.m., they experienced a slight decrease from 4 p.m. to 6 p.m.

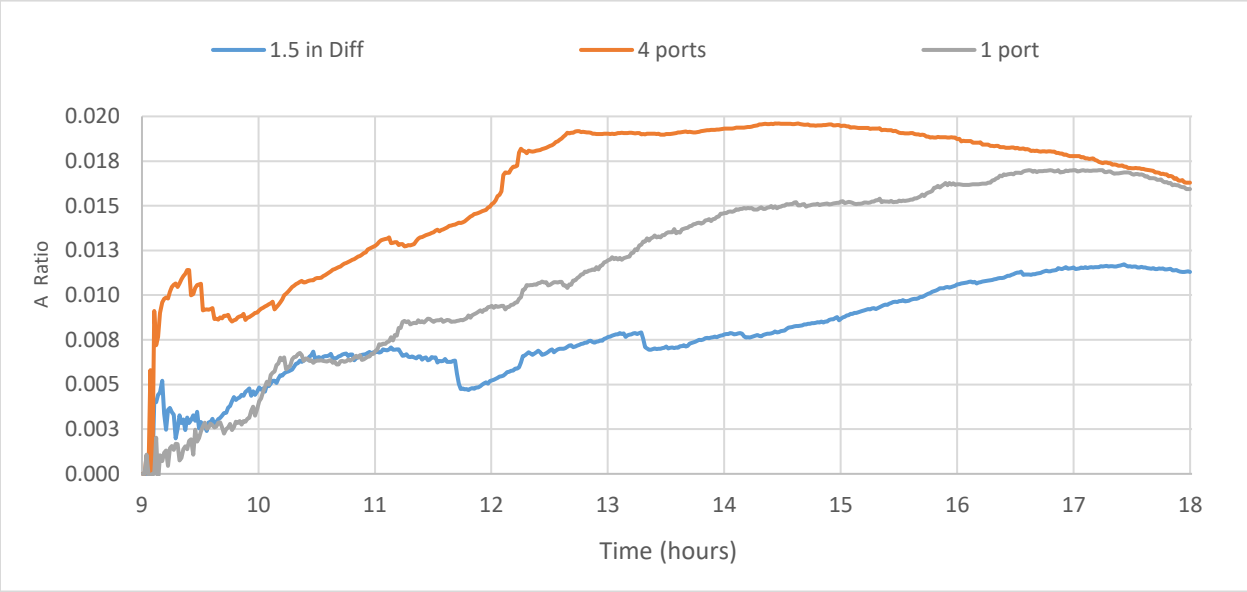


Figure 6-14 Availability ratios for three inlet devices in low average PV power and cold tank conditions.

Figure (6-15) shows the average availability ratios in a cold SDHW tank using the three hot water inlet devices. The average availability ratios for 1.5-inch diffuser, four-port and one-port inlet devices were 0.008, 0.16 and 0.12 MJ, respectively. After normalizing the PV average power and the dead-state temperature, the availability ratios of the 1.5-inch diffuser, four-port manifold and one-port tube were 0.009, 0.016 and 0.01, respectively.

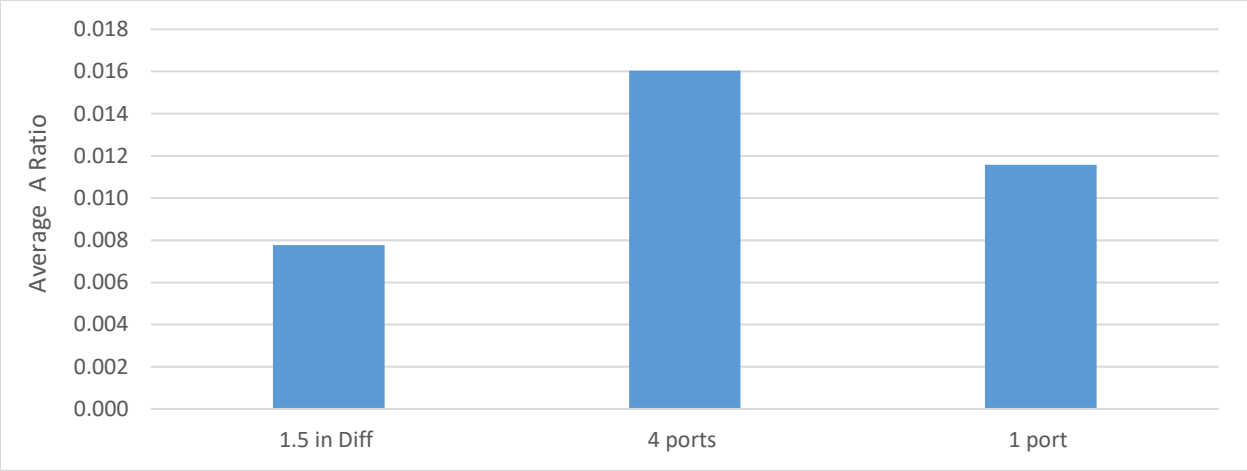


Figure 6-15 Average availability ratio for three inlet device in low average PV power and cold tank conditions.

### 6.1.5. Entropy

The entropy ratios and merit factors were analyzed and discussed for each cold tank condition test using the three inlet hot water devices.

#### 6.1.5.1. Merit Factor

As shown in equation 4-19, this basic approach was used to calculate the difference in the entropy of the perfect tank and the entropy of the experimental tank. The result is then divided by the difference of the entropy of a perfect tank and the fully mixed tank. Hence, when the entropy of the experimental tank equals the entropy of perfect tank the merit factor will be highest.

Figure (6-16) shows the merit factor from 9 a.m. to 6 p.m. At the beginning of the experiment, the merit factor for the one-port tube inlet device was 0.42. A slight decrease from 0.42 to 0.40 occurred between 9 a.m. and 10 a.m. Then, due to the effects of destratification, a sharp decrease from 0.40 to 0.25 occurred between 10 a.m. and 2 p.m. At the end of the test, the merit factor was 0.30, as shown in Figure (6-16).

At the beginning of the experiment, using a 1.5-inch diffuser inlet device, the merit factor increased and then slightly decreased from midday to the end of the operation. At the end of the test, the

merit factor was 0.4, as shown in Figure (6-17). Using a four-port manifold, the merit factor increased gradually until reaching a high of 0.50 at mid-day. This was followed by a slight decrease such that by the end of the experiment, the merit factor was 0.45. The graphs illustrate that the merit factor change rate for the four-port manifold was the highest. Specifically, the merit factors change rates were 0.11, 0.33 and -0.11, respectively, for the 1.5-inch diffuser, four-port manifold, and one-port tube,

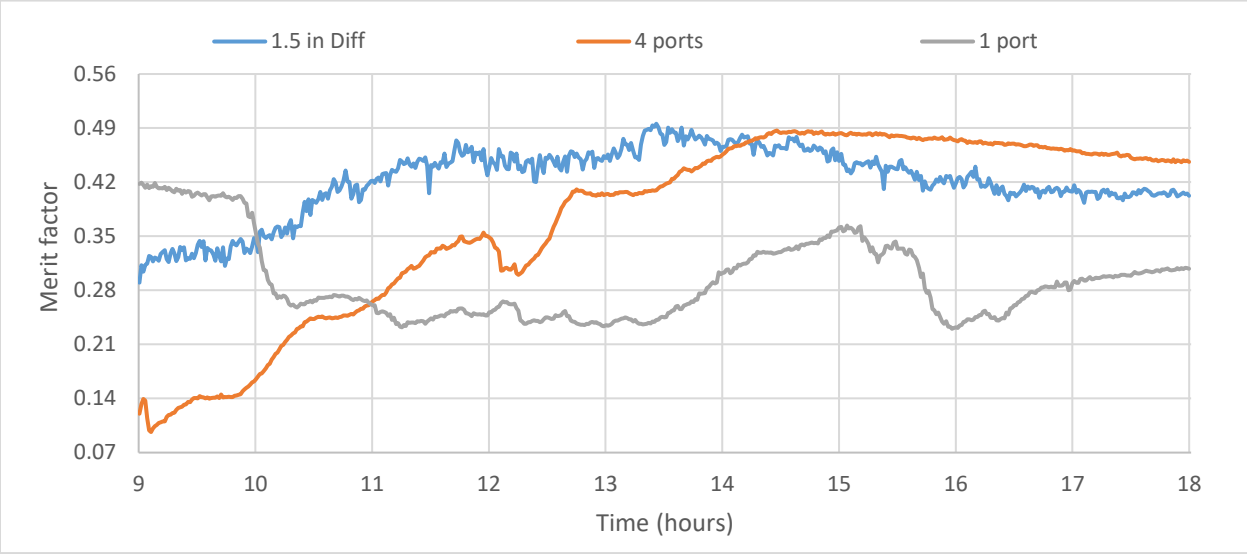


Figure 6-16 Merit factor for three hot water inlet devices in cold tank conditions.

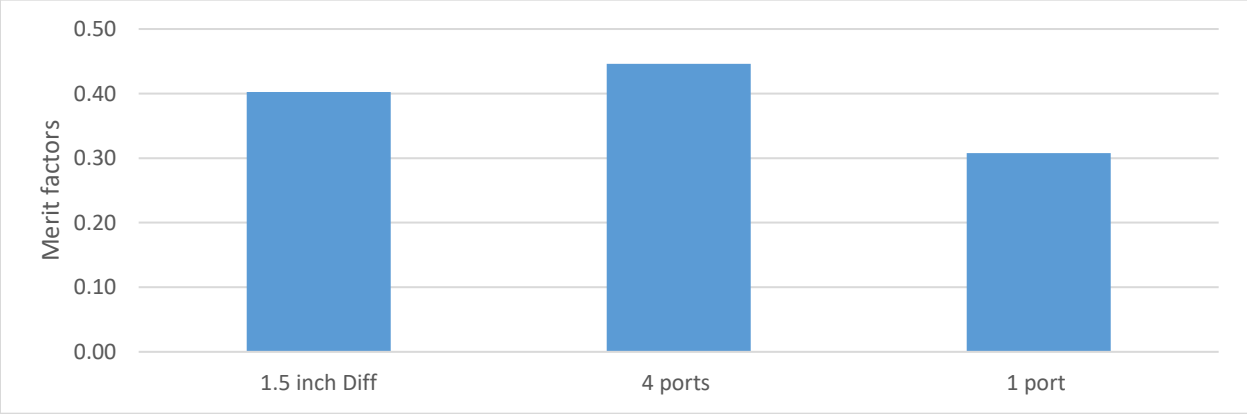


Figure 6-17 Merit factor for three hot water inlet devices at the end of the test in cold tank conditions.

### 6.1.5.2. Entropy Ratio

Figures (6-18) and (6-19) show the entropy ratios for a cold SDHW tank, using the three aforementioned hot water inlet devices. The entropy ratios for the four-port manifold, one-port tube, and 1.5-inch diffuser were 0.9954, 0.9979 and 0.9986, respectively. In comparison to all other designs, the four-port hot water inlet design had a lower entropy ratio than either the four-port or the 1.5-inch diffuser designs. A low entropy ratio is preferable. The difference between the four-port and one-port hot water inlet designs was 0.0025, which is so small to be nearly unnoticeable. As shown in figure (6-20a, 6-20b, and 6-20c) the reason for the difference between these two designs is that the difference in actual entropy, perfect entropy and mixed entropy is so negligible that it had very little to no impact on the final calculations.

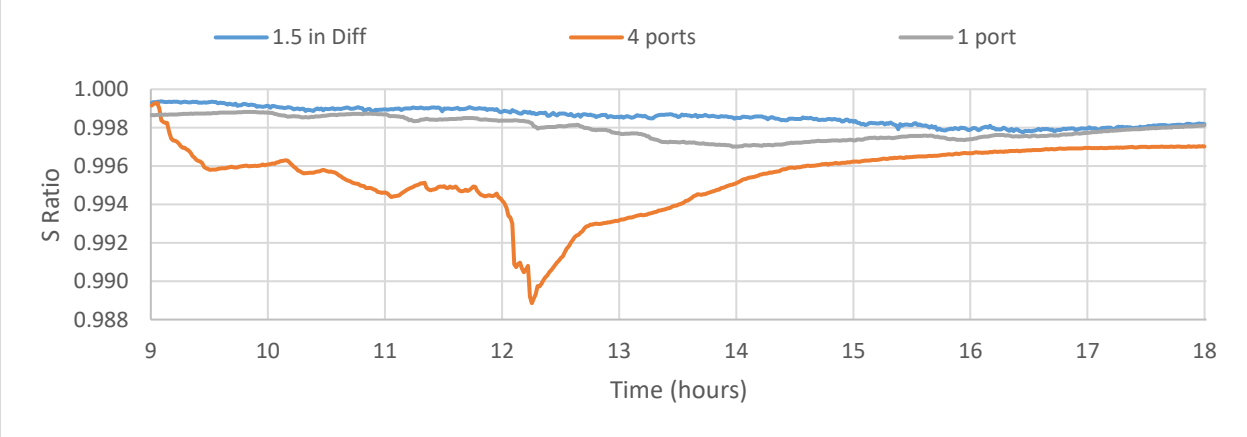


Figure 6-18 Entropy ratios of three inlet devices in low average PV power and cold tank conditions.

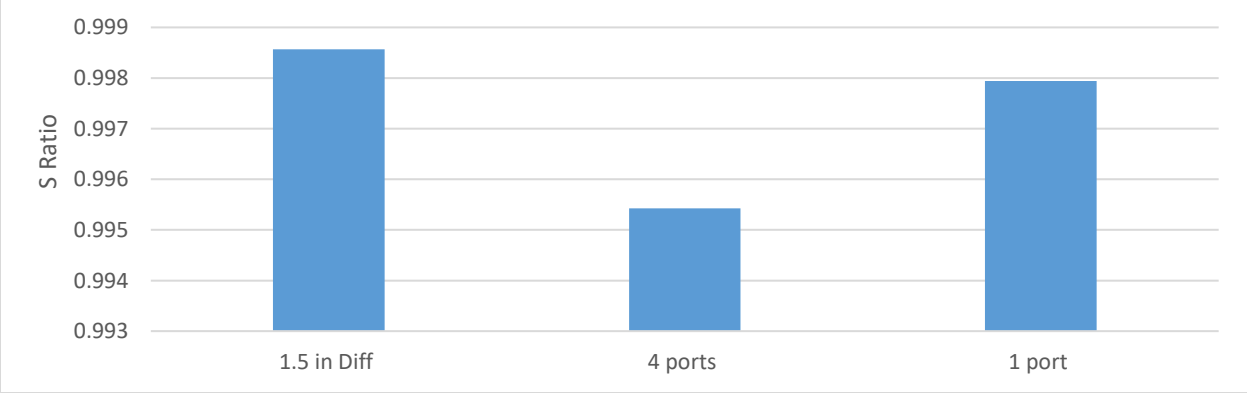


Figure 6-19 Entropy ratios of three inlet devices in low average PV power and cold tank conditions.

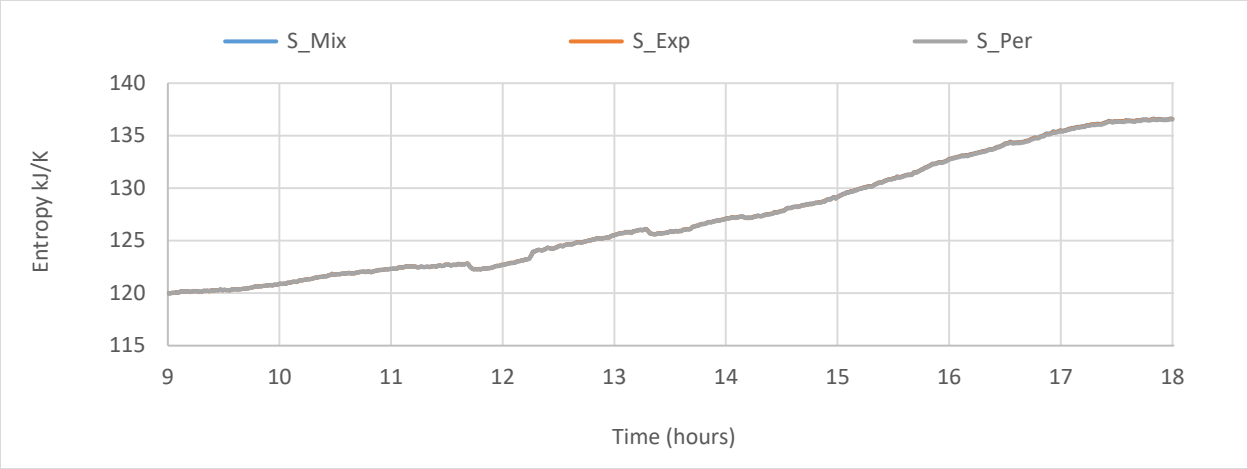


Figure (6-20a). Entropy of 1.5-inch diffuser for inlet devices in low average PV power and cold tank conditions.

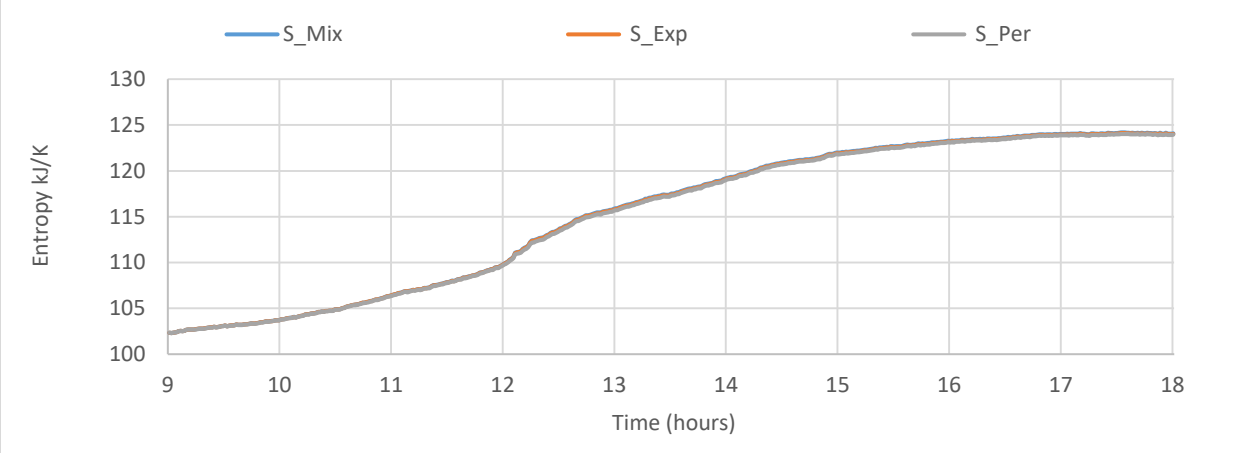


Figure (6-20b). Entropy of four ports manifold for inlet devices in low average PV power and cold tank conditions.

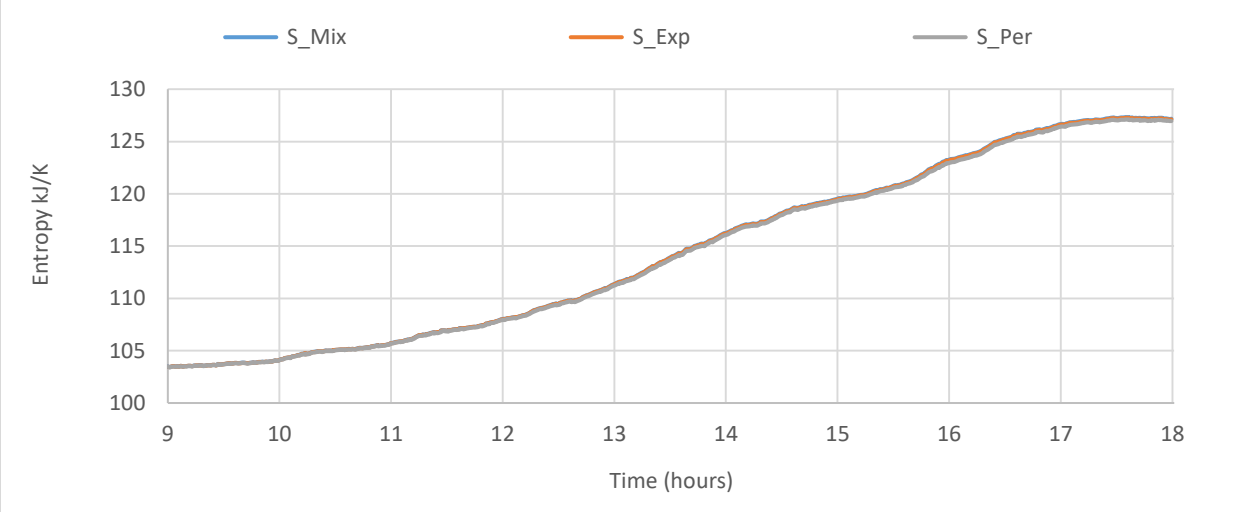


Figure (6-20c). Entropy of one port copper tube for inlet devices in low average PV power and cold tank conditions.

Figure 6-20 Entropy inside the DHW Tank of three hot water inlet devices

#### 6.1.5.3. Internal Entropy Generation

Figure (6-21) shows internal entropy generation in a cold tank using the three aforementioned hot water inlet devices. There is a sharp decrease in the levels of internal entropy generation in the four-port manifold from 9 a.m. to 12:30 p.m. This is followed by a slight gradual increase until the end of the operation.

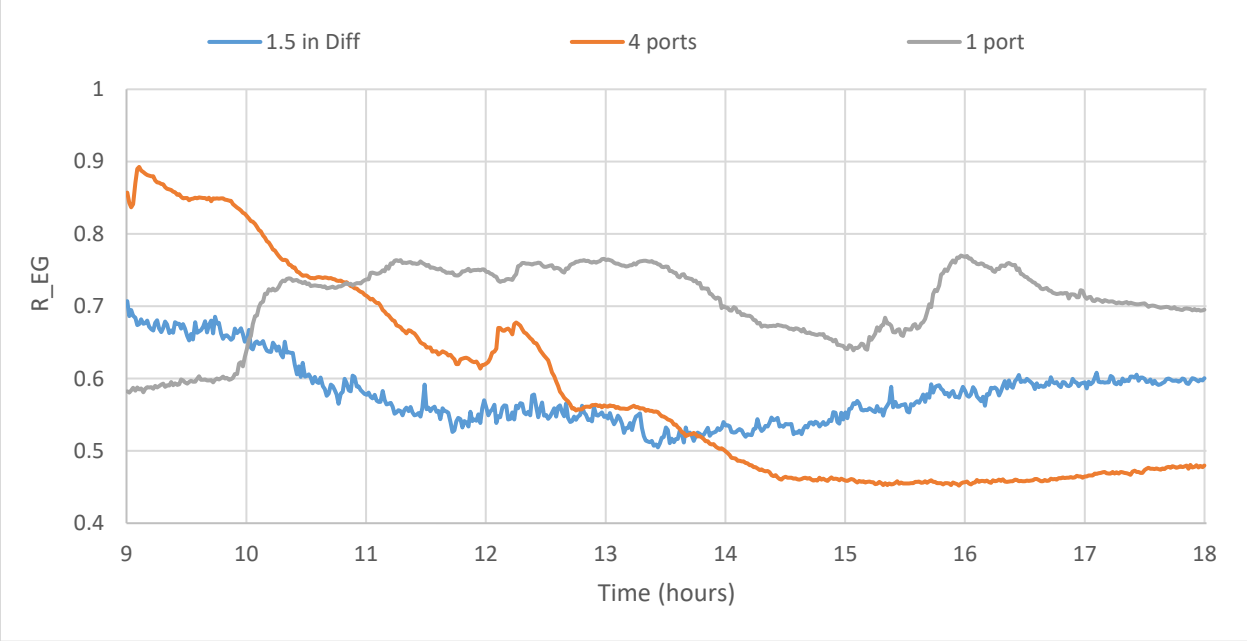


Figure 6-21 Internal entropy generation of inlet devices in low average PV power and cold tank conditions.

Figure (6-22) shows the internal entropy generation at the end of the tests. The internal entropy generation for the 1.5-inch diffuser, four-port, and one-port inlet devices were 0.6, 0.5 and 0.7, respectively. Compared to the other designs, the four-port manifold hot water inlet design had a lower internal entropy generation than the other inlet devices. Therefore, according to these calculations, the four-port manifold is the best option. The graphs illustrate that the internal entropy generation change rate of the four-port manifold was the highest. Specifically, the internal entropy generation change rates of the 1.5-inch diffuser, four-port manifold and one-port tube were -0.1, -0.37 and 0.11, respectively.

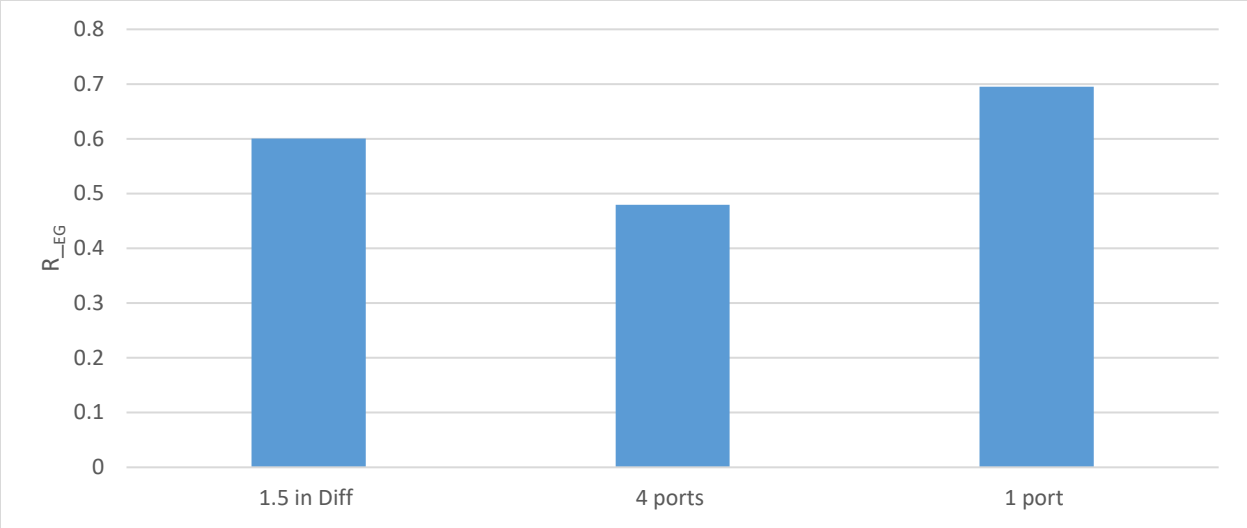


Figure 6-22 Internal entropy generation of three inlet devices in low average PV power and cold tank conditions.

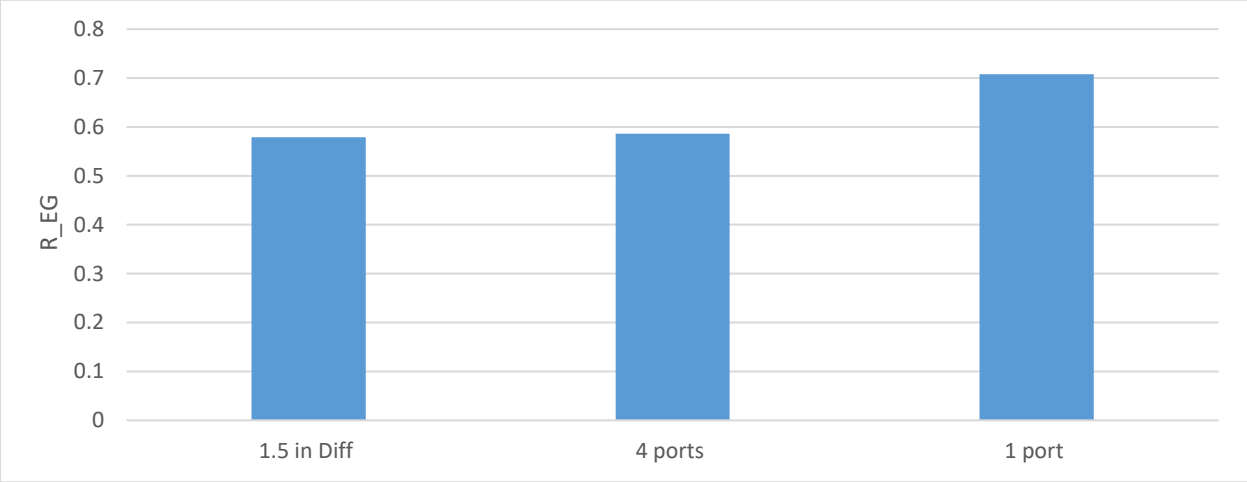


Figure 6-23 Average internal entropy generation of three inlet devices in low PV power and cold tank conditions.

### 6.1.6. Energy Delivery

One important element in the design of the side-arm heater and inlet hot water device is that it should have a highest energy delivery. In other words, this design ensures the hottest water temperature at the top of the domestic hot water tank early in the day. During the tests, the energy levels within the water in the storage tank changed as the temperatures of the hot water within the storage tank changed over a certain period of time [9].

Figure (6-24) shows the calculation of energy delivery in a cold tank using the three aforementioned hot water inlet devices. At the beginning of the test, the delivered energy from the four-port manifold was 0.5 MJ and reached a high of 3.5 MJ at mid-day, where it remained at the same level for the rest of the test. However, when comparing hot water inlet designs according to differences in energy delivery quality, we need to take into account PV heater power and dead-state temperature, as shown in Figure (6-25). This graph illustrates that the mains water supply temperature and the PV heater power differed for each experimental test, and that the calculation of energy delivery is reliant on PV heater power and dead-state temperature. Furthermore, Figure (6-25) illustrates that the test using the four-port inlet device also used the same dead-state temperature as the one-port device, and that while it has less PV heater power than the one-port device, the four-port device provides the highest energy delivery to consumers. The energy delivery for the 1.5-inch diffuser, four-port and one-port inlet devices were 1.8, 2.8 and 2.5 MJ, respectively. After normalizing the PV average power and dead-state temperature, the delivered energy for the 1.5-inch diffuser, four-port and one-port inlet devices were 1.9, 2.8 and 2.3 MJ, respectively.

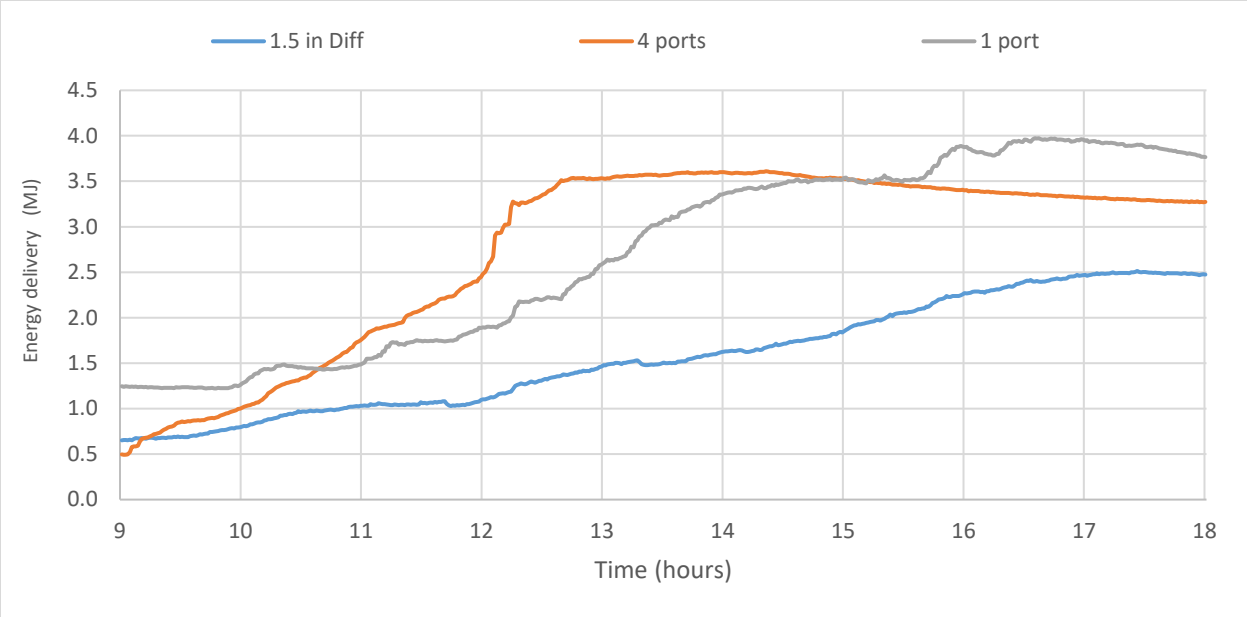


Figure 6-24 Energy delivery for three inlet devices in low average PV power and cold tank conditions.

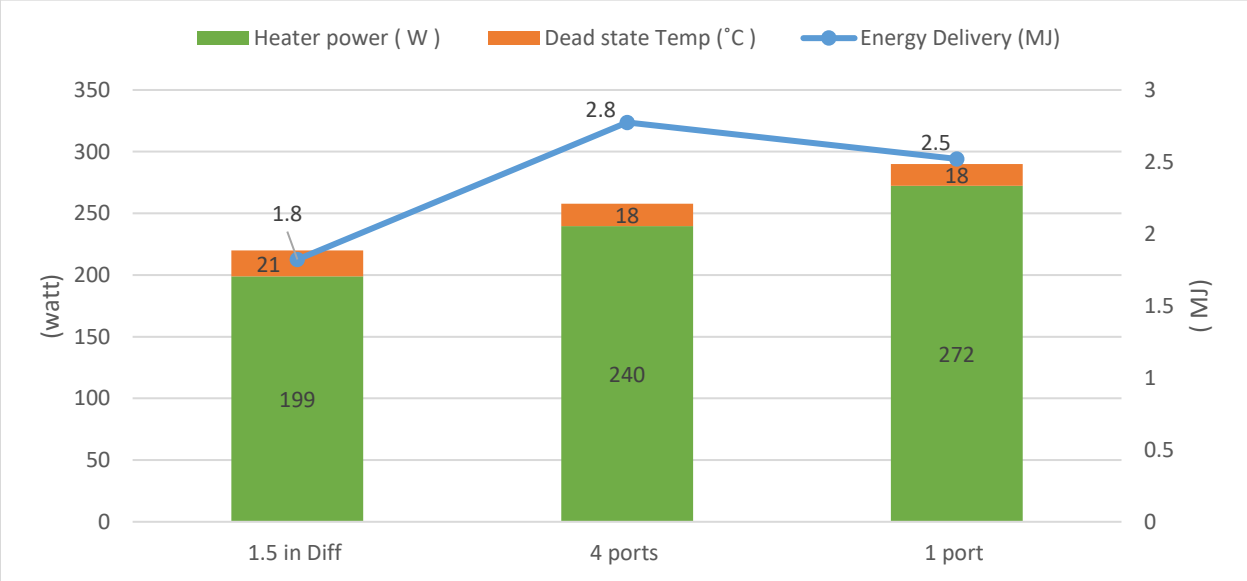


Figure 6-25 Energy delivery, low PV power, and dead-state temperature of the three devices in cold tank conditions.

## 6.2. Hot Tank Conditions Tests

### 6.2.1. Power and Hot Water Flow Rate

Figure (6-26) shows the PV heater power plots from 9 a.m. to 6 p.m. during the low average PV power tests for hot tank conditions. With these tests we started with a tank that had been brought to temperatures higher than the mains water temperature due to heat provided by the PV heater on the previous day. In the tests, a 1.5-inch diffuser, a four-port manifold, and a one-port copper tube are used. The average PV heater power of these three devices was 284, 332 and 262 watts, respectively. Figure (6-27) shows the hot water flow rate inside the side-arm heater plots from 9 a.m. to 6 p.m. during the low average heat power experiments and hot tank conditions. A 1.5-inch diffuser, four-port manifold, and one-port copper tube are used.

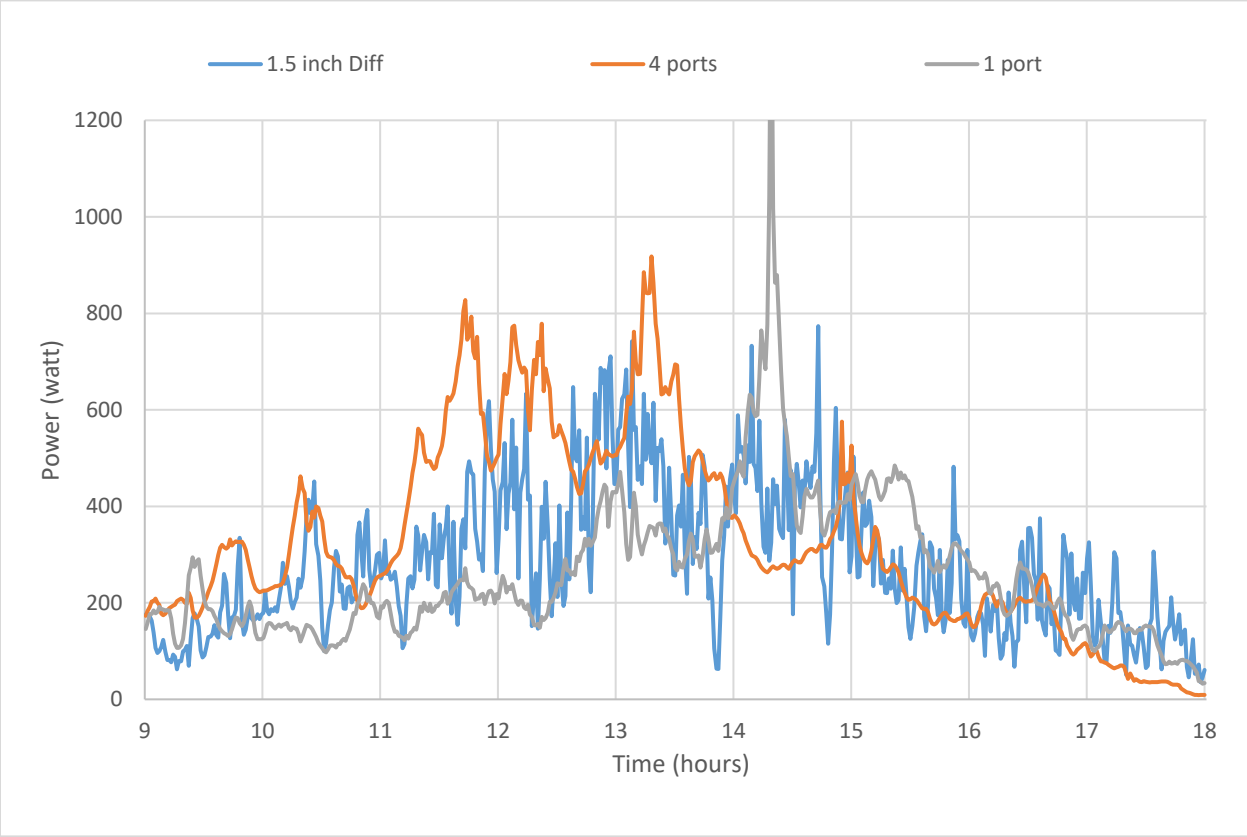


Figure 6-26 Low PV power heater during testing of three hot water inlet devices in hot tank conditions.

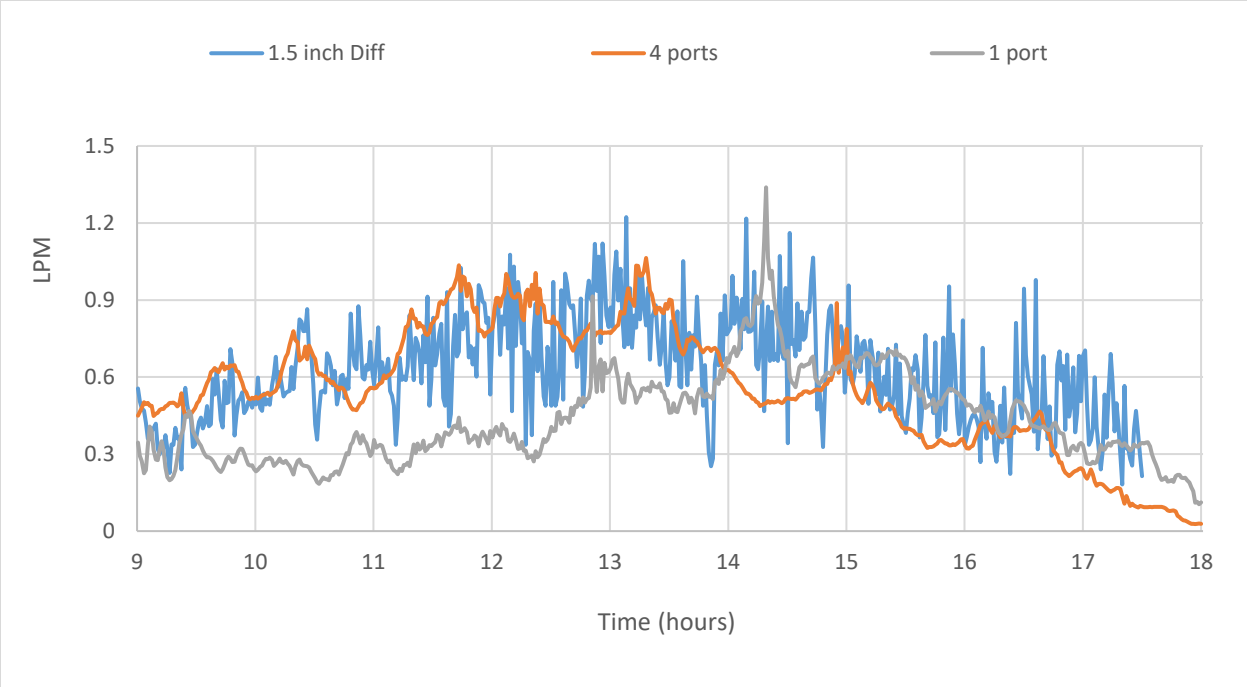


Figure 6-27 Hot water flow rate inside side-arm heater for low PV power and hot tank conditions.

Figure (6-24) shows the average PV heater power and tank temperature at the beginning of the experimental tests for low average PV power and hot tank conditions.

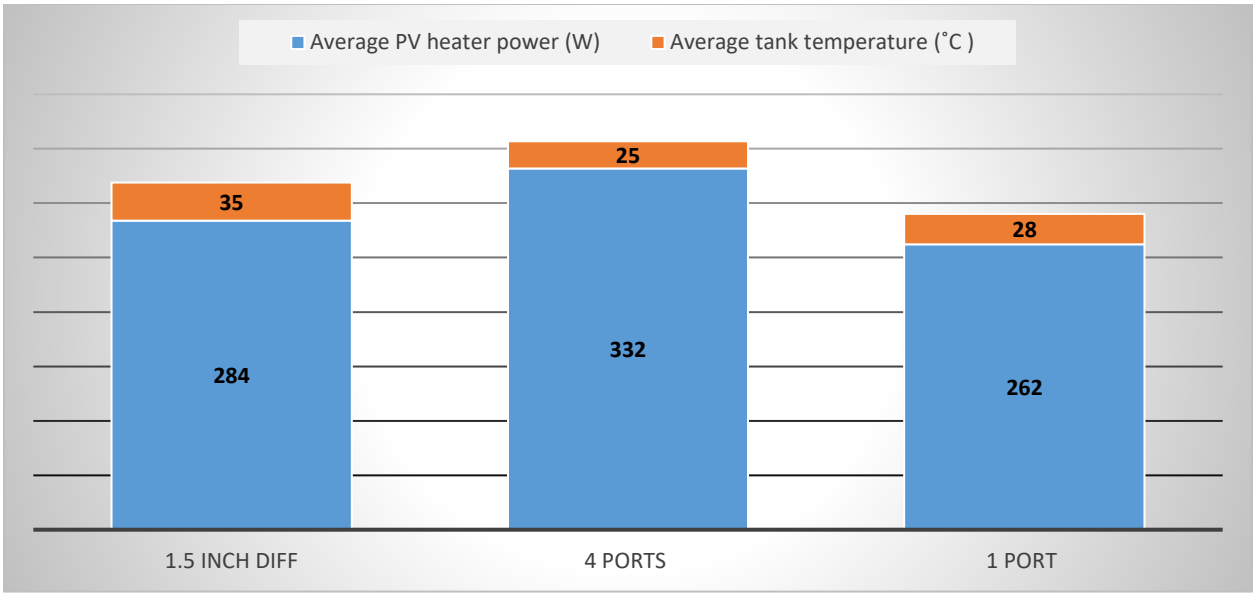


Figure 6-28 Average PV power and tank temperature for low average PV power and hot tank conditions.

### 6.2.2. Temperature

In Figure (6-29), the tank temperature has been plotted for a side-arm heater with three inlet hot water design devices. The figure shows the temperature distribution inside the domestic hot water tank for low PV power when using a 1.5-inch diffuser inlet device. The average tank temperature at the beginning of the operation was 35˚C, and the temperatures of the top ten layers of the tank were all approximately the same. Specifically, the difference between the top and bottom layers was only 0.8˚C. Furthermore, there was only a slight increase in the temperature of the middle layers until 11 a.m. but no change in the temperature of the top layers until 12 p.m. The highest temperature recorded during the test was 38˚C at 3 p.m. This was followed by a constant decrease in temperature until the end of the test. The difference in the top layer temperatures between the beginning of the test and the highest reading was 2.5˚C. Moreover, the temperature change rate for the top layers was very slow. As shown in Table (6-2), the temperature change rate for the top layers between the highest temperature and the start-up temperature was 0.5˚C/h. This magnitude of change led to a decrease in availability and energy delivery. Therefore, consumers would not be able to use hot water early in the day.

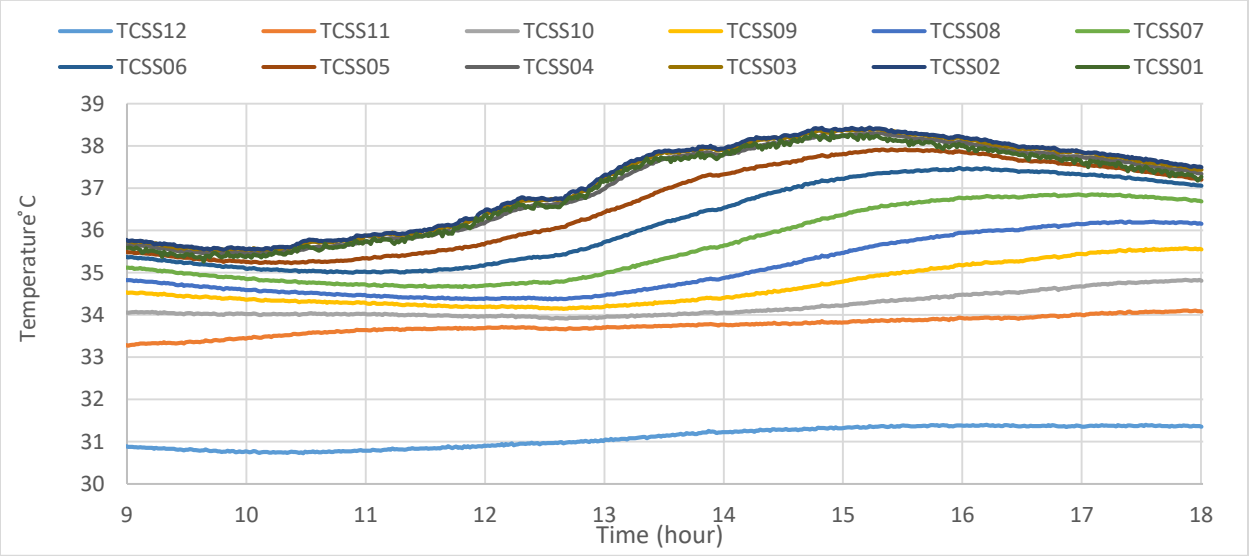


Figure 6-29 Graph showing 1.5-inch diffuser inlet device and low average PV power in hot tank conditions.

Figure (6-30) shows the temperature distribution in a hot SDHW tank with low PV power and a four-port manifold. The average tank temperature at the beginning of the operation was 25˚C the temperature at the top layer of the tank was 27˚C, and the temperature at the bottom of the tank was 21˚C. The graph shows that there was a gradual increase in the temperature at the top of the tank, with the water temperature there reaching 35˚C at 1:30 p.m. However, after 1:30 p.m., there was a slight decrease in the top layer temperature but an increase in the middle layer temperature. The difference in top layer temperature between the start and end of the experiment was 7˚C. As shown in Table (6-2), the top tank temperature change rate between the highest temperature and the top layer start-up temperature was 1.8˚C/h. This shows that the four-port manifold strategy keeps the top layer at a constant temperature, which increases the stratification and the energy delivery to consumers.

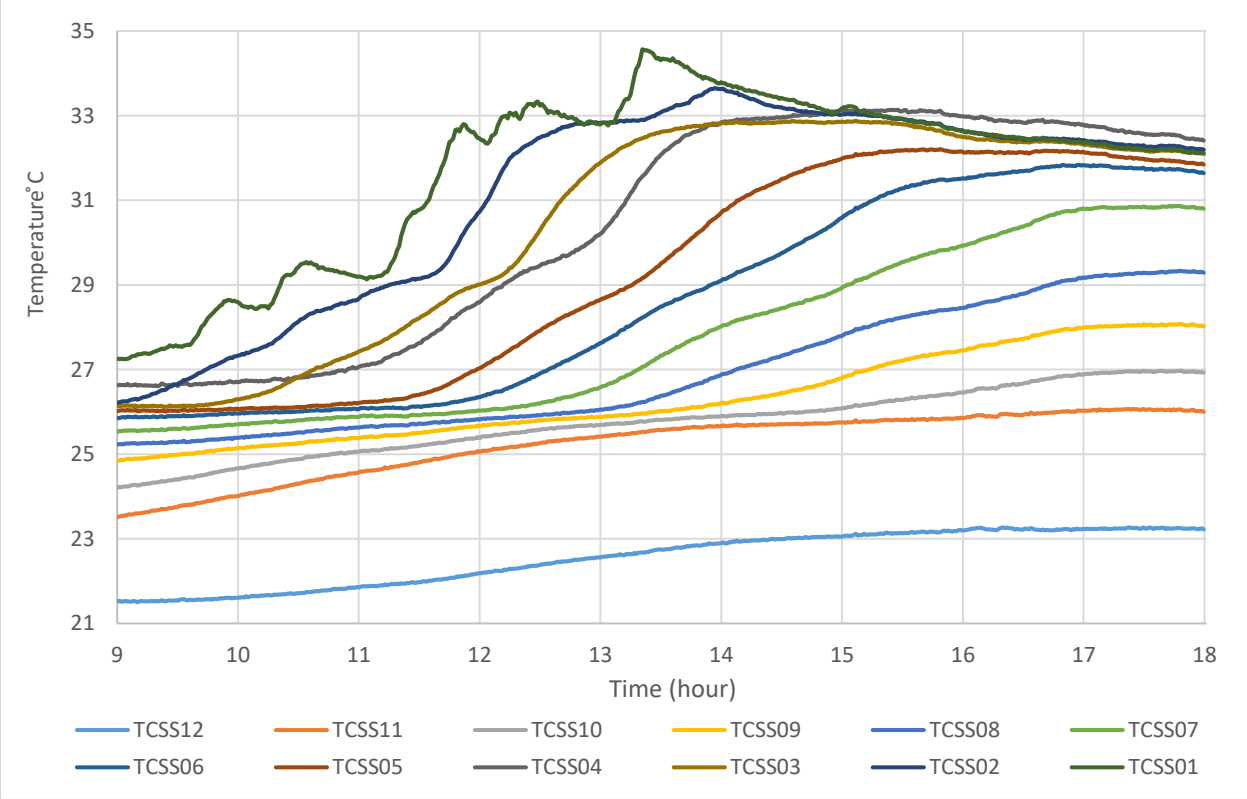


Figure 6-30 Graph showing four-port manifold inlet device and low average PV power in hot tank conditions.

Figure (6-31) shows the temperature distribution in a hot SDHW tank with low PV power and a copper tube with one port at the top of the tank. The average tank temperature at the beginning of the operation was 28˚C. Specifically, the temperature at the top layer of the tank was 31.5˚C and the temperature at the bottom layer of the tank was 21˚C. The graph shows that there was a decrease in the temperature of the top layers, with water temperature at 12:30 p.m. dropping to 29.5˚C. This dip in temperature indicates that the hot water being delivered through the one-port tube is flowing downwards to the bottom of the tank. This downward movement is due to the water entering the top of the tank being colder than the water at the top layers of the tank. As a consequence, there is a decline in the temperature of the top layers of the tank, which leads to a decrease in the quality of the hot water.

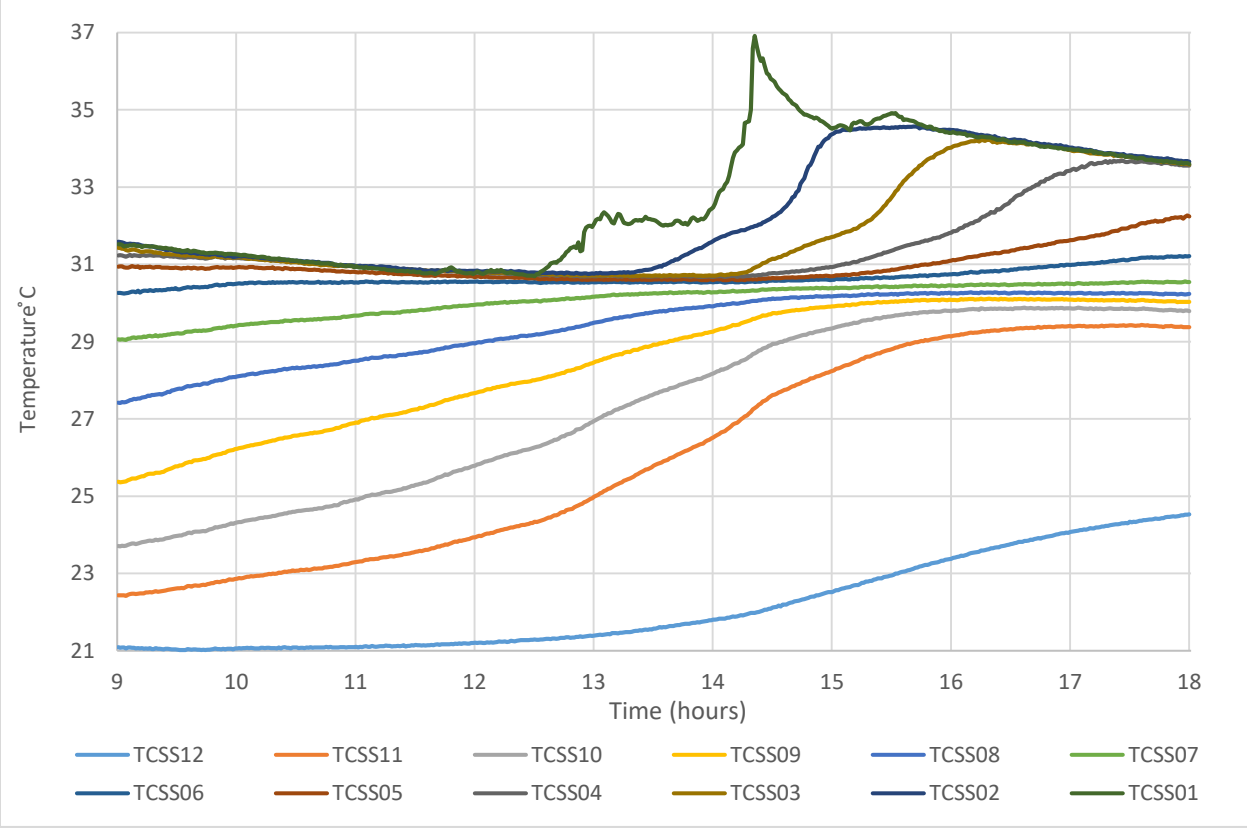


Figure 6-31 Graph showing one-port copper tube inlet device and low average PV power in hot tank conditions.

As illustrated in Figure (6-31), there is an increase in temperature from 1 p.m. to 3 p.m., followed by a steady decrease until the end of the operation. The difference in the temperature of the top layers between the beginning of the test and the highest reading was 5˚C. Thus, the temperature change rate between the highest temperature and the top layers' start-up temperature was 1.1˚C/h, as shown in Table (6-2). This shows us that the copper tube pipe line with one port at the top decreases stratification and would have an impact on the delivery of hot water to consumers early in the morning.

Table 6-2 Temperature Change Rate of the three tank Top Layers Low PV power and Hot Tank Condition.

| 1.5-Inch Diffuser | 4 Ports | 1 Port |
|---|---|---|
| ˚C/h | ˚C/h | ˚C/h |
| 0.5 | 1.8 | 1.1 |

### 6.2.3. Degree of Stratification

Figure (6-32) shows the degree of stratification (DOS) inside the storage tank under hot tank conditions and low PV power heater. From the start of the test until mid-day, the 1.5-inch diffuser does not show any significant change in DOS. However, from mid-day onwards, the DOS increases until reaching a maximum value of 40 DOS, after which it decreases to a value of 31 at the end of the experiment. With the one-port manifold the DOS decreases from 73 at the start to 65 at 12 p.m., reaching a high value of 75 between midday and 2 p.m. Between 2 p.m. and the end of the experiment, the tank with the one-port manifold experiences a sharp decrease in DOS, falling to a value of 53. The figure also shows that the four-port manifold had the highest DOS value early in the morning and topped out at 76 at mid-day. The DOS then started gradually decreasing between noon and 4 p.m., after which it remained at 62 until the end of the experiment.

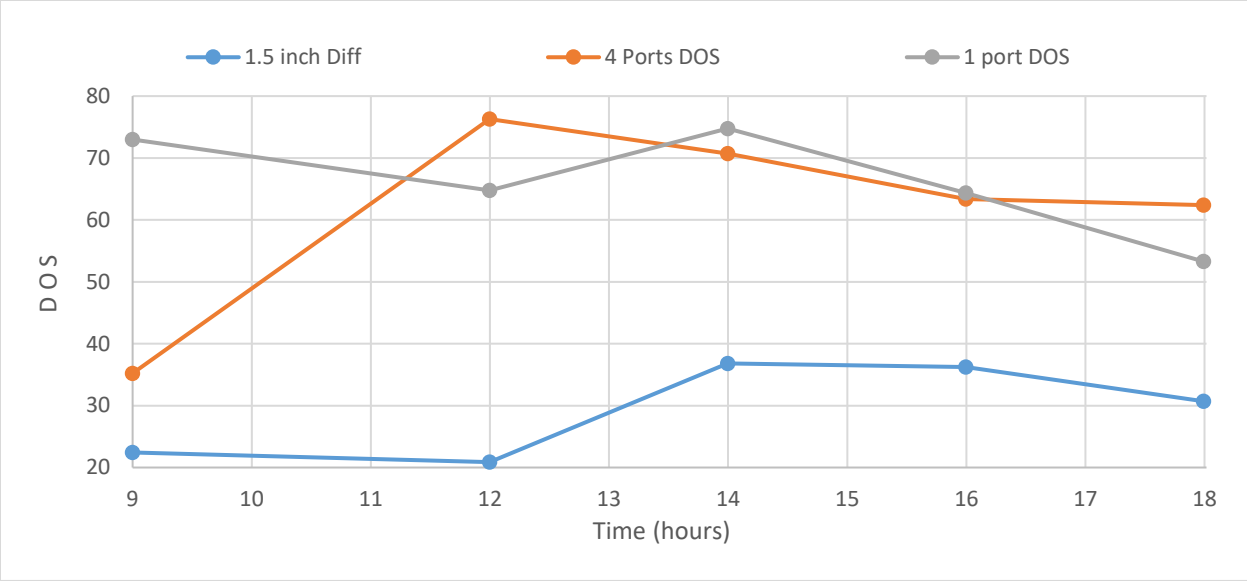


Figure 6-32 DOS of three inlet devices in low average PV power and hot tank conditions.

Figure (6-33) shows the average DOS for the three hot water inlet devices inside the storage tank. The four-port manifold had the highest average DOS from start-up until mid-day and then experienced a decline, reaching the same value as the one-port copper tube by the end of the test. The one-port tube experienced variable average degrees up to the end of the test. However, the 1.5-inch diffuser declined to the lowest value of DOS by mid-day and then increased between 12 p.m. and 2 p.m., after which it maintained a constant low average DOS value of 6 to the end of the experiment.

The DOS is determined by looking at the difference between the slopes of the lines in the thermocline region of the elevation curves. To calculate the degree of stratification in the SDHW tank, the rate of change in temperature per the change in the difference between the layers was determined for all levels. As no precise rules could be found regarding the exact gradient to use for a stratified tank, 5°C/m was chosen as the cut-off measure. Thus, any DOS of less than 5°C/m between two layers was not considered during the evaluation. The sum of DOS of all layers was then taken for each period. Larger number of the sum, the higher quality of stratification [44]. The

average value of DOS was determined using only those values that were greater than 1/10 of the maximum DOS for each period [45].

The graphs in Figures (6-32) and (6-33) illustrate that the four-port manifold has the highest DOS in the tank early in the morning and that it remains relatively unchanged to the end of the test.

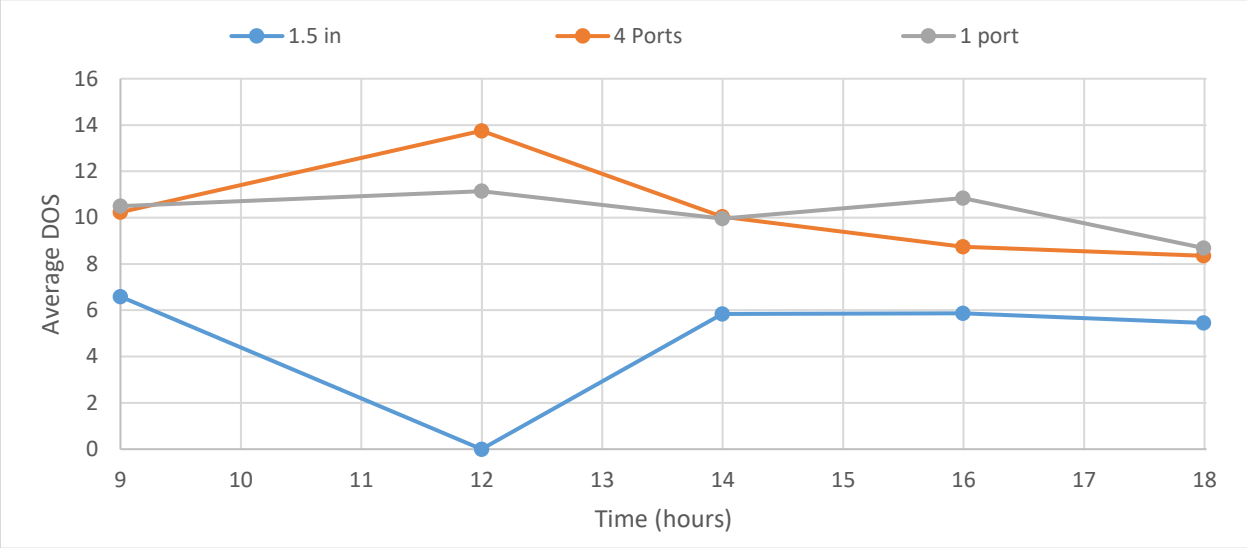


Figure 6-33 Average DOS of three inlet devices in low average PV power and hot tank conditions.

Figure (6-34) shows the temperature distribution in the tank with low PV power heater and a 1.5-inch diffuser inlet device. The temperature curves represent the water temperature at each level at start-up, mid-day, 2 p.m., 4 p.m., and the end of the experiment. At start-up, the temperatures of the tank layers were stratified between 31°C at the bottom of the tank and 36°C at the top. There was no difference between the start-up and 12 p.m. curves. Furthermore, there was a minor decrease in the lower layers and an insignificant increase of 0.2°C in the top four layers. The curves show that these four layers maintained the same temperature and that the temperature change rate for the top layers was very slow. There was only a 2˚C difference in the top layer temperature at start-up and the highest temperature curves. In addition, there was a decrease in the temperature of the top layers at the 4 p.m. curve as well as an increase in that of the lower layers,

which means that the 1.5-inch diffuser acquired a mixture storage tank temperature, leading to a decrease in energy delivery.

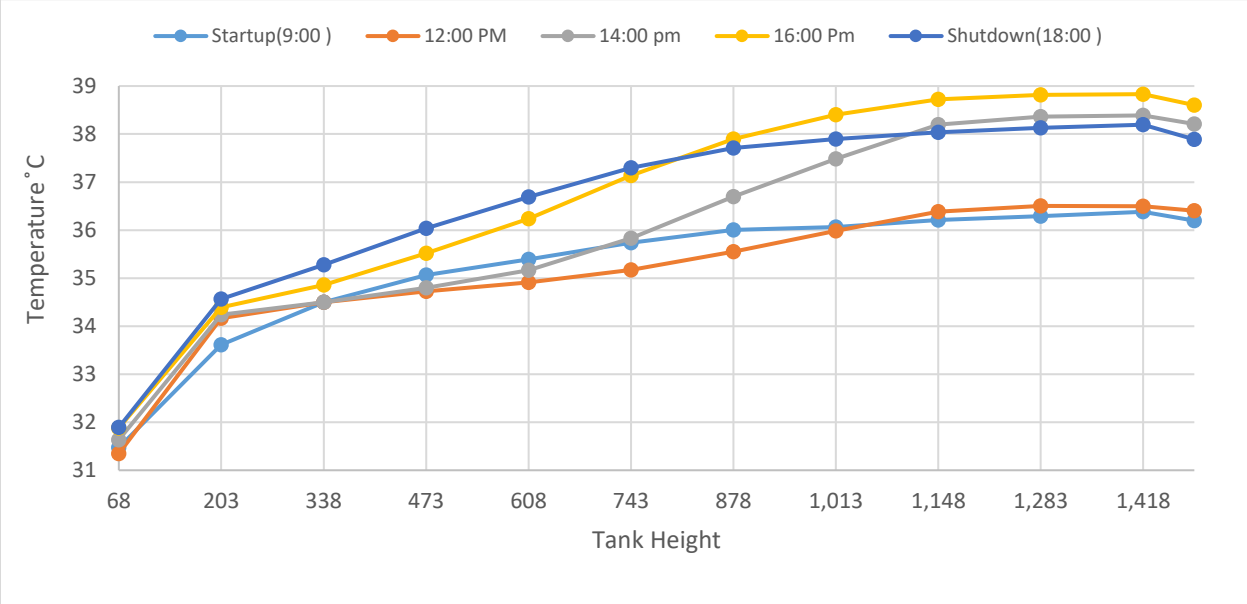


Figure 6-34 Graph showing 1.5-inch diffuser inlet device with low PV power and hot tank conditions.

Figure (6-35) shows the temperature distribution in the tank with low PV power heater and a four-port inlet device. At the start of the experiment, the temperatures of the tank layers were stratified between 22°C at the bottom of the tank and 27°C at the top. There was clear stratification among the curves, with a 7˚C difference between the top layer temperature at start-up and the highest temperature curves. Moreover, the curves show that the four-port manifold strategy responded earlier in the day compared to the traditional designs and maintained a top tank temperature as high as possible. This enhanced the stratification and thus allowed consumers to use hot water early in the morning.

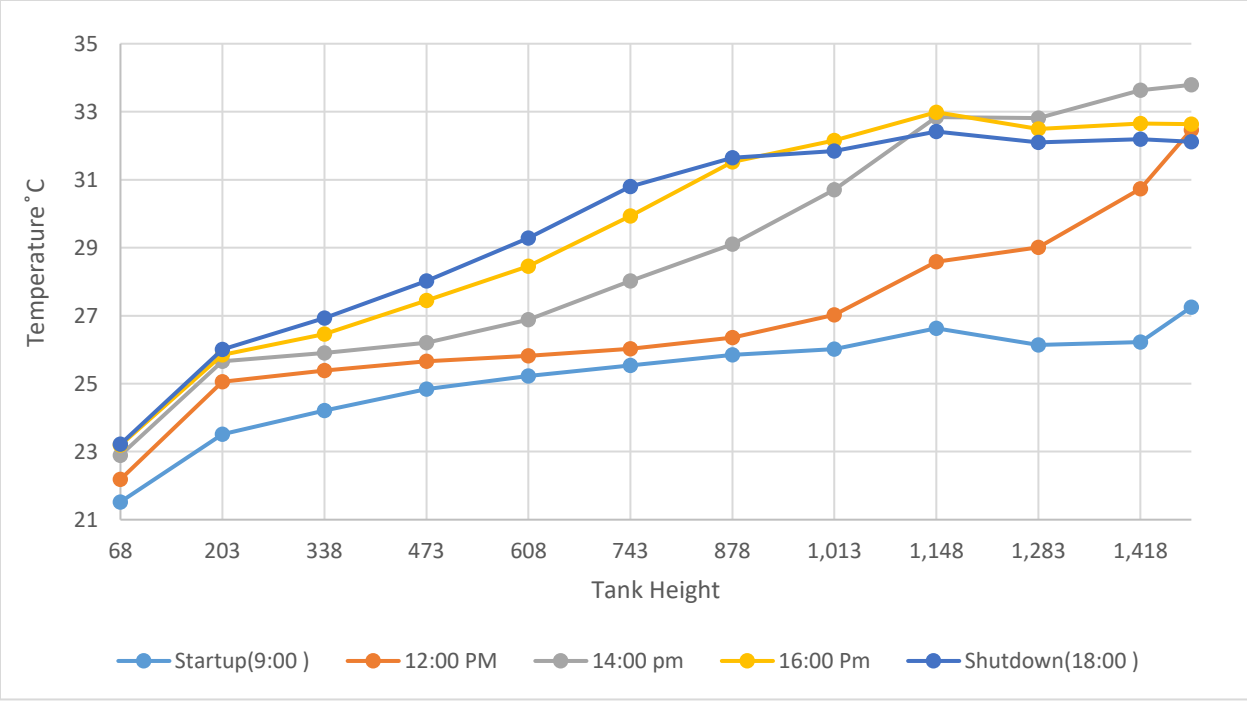


Figure 6-35 Graph showing four-port manifold inlet device with low average PV power and hot tank conditions.

Figure (6-36) shows the temperature distribution in the tank with low PV power heater and a one-port inlet device. At the start, the temperature of the tank layers was stratified between 22°C at the bottom of the tank and 30°C at the top. The curve at 12 p.m. indicates there was a decrease in the top layer temperatures and an increase in the bottom layer temperatures, which means that the delivery hot water was cold compared to the water at the top of the tank. This resulted from the delivery water sinking downward to meet the matched water temperature at the middle and bottom layers. On its way down, it mixed with the warmed water at the top and middle layers and cooled them down. The difference in the top layer temperature at the start-up and the highest temperature curves was 3.6˚C.

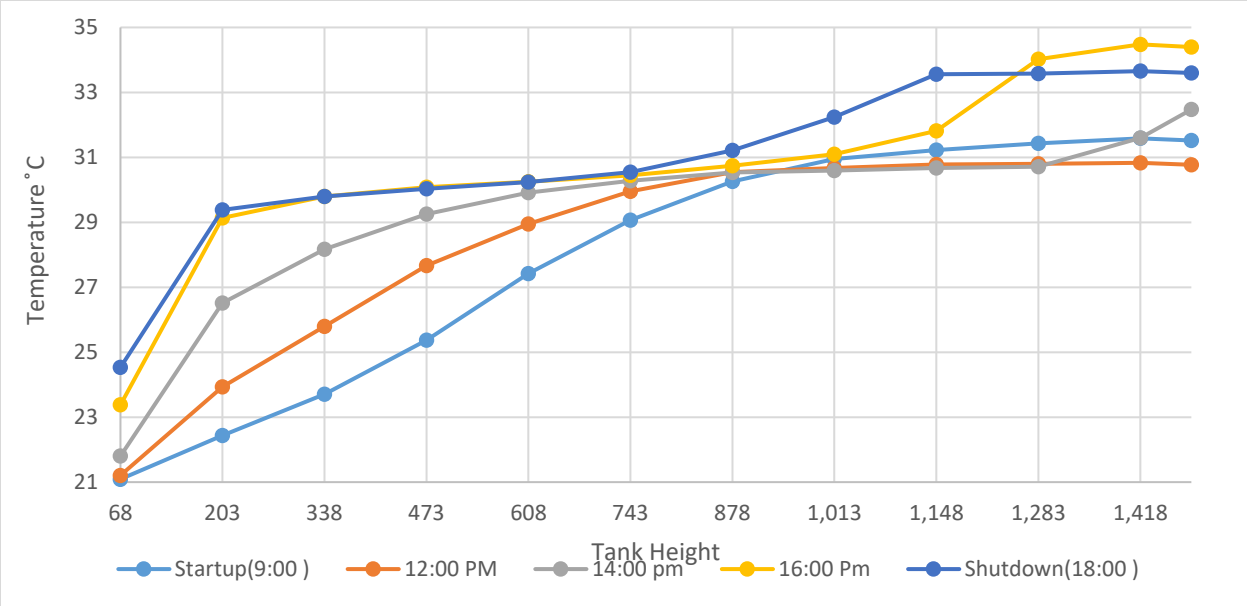


Figure 6-36 Graph showing one-port copper tube inlet device with low PV power and hot tank conditions.

### 6.2.4. Availability and Availability Ratio

The availability ratios were analyzed and discussed for each hot tank condition test using the three inlet devices. Figure (6-37) shows the availability over time in a hot SDHW tank with low PV heater power and three inlet hot water devices. The graph shows that for the 1.5-inch diffuser and one-port inlet devices, there was no significant change in availability from the start of the experiment to 12:30 p.m. However, there was a sharp increase in the availability change for the four-port inlet device between 10 a.m. and 2:30 p.m.

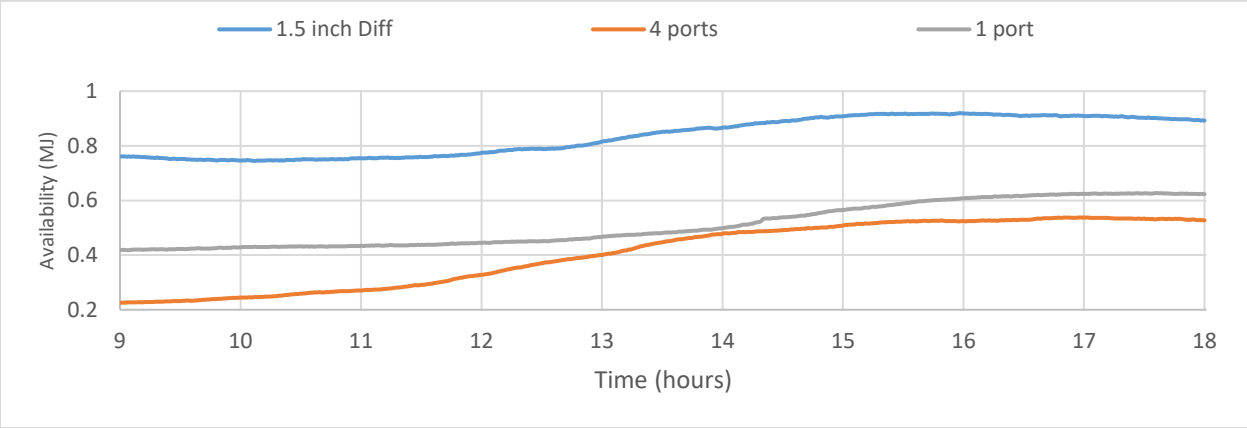


Figure 6-37 Availability of three inlet devices with low average PV power and hot tank conditions.

Figure (6-38) shows availability change, average PV heater power, and average tank temperature for hot tank conditions and three inlet hot water devices. The graph shows that the availability change of the four-port device was the highest at 0.30 MJ, while the one-port tube was 0.20 MJ and the 1.5-inch diffuser was 0.13 MJ. Although the four-port manifold experimental test has the lowest average tank temperature, it was still the best compared to the other hot water inlet devices. When we normalized the PV average power and the tank average temperature, the availability change of the four-port manifold remained the highest value. The availability changes of the 1.5-inch diffuser, four-port manifold and one-port tube were 0.11, 0.31 and 0.22 MJ, respectively.

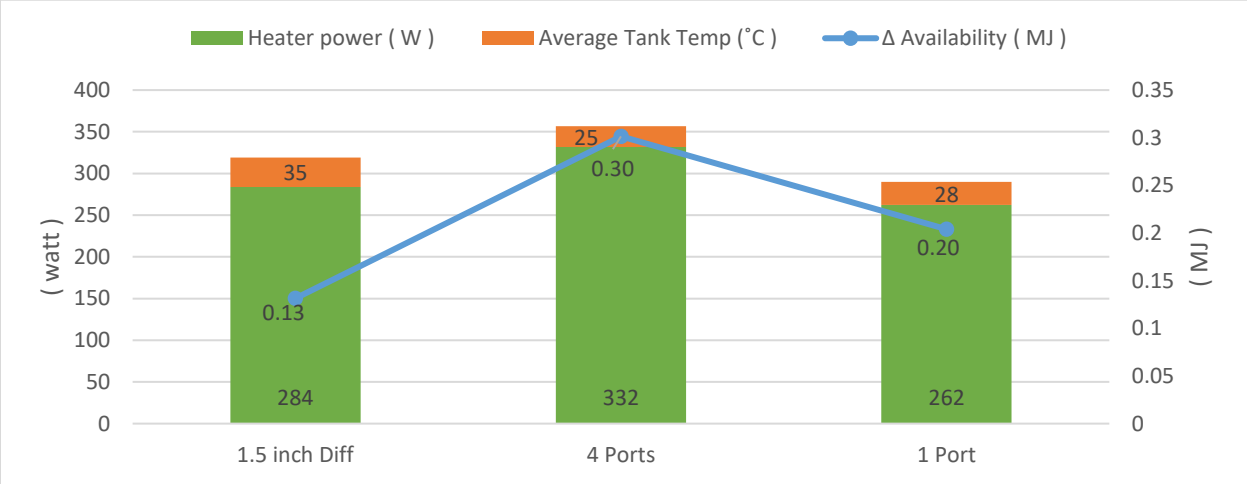


Figure 6-38 Availability change of hot water inlet devices with low average PV power and hot tank conditions.

Figure (6-39) illustrates the availability ratios for the three hot water inlet devices in hot tank conditions and low PV power heater from 9 a.m. to 6 p.m. The graph shows that the availability ratios for the four-port manifold rapidly increased from the test start-up to 1:30 p.m., remained stable until 3:30 p.m., and then slightly decreased to the end of the test period. The graph indicates that the four-port curve held the highest value from the beginning until approximately the end of the experiment. Figure (6-40) shows the average availability ratios of a hot SDHW tank using three hot water inlet devices. The average availability ratios for the 1.5-inch diffuser, four-port and one-

port inlet devices were 0.016, 0.034 and 0.021 MJ, respectively. When we normalized the PV average power and average tank temperature, the availability ratios of the 1.5-inch diffuser, four-port manifold and one-port tube were 0.011, 0.034 and 0.023, respectively.

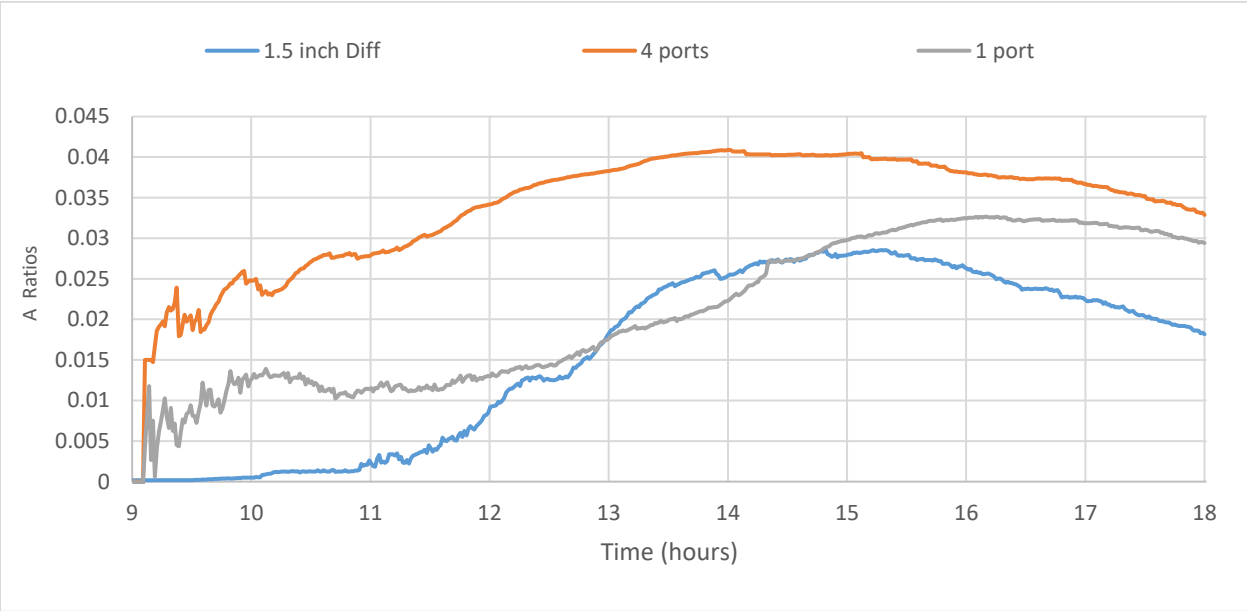


Figure 6-39 Availability ratio of three inlet devices with low average PV power and hot tank conditions.

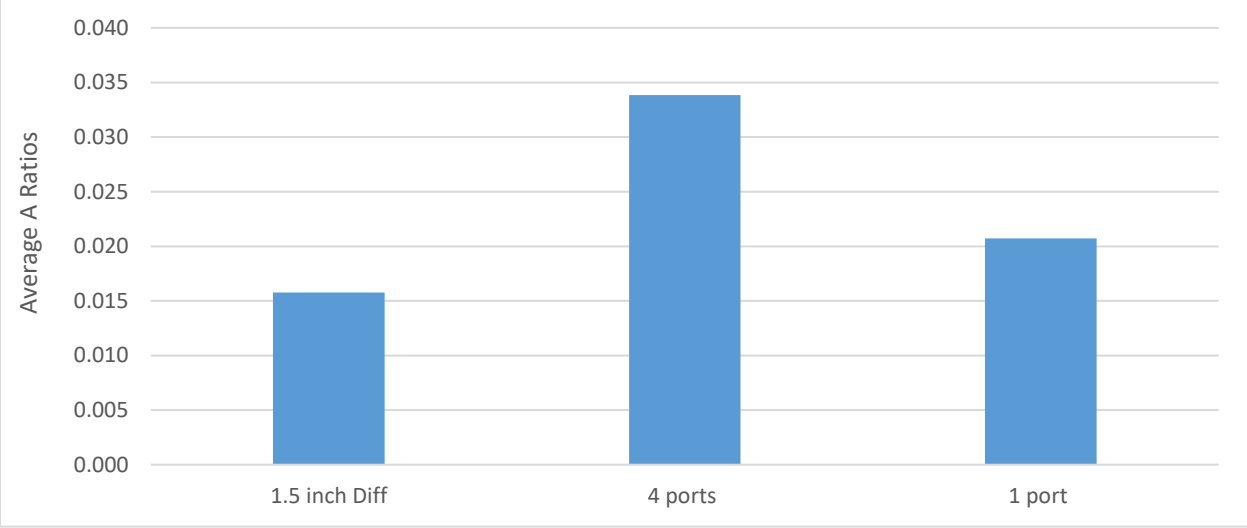


Figure 6-40 Average availability ratio of three inlet devices with low average PV power and hot tank conditions.

### 6.2.5. Entropy

In this part of the experimental tests, the entropy ratios, merit factors, and internal entropy generation were analyzed for each assessment of hot tank conditions and low PV power, using a 1.5-inch diffuser, four-port manifold, and one-port copper tube.

#### 6.2.5.1. Merit Factor

Figure (6-41) shows the calculation of the merit factors from 9 a.m. to 6 p.m. for hot tank conditions and low PV power. The graph illustrates that from the beginning of the experiment until 2:30 p.m., the merit factor for the one-port tube inlet device sharply decreased from 0.5 to 0.07. This was followed by a slight increase from 2:30 to the end of the test, where it became 0.12. Moreover, the graph shows there was no significant change in the 1.5-inch diffuser. In contrast, the four-port inlet device sustained the exact same merit factor until 11:30 a.m. After that time, it experienced a gradual increase until the end of the test, reaching 0.25, as shown in Figure (6-41). The merit factor end results for the 1.5-inch diffuser, four-port and one-port inlet devices were 0.12, 0.25 and 0.18, respectively, as shown in Figure (6-42). When we normalized the PV average power and the average tank temperature, the merit factors for the three aforementioned devices were 0.09, 0.25 and 0.15, respectively. The graph shows that the merit factor change rate of the four-port manifold was the highest. Overall, the merit factor change rate for the 1.5-inch diffuser, four-port manifold and one-port tube was 0.02, 0.14 and -0.21, respectively.

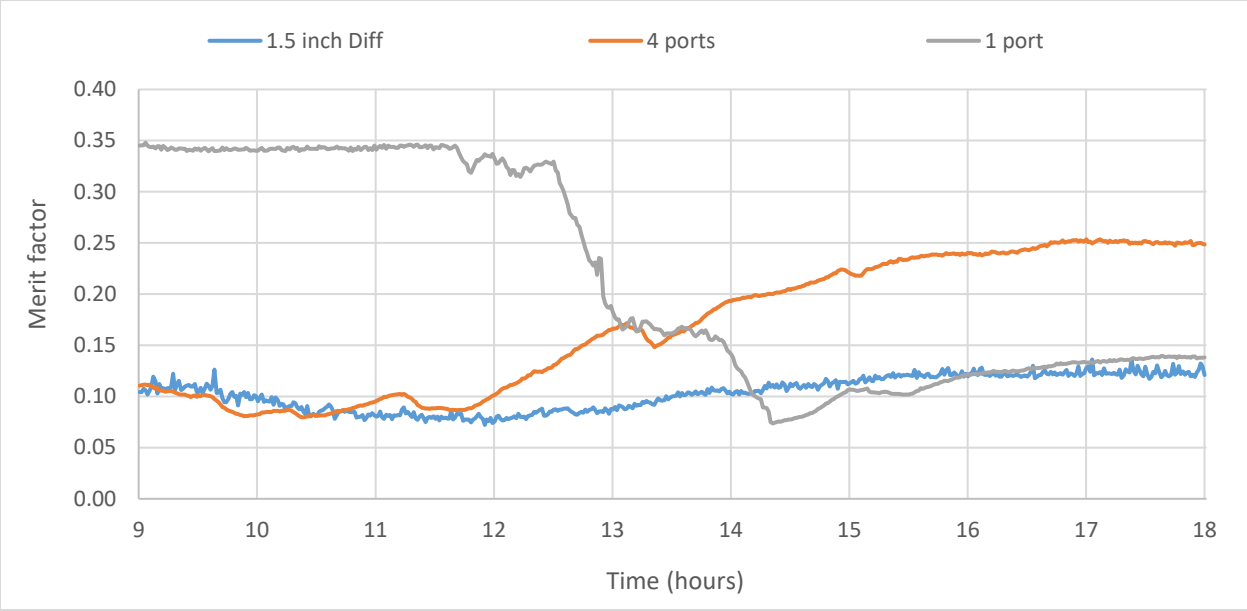


Figure 6-41 Merit factors for the three inlet devices with low average PV power and hot tank conditions.

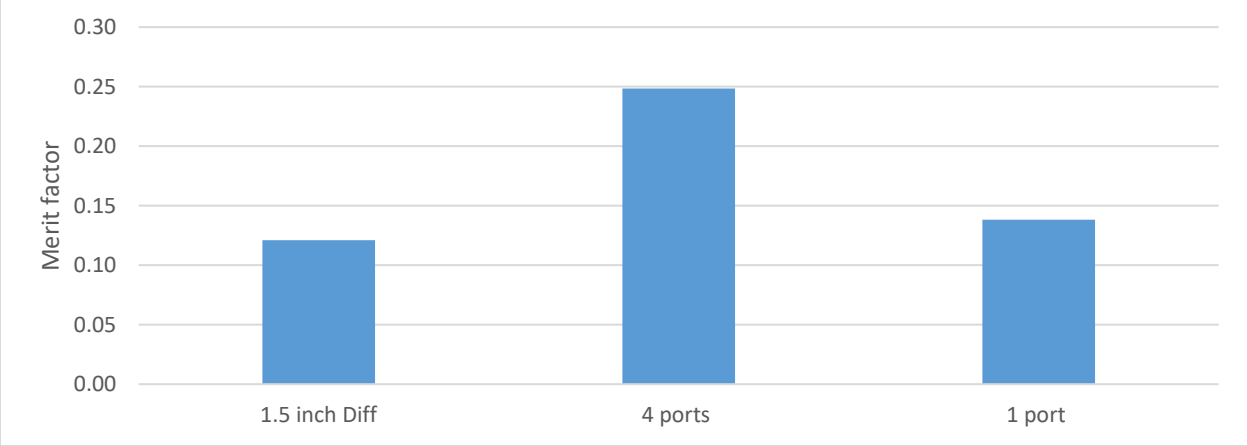


Figure 6-42 Merit factors for inlet device experimental tests with low average PV power and hot tank conditions.

#### 6.2.5.2. Entropy Ratio

Figures (6-43) and (6-44) show the entropy ratios for hot tank conditions and low PV power using the three hot water inlet devices. The entropy ratios for the 1.5-inch diffuser, four-port and one-port inlet devices were 0.9977, 0.9943 and 0.9954, respectively. Compared to the two other designs, the four-port hot water inlet design had lower entropy ratios. Specifically, the difference in entropy ratio between the one-port and four-port hot water inlet designs was 0.0011, which is

quite small. The difference, which was caused by calculation variances among actual entropy, perfect entropy and mixed entropy, had very little to no impact on the final calculations as shown in Figures (6-45a, 6-45b, and 6-45c).

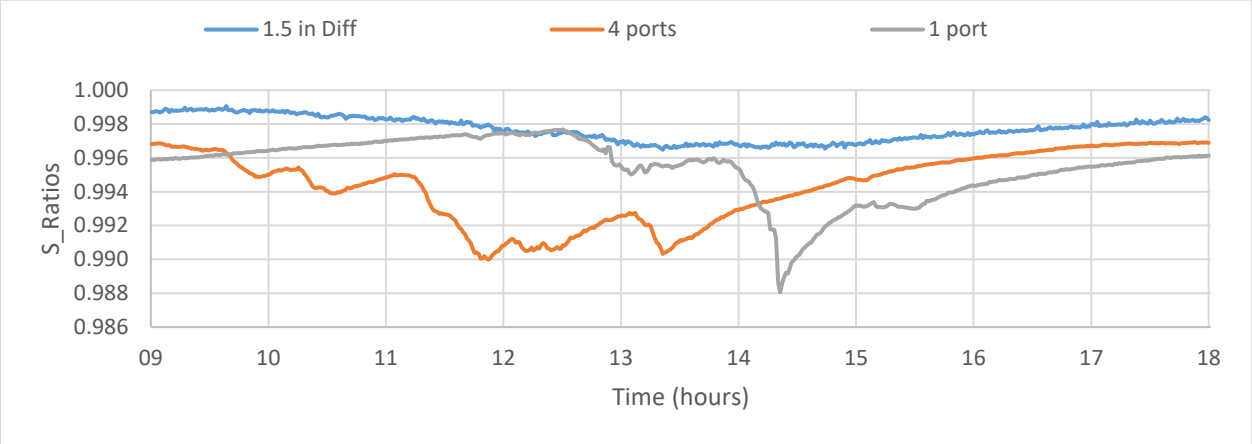


Figure 6-43 Entropy ratios of the three inlet devices with low average PV power and hot tank conditions.

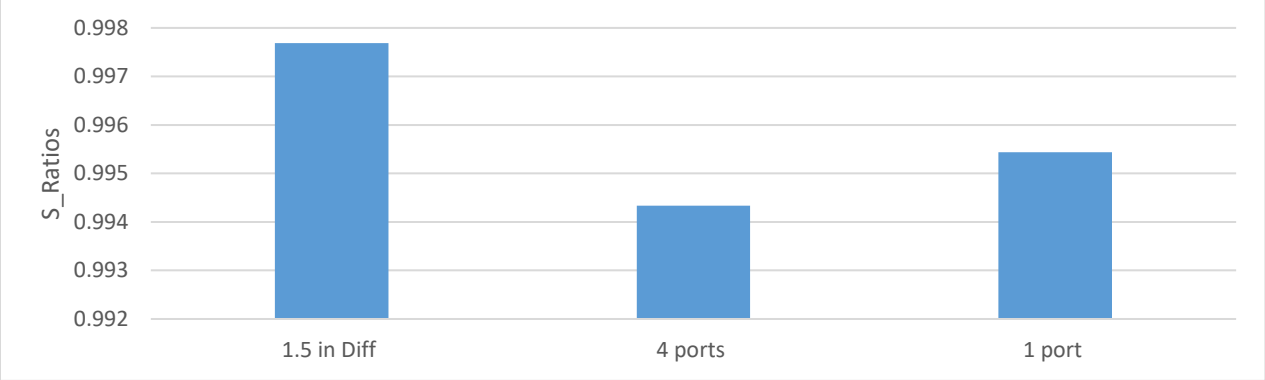


Figure 6-44 Entropy ratios of inlet devices at the end of the test in hot tank conditions and low PV power.

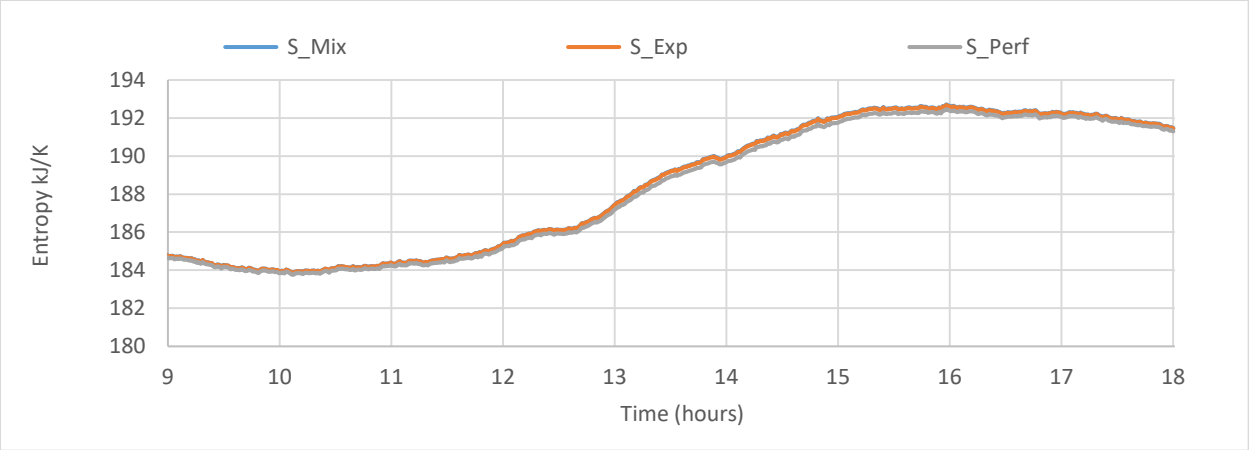


Figure (6-45a). Entropy of 1.5-inch diffuser for three inlet devices in low average PV power and cold tank conditions.

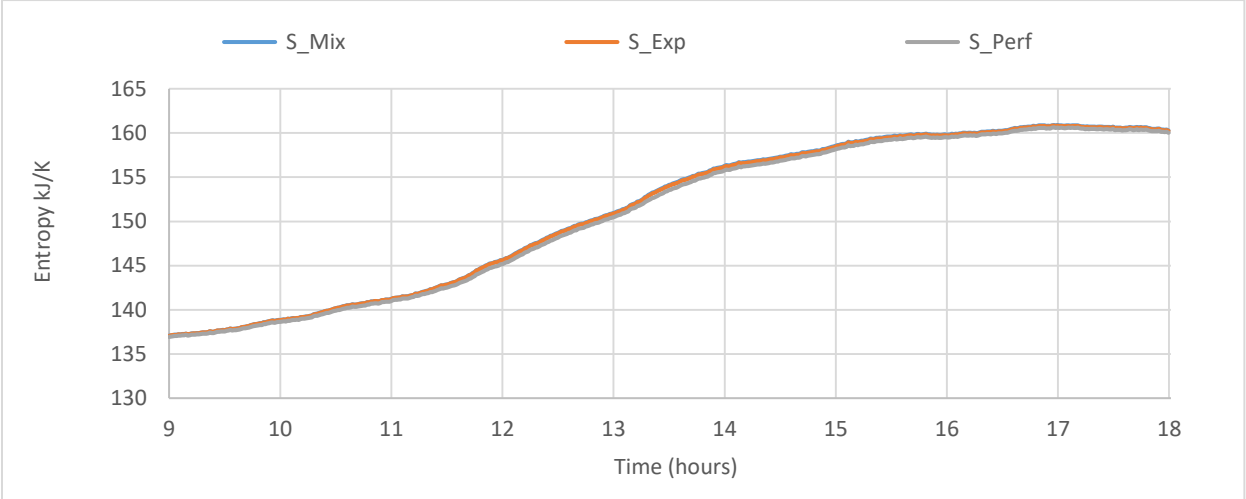


Figure (6-45b). Entropy of four ports manifold for three inlet devices in low average PV power and cold tank conditions.

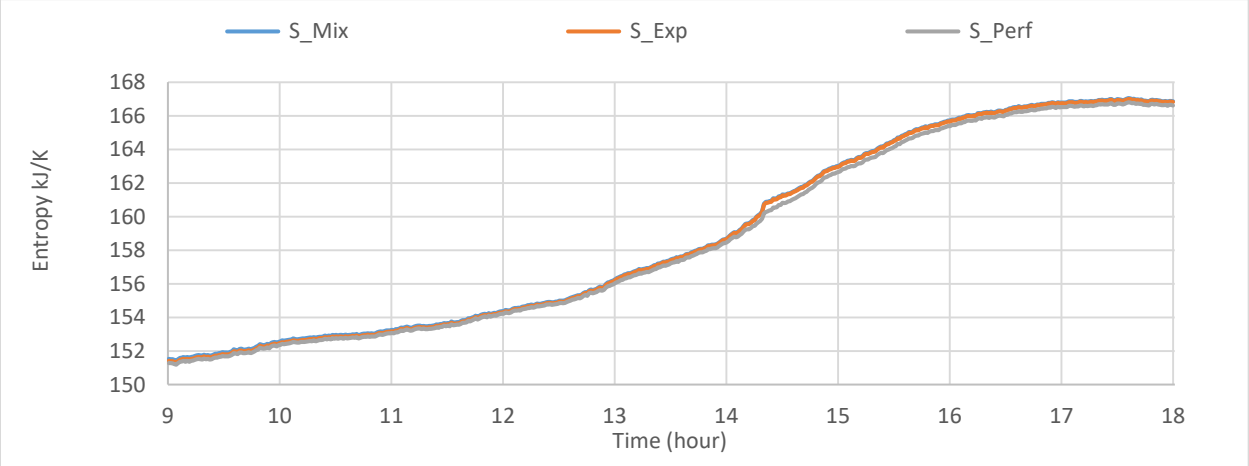


Figure (6-45c). Entropy of one port copper tube for three inlet devices in low average PV power and cold tank conditions.

Figure 6-45 Entropy inside the DHW Tank of three hot water inlet devices

#### 6.2.5.3. Internal Entropy Generation

Figure (6-46) shows the calculation of the internal entropy generation in hot tank conditions and low PV power using the three aforementioned hot water inlet devices. As can be seen, there was a rapid decrease in the levels of internal entropy generation of the four-port inlet device until it reached 0.65 at the end of the experimental test. There was also a slight decrease in the 1.5-inch diffuser, with the value reaching 0.85. However, the complete opposite occurred in the one-port manifold, where the value increased from 0.55 to 0.8. In general, a lower value of internal entropy generation is better.

Figure (6-47) shows the internal entropy generation values at the end of the experimental tests. Compared to the other two, the four-port inlet design had a lower internal entropy generation. Hence, the four-port manifold is the best strategy to use for hot water tanks with less solar energy power. The graph shows that the internal entropy generation change rate of the four-port device was the highest. Overall, the internal entropy generation change rate of the 1.5-inch diffuser, four-port manifold and one-port tube was -0.01, -0.2 and 0.23, respectively.

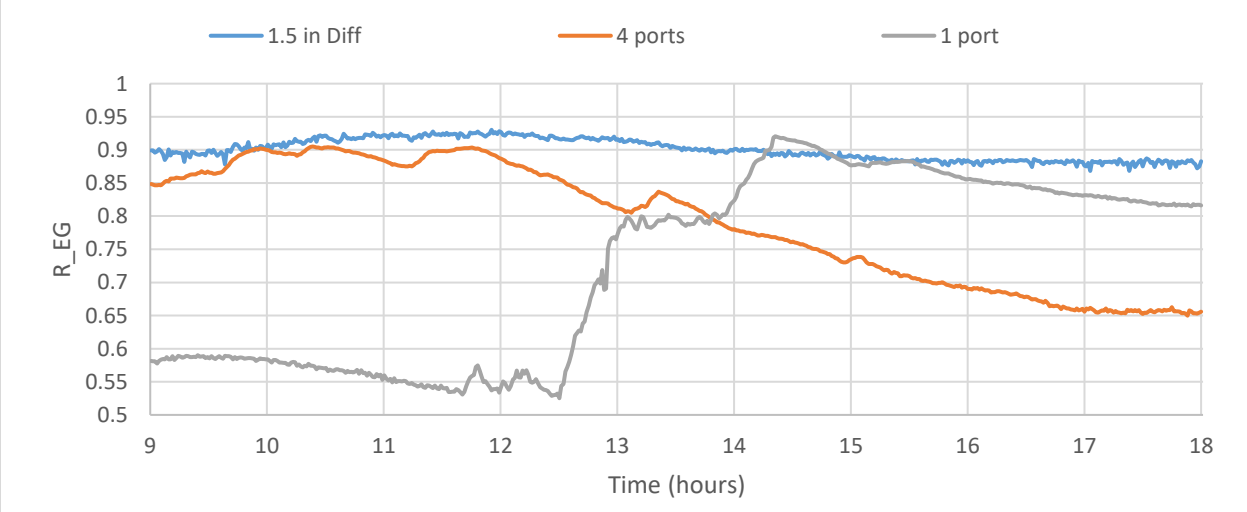


Figure 6-46 Internal entropy of the inlet devices with low average PV power and hot tank conditions.

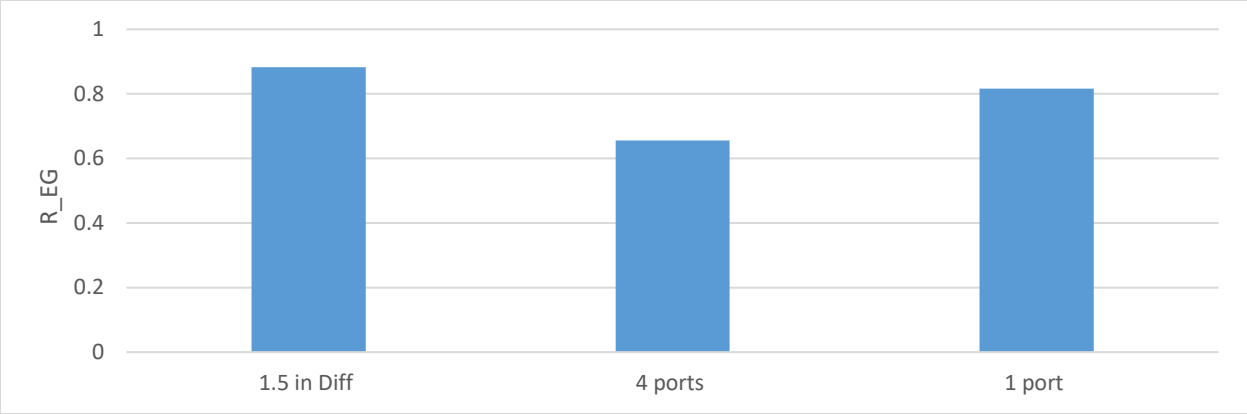


Figure 6-47 Internal entropy generation of inlet devices tests with low average PV power and hot tank conditions.

### 6.2.6. Energy Delivery

Figure (6-48) shows the calculation of the energy delivery in hot tank conditions and low PV power using the three aforementioned hot water inlet devices. At the beginning of the test, the energy delivery for the four-port device was 3.5 MJ and reached a high of 6.5 MJ at 1:30 p.m. When the solar radiation decreased, the energy delivery also slightly decreased from 6.5 to 6 MJ. Moreover, for the 1.5-inch diffuser and one-port inlet devices, the graph shows no change in the delivery energy from the start-up of the experiment until 12:30 p.m., whereas there was an increase in the energy delivery for the four-port device in the morning. In addition, it is worth noting that the difference in the energy delivery for the 1.5-inch diffuser from 1 p.m. until the end of the test was very small. The graph shows that from the beginning of the experiment until 1:30 p.m., the energy delivery for the one-port tube inlet device decreased. This was followed by a slight increase to the end of the operation test, reaching 6.5 MJ.

Figure (6-49) illustrates the change in energy delivery, average PV heater power, and average tank temperature for hot tank conditions using the three hot water inlet devices. The graph shows that the change in energy delivery of the four-port manifold was the highest at 2.3 MJ, and that the one-port tube was 0.9 MJ and the 1.5-inch diffuser 0.7 MJ. When we normalized the PV average

power and the average tank temperature, the energy delivery for the three aforementioned devices were 0.5, 2.4 and 0.9 MJ, respectively. These results indicate that the four-port strategy responds earlier in the day than the traditional designs, thus enhancing stratification and allowing consumers to access hot water early in the day.

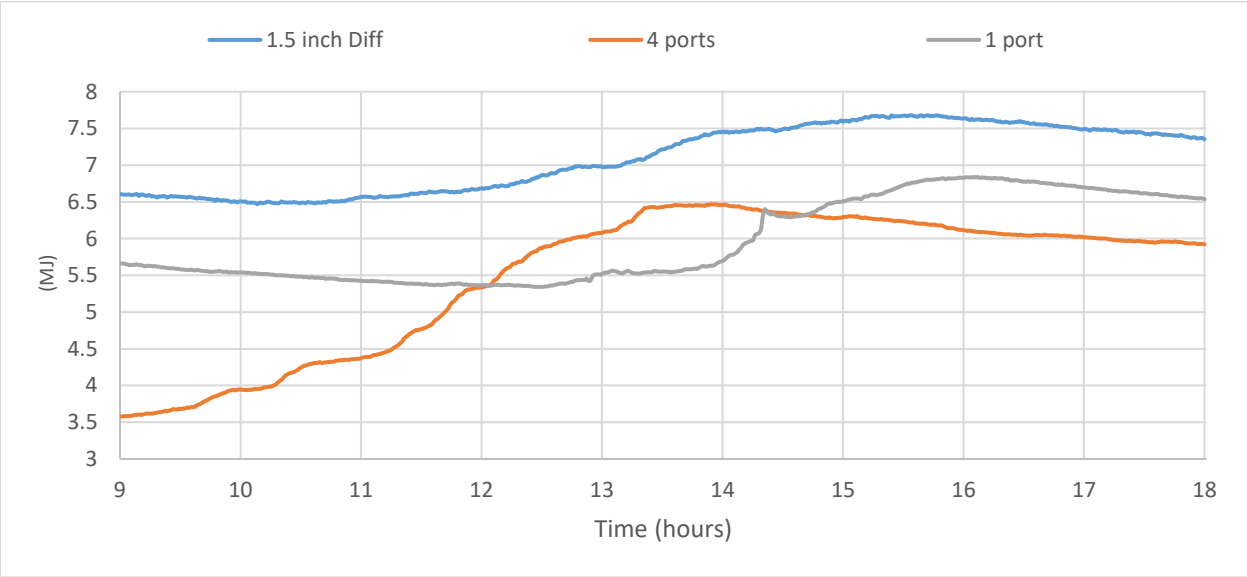


Figure 6-48 Energy delivery of the three inlet devices with low average PV power and hot tank conditions.

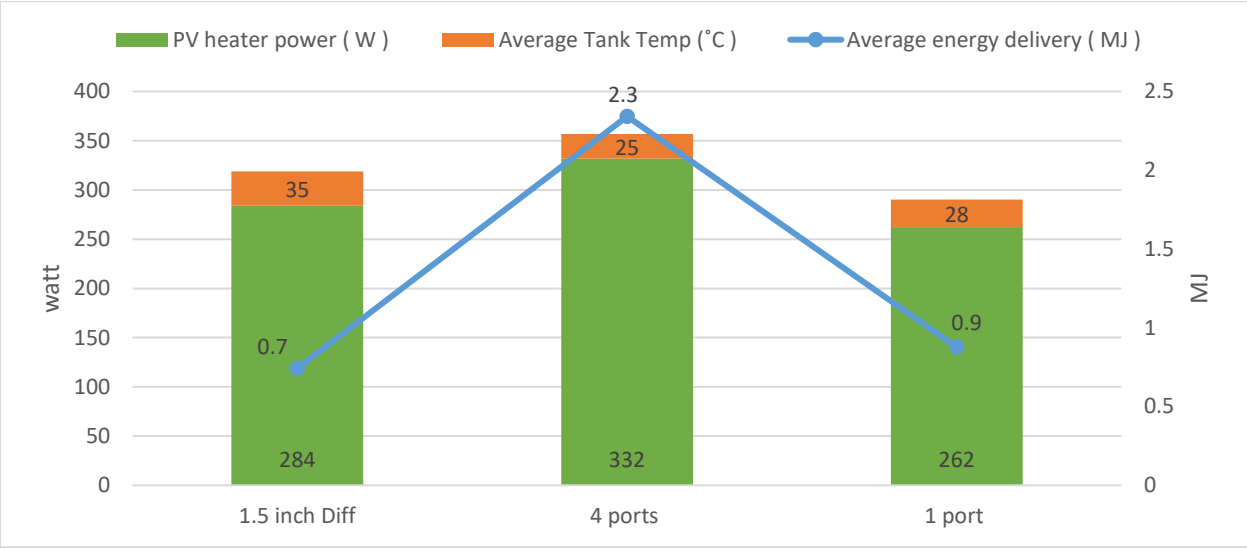


Figure 6-49 Chart showing energy delivery, low PV power, average tank temperature, and hot tank conditions.

## 6.3. Results

Figure (6-50) shows the average PV power and dead-state temperature in cold tank conditions for all the experimental tests, while Figure (6-51) shows the average PV power and average tank temperature in hot tank conditions for the same tests.

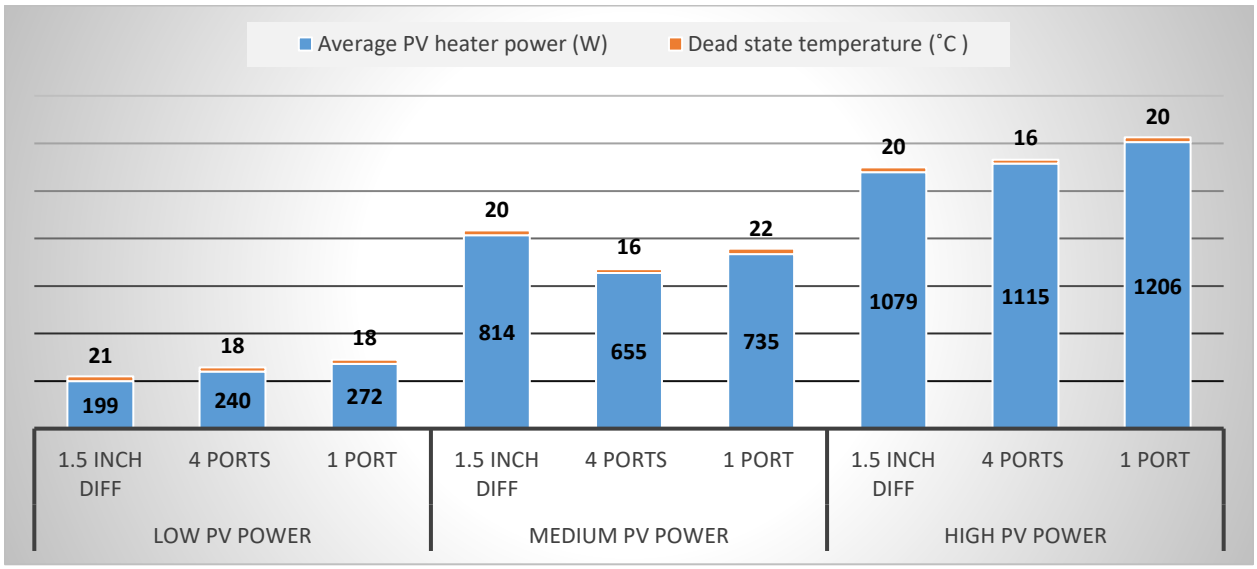


Figure 6-50 Average PV power heater and dead-state temperature in cold tank conditions for all experimental tests.

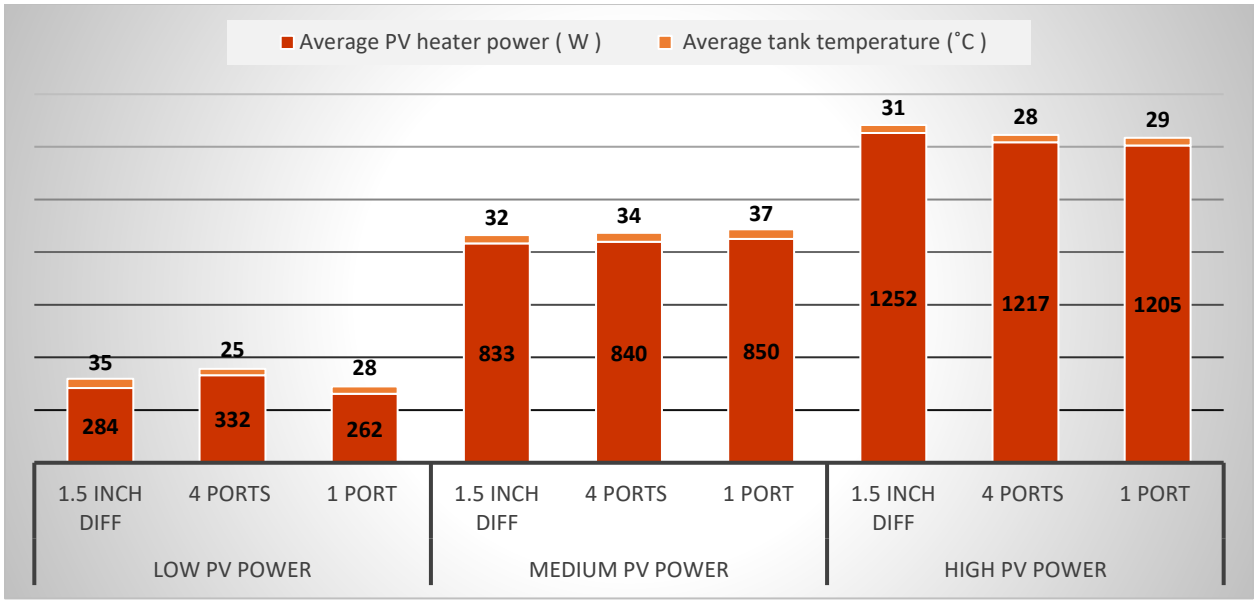


Figure 6-51 Average PV power heater and average tank temperature in hot tank conditions for all experimental tests.

### 6.3.1. Flow Visualization

Flow visualization was used to view the flow of hot water through the inlet devices inside the tank in order to determine the cause of destratification. A color dye, which allowed for the observation of inlet jet mixing and plume entrainment, was inserted into the side-arm heater injection system to visualize the flow pattern from the outlet of the inlet hot water devices. A syringe was used to inject 60 ml of dye into the side-arm heater to visualize the hot water flow pattern inside the domestic hot water tank. A few seconds after the injection the dye, a video camera was used to record the flow pattern.

The first tests were high PV power heater experiments, as shown in Figures (6-52a), (6-52b) and (6-52c). The flow visualization occurred when the side-arm heater and inlet devices injected warmer water into the cold tank. Figures (6-52a) and (6-52b) depict the ink being injected into hot water flowing through a four-port manifold and one-port tube. Most of the hot water delivered through those two inlet devices was distributed horizontally at the top layers of the storage tank. Because the density of the water entering the tank was lower than the water in the tank, the entering water rose to the top of the tank. We observed that the water with highest temperature always rose to the top level of the tank and replaced the dyed layer at the top. This process of circulation enhances stratification in SDHW tanks. However, our observations of the 1.5-inch diffuser indicated that the dye color was delivered in the middle of the tank, a strategy which mixed all the water in the tank and decreased stratification, as shown in the photo in Figure (6-52c).


Figure 6-52 High PV power heater flow pattern from a) four-port, b) one-port and c) 1.5-inch diffuser devices.

The second tests were low PV power heater experiments, as shown in Figures (6-53a), (6-53b) and (6-53c). In these tests, the flow visualization occurred when the outlet hot water temperature varied during the experiment due to fluctuations in solar radiation, causing the temperature of the delivered hot water to be lower than that of the water at the top of the tank. Low heater power often occurs early in the morning or late afternoon due to decreases in the amount of solar radiation energy. When ink was injected into the hot water flowing through the one-port tube or 1.5-inch diffuser devices, we observed that a decrease in the PV power heater input to the side-arm heater led to a decrease in the outlet hot water temperature from the side-arm heater. The delivered water from the side-arm heater had a higher density than the water inside the tank, causing a plume entrainment that led to water mixing and a decrease in thermal stratification, and thus a decrease in energy delivery to consumers. Therefore, using the four-port manifold during solar radiation energy fluctuations caused enhanced stratification in the SDHW tanks, whereas the one-port and 1.5-inch diffuser devices were ineffective at maintaining or establishing thermal stratification.

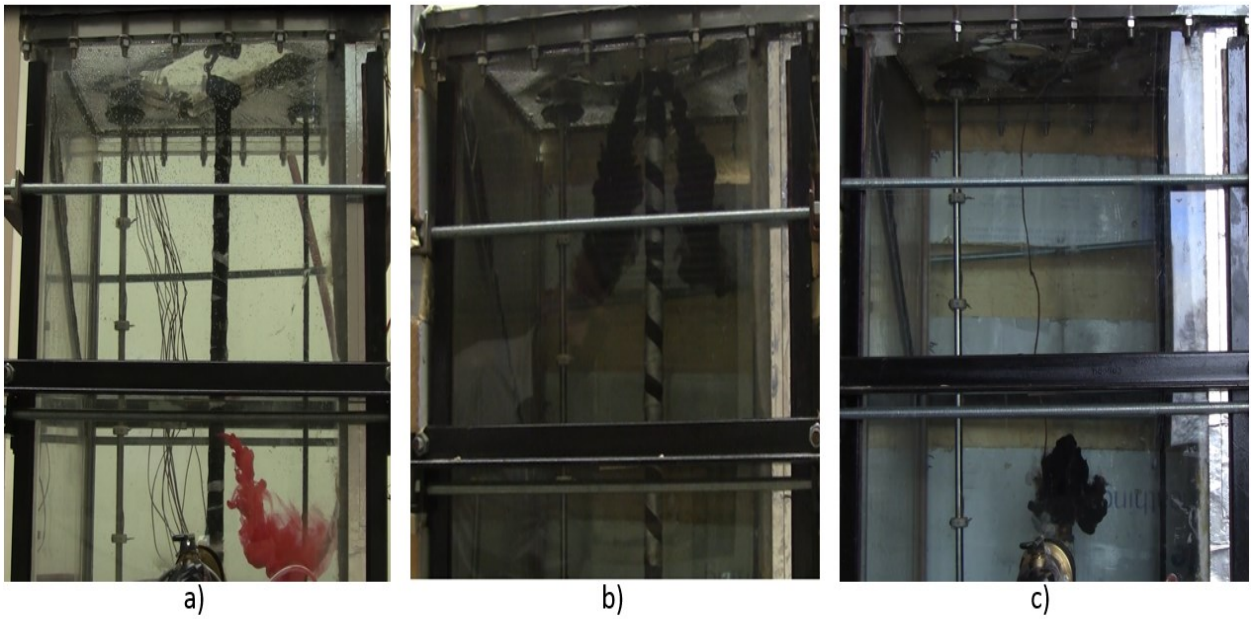


Figure 6-53 Low PV power heater flow patterns from a) 4-port, b) one-port and c) 1.5-inch diffuser devices.

Furthermore, as shown in Figure (6-52b), we noticed that there was a high discharge velocity flow rate when using a one-port copper tube at the top of the storage tank or a four-port manifold under high PV power, which led to destratification. Based on this observation, the exit velocities should be reduced by increasing the resistance in the sidearm loop by using smaller diameter piping, orifices, or a throttling valve to enhance stratification.

### 6.3.2. DOS and Temperature Results

The top layer temperature change rates for the inlet hot water 1.5-inch diffuser were very slow, which led to a decrease in availability and energy delivery. Therefore, consumers would not be able to use hot water early in the morning.

Plume entertainment is often the result of decreases in the amount of solar energy radiation. Using a one-port copper tube at the top of the tank led to a downward-flowing plume, as the water entering the tank was cooler than the water at the top layers of the tank. The downward-flowing plume caused a decline in the temperature of the top layers of the tank, resulting in a decrease in

the quality of the hot water. Thus, the copper tube pipe line design with one port at the top decreases stratification and therefore would have an impact on the delivery of hot water to consumers early in the day.

After studying and comparing all the graphs, it was found that the four-port manifold had the highest degree of stratification as well as the highest change rate for the top tank temperature layers. The four-port design also responded earlier in the day than the other two traditional designs for most of the experimental tests. Furthermore, the four-port manifold maintained a constant level of DOS throughout the experimental tests, which means this type of manifold will enhance stratification in the tank, leading to increased energy levels. During the tests, whenever energy was added to the SDHW tank through the four-port inlet manifold design, there was always a high degree of stratification and high energy delivery to consumers.

Figures (6-54a) and (6-54b) show screen shots of a four-port manifold during testing under cold and hot tank conditions. From these screen shots, we noticed that it was difficult to prove that cold water was being drawn into the manifold from the lower ports at the middle of tank and mixed with hot water delivered from the side-arm heater inside the manifold, leading to decreases in the quality of the hot water delivered to the top of the tank. To prove, we need more accurate temperature measurement instrumentation to measure the water temperature surrounding the manifold ports.

Table 6-3 Temperature Change Rate of the three tank Top Layers for all experimental tests

| PV power average | Tank conditions | 1.5-inch Diffuser | 4 Ports | 1 Port |
|---|---|---|---|---|
| | | ˚C/h | ˚C/h | ˚C/h |
| Low | Cold | 0.7 | 2.8 | 1.8 |
| | Hot | 0.5 | 1.8 | 1.1 |
| Medium | Cold | 2.1 | 5.5 | 7 |
| | Hot | 1.7 | 2.4 | 2.2 |
| High | Cold | 2.4 | 4.2 | 4.3 |
| | Hot | 2.3 | 3.7 | 3.3 |

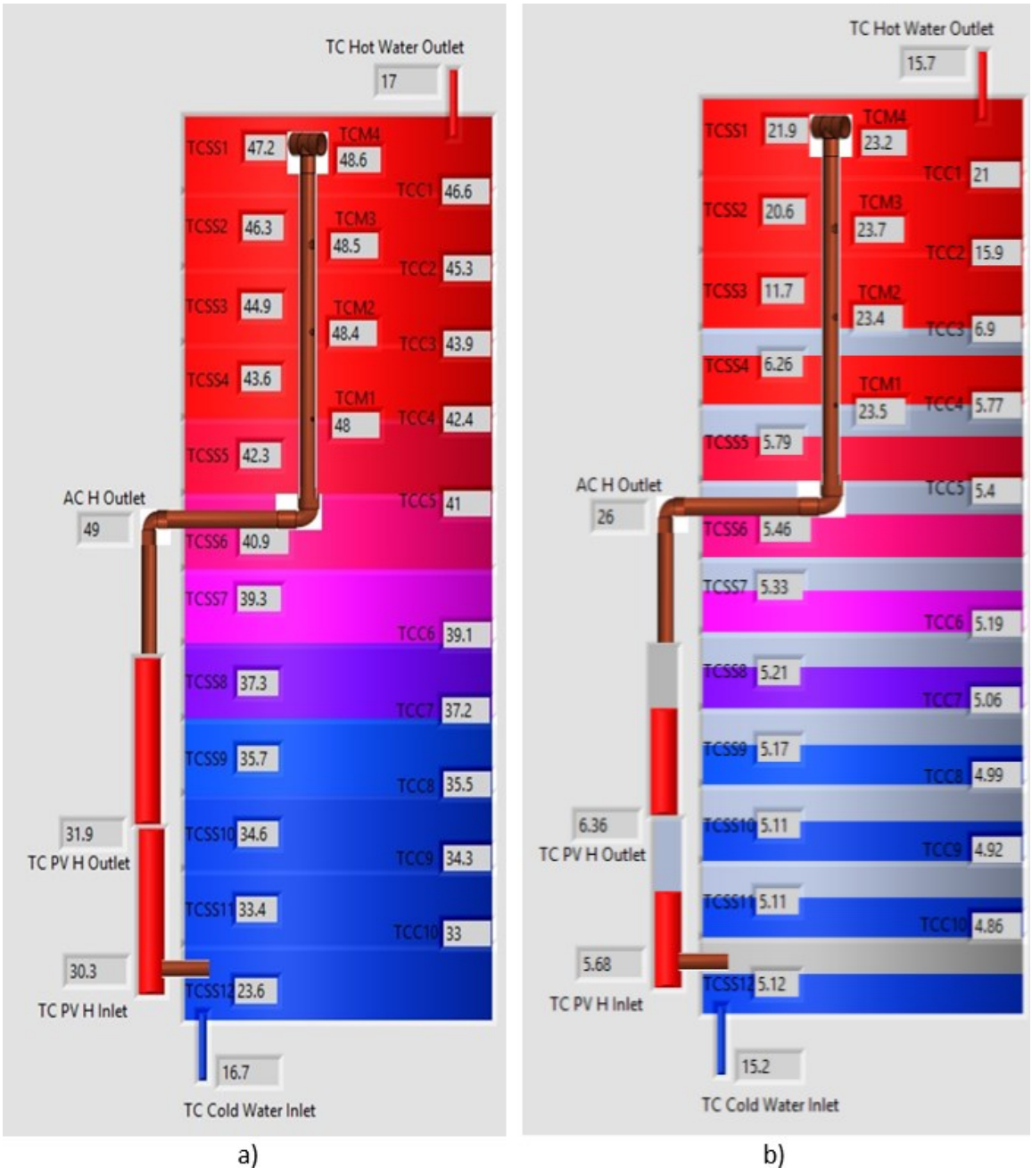


Figure 6-54 Temperature measurements inside a four-port manifold for a) hot tank and b) cold tank conditions.

#### 6.3.2.1. PV heater temperature difference

Figure (6-55) a, b, c and (6-56) a, b, c show the difference between the outlet hot water temperature and inlet cold water temperature to the side-arm PV heating element, when using a 1.5 inch diffuser, a four-port hot water inlet device, and a one-port hot water inlet device using the low, medium, and high PV heater power during cold and hot tank conditions (the position of inlet and outlet PV heater are shown in Figure (4-7)).

The results shows that the higher the PV heater power to the heating element, the greater the temperature difference across the side-arm heater.

Table (6-4) and (6-5) show the one-port hot water inlet device had the highest temperature difference under low and medium PV heater power. This is the result of first the discharge velocity flow rate inside the side arm heater being very slow, and second the location of the discharge port at the top of the tank which causes water to stay for longer periods near the heating element.

Tables 6-4 and 6-5 also show that the four-port manifold had a higher temperature difference across the side-arm PV heater than the one-port under high PV power.

Table 6-4 Temperature difference across the heater, and PV power under all tests for a cold tank condition.

| Cold Tank Conditions | | | | | | | | |
|---|---|---|---|---|---|---|---|---|
| | | | Power (W) | | | ΔT (°C) | | |
| | Figure # | Time | 1.5 Diff | 4 port | One port | 1.5 Diff | 4 port | One port |
| Low | 6-51 a | 01:05 | 166 | 373 | 377 | 5.1 | 7.8 | 8.5 |
| Medium | 6-51 b | 11:03 | 400 | 927 | 720 | 7 | 12.6 | 13.2 |
| High | 6-51 c | 01:28 | 1547 | 1531 | 1421 | 18.5 | 20.3 | 18.9 |

Table 6-5 Temperature difference across the heater, and PV power under all tests for a hot tank condition.

| Hot Tank Conditions | | | | | | | | |
|---|---|---|---|---|---|---|---|---|
| | | | Power (W) | | | ΔT (°C) | | |
| | Figure # | Time | 1.5 Diff | 4 port | One port | 1.5 Diff | 4 port | One port |
| Low | 6-52 a | 10:55 | 233 | 223 | 200 | 5.7 | 6.2 | 8.2 |
| Medium | 6-52 b | 16:17 | 659 | 522 | 861 | 9 | 11.3 | 13.8 |
| High | 6-52 c | 11:00 | 1225 | 1560 | 1542 | 13.9 | 19 | 17.3 |

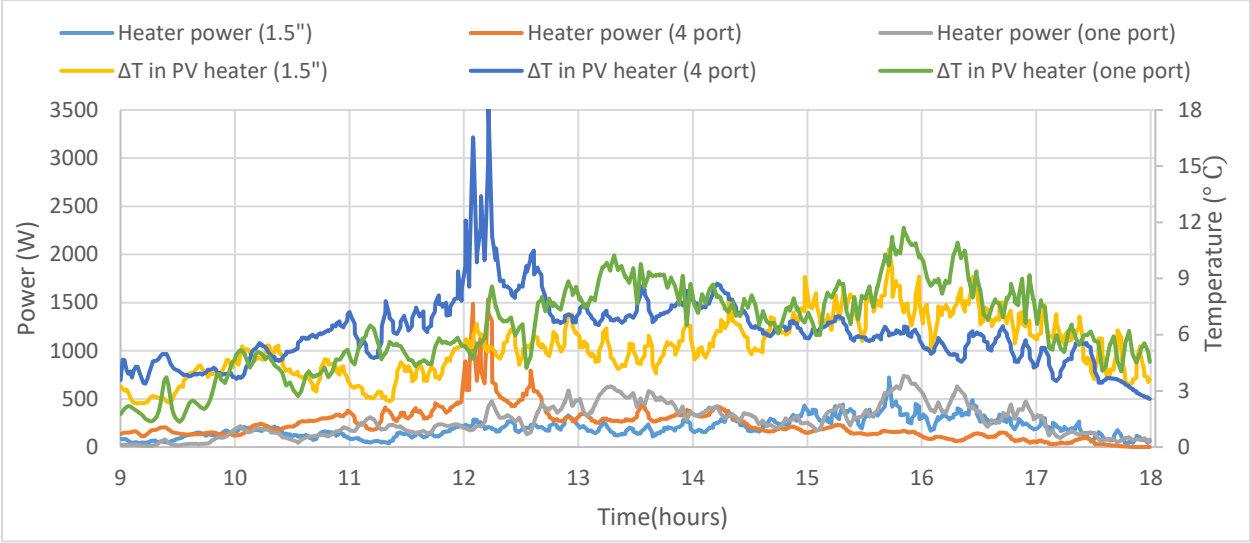


Figure 6-55 a PV heater temperature difference during low PV power of all devices of cold tank condition

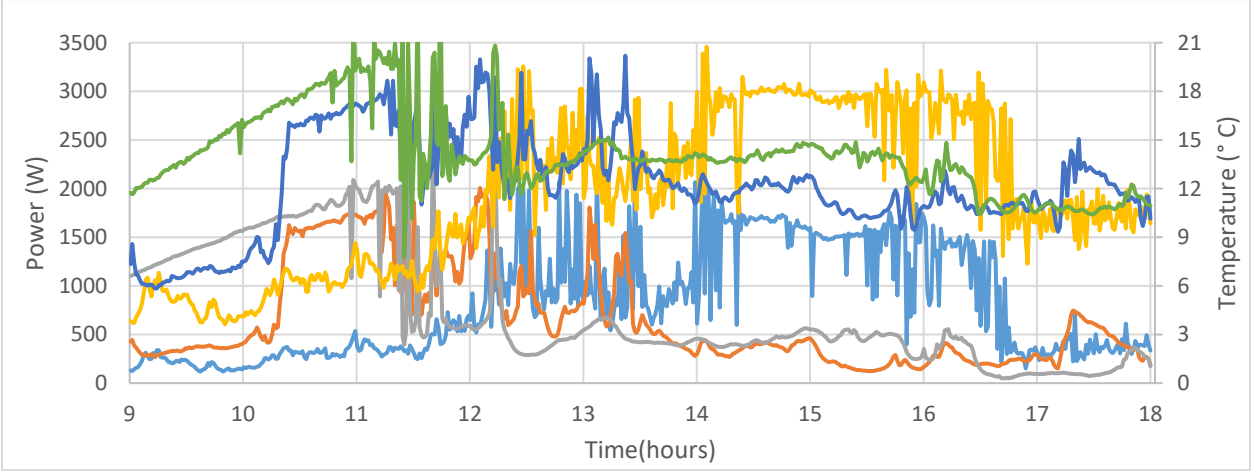


Figure 6-55 b PV heater temperature difference during medium power of all devices of cold tank condition

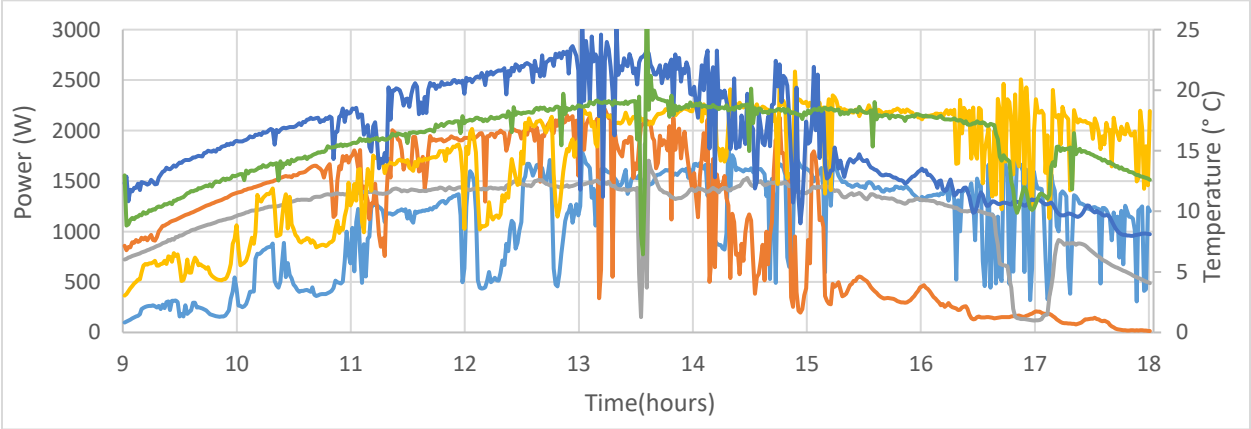


Figure 6-55 c PV heater temperature difference during high PV power of all devices of cold tank condition

Figure 6-55 PV heater temperature difference for cold tank condition for all power categories tests

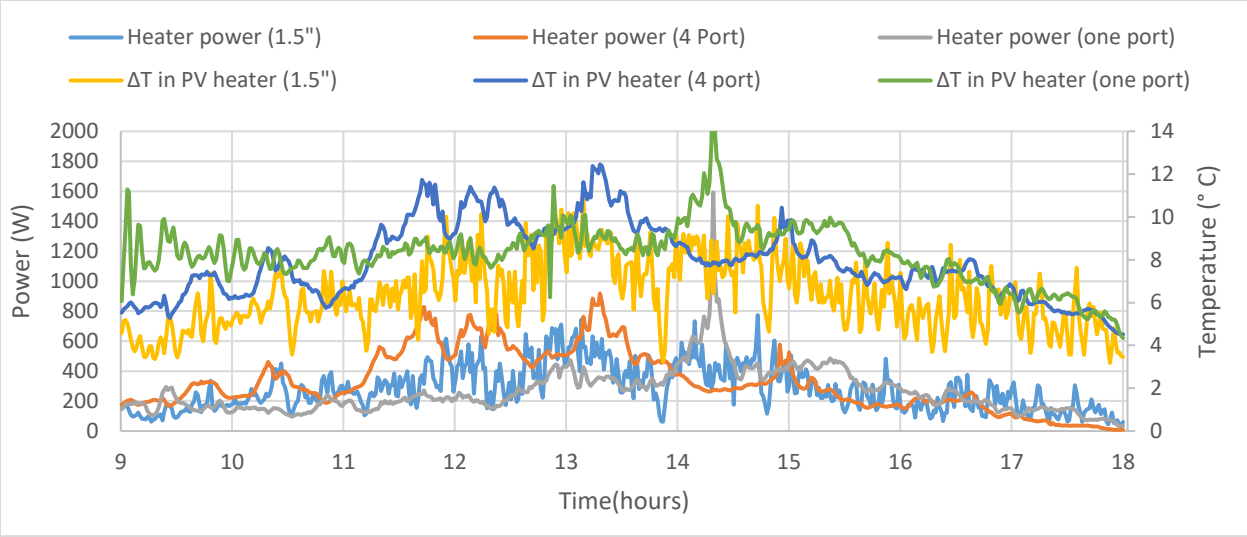


Figure 6-56 a PV heater temperature difference during low PV power of all devices of hot tank condition

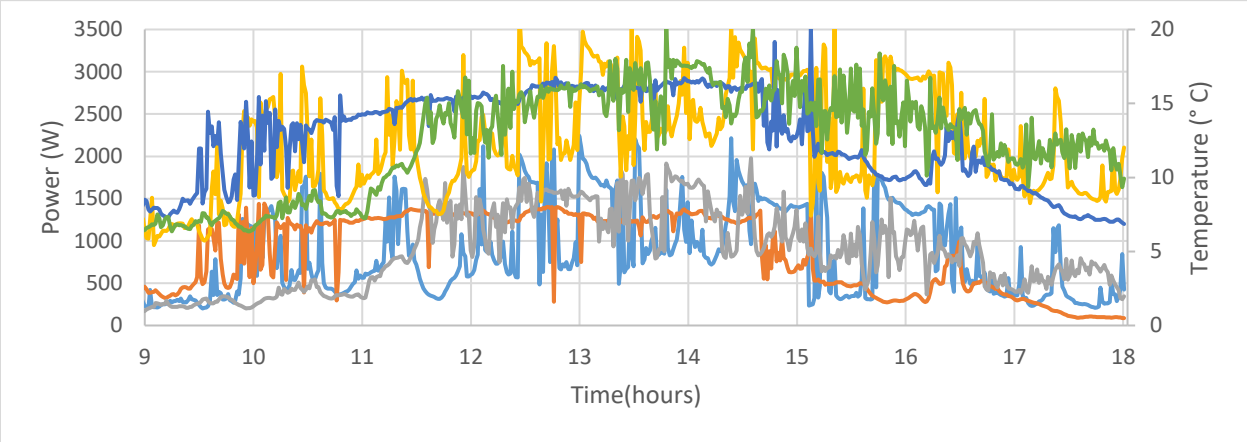


Figure 6-56 b PV heater temperature difference during medium power of all devices of hot tank condition

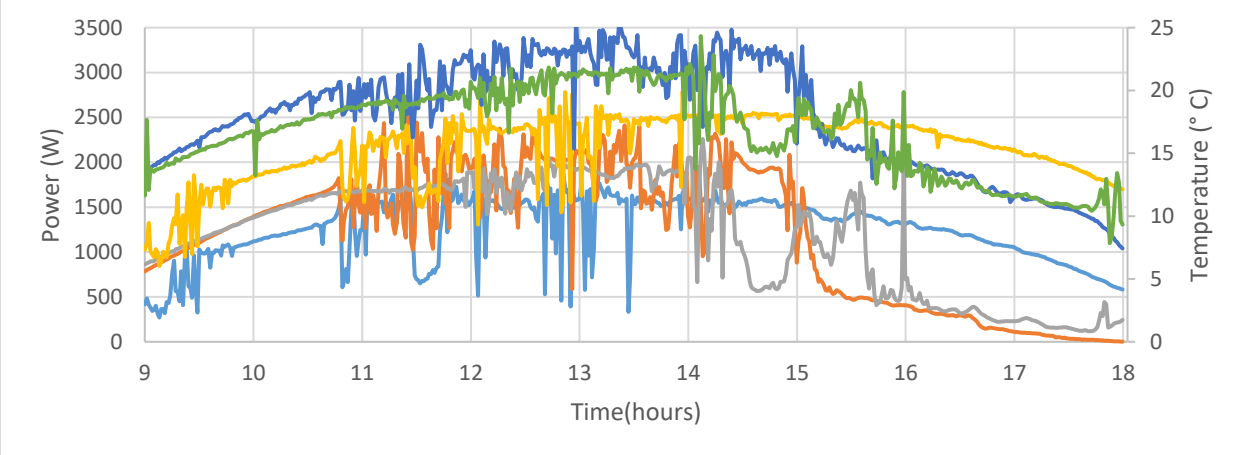


Figure 6-56 c PV heater temperature difference during high PV power of all devices of hot tank condition

Figure 6-56 PV heater temperature difference for cold tank condition for all power categories tests

### 6.3.3. Availability

#### 6.3.3.1. Change in Availability

When comparing the thermal performance of the inlet hot water devices for cold or hot storage tanks, we have to consider in our evaluation the average PV power heater value and the dead-state temperature for cold tank conditions, as well as the average tank temperature for hot tank conditions. To make a good evaluation a normalization was performed. Normalization is to bring all the PV power values, dead state temperatures for a cold tank, and average tank temperatures for hot tank conditions to an equal level for comparison. For example, the normalization of availability change is shown in table (6-6).

Table 6-6 Normalization of availability change for low, medium, and high PV power under cold tank condition

| Availability Change (MJ) | | | | | | | | | |
|---|---|---|---|---|---|---|---|---|---|
| Cold Tank Condition | | | | | | | | | |
| | Low PV Power | | | Medium PV Power | | | High PV Power | | |
| | Diff | 4 port | 1 port | Diff | 4 port | 1 port | Diff | 4 port | 1 port |
| Experimental result | 0.09 | 0.13 | 0.15 | 0.77 | 0.59 | 0.62 | 1.27 | 1.26 | 1.37 |
| Heater average power W | 199 | 240 | 272 | 814 | 655 | 735 | 1079 | 1115 | 1206 |
| Normalization power | 0.11 | 0.13 | 0.13 | 0.7 | 0.66 | 0.62 | 1.31 | 1.26 | 1.27 |
| Dead State $T_0$ ˚C | 21 | 18 | 18 | 20 | 16 | 22 | 20 | 16 | 20 |
| Normalization dead state | 0.09 | 0.13 | 0.13 | 0.7 | 0.83 | 0.56 | 1.31 | 1.58 | 1.27 |

The results from the availability change rate, as shown in Figure (6-57), show that the four-port hot inlet device availability was the best option for all average PV heater power in cold and hot tank conditions.

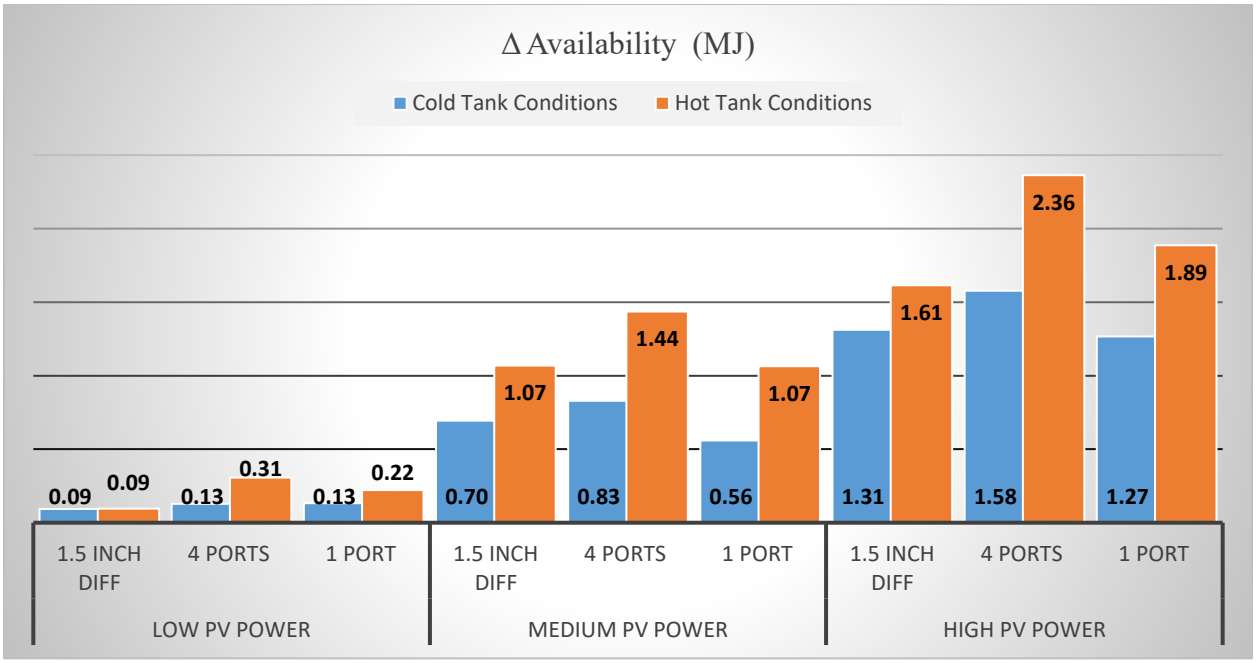


Figure 6-57 Availability change in cold and hot tank conditions for all experimental tests.

### 6.3.3.2. Availability Ratios

As a result of the thermal performance parameter plots of availability ratios as shown in Figure (6-58), the four-port manifold is suitable for use with all average PV power loads in both cold and hot tank conditions.

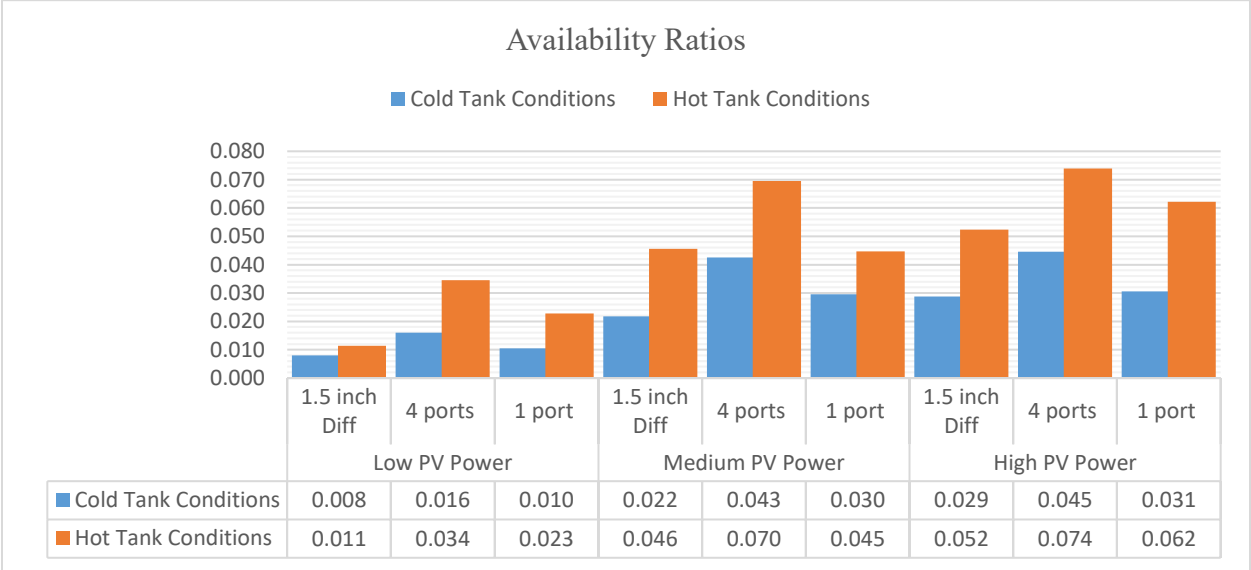


| | | | | | | | | | |
|---|---|---|---|---|---|---|---|---|---|
| Cold Tank Conditions | 0.008 | 0.016 | 0.010 | 0.022 | 0.043 | 0.030 | 0.029 | 0.045 | 0.031 |
| Hot Tank Conditions | 0.011 | 0.034 | 0.023 | 0.046 | 0.070 | 0.045 | 0.052 | 0.074 | 0.062 |

Figure 6-58 Average availability ratios of cold and hot tank conditions for all experimental tests.

### 6.3.4. Energy Delivery

Figure (6-59) shows the delivered energy calculations for cold and hot tank conditions in all experimental tests. The four-port hot water inlet device had the highest energy delivery value when using low, medium, and high average PV power for cold or hot tank conditions.

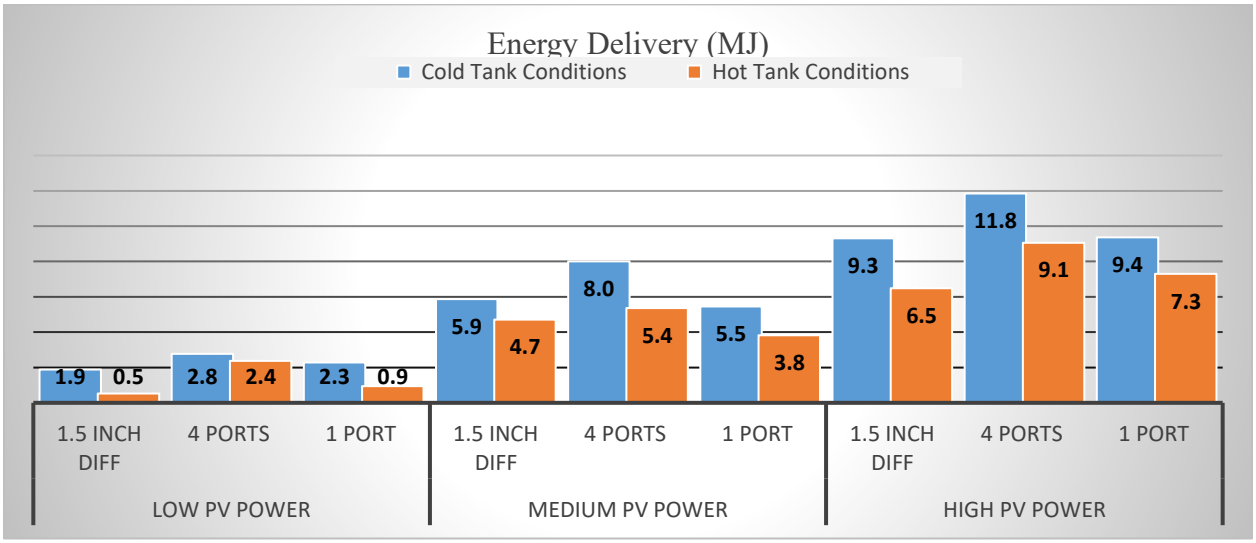


Figure 6-59 Energy delivery in cold and hot tank conditions for all experimental tests.

### 6.3.5. Entropy

#### 6.3.5.1. Merit Factors

Figure (6-60) shows the merit factor calculations for cold and hot tank conditions in all experimental tests. The four-port hot water inlet device had the highest merit factors value when using low average PV power for both cold and hot tank conditions and medium average PV power for cold tank conditions. However, the calculation of the thermal performance of merit factors showed that the one-port hot water inlet device had the highest merit factor for high average PV power and hot tank conditions. The difference between the one port and the four-port hot water inlet device was 0.01 MJ. Also, the 1.5-inch inlet device had the highest merit factor when using a medium average PV power heater for a hot tank and a high average PV power heater for a cold

tank. The difference between the 1.5-inch diffuser and the four-port hot water inlet device was 0.03 MJ.

In addition, and for further clarification, Figure (6-61) shows the merit factors of a 1.5-inch diffuser. This device started at a higher value than the other hot water inlet devices but then declined until mid-day. From noon until 1:30 p.m., there was a slight increase, after which the readings remained approximately unchangeable until the end of the experimental test. The merit factor change rates for the 1.5-inch diffuser, four-port manifold and one-port tube under medium average PV power and hot tank conditions were -0.06, 0.07 and -0.04, respectively, indicating that the four-port device gave the best outcome.

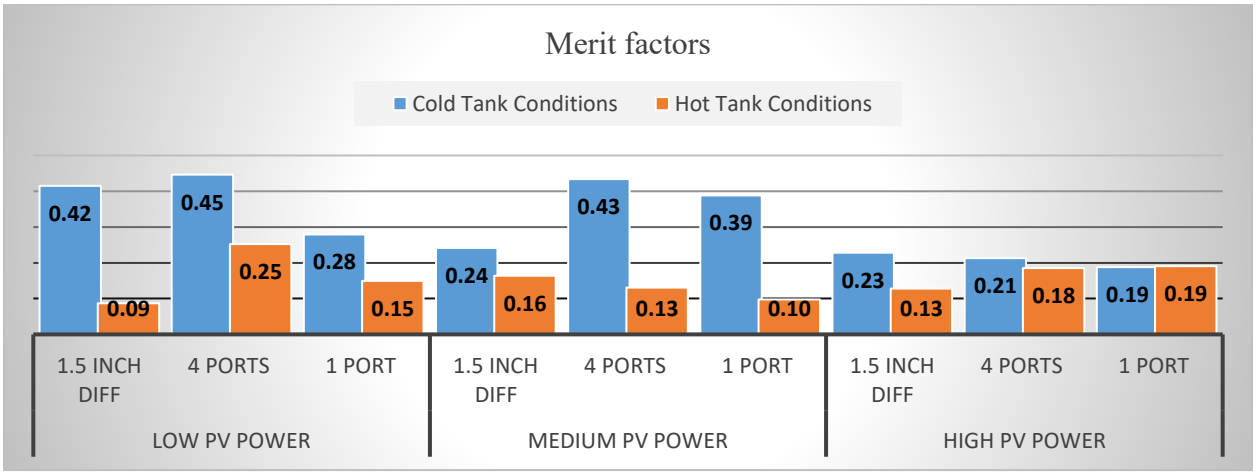


Figure 6-60 Merit factors under cold and hot tank conditions for all experimental tests.

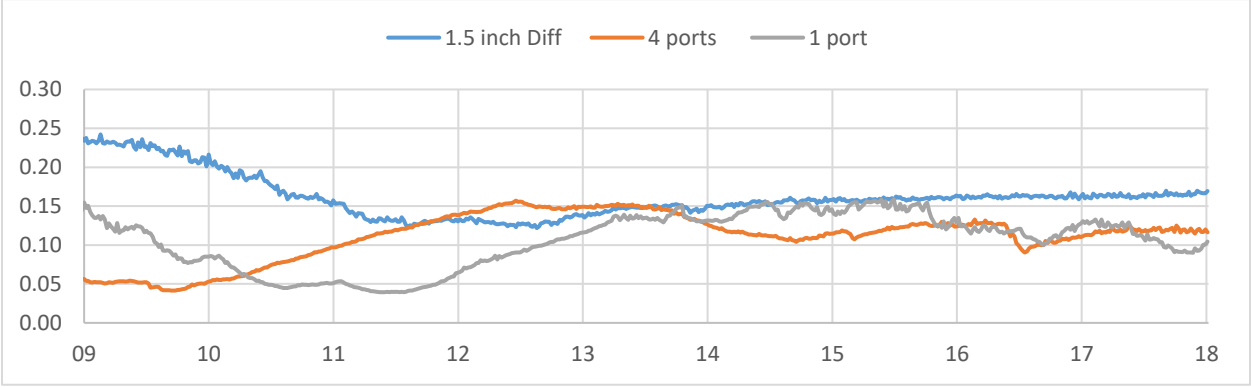


Figure 6-61 Merit factors for inlet devices under medium average PV power and hot tank conditions.

#### 6.3.5.2. Entropy Ratios

Figure (6-62) shows the entropy ratio calculations for cold and hot tank conditions for all experimental tests. The four-port hot water inlet device had the lowest entropy ratio value for most of average PV powers in both cold and hot tank conditions. However, the one-port hot water inlet device had the same entropy ratios of the four-port manifold for the medium average PV power and cold tank conditions. Furthermore, the difference between the inlet hot water inlet designs regarding entropy ratios was quite small. The difference was caused by calculation differences among actual entropy, perfect entropy and mixed entropy and was so minor as to have very little to no impact on the final calculations. To make a good evaluation a normalization was performed. Normalization is to bring all the PV power values, dead state temperatures for a cold tank, and average tank temperatures for hot tank conditions to an equal level for comparison. For example, the normalization of entropy ratio as shown in table (6-7).

Table 6-7 Normalization of availability change for low, medium, and high PV power under cold tank condition

| Entropy Ratio | | | | | | | | | |
|---|---|---|---|---|---|---|---|---|---|
| Cold Tank Condition | | | | | | | | | |
| | Low PV Power | | | Medium PV Power | | | High PV Power | | |
| | Diff | 4 port | 1 port | Diff | 4 port | 1 port | Diff | 4 port | 1 port |
| Experimental result | 0.9986 | 0.9954 | 0.9979 | 0.9964 | 0.9928 | 0.9928 | 0.9958 | 0.9910 | 0.9918 |
| Heater Power W | 199 | 240 | 272 | 814 | 655 | 735 | 1079 | 1115 | 1206 |
| Normalization power | 1.2 | 0.9954 | 0.879 | 0.899 | 1.11 | 0.9928 | 1.029 | 0.9910 | 0.917 |
| Dead State $T_0$ ˚C | 21 | 18 | 18 | 20 | 16 | 22 | 20 | 16 | 20 |
| Normalization $T_0$ | 1.03 | 0.9954 | 0.879 | 0.899 | 1.391 | 0.903 | 1.029 | 1.239 | 0.917 |

We did not consider average PV power heater value, dead-state temperature for cold tank conditions, or average tank temperature for hot tank conditions in our evaluation because when using a normalization, the entropy ratio results are greater than one, which is an unrealistic value. Furthermore, according to thermodynamics, lower entropy indicates more stratification in a tank,

but it is difficult to determine which inlet device was the most effective based on such small differences. Due to this issue, we did not recognize this parameter in our evaluations.

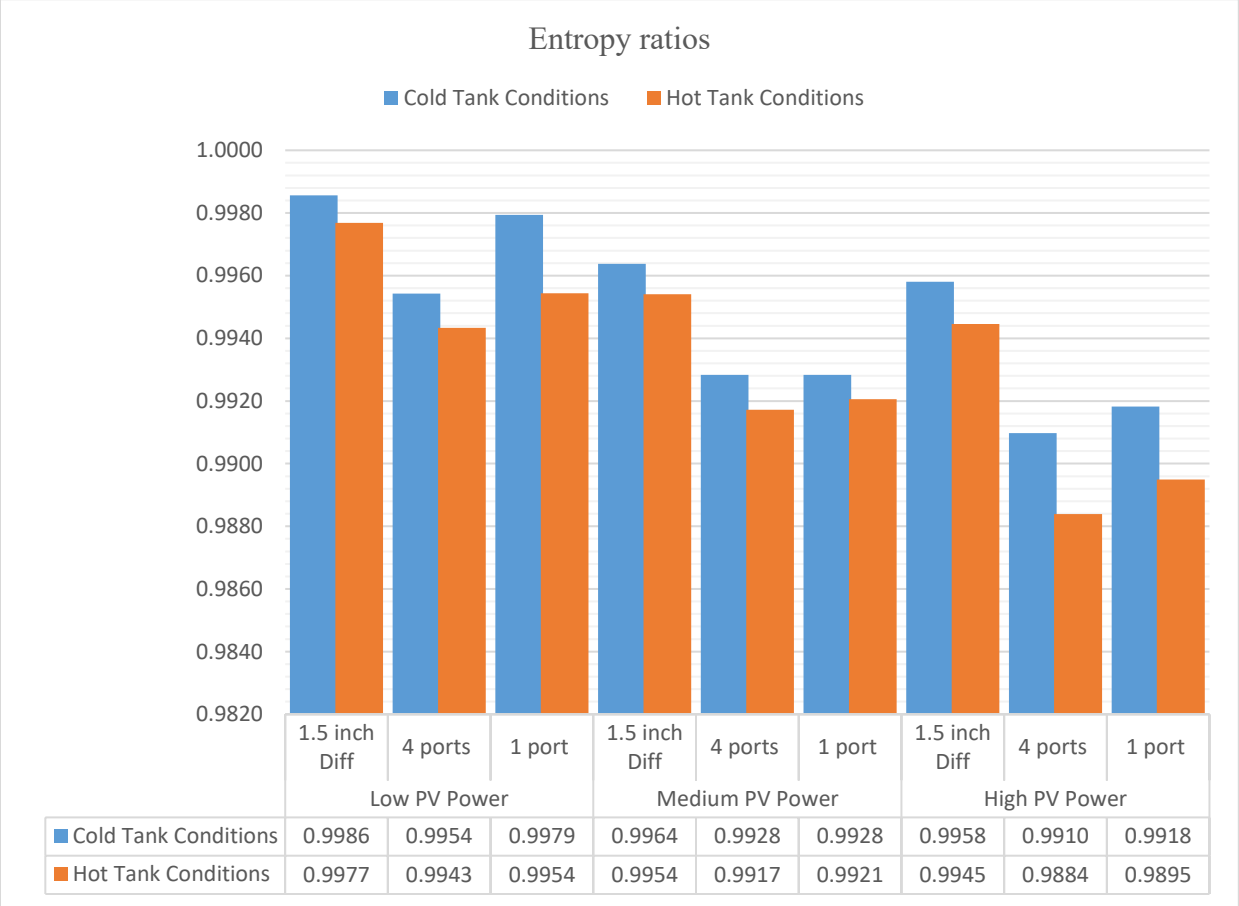


| | 1.5 inch Diff | 4 ports | 1 port | 1.5 inch Diff | 4 ports | 1 port | 1.5 inch Diff | 4 ports | 1 port |
|---|---|---|---|---|---|---|---|---|---|
| | Low PV Power | | | Medium PV Power | | | High PV Power | | |
| Cold Tank Conditions | 0.9986 | 0.9954 | 0.9979 | 0.9964 | 0.9928 | 0.9928 | 0.9958 | 0.9910 | 0.9918 |
| Hot Tank Conditions | 0.9977 | 0.9943 | 0.9954 | 0.9954 | 0.9917 | 0.9921 | 0.9945 | 0.9884 | 0.9895 |

Figure 6-62 Average entropy ratios in cold and hot tank conditions for all experimental tests.

#### 6.3.5.3. Internal Entropy Generation

Figure (6-63) shows the internal entropy calculations for cold and hot tank conditions in all experimental tests. The four-port hot water inlet device had the lowest internal entropy generation value when using low average PV power for cold and hot tank conditions. To perform the internal entropy generation calculation, the entropy difference of the mixture tank should be greater than the entropy difference of the experimental tank, and the entropy difference of the perfect tank must be less than the entropy difference of the experimental tank. In addition, the figure shows that the

one-port design had the lowest value of internal entropy generation under medium power for cold tank conditions and under high power for hot tank conditions. However, the 1.5-inch diffuser design was the best medium average PV power heater for hot tank conditions as well as the best high average PV power heater for cold tank conditions. The differences in internal entropy generation among the three hot water inlet designs were very small and caused by differences in calculating actual entropy, perfect entropy, and mixed entropy. As these differences were only minor, they had little to no impact on the final calculations. Furthermore, in our evaluations, we did not consider either the average PV power heater value, the dead-state temperature for cold tank conditions, or the average tank temperature for hot tank conditions. We chose not to use these measurements because it was very sensitive to dead state temperature, average tank temperature. Due to this issue, we chose not to recognize this particular parameter in our evaluations.

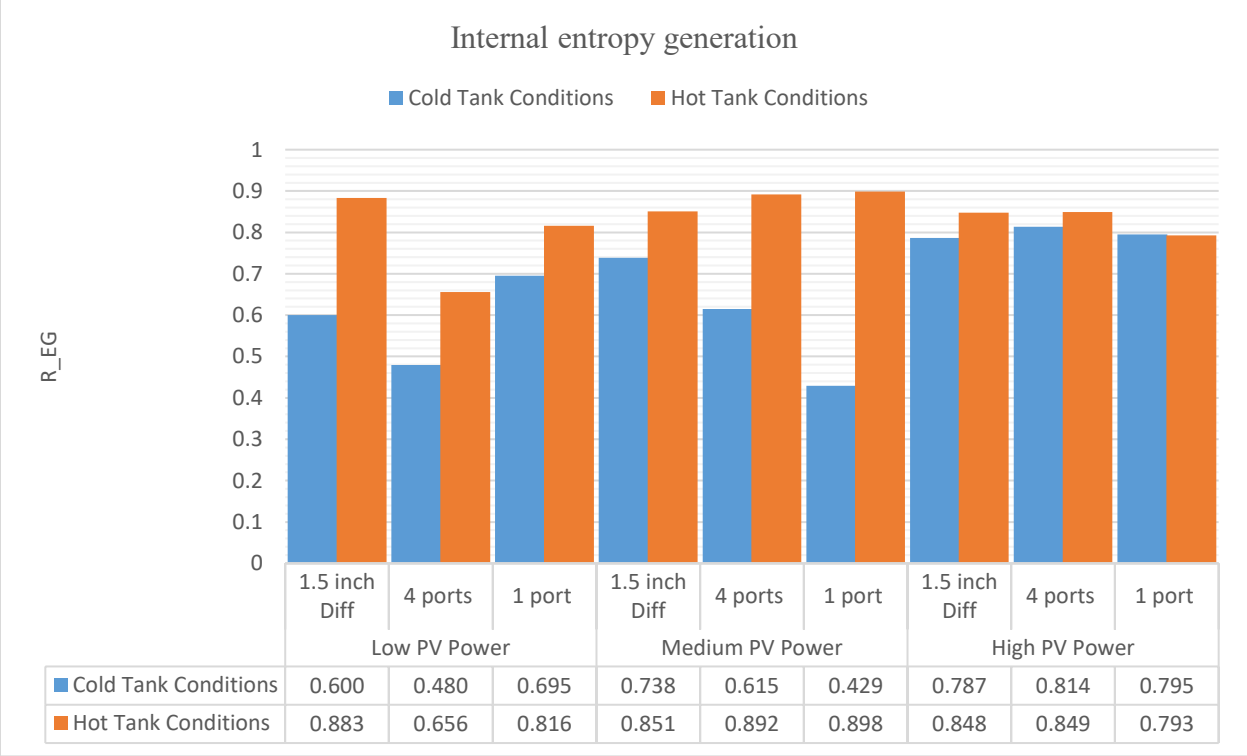


| | 1.5 inch Diff | 4 ports | 1 port | 1.5 inch Diff | 4 ports | 1 port | 1.5 inch Diff | 4 ports | 1 port |
|---|---|---|---|---|---|---|---|---|---|
| | Low PV Power | | | Medium PV Power | | | High PV Power | | |
| Cold Tank Conditions | 0.600 | 0.480 | 0.695 | 0.738 | 0.615 | 0.429 | 0.787 | 0.814 | 0.795 |
| Hot Tank Conditions | 0.883 | 0.656 | 0.816 | 0.851 | 0.892 | 0.898 | 0.848 | 0.849 | 0.793 |

Figure 6-63 Internal entropy generation in cold and hot tank conditions for all experimental tests.

# Chapter 7: Conclusions

The experiments for this research were conducted at the Renewable Energy Laboratory at Dalhousie University. Sixty-two experiments were conducted on a side-arm PV water heater with three types of hot water inlet devices. The experimental tests were conducted from June to October 2018. Over this time, the main water supply temperatures changed from 16 to 21℃. The experimental work was undertaken to identify a side-arm heater, connected with various types of hot water distributor devices, which would enhance thermal stratification in an SDHW system tank. The evaluation of the performance of the hot water inlet devices was based on the assessment of flow visualization, temperature distribution inside the storage tank, degree of stratification (DOS), availability, availability ratio, energy delivery, entropy ratio, merit factor and internal entropy generation. The most effective hot water inlet device is the one which has a high DOS, availability change, merit factor, energy delivery, and average availability ratios. Furthermore, it has a low entropy ratio and a low internal entropy generation. Based on the results from this experimental research work, we determined the following:

- The availability is inversely proportional to dead state temperature and the entropy is directly proportional to dead state temperature. Selection of the dead state temperature is a critical parameter for a precise evaluation. In this research, the main water supply temperature was selected as the dead state temperature because if the water temperature is equal to the main water supply temperature, there will be no useful energy for the SDHW system user.

- The hot water from the side-arm heater rose in the four-port manifold, maintaining a pressure difference with the hot water in the tank until it reached the level at which the manifold density matched that of the hot water in the tank.
- An experimental method to enhance stratification in the SDHW system using PV power will contribute to the industry by providing important information on the ability and effectiveness of using photovoltaics to provide low-grade heat.
- By graphing results we found that for the most of experimental tests the four port manifold had the highest degree of stratification, and high change rate for the temperature of the top tank layers, and responded earlier in the day than the other two designs for the most of experimental tests. This means the four-port manifold had the ability to enhance stratification to a higher degree than the single-port manifolds.
- According to flow visualization tests, using the four-port manifold during periods of fluctuating solar radiation led to enhanced stratification. The results of this testing indicated that using a four-port manifold that increases gradually from a small lower-port diameter to a large upper-port diameter is a workable solution to enhance stratification.
- According to thermodynamics, a more stratified storage tank will have a lower entropy. The four-port hot water inlet device had the lowest entropy ratio value in most of the tests. However, due to the very small differences in entropy between the tests with the three manifolds, it was impossible to use entropy ratio, as parameters to determine which inlet device was the most effective. In addition, with normalization, the entropy results was greater than one, which is an unrealistic value. Due to this issue it was difficult to recognize this parameter in our evaluations.

- Due to fluctuating mains water supply temperature, and average tank temperature, the internal entropy generation parameters were producing infrequent results. Due to the inconstant results in internal entropy generation between the tests with the three manifolds, it was impossible to use the internal entropy generation, as parameters to determine which inlet device was the most effective.
- There was a high velocity discharge flow rate when using a one port copper tube at the top of the storage tank or a four-port manifold under high PV power, which led to destratification.
- Water colder than water at the top layers of the tank, delivered through the one-port tube flows downwards to the bottom of the tank. Due to this action a decline in the temperature of the top layers of the tank occurs, which leads to decreases in the quality of the hot water.
- With the four-port manifold, it was difficult to establish that there was cold water sucked into the lower ports of the manifold at the middle of tank. This cold water may have mixed with hot water delivered from the side-arm heater inside the manifold, which led to decreases in the quality of the hot water at the top of the tank.
- The decay of the stratification over time is caused by heat transfer to the environment. Measurement of heat losses to the environment is based on the difference between temperature surrounding the tank and the average temperature of each layer in the storage tank at the start and at the end of the experimental test. It is obvious from the tests that the temperature of storage tank layers were decreased due to standby heat losses. Heat can be transferred from a hot medium to a cold medium via a heat conducting wall, and this mechanism destroys thermal stratification. Consequently, enhanced thermal stratification may be obtained by using a well-insulated storage tank.

## 7.1. Recommendations and Future Work

While this research has successfully investigated the enhancement of thermal stratification in a SDHW tank using a side-arm heater with four ports inlet device, there is still other experimental and modelling work to be done. The following recommendations are made for additional research:

- The effect of hot water draws from the side-arm heater and the performance of the SDHW tank should be investigated experimentally. Furthermore, based on this observation, it is recommended that experiments be conducted by increasing the resistance in the sidearm loop by using smaller diameter piping, orifices, or a throttling valve to reduce the exit velocities. In addition, different side-arm heater diameters also need to be tested in order to be applicable for commercial domestic hot water tanks.
- To test the system with constant AC power future research should use a 120 V, 1500 W AC element heater to simulate a sunny day, and a 240 V, 3000 W set to 120 V to simulate a cloudy day.
- Research should be conducted by using a model to predict the PV power, dead state temperature, and temperature distribution in the SDHW Tank as well as the side-arm heater. The result of these models should be compared with the experimental results with similar configurations and similar conditions.
- A flow meter measurement device should be assembled to measure flow rate after the sidearm heater instead of using a numerical calculation. To improve the estimate of hot water flow rate.
- We recommend using more accurate temperature measurement surrounding the manifold ports to prove there was cold water sucked from the lower ports of four port manifold at

the middle of tank, which leads to decrease the water quality of the hot water at the top of the tank.

- The effect of the reverse flow through the side-arm heater and the manifold under the night and low PV power conditions should be studied to protect the system from this phenomenon could be a practical feature in the design.

# References


[1] Al-Badi, A.H. and Albadi, M.H. "Domestic Solar Water Heating System in Oman: Current Status and Future Prospects." Renewable and Sustainable Energy Reviews 16.8 (2012): 5727-731. Web.

[2] Alsagheer, F. (2011). An investigation of methods to enhance stratification in solar domestic hot water tanks. Ph.D. thesis, Dalhousie University, Nova Scotia, Canada.

[3] Altuntop, N., Arslan, M., Ozceyhan, V., & Kanoglu, M. (2005). Effect of obstacles on thermal stratification in hot water storage tanks. Applied Thermal Engineering, 25(14-15), 2285-2298. doi:10.1016/j.applthermaleng.2004.12.013.

[4] Al-Najem, N. M., & El-Refaee, M. M. (1997). A numerical study for the prediction of turbulent mixing factor in thermal storage tanks. Applied Thermal Engineering, 17(12), 1173-1181. doi:10.1016/S1359-4311(97)00030-6

[5] Altuntop, N., Tekin, Y., Ozceyhan, V., Gunes, S. (2008). The effect of obstacle geometry and position on thermal stratification in solar hot water storage tanks. Proceedings of the ASME Summer Heat Transfer Conference, HT 2008, v 3, p 479-484, 2009.

[6] Andersen, E., Furbo, S., & Fan, J. (2007). Multilayer fabric stratification pipes for solar tanks. Solar Energy, 81(10), 1219–1226. doi:10.1016/j.solener.2007.01.008.

[7] Ashkenazy, H. (2012).Photovoltaic heater. EDS-USA Inc. Publication number: EP2513735 Publication date: 10/24/2012.

[8] Cabeza, Luisa F. Advances in Thermal Energy Storage Systems: Methods and Applications. Cambridge: Elsevier/Woodhead, 2015. Print. Woodhead Publishing in Energy; Number 66.

[9] Cruickshank, C.A. 2006. Simulation and testing of stratified multi-tank thermal storages for solar heating systems. Master of applied Science Thesis, Queen‘s University, Kingston, ON, Canada.

[10] Dahghan, A. A., Hosni, M. H., Hoda, S.(2005). Experimental evaluation of the thermal behavior of a vertical solar tank using energy and exergy analysis. Energy Conversion and Resources, 2005, pp. 375-380.

[11] Davidson J.H., Adams D.A., Miller J.A. (1994). Coefficient to characterize mixing in solar water storage tanks. Journal of Solar Energy Engineering, Transactions of the ASME, 116 (2), pp. 94-99.

[12] Dougherty, B. P., Fanney, A. H., Richardson, J. O. (2002). Field test of a photovoltaic water heater. ASHRAE Transactions, v 108 PART 2, pp. 780-791, 2002.

[13] Dinçer, İbrahim, and Rosen, Marc. Thermal Energy Storage: Systems and Applications. 2nd ed. Hoboken, N.J.: Wiley, 2011.

[14] Eames, P.C., Norton, B. (1998).The effect of tank geometry on thermally stratified sensible heat storage subject to low Reynolds number flows. International Journal of Heat and Mass Transfer, 41, (14), pp. 2131-2142.

[15] Fraunhofer, I. S. E. (2017). Photovoltaics report, updated: 12 July 2017. Technical Report, Fraunhofer Institute for Solar Energy Systems, ISE.

[16] García-Marí, E., Gasque, M., Gutiérrez-Colomer, R. P., Ibáñez, F., & González-Altozano, P. (2013). A new inlet device that enhances thermal stratification during charging in a hot water storage tank. Applied Thermal Engineering, 61(2), 663–669. doi:10.1016/j.applthermaleng.2013.08.023.

[17] Gari H.N., Loehrke R.I. (1982). Controlled buoyant jet for enhancing stratification in a liquid storage tank. Journal of Fluids Engineering, Transactions of the ASME, 104 (4) , pp. 475-481.

[18] Hahne E., & Chen Y. (1998).Numerical study of flow and heat transfer characteristics in hot water stores, Solar Energy, 64 (1-3) , pp. 9-18.

[19] Haller, M. Y., Cruickshank, C. a., Streicher, W., Harrison, S. J., Andersen, E., & Furbo, S. (2009). Methods to determine stratification efficiency of thermal energy storage processes – Review and theoretical comparison. Solar Energy, 83(10), 1847–1860. doi:10.1016/j.solener.2009.06.019.

[20] Hermansson, R. 1993. Short term water heat storage. Ph.D. Thesis, Division of Energy Engineering, Lulea University of Technology, Lulea, Sweden.

[21] Hollands, K.G.T., Lightstone, M.F. (1989). Review of low-flow, stratified-tank solar water heating systems. Solar energy, 43, (2), p 97-105.

[22] Han, Y. M., Wang, R. Z., & Dai, Y. J. (2009). Thermal stratification within the water tank. Renewable and Sustainable Energy Reviews, 13(5), 1014–1026. doi:10.1016/j.rser.2008.03.001.

[23] International Energy Agency; Energy Technology Systems Analysis Program (ETSAP); International Renewable Energy Agency. Thermal Energy Storage, Technology Brief E17. January 2013. Available online: https://www.irena.org/DocumentDownloads/Publications/IRENA-ETSAP%20Tech%20Brief%20E17% 20Thermal%20Energy%20Storage.pdf.

[24] Jaluria, Y., & Gupta, S.K. (1982). Decay of thermal stratification in a water body for solar energy storage. 28, (2), pp. 137-143.

[25] Jordan, U., & Furbo, S. (2005). Thermal stratification in small solar domestic storage tanks caused by draw-offs. Solar Energy, 78(2), 291–300. doi:10.1016/j.solener.2004.09.011

[26] Knudsen, S., Morrison, G. L., Behnia, M., & Furbo, S. (2005). Analysis of the flow structure and heat transfer in a vertical mantle heat exchanger. Solar Energy, 78(2), 281-289. doi:10.1016/j.solener.2004.08.019.

[27] Knudsen, S. (2002). Consumers' influence on the thermal performance of small SDHW systems—Theoretical investigations. Solar Energy, 73(1), 33-42. doi:10.1016/S0038-092X(02)00018-X.

[28] Lavan, Z, Thompson, J. (1977).Experimental study of thermally stratified hot water storage tanks. Solar Energy, 19, (5), pp. 519-524.

[29] Lichtenberger, M. (2014). Solar photovoltaic water heating system utilizing microprocessor control and water heater retrofit adaptor. Publication Number: US20140112647, publication date: 04/24/2014.

[30] Loehrke R.I., Holzer J.C., Gari H.N., Sharp M.K.(1979). Stratification enhancement in liquid thermal storage tanks. Journal of energy, 3,(3), pp. 129-130.

[31] Miller,C. W.(1977). Effect of conducting wall on a stratified fluid in a cylinder, AIAA 12th Thermophysics conference, 77-792.

[32] Moran, Michael J., Shapiro, Howard N., Boettner, Daisie D., and Bailey, Margaret B. Fundamentals of Engineering Thermodynamics. 8/e. ed. Hoboken, NJ: Wiley, 2014. Print.

[33] Newman, M., Newman, G. (2005). Solar photovoltaic water heating system. Energy Laboratories, Inc. Publication number: US20140153913, publication date: 06/05/2014.

[34] Outtrim, Richard Victor, and Dalhousie University. Dept. of Mechanical Engineering. An Experimental Study of Immersed Thermosiphon Heat Exchangers for Solar Domestic Hot Water Systems (2004)

[35] Panthalookaran, V., Heidemann, W., & Müller-Steinhagen, H. (2007). A new method of characterization for stratified thermal energy stores. Solar Energy, 81(8), 1043-1054. doi:10.1016/j.solener.2006.11.012.

[36] Renewable Energy Policy Network for the 21st Century. (2018). Renewables 2018: Global Status Report. http://www.ren21.net/ wp-content/uploads/2018/06/178652_GSR2018_FullReport_web_final_.pdf.

[37] Rosengarten G., Morrison G., Behnia M. (1999). A second law approach to characterizing thermally stratified hot water storage with application to solar water heaters. Journal of Solar Energy Engineering, Transactions of the ASME, 121, (4), pp. 194-200.

[38] Rosen, M., Pedinelli, N., Dincer, I. (1999). Energy and exergy analyses of cold thermal storage systems. International Journal of Energy Research, 23, (12), pp. 1029-1038.

[39] Rosen, M.A., Hooper, F.C. (1992). Modelling the temperature distribution in vertically stratified thermal energy storages to facilitate energy and exergy evaluation. Thermodynamics and the Design, Analysis, and Improvement of Energy Systems. 27, pp. 247-252.

[40] Sarbu, I., & Sebarchievici, C. (2018). A comprehensive review of thermal energy storage. Sustainability, 10(1), 191.

[41] Shah, L. J., & Furbo, S. (2003). Entrance effects in solar storage tanks. Solar Energy, 75(4), 337–348. doi:10.1016/j.solener.2003.04.002.

[42] Shah, L. J., Andersen, E., & Furbo, S. (2005). Theoretical and experimental investigations of inlet stratifiers for solar storage tanks. Applied Thermal Engineering, 25(14-15), 2086-2099. doi:10.1016/j.applthermaleng.2005.01.011.

[43] Shyu R.J., Hsieh C.K. (1987). Unsteady natural convection in enclosures with stratified medium. Journal of Solar Energy Engineering, Transactions of the ASME, 109 (2), pp. 127-133.

[44] Sliwinski, B.J., Mech, A.R., and Shih, R.S. (1997). Stratification in thermal storage during charging, 6th international Heat Transfer conference, Toronto, ON, 149-154.

[45] Spaulding, W. J., & Rush, C. K. (1988). Thermal stratification within a hot water storage tank. In Advances in Solar Energy Technology (pp. 1167-1171).

[46] Swamee, Prabhata K., and Sharma, Ashok K. Design of Water Supply Pipe Networks. Hoboken, N.J.: Wiley-Interscience, 2008.

[47] Teahan, M. (2006). Is it time to introduce photovoltaic powered water heating system? Engineering Technology, v 8, n 10, pp. 16-20, January 2006.

[48] Thomasson, S. (2009). PV water heater with adaptive control. Publication number: US 20090188486, Publication date: 07/30/2009.

[49] Zachar A., Farkas I., Szlivka F. (2003). Numerical analyses of the impact of plates for thermal stratification inside a storage tank with upper and lower inlet flows, Solar Energy, 74 (4), pp. 287-302.

[50] Zurigat Y.H., Liche P.R., Ghajar A.J. (1988). Turbulent mixing correlations for a thermocline thermal storage tank, AIChE Symposium Series, 84 (263), pp. 160-168.

[51] Zurigat Y.H., Liche P.R., Ghajar A.J. (1991). Numerical study of the effect of inlet geometry on stratification in thermal energy storage, Heat Transfer, 19, (1), pp. 65-83.

[52] Mukhopadhyaya, K .&Forssellb, O . (2005). An empirical investigation of air pollution fossil fuel combustion and its impact on health in India during 1973 – 1974 to 1996 – 1997,Ecological Economics, 55 235 – 250. Retrieved from http:// www.elsevier.com/locate/ecolecon

# Appendix A

The following graphs present the results of the medium PV power for cold tank and hot tank Figures (62-101), and Figures from (102-145) present the high PV average power for cold and hot tank.

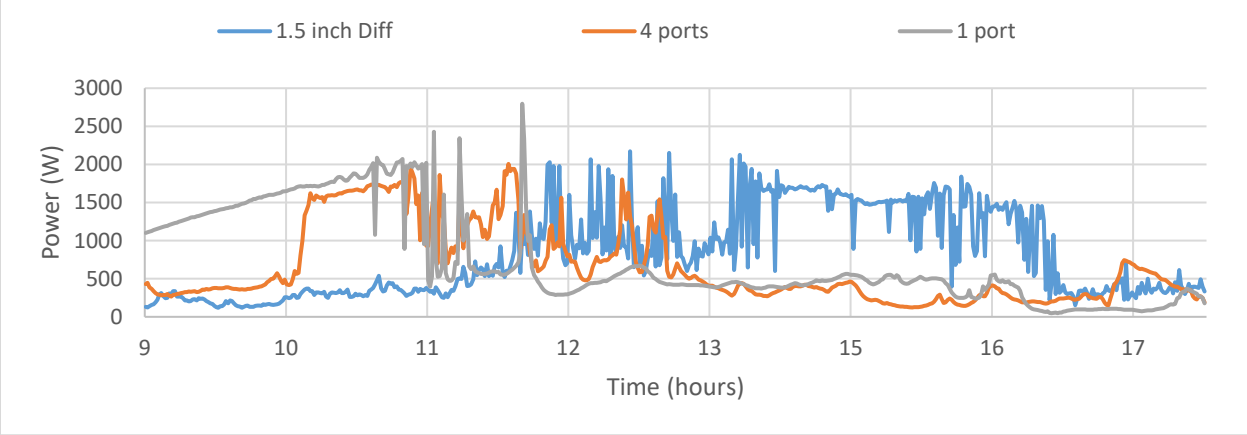


Figure 6-64 Medium PV power heater during three hot water inlet device tests for cold tank conditions.

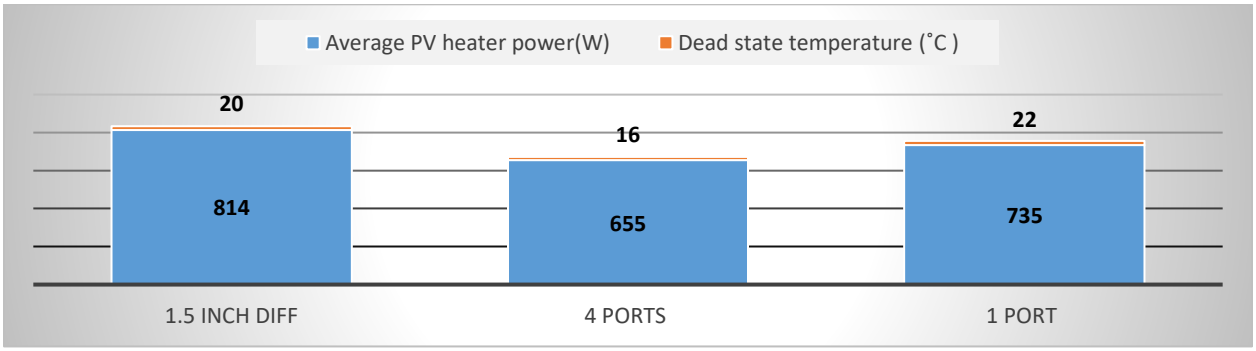


Figure 6-65 Medium average PV power and cold tank condition tests.

Table 6-8 Temperature Change Rate of three the tank Top Layers for Medium PV power and Cold Condition

| 1.5 inch diffuser | 4 ports | 1 port |
|---|---|---|
| ˚C/h | ˚C/h | ˚C/h |
| 2.1 | 5.5 | 7 |

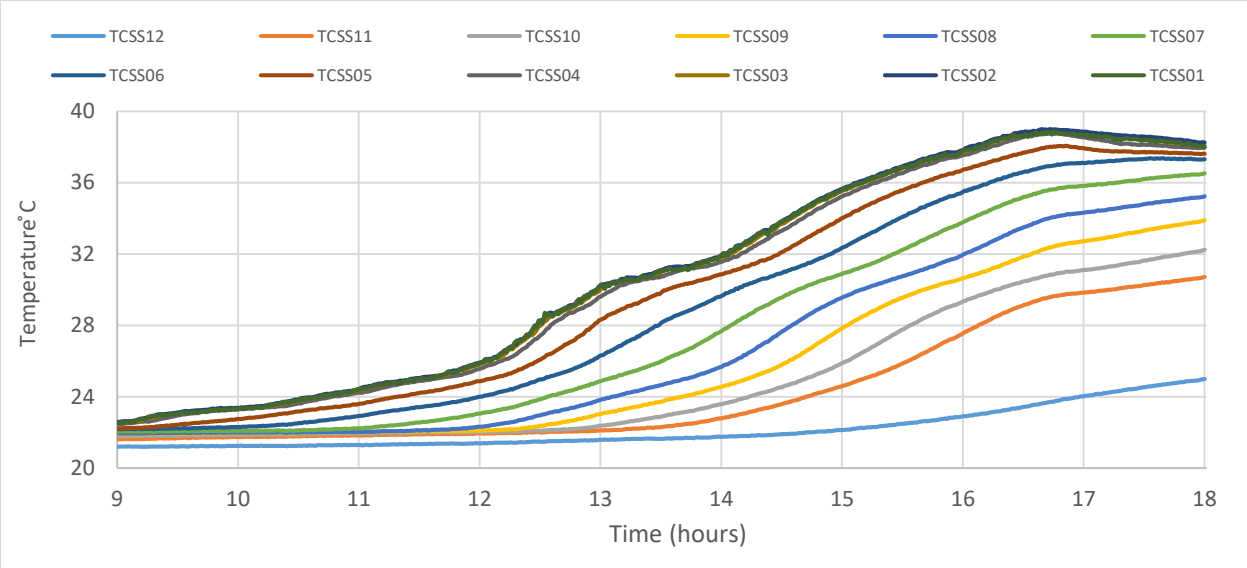


Figure 6-66a Graph showing 1.5-inch diffuser inlet device, medium average PV power, and cold tank conditions.

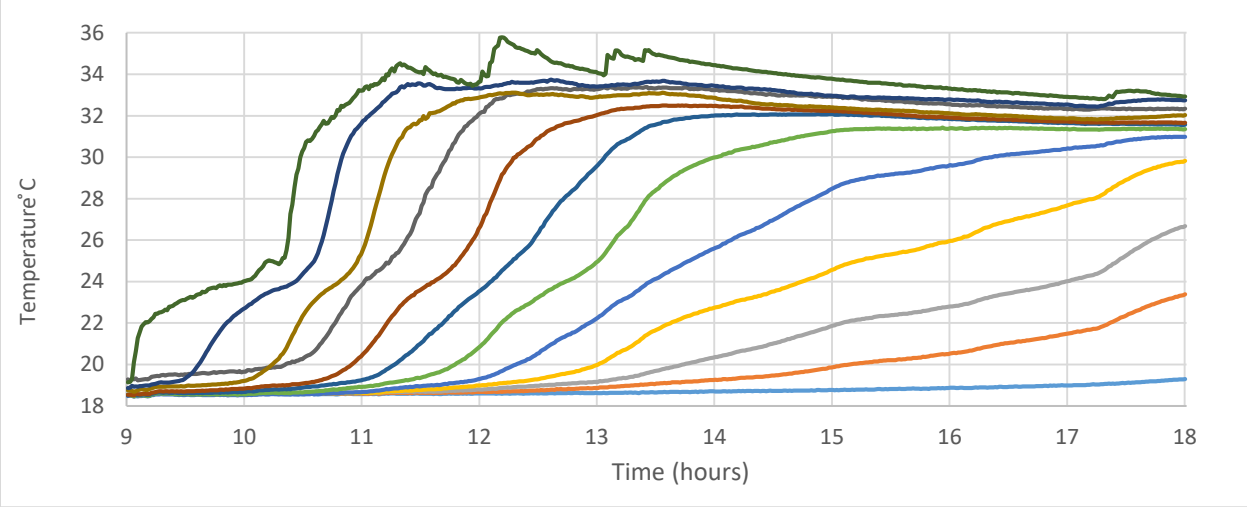


Figure 6-66b Graph showing four-port manifold inlet device, medium average PV power, and cold tank conditions.

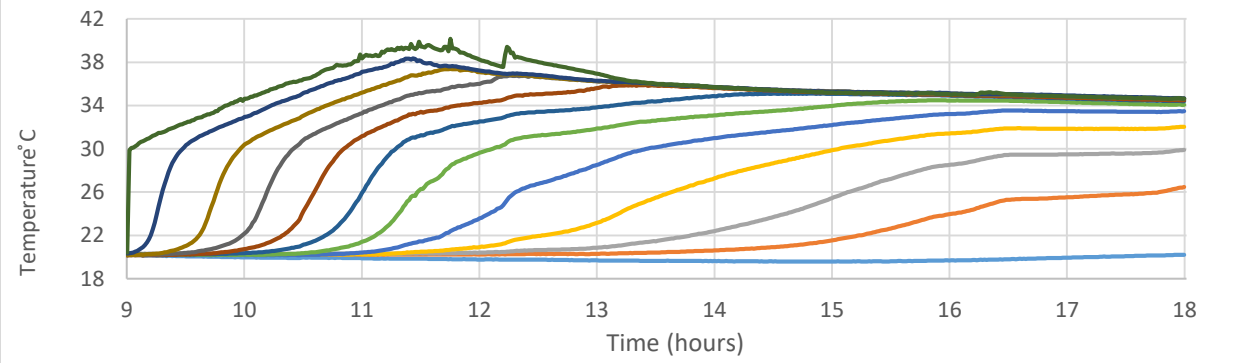


Figure 6-66c. Graph showing one-port tube inlet device, medium average PV power, and cold tank conditions.
Figure 6-66 Temperature distribution inside DHW tanks using three hot water inlet devices.

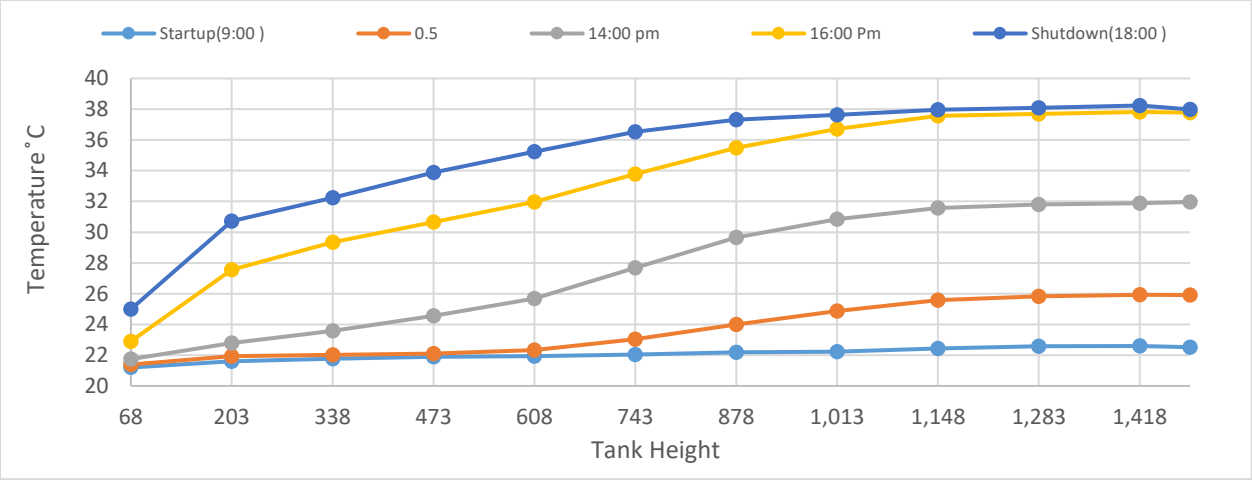


Figure 6-67a Graph showing 1.5-inch diffuser inlet device, medium average PV power, and cold tank conditions.

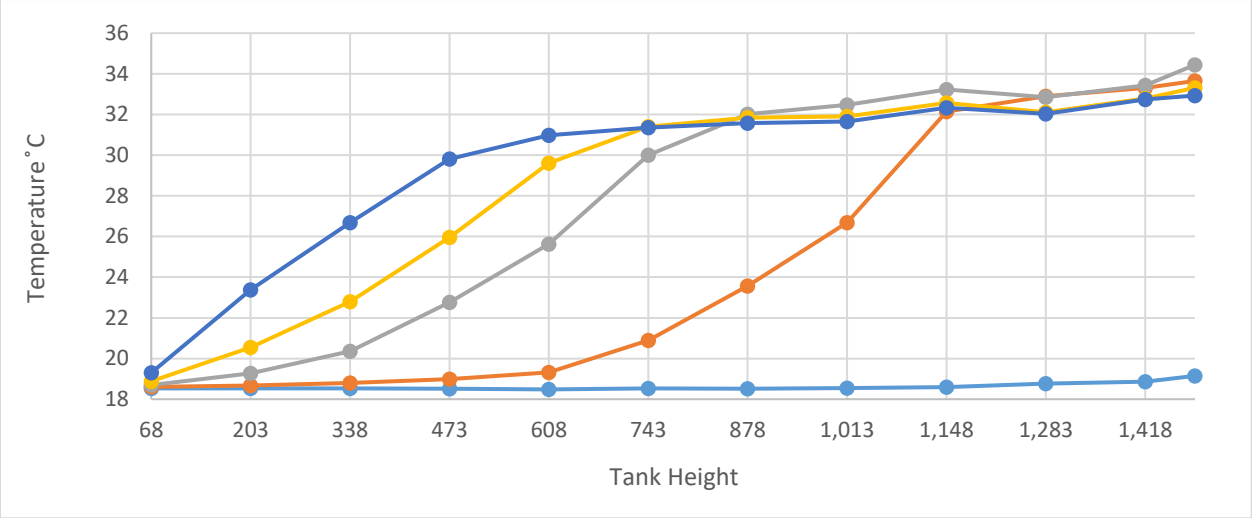


Figure 6-67b Graph showing four-port manifold inlet device, medium average PV power, and cold tank conditions.

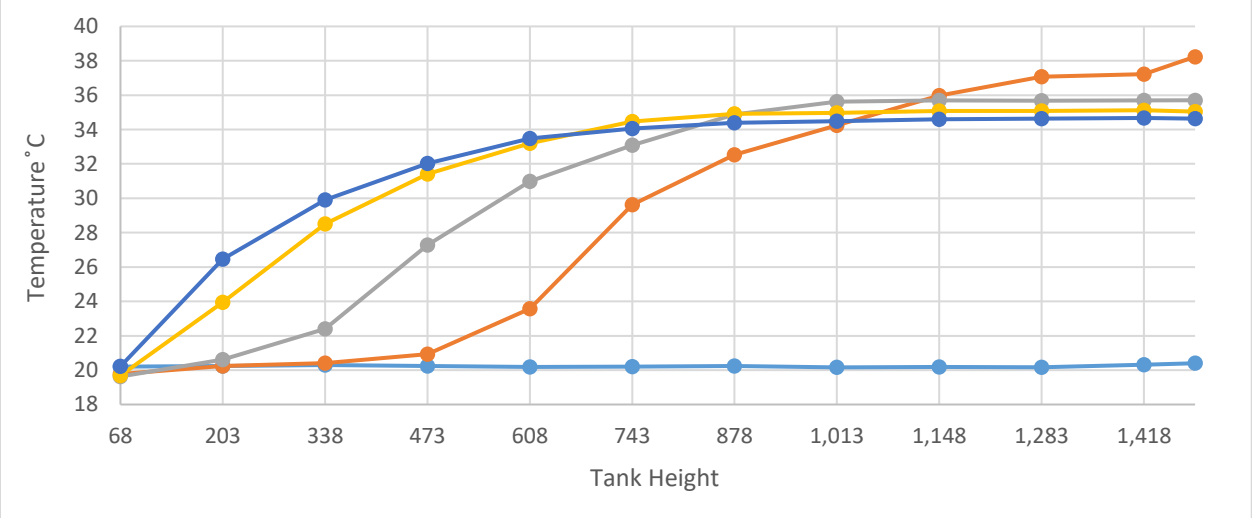


Figure 6-67c Graph showing one-port copper inlet device, medium average PV power, and cold tank conditions
Figure 6-67 Temperature distribution inside DHW tanks using hot water inlet devices.

.

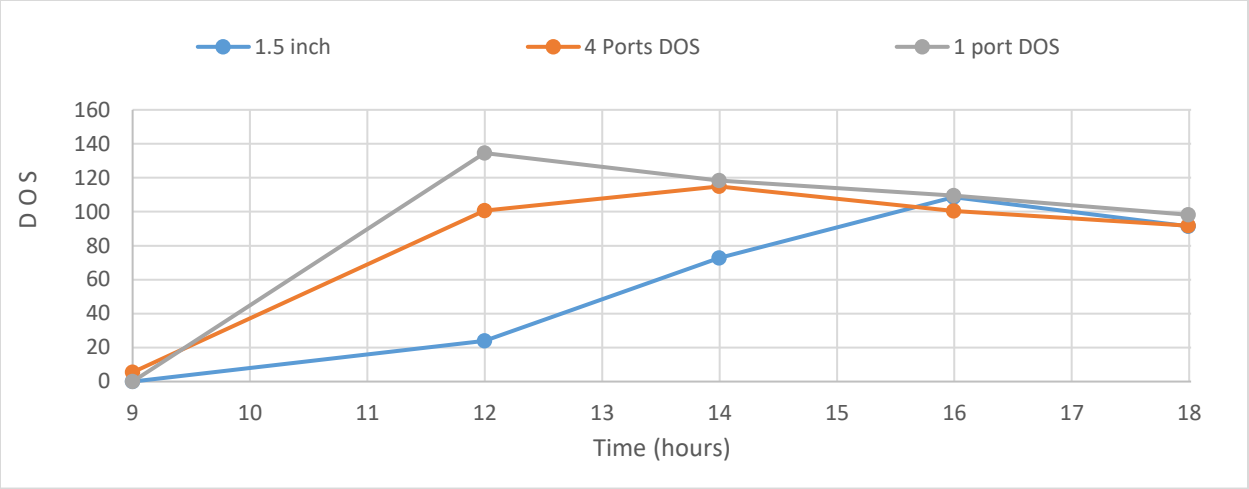


Figure 6-68 Degree of stratification of three hot water inlet devices, medium average PV power, and cold tank conditions.

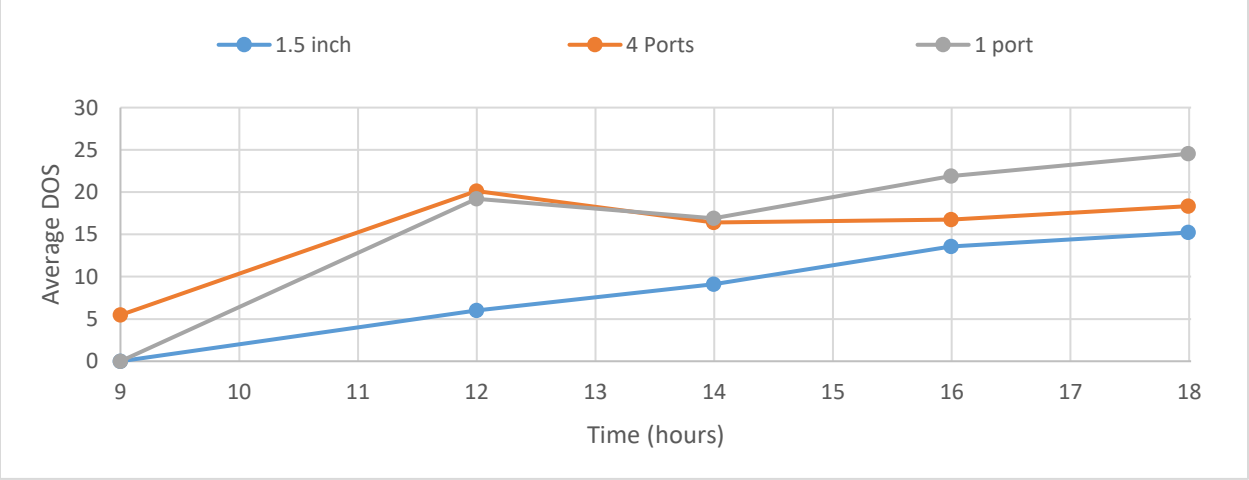


Figure 6-69 Average DOS of three inlet devices, medium average PV power, and cold tank conditions.

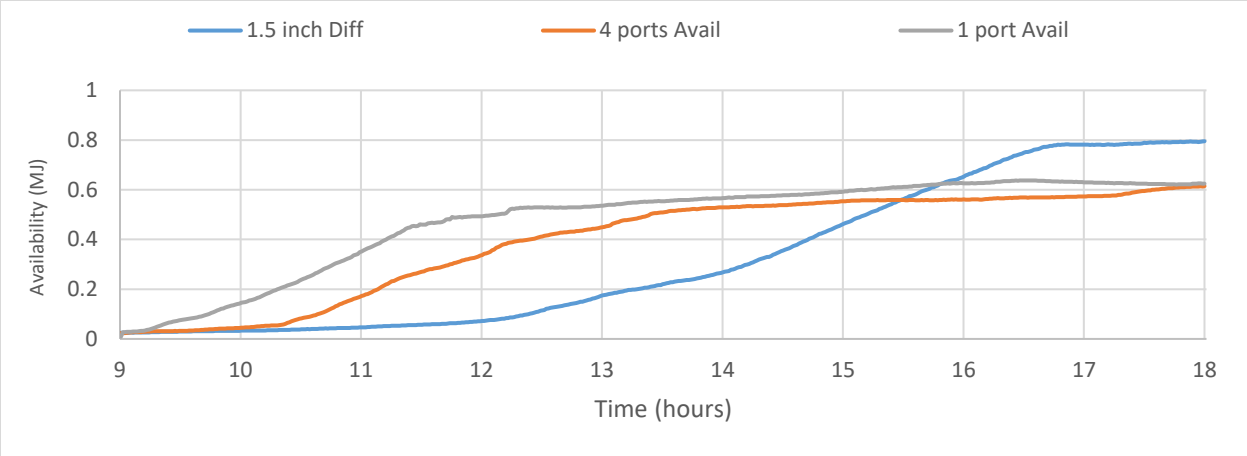


Figure 6-70 Availability for three inlet devices in medium average PV power and cold tank conditions.

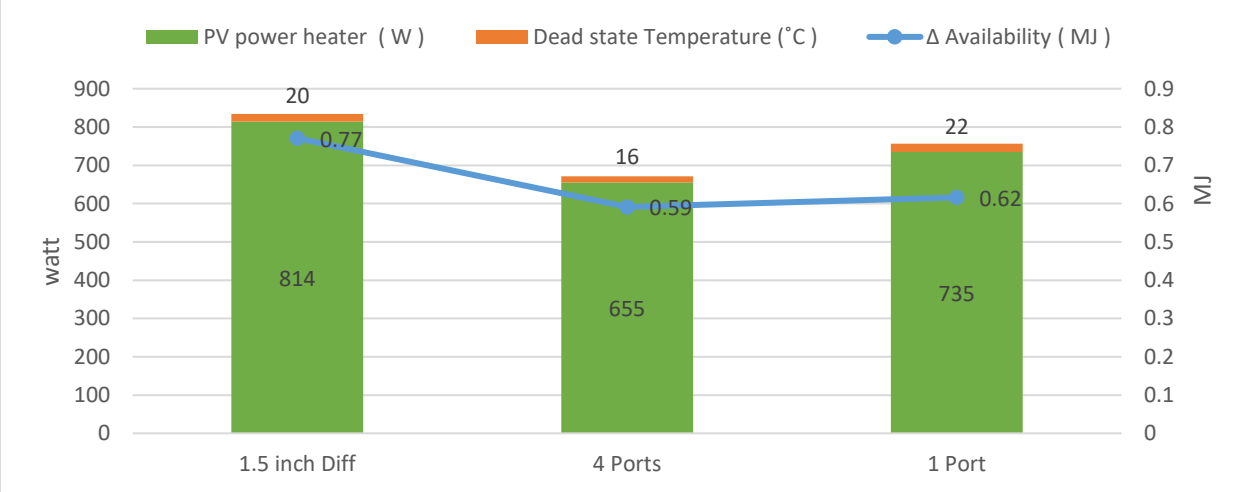


Figure 6-71 Availability change for three inlet devices in medium average PV power and cold tank conditions.

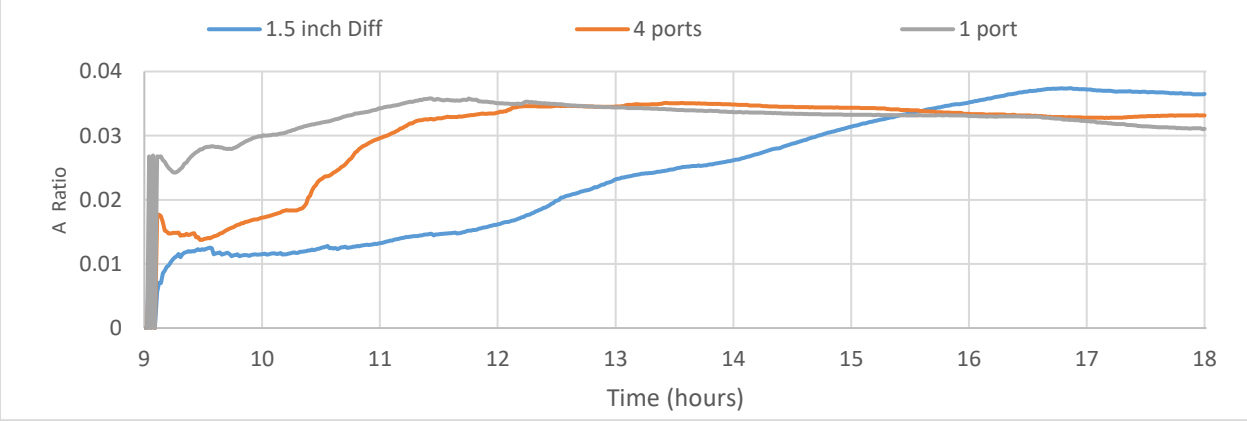


Figure 6-72 Availability ratios for three inlet devices in medium PV power and cold tank conditions.

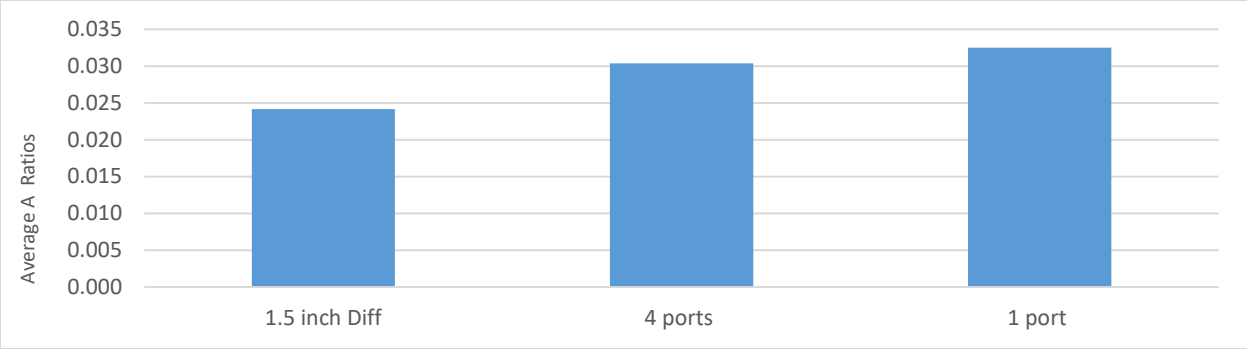


Figure 6-73 Average availability ratio for three inlet devices in medium PV power and cold tank conditions.

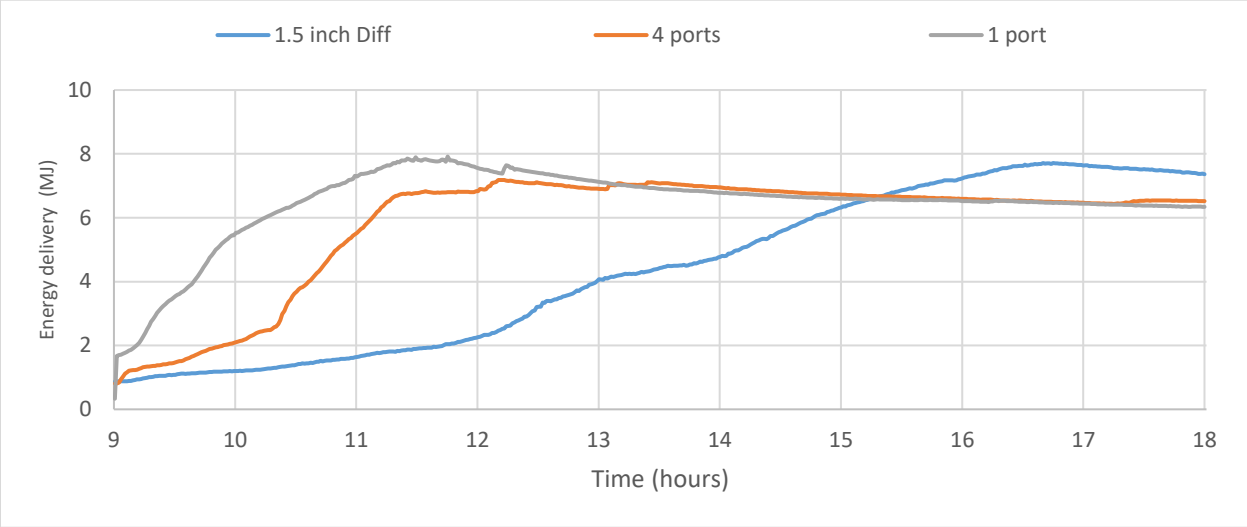


Figure 6-74 Energy delivery for three inlet devices in medium PV power and cold tank conditions.

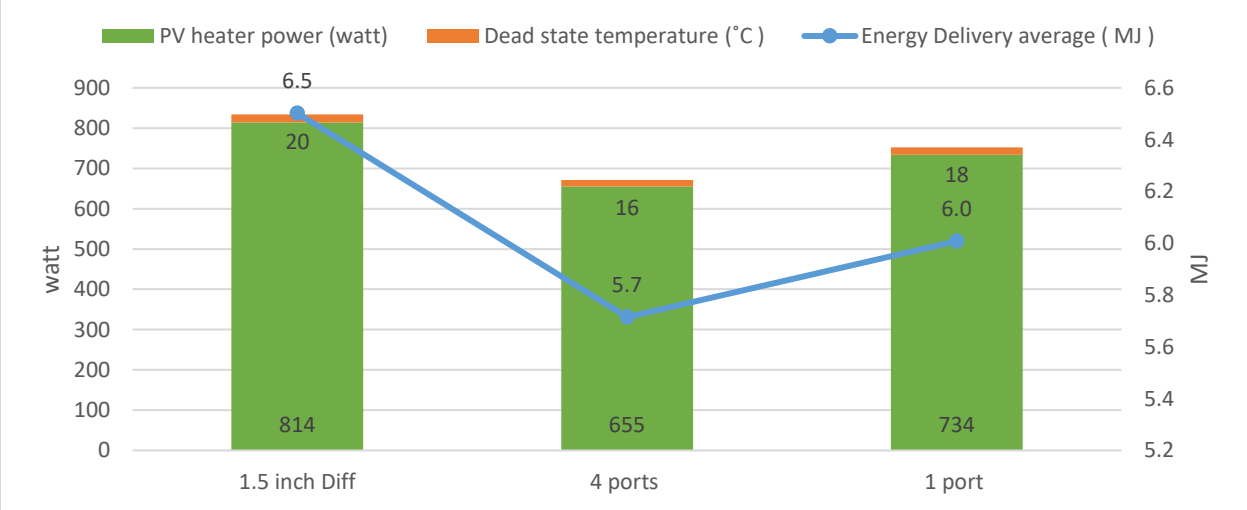


Figure 6-75 Energy delivery, medium PV power, and dead-state temperature of the three devices in cold tank conditions.

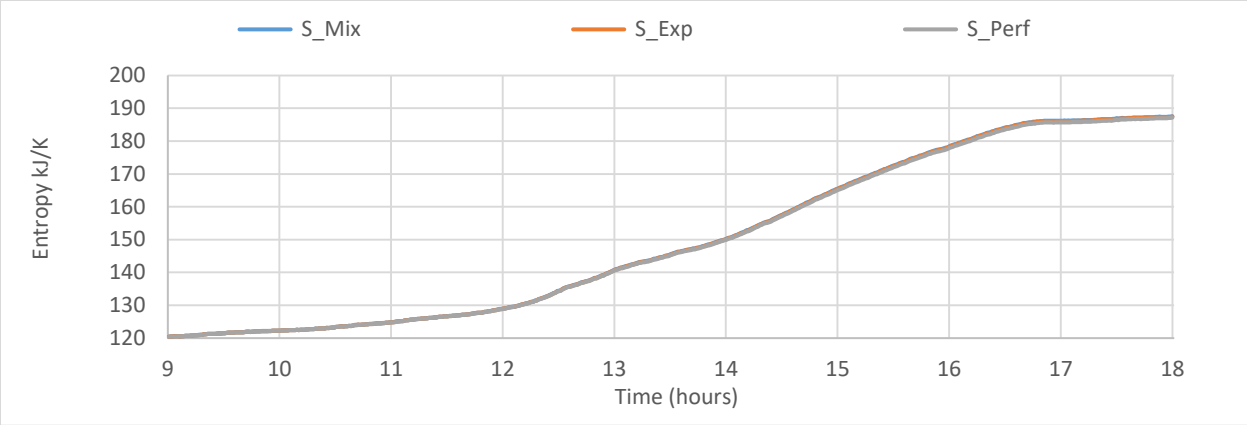


Figure 6-76a Entropy of 1.5-inch diffuser for three inlet devices in medium average PV power and cold tank conditions.

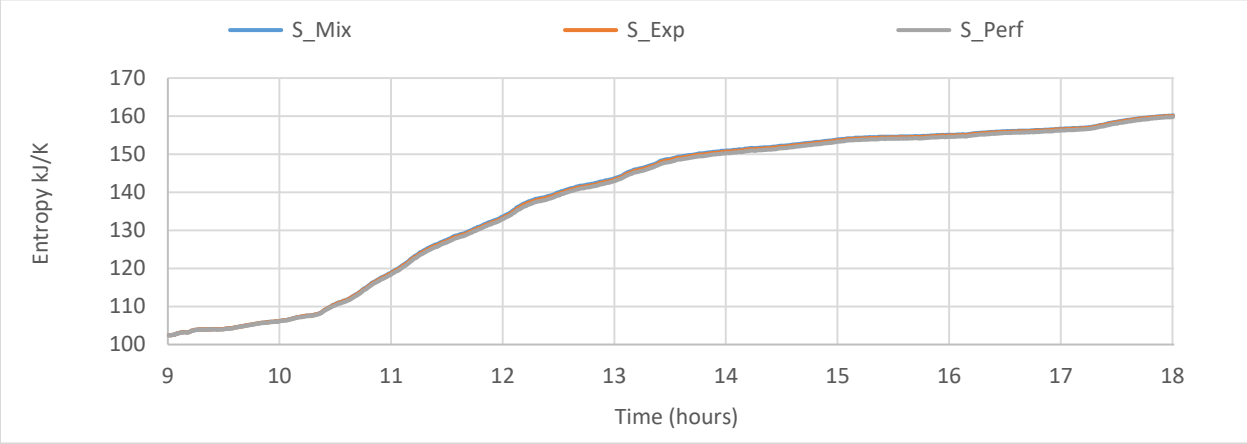


Figure 6-76b Entropy of four ports manifold for three inlet devices in medium average PV power and cold tank conditions.

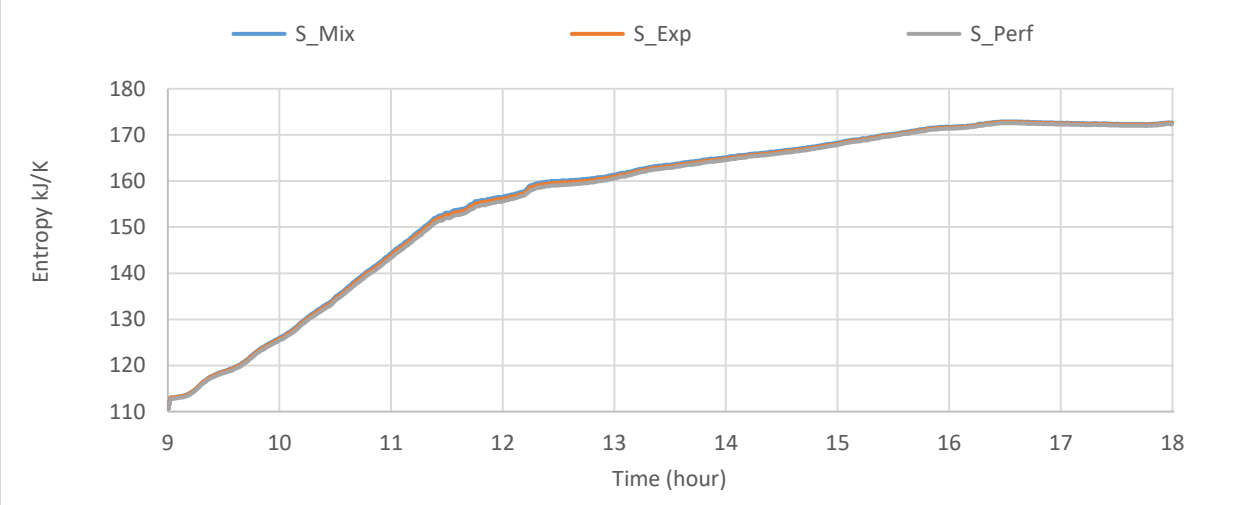


Figure 6-76c Entropy of one port copper tube for three inlet devices in medium average PV power and cold tank conditions.

Figure 6-76 Entropy inside the DHW Tank of three hot water inlet devices

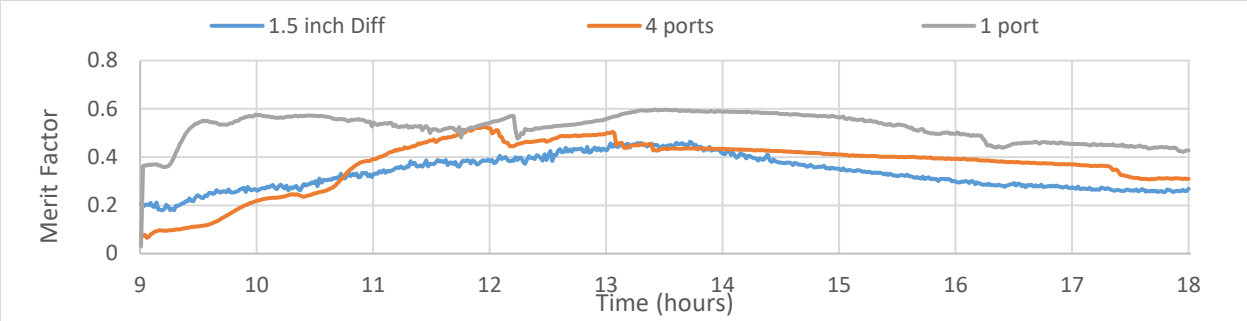


Figure 6-77 Merit factor for three hot water inlet devices in medium average PV power, and cold tank conditions.

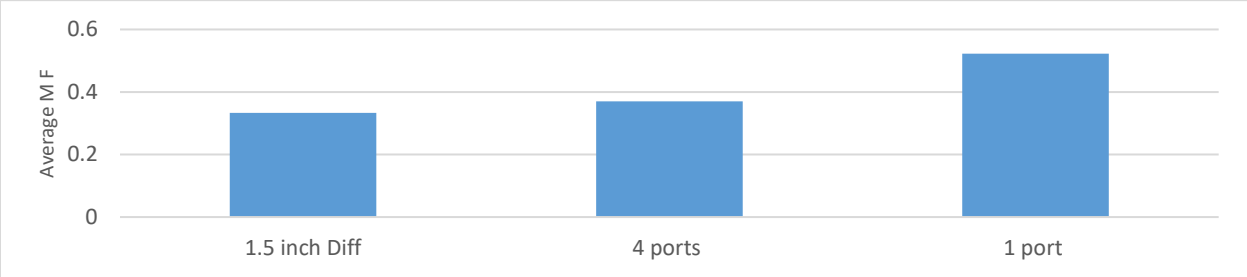


Figure 6-78 Merit factor for three hot water inlet devices at the end of the test in cold tank conditions.

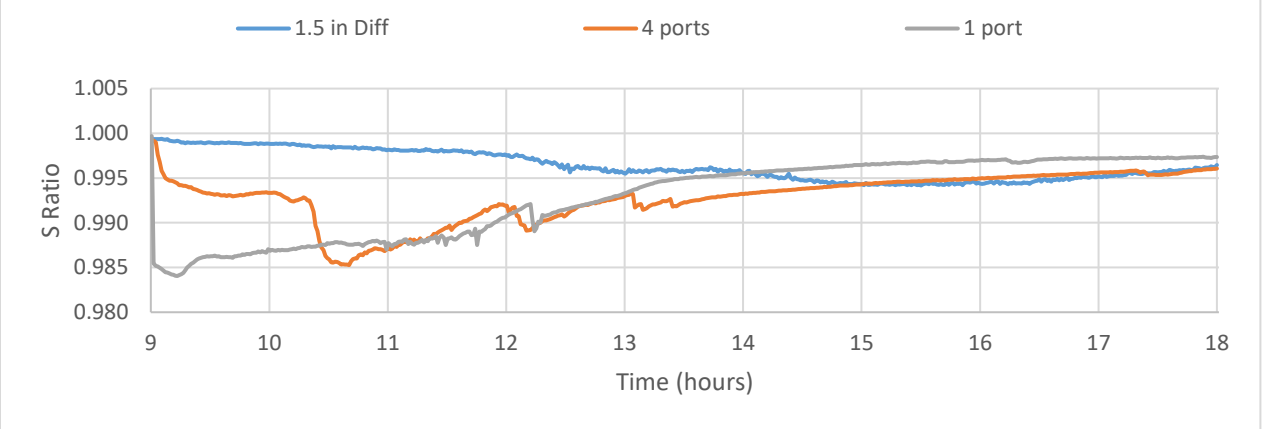


Figure 6-79 Entropy ratios of inlet devices in medium average PV power and cold tank conditions.

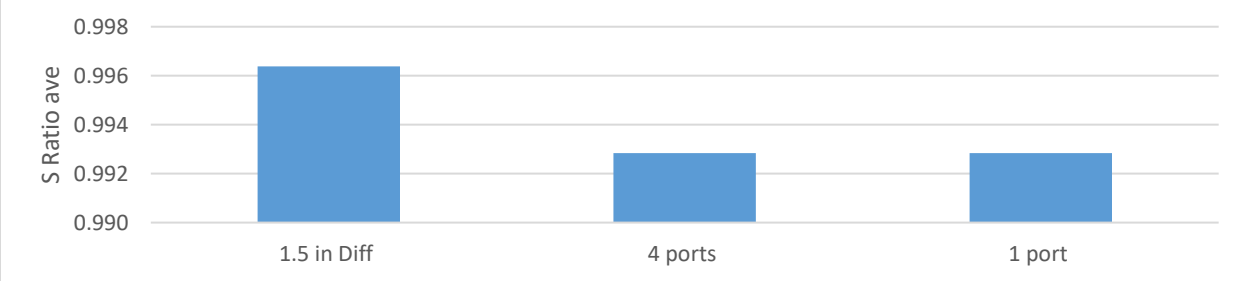


Figure 6-80 Entropy ratios of three inlet devices in medium average PV power and cold tank conditions.

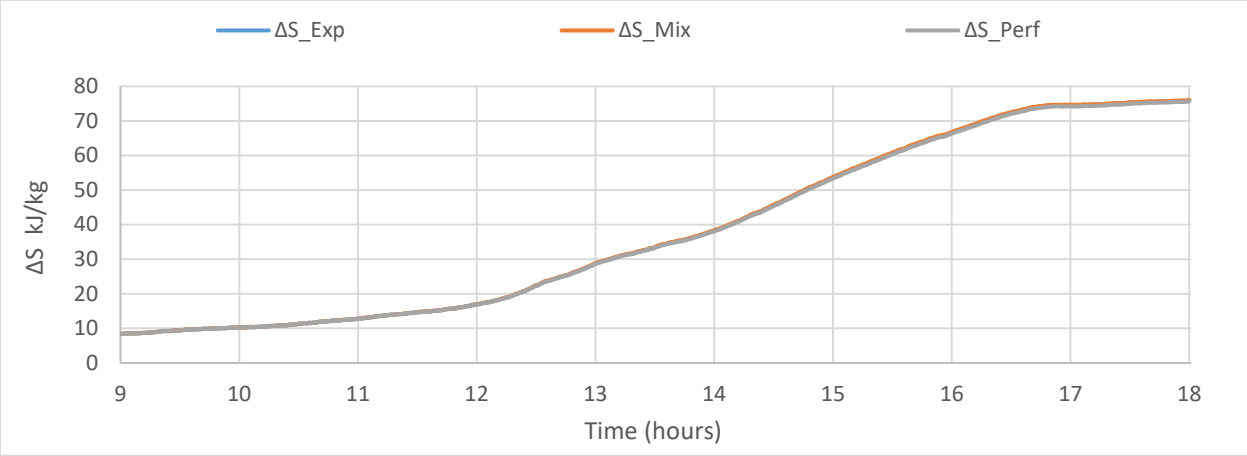


Figure 6-81a Entropy difference of 1.5-inch diffuser in medium average PV power and cold tank conditions.

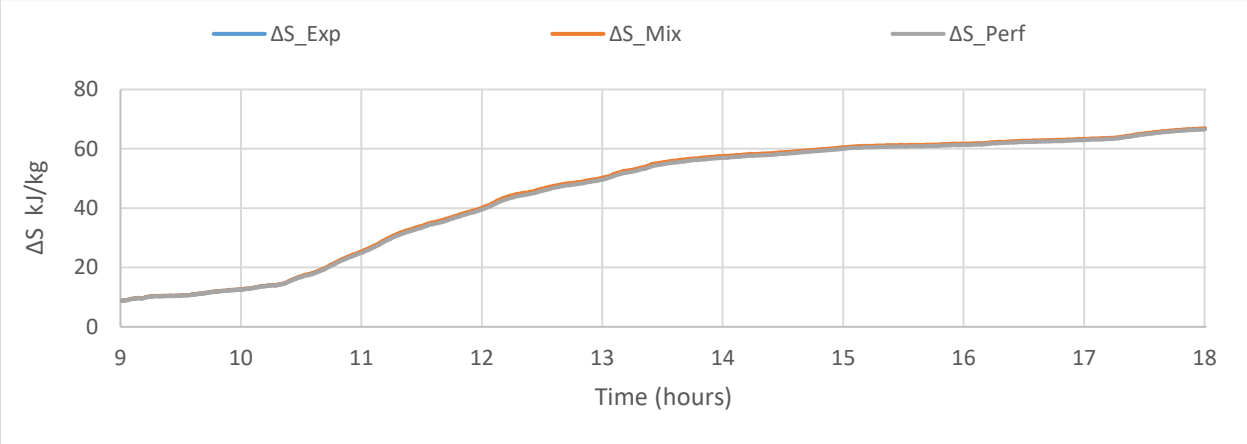


Figure 6-81b Entropy difference of four ports manifold in medium average PV power and cold tank conditions

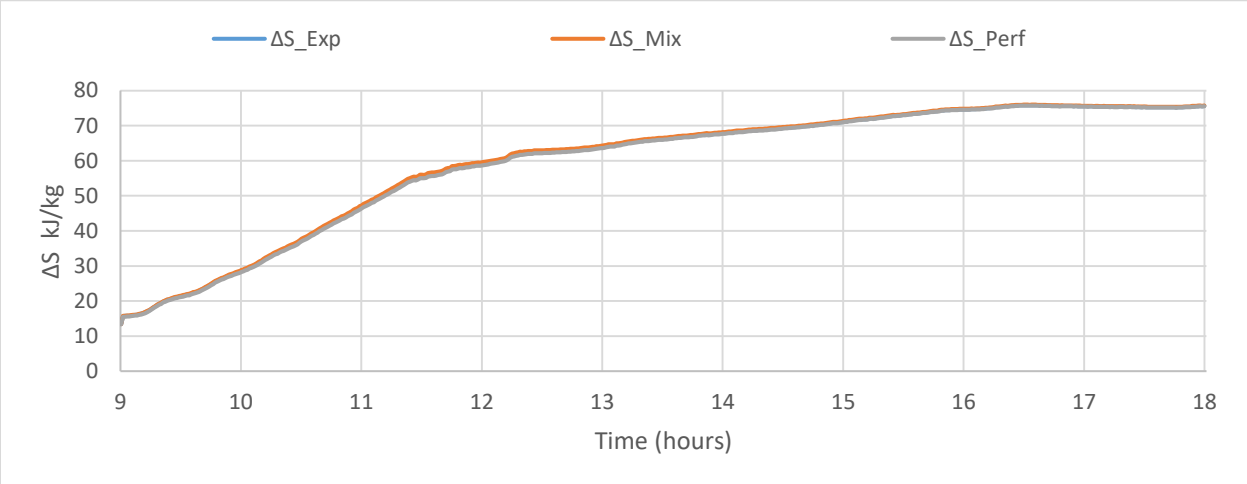


Figure 6-81c Entropy difference of one port copper tube in medium average PV power and cold tank conditions

Figure 6-81 Entropy difference inside the DHW Tank of three hot water inlet devices

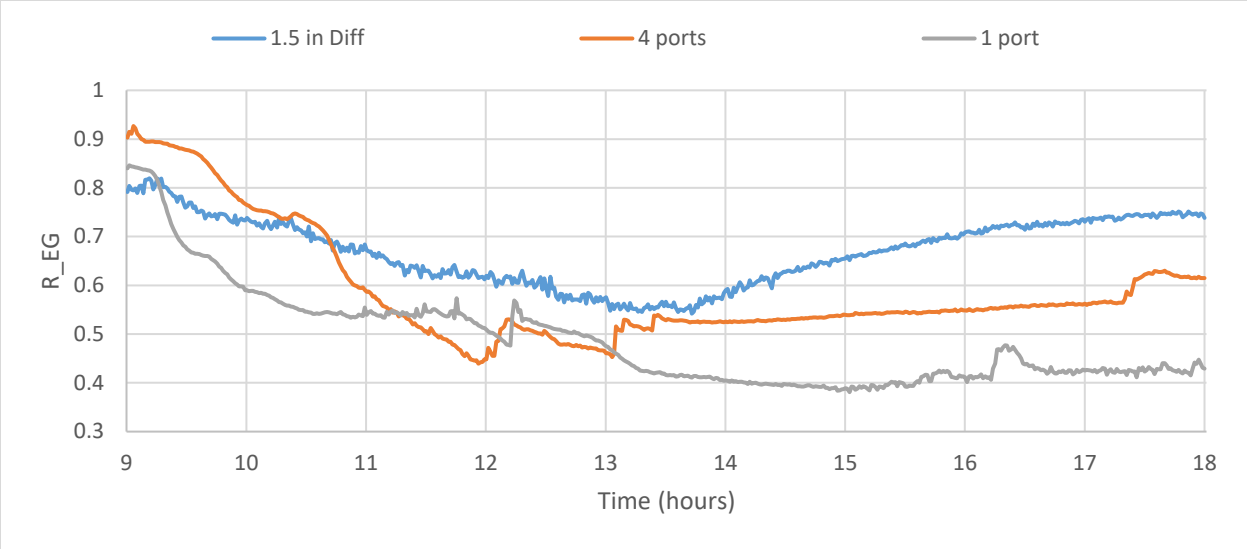


Figure 6-82 Internal entropy generation of inlet devices in medium average PV power and cold tank conditions.

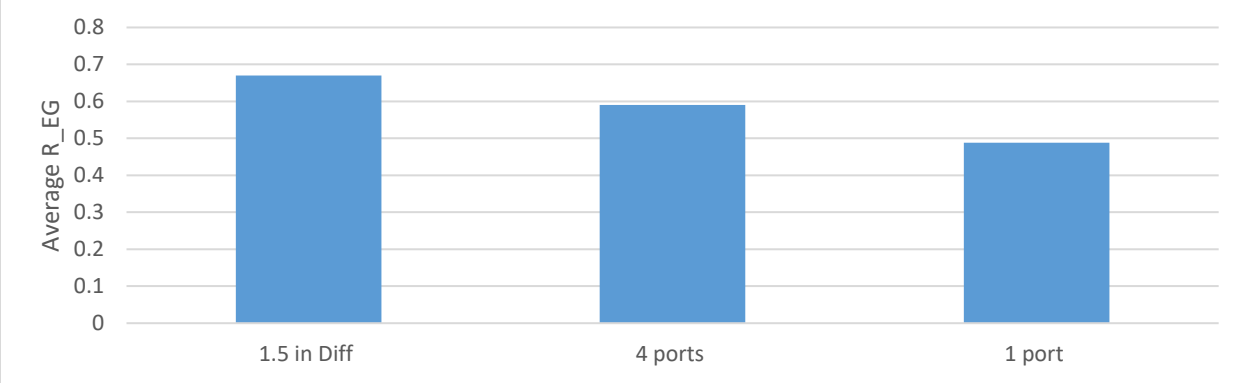


Figure 6-83 Average internal entropy generation of three inlet devices in medium average PV power and cold tank conditions.

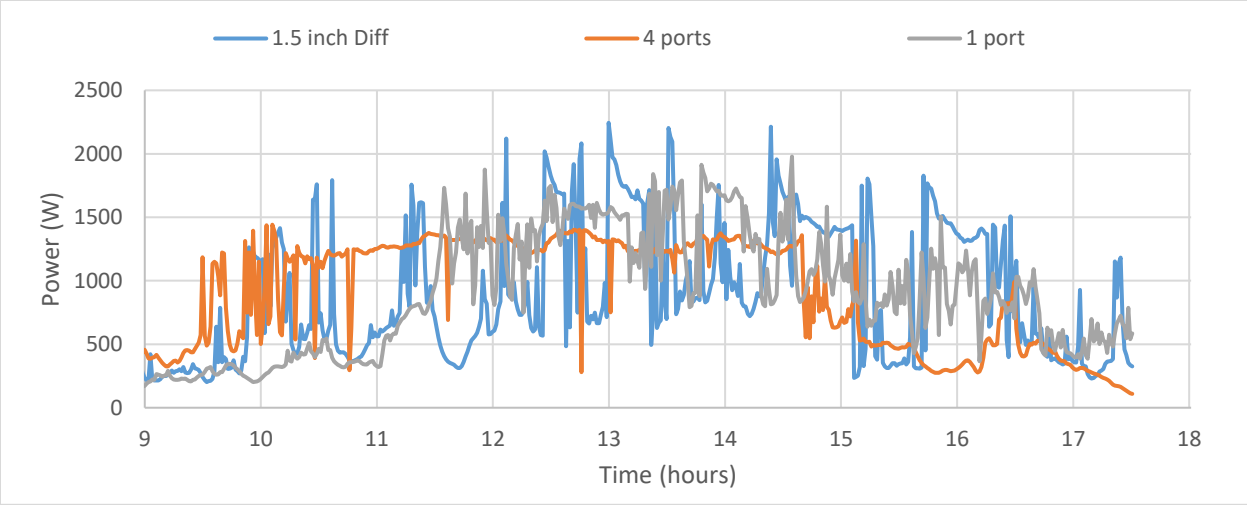


Figure 6-84 Medium PV power heater during three hot water inlet device tests for hot tank conditions.

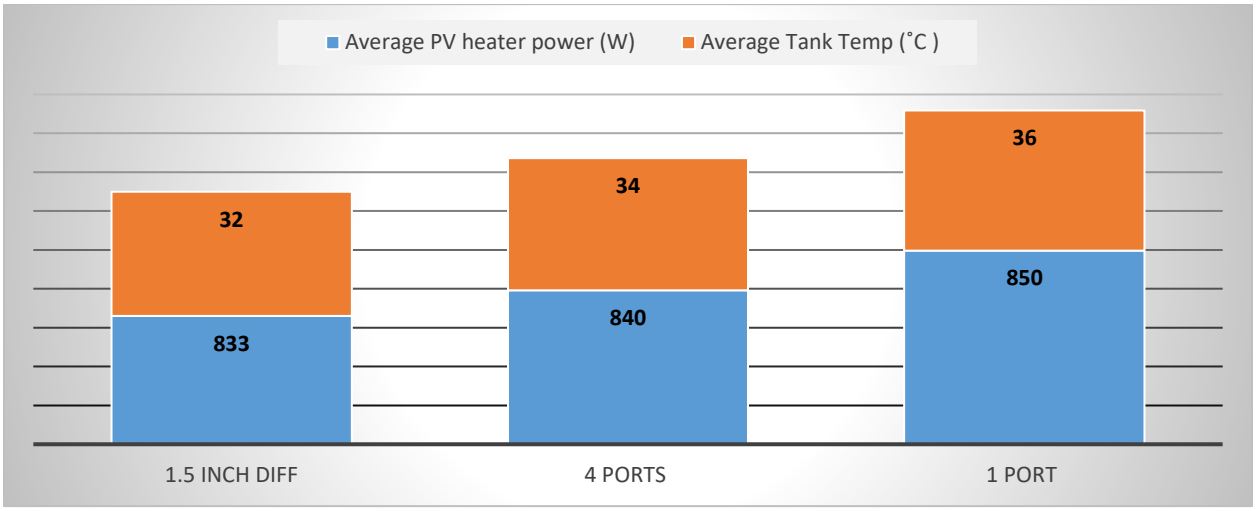


Figure 6-85 Medium average PV power and hot tank condition tests.

Table 6-9 Temperature Change Rate of the three tank Top Layers for Medium Average PV power and Hot Tank Condition

| 1.5 inch diffuser | 4 ports | 1 port |
|---|---|---|
| ˚C/h | ˚C/h | ˚C/h |
| 1.7 | 2.4 | 2.2 |

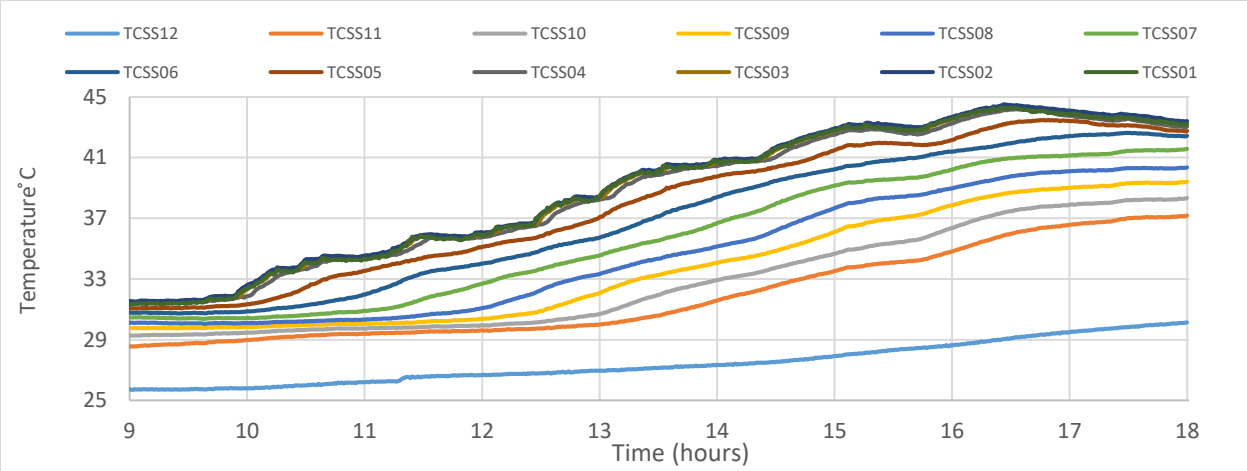


Figure 6-86a Graph showing 1.5-inch diffuser inlet device, medium average PV power, and hot tank conditions.

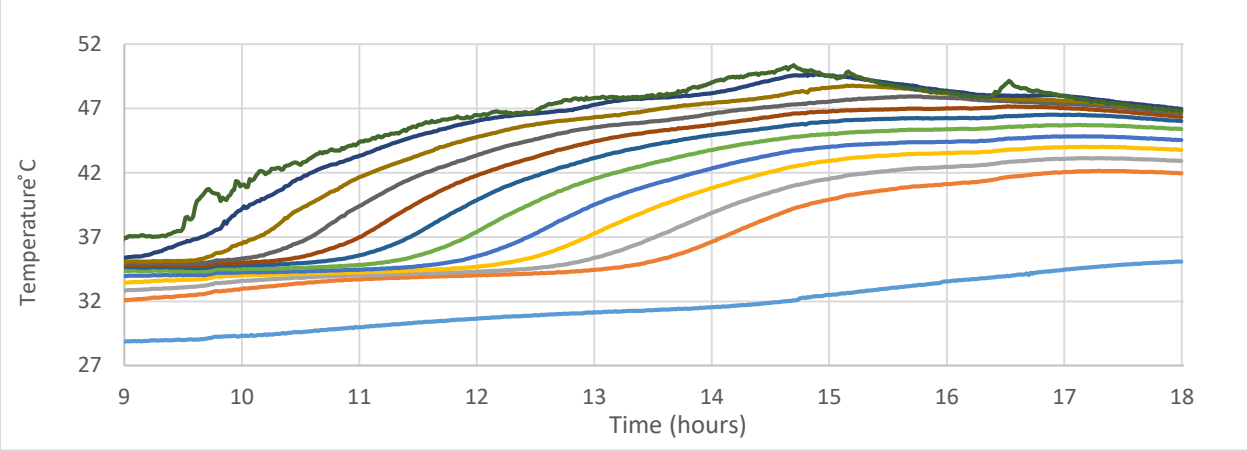


Figure 6-86b Graph showing four-port manifold inlet device, medium average PV power, and hot tank conditions.

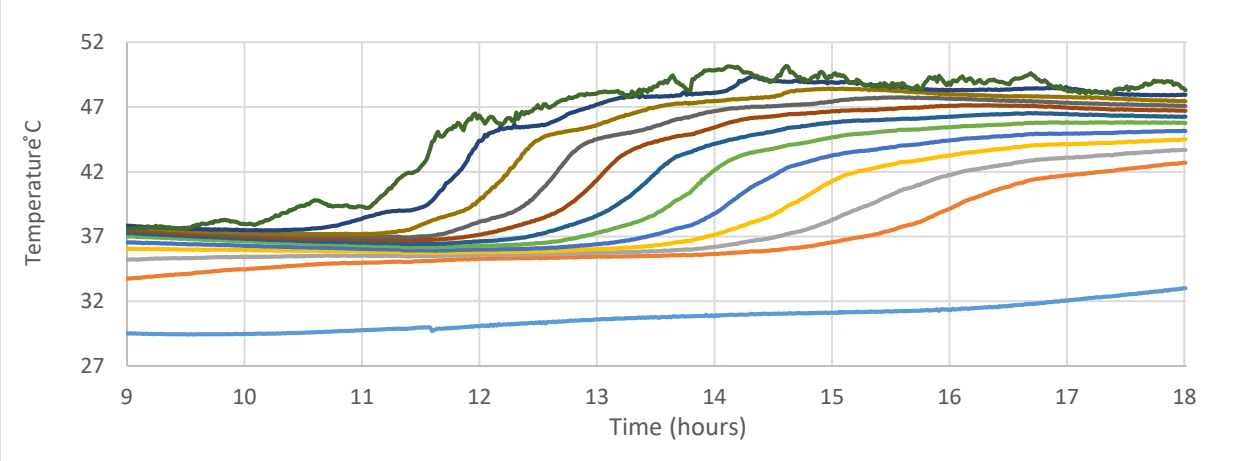


Figure 6-86c Graph showing one-port tube inlet device, medium average PV power, and hot tank conditions.

Figure 6-86 Temperature distribution inside DHW tanks using three hot water inlet devices.

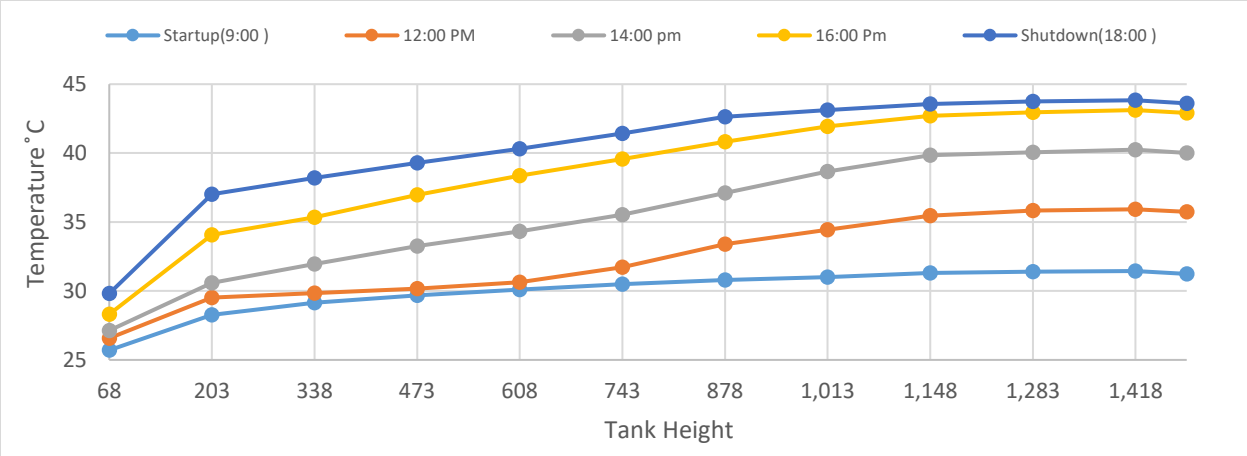


Figure 6-87a Graph showing 1.5-inch diffuser inlet device, medium average PV power, and hot tank conditions.

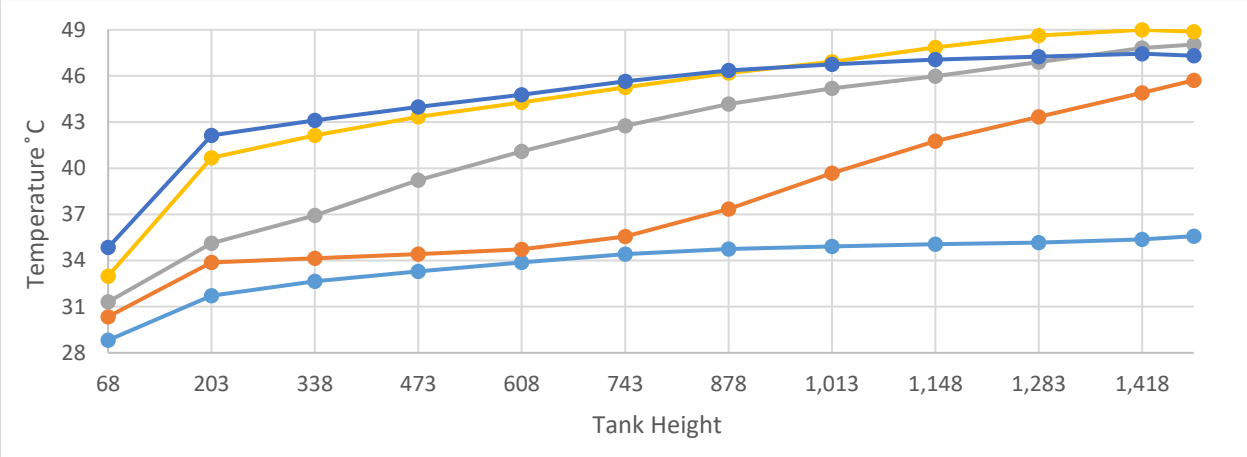


Figure 6-87b Graph showing four-port manifold inlet device, medium average PV power, and hot tank conditions.

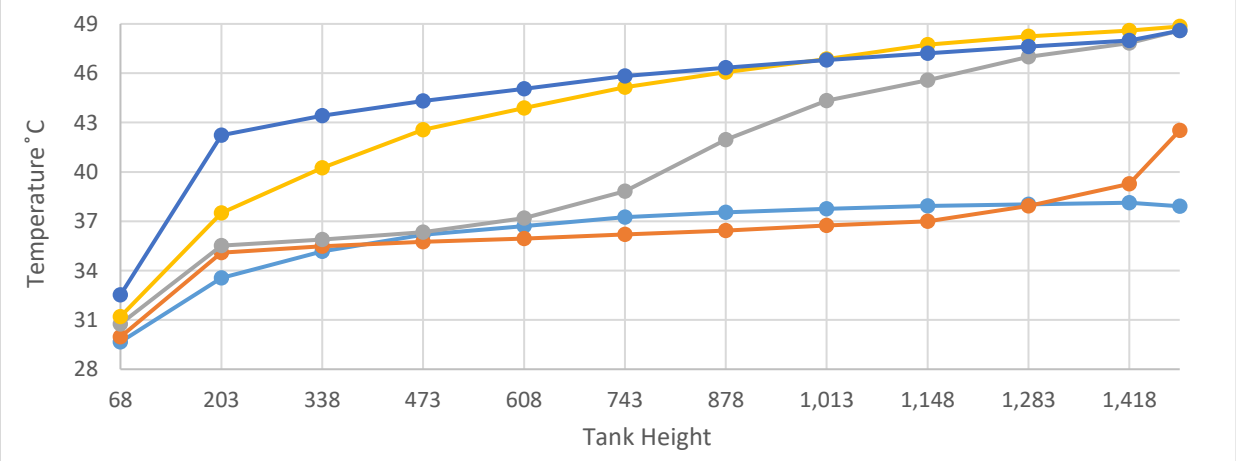


Figure 6-87c Graph showing one-port copper inlet device, medium average PV power, and hot tank conditions.

Figure 6-87 Temperature distribution inside DHW tanks using hot water inlet devices.

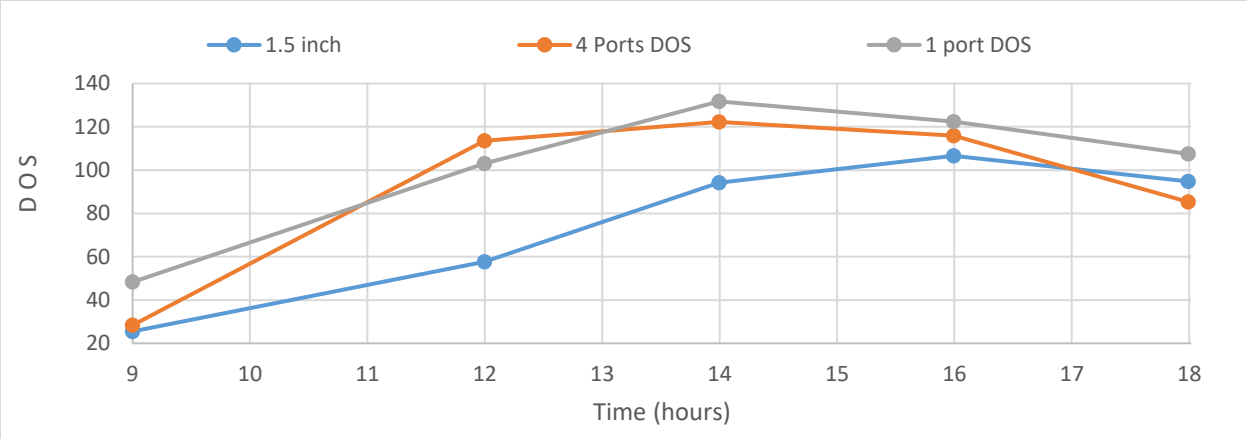


Figure 6-88 Degree of stratification of three hot water inlet devices, medium average PV power, and hot tank conditions.

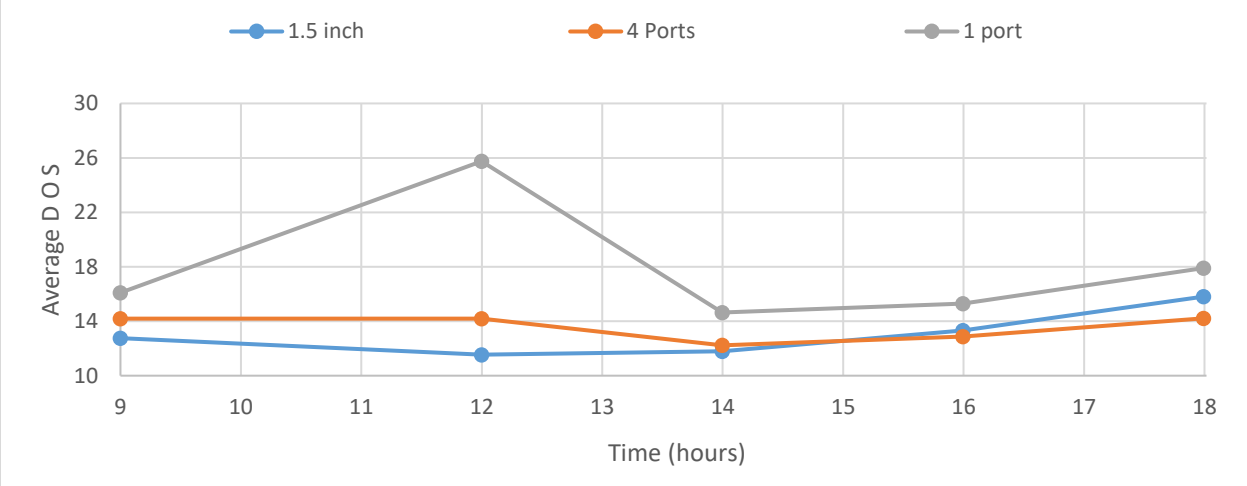


Figure 6-89 Average DOS of three inlet devices, medium average PV power, and hot tank conditions.

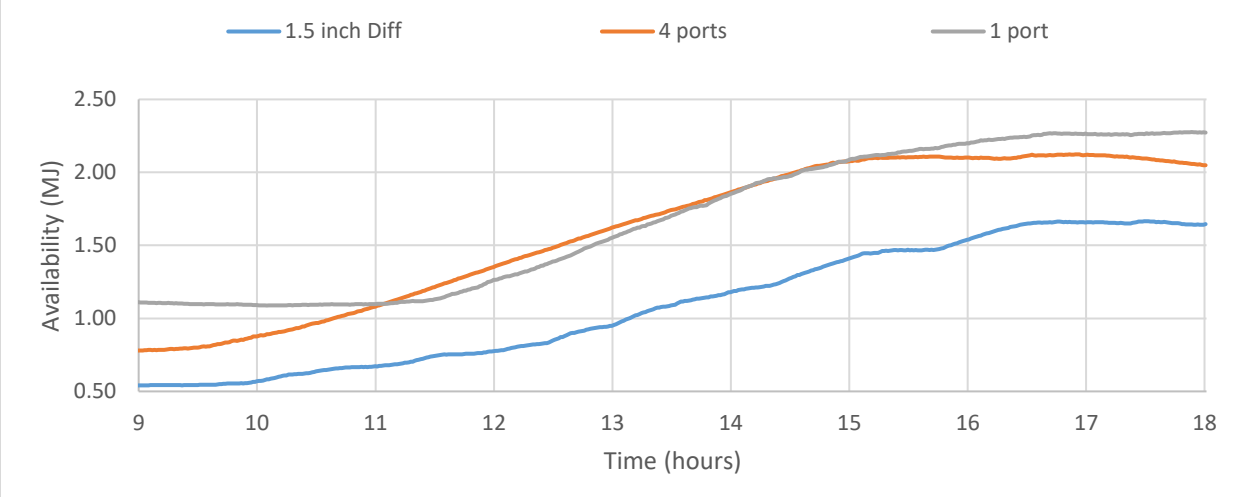


Figure 6-90 Availability for three inlet devices in medium average PV power and hot tank conditions.

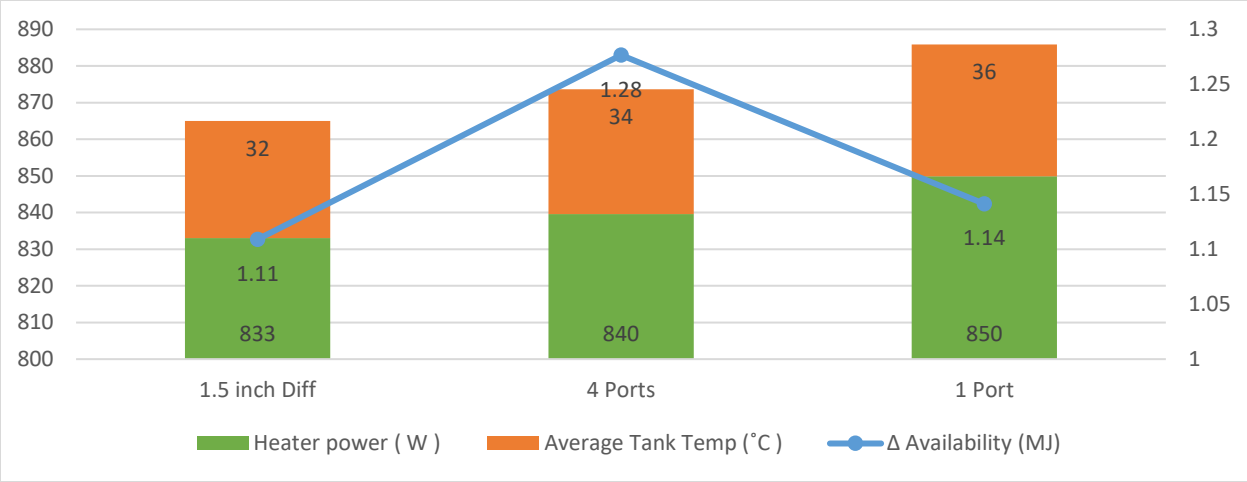


Figure 6-91 Availability change for three inlet devices in medium average PV power and hot tank conditions.

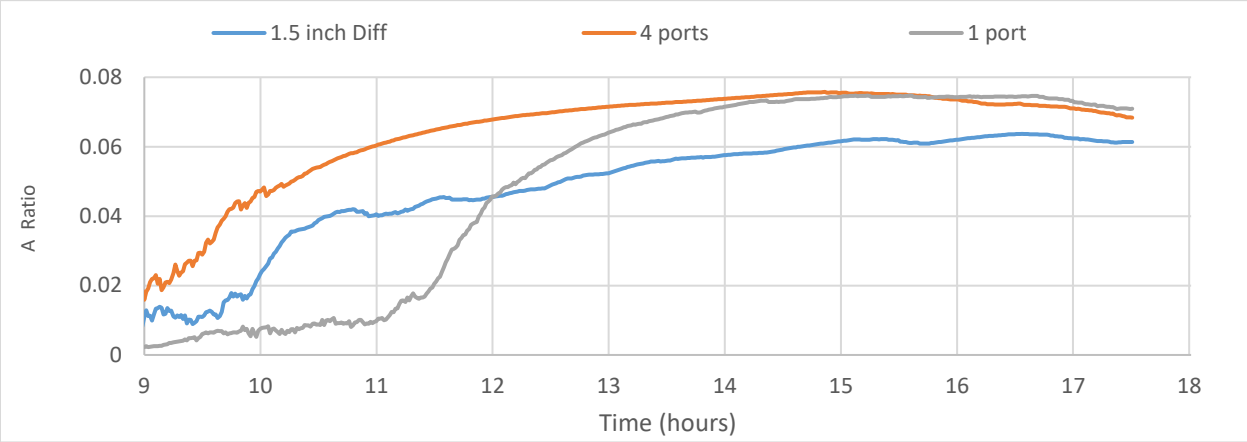


Figure 6-92 Availability ratios for three inlet devices in medium average PV power and hot tank conditions.

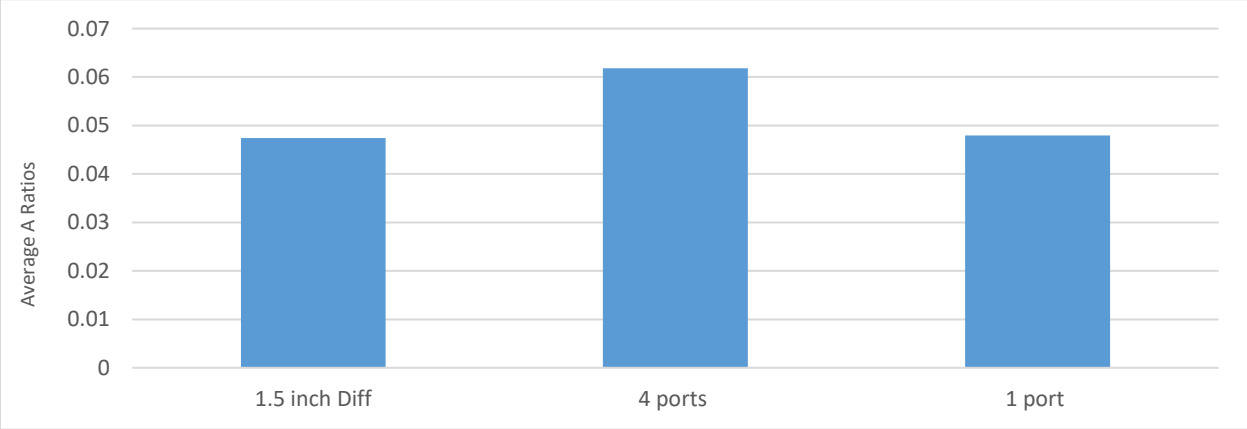


Figure 6-93 Average availability ratio for three inlet devices in medium average PV power and hot tank conditions.

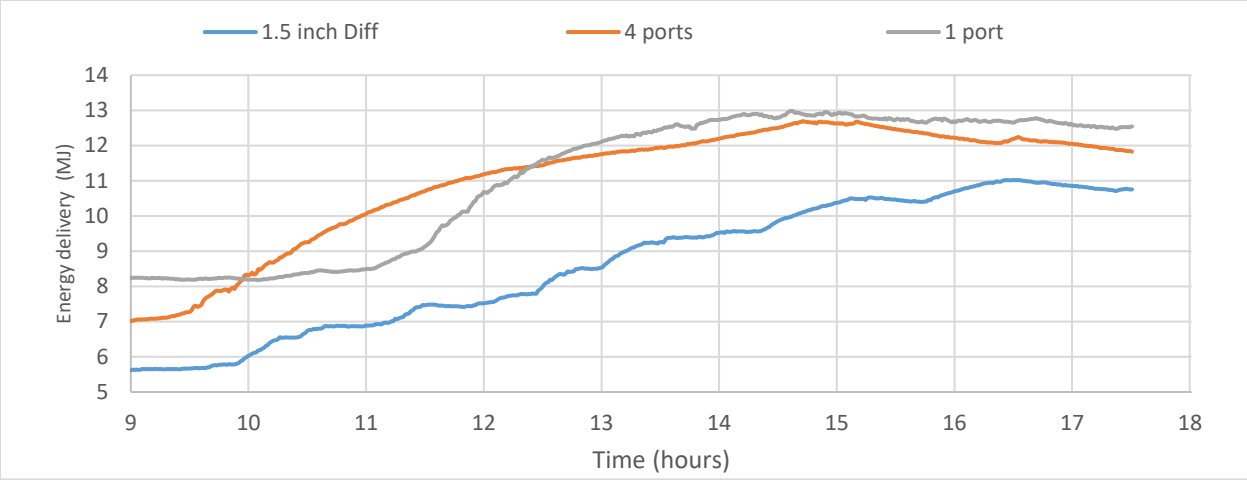


Figure 6-94 Energy delivery for three inlet devices in medium average PV power and hot tank conditions.

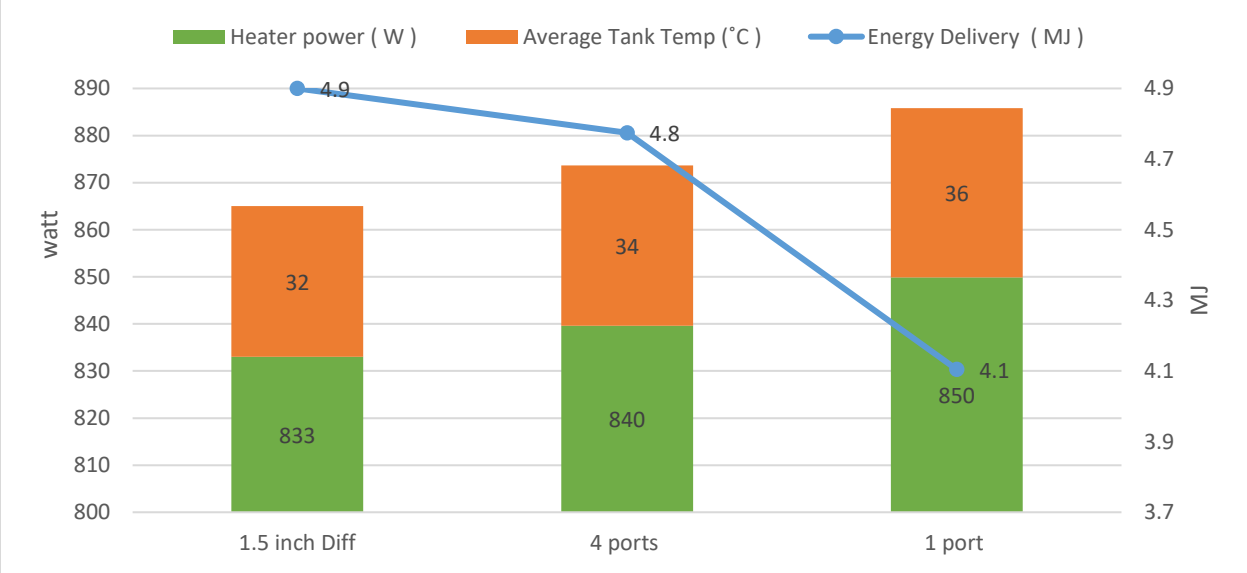


Figure 6-95 Energy delivery, medium PV power, and dead-state temperature of the three devices in hot tank conditions.

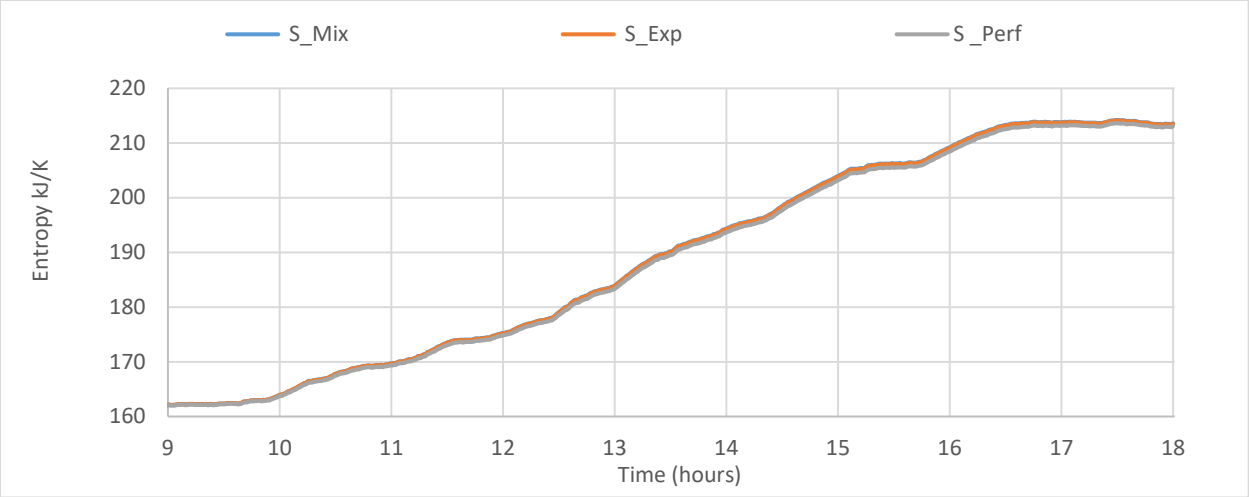


Figure 6-96a Entropy of 1.5-inch diffuser for three inlet devices in medium average PV power and hot tank conditions.

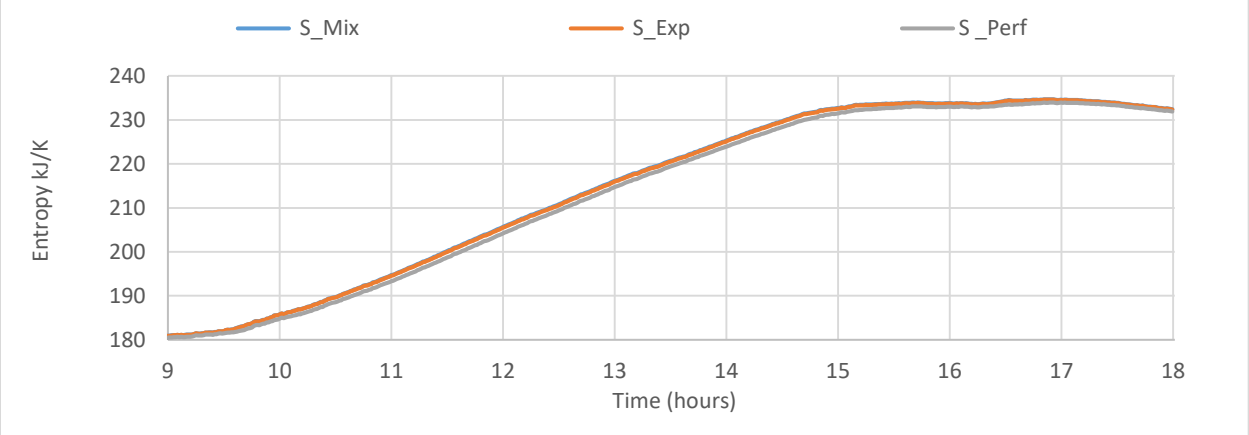


Figure 6-96b Entropy of four ports manifold for three inlet devices in medium average PV power and hot tank conditions.

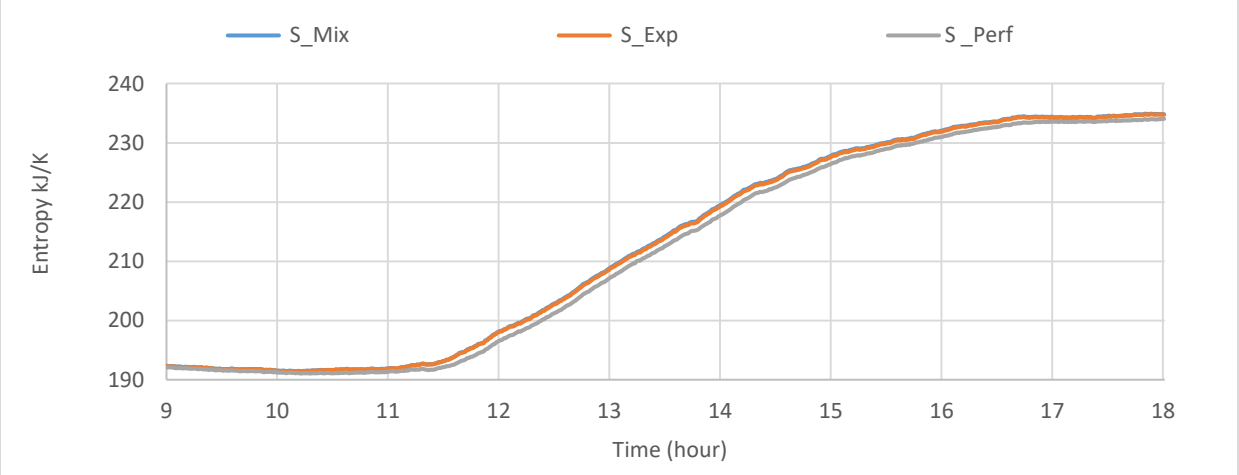


Figure 6-96c Entropy of one port copper tube for three inlet devices in medium average PV power and hot tank conditions.

Figure 6-96 Entropy inside the DHW Tank of three hot water inlet devices

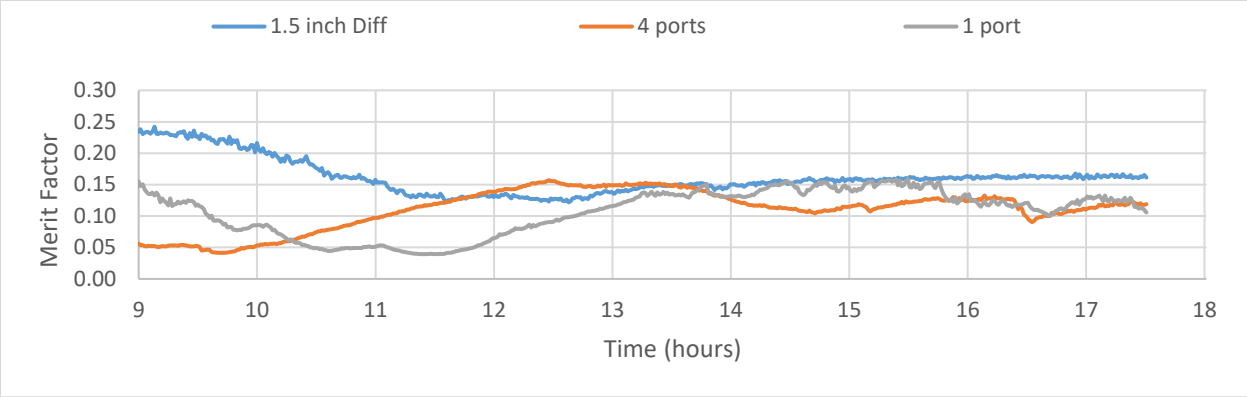


Figure 6-97 Merit factor for three hot water inlet devices in medium average PV power, and hot tank conditions.

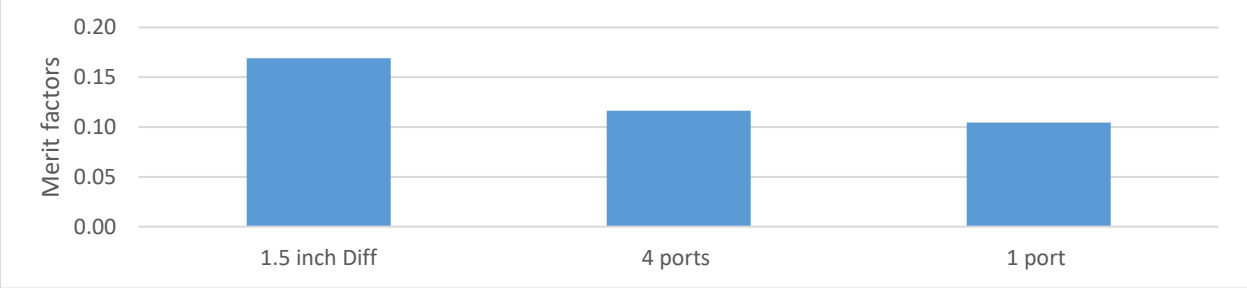


Figure 6-98 Merit factor for three hot water inlet devices at the end of the test in hot tank conditions.

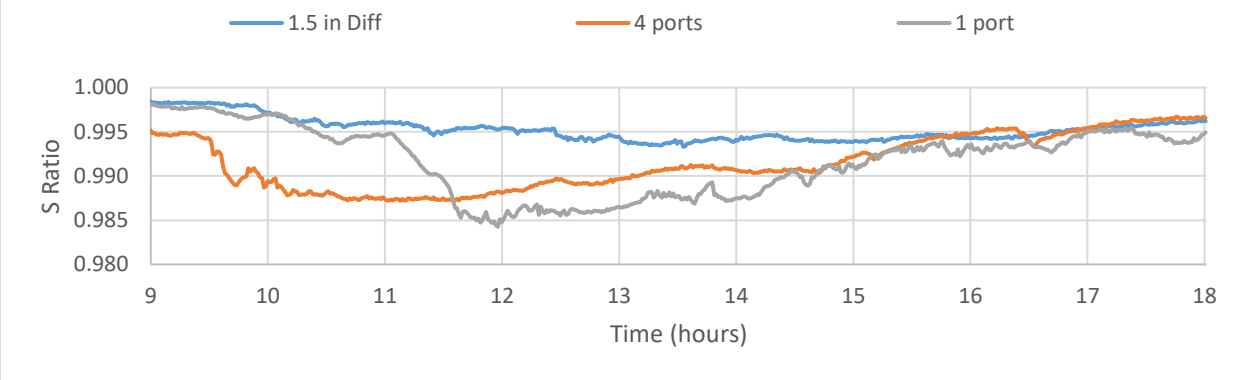


Figure 6-99 Entropy ratios of inlet devices in medium average PV power and hot tank conditions.

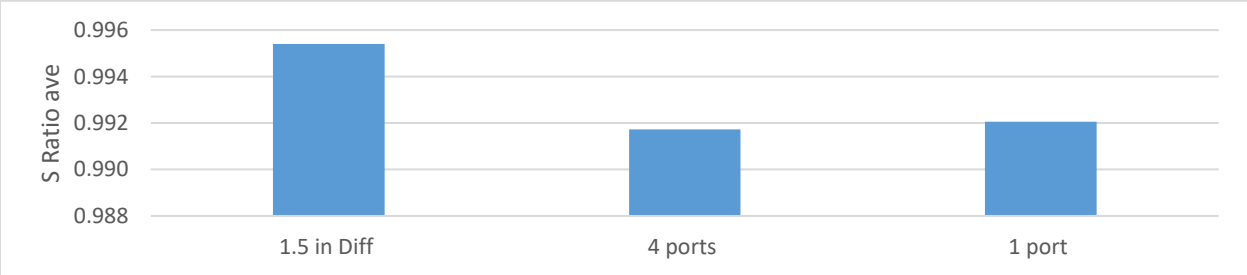


Figure 6-100 Entropy ratios of inlet devices in medium average PV power and hot tank conditions.

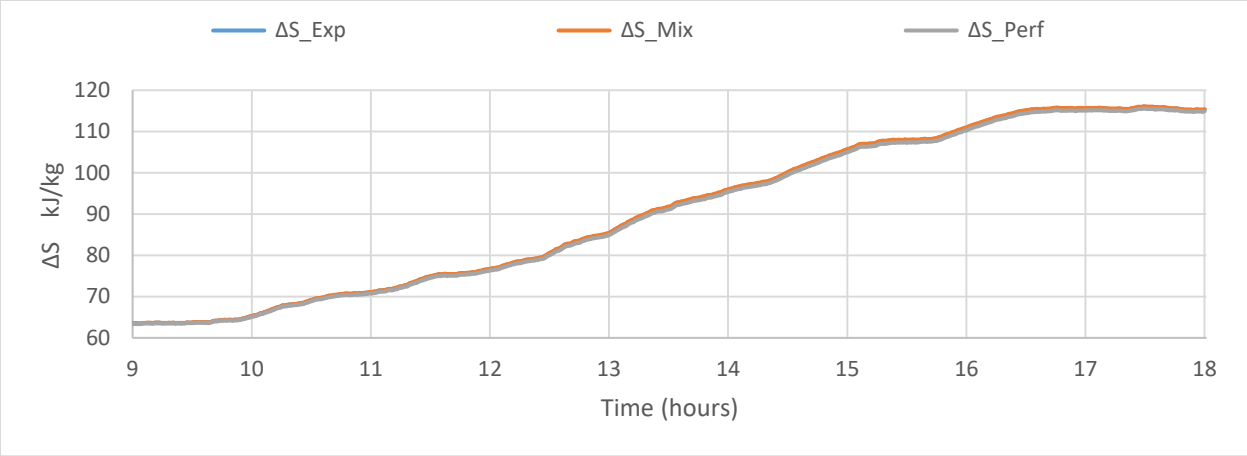


Figure 6-101a Entropy difference of 1.5-inch diffuser in medium average PV power and hot tank conditions.

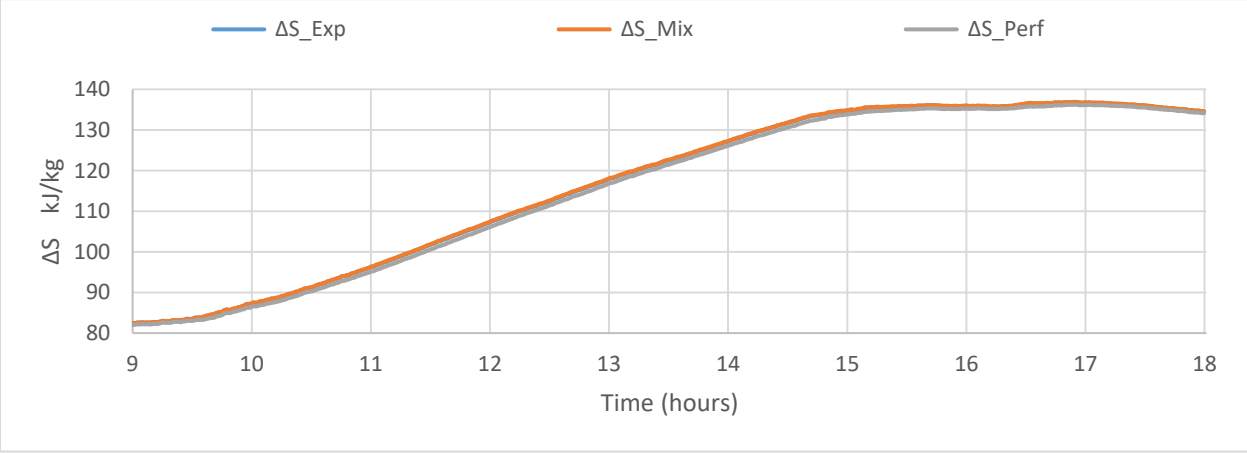


Figure 6-101b Entropy difference of four ports manifold in medium average PV power and hot tank conditions

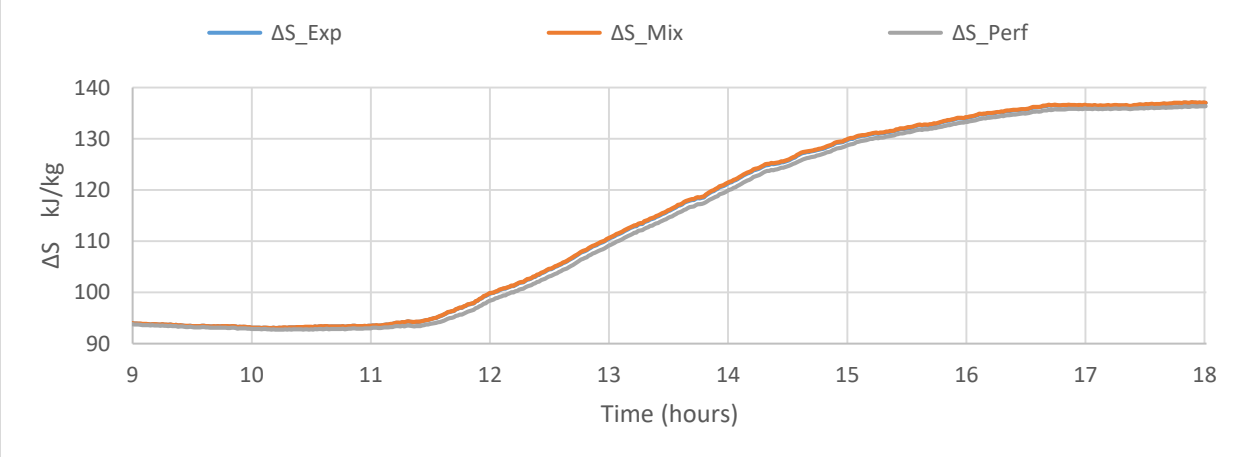


Figure 6-101c Entropy difference of one port copper tube in medium average PV power and hot tank conditions

Figure 6-101 Entropy difference inside the DHW Tank of three hot water inlet devices

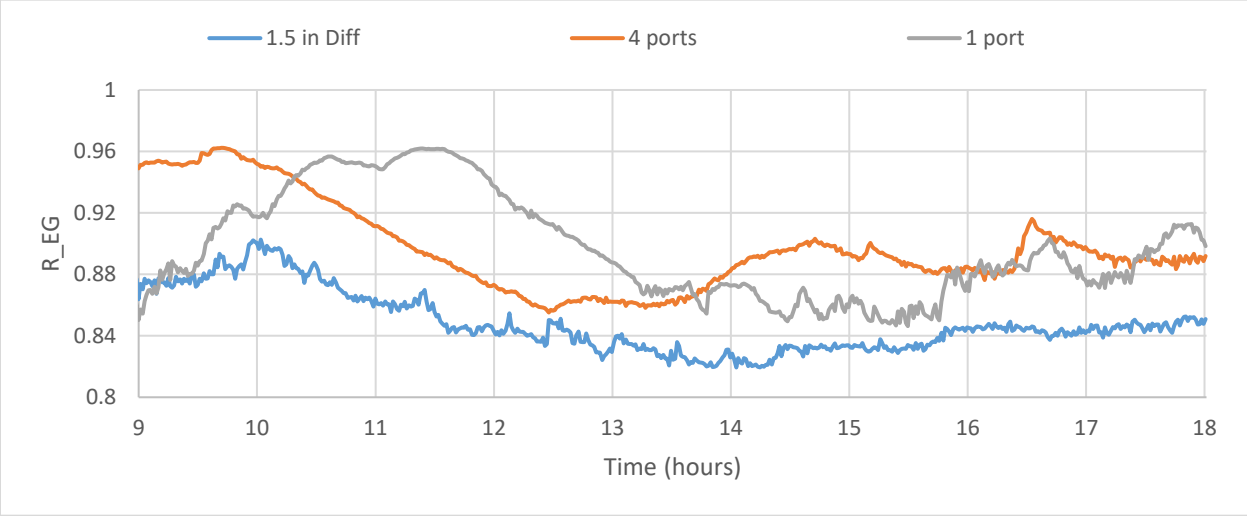


Figure 6-102 Internal entropy generation of inlet devices in medium average PV power and hot tank conditions.

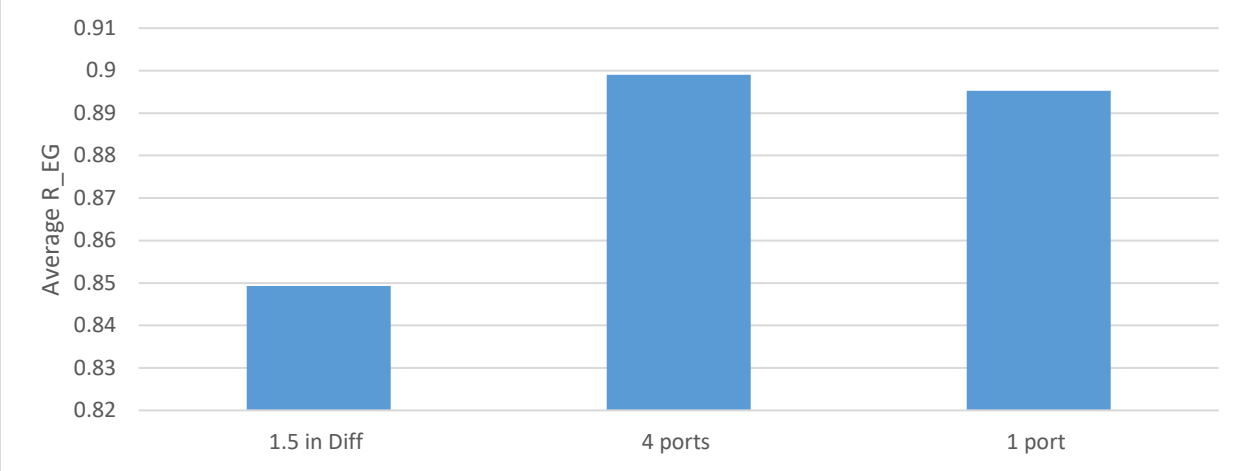


Figure 6-103 Average internal entropy generation of three inlet devices in medium average PV power and hot tank conditions.

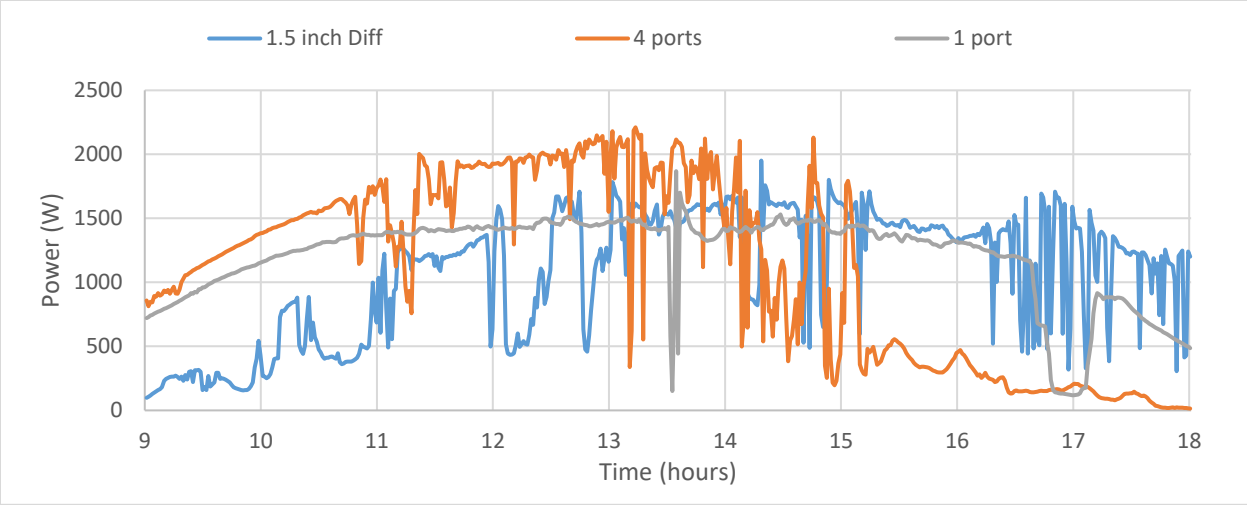


Figure 6-104 High PV power heater during three hot water inlet device tests for cold tank conditions.

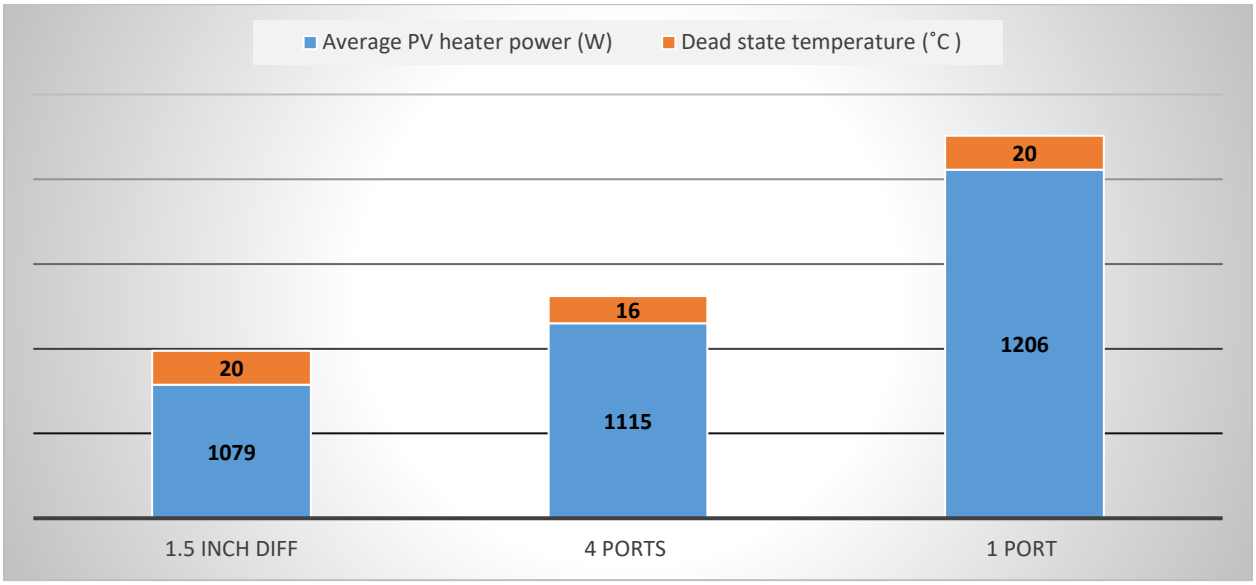


Figure 6-105 High average PV power and cold tank condition tests.

Table 6-10 Temperature Change Rate of the three tank Top Layers for High Average PV power and Cold Tank Condition

| 1.5 inch diffuser | 4 ports | 1 port |
|---|---|---|
| ˚C/h | ˚C/h | ˚C/h |
| 2.4 | 4.2 | 4.3 |

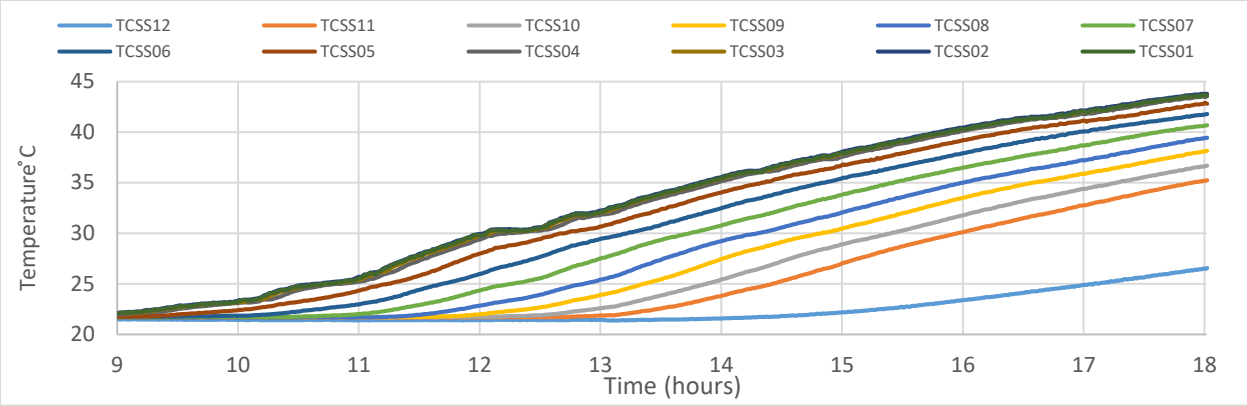


Figure 6-106a Graph showing 1.5-inch diffuser inlet device, high average PV power, and cold tank conditions.

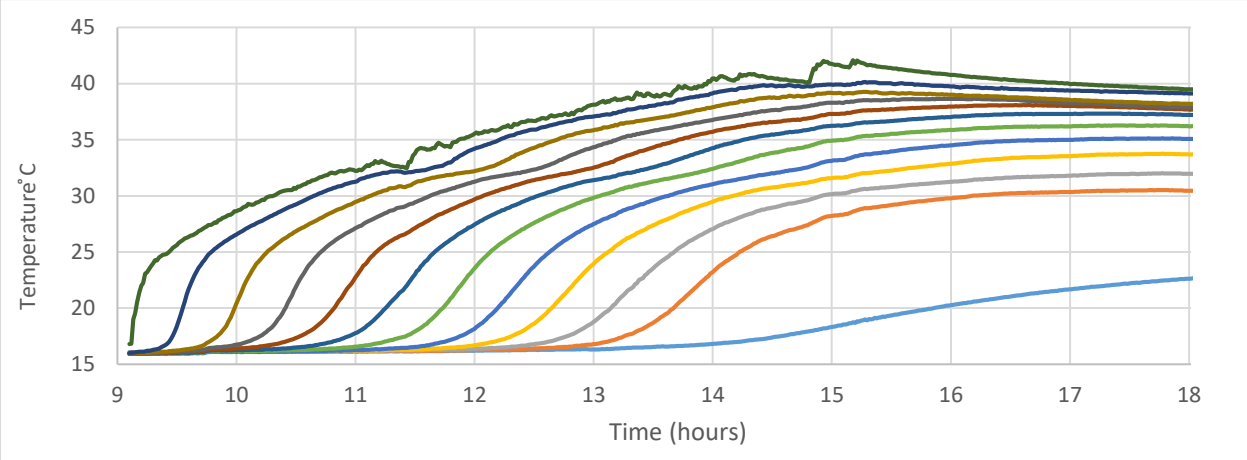


Figure 6-106b Graph showing four-port manifold inlet device, high average PV power, and cold tank conditions.

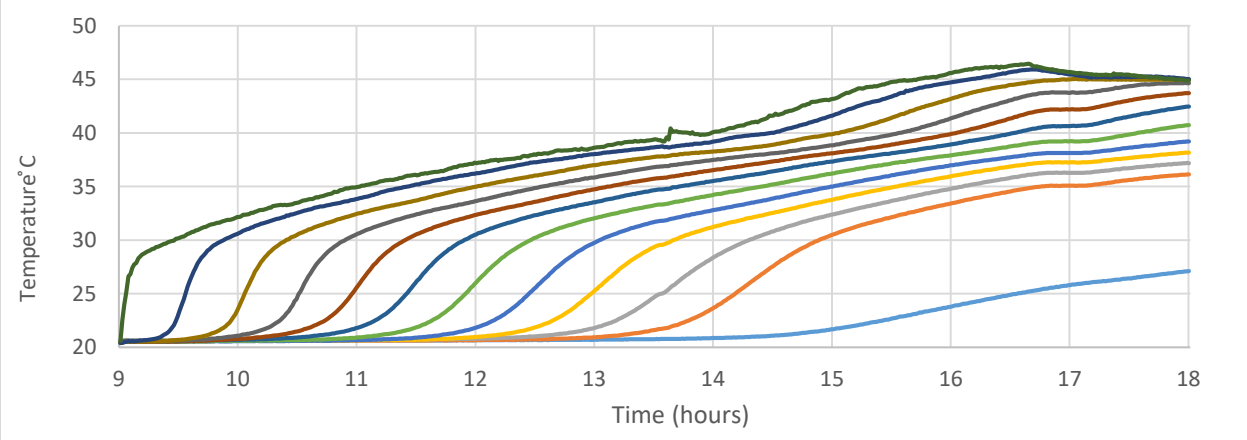


Figure 6-106c Graph showing one-port tube inlet device, high average PV power, and cold tank conditions.

Figure 6-106 Temperature distribution inside DHW tanks using three hot water inlet devices.

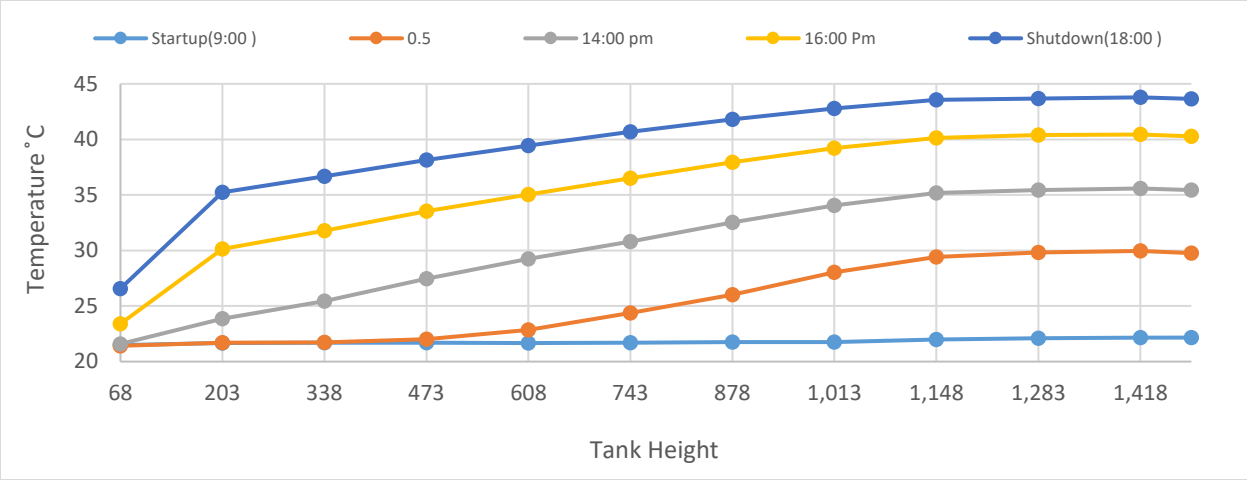


Figure 6-107a Graph showing 1.5-inch diffuser inlet device, high average PV power, and cold tank conditions.

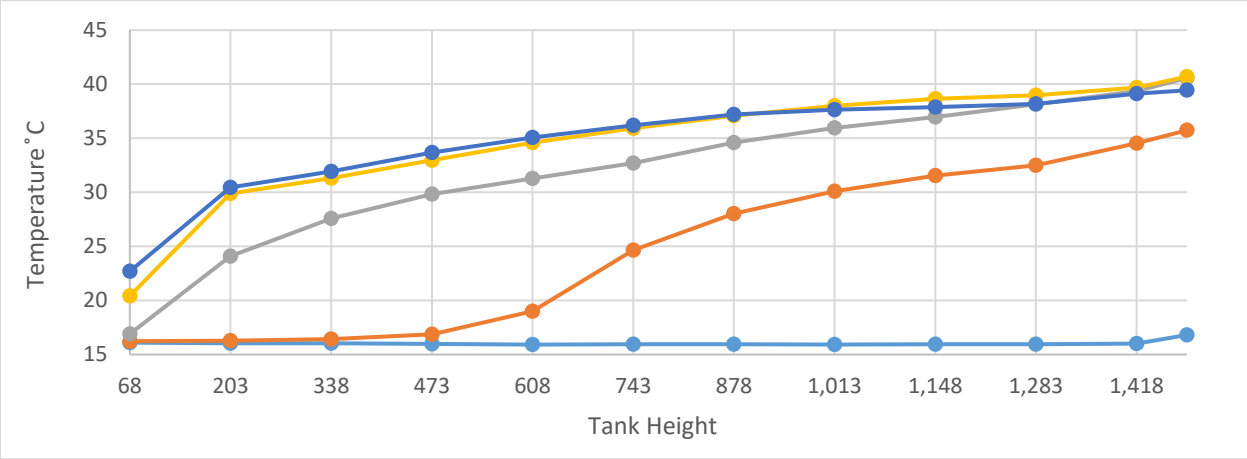


Figure 6.107b Graph showing four-port manifold inlet device, high average PV power, and cold tank conditions.

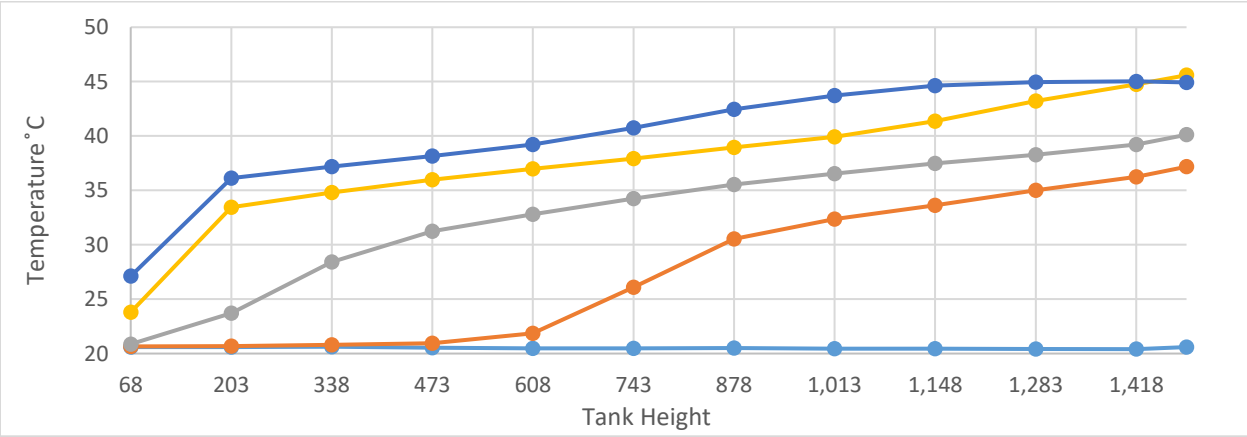


Figure 6-107c Graph showing one-port copper inlet device, high average PV power, and cold tank conditions.

Figure 6-107 Temperature distribution inside DHW tanks using hot water inlet devices.

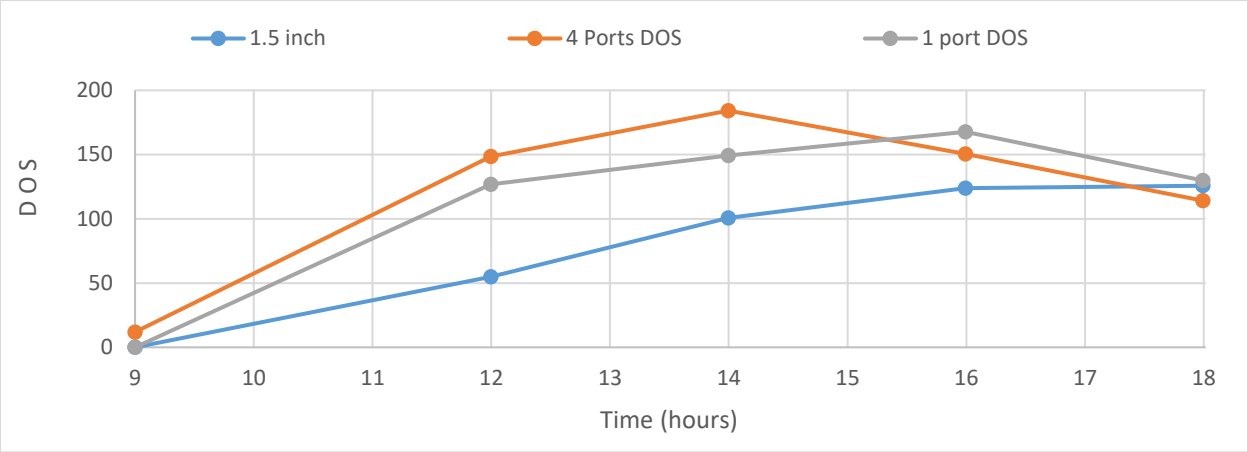


Figure 6-108 Degree of stratification of three hot water inlet devices, high average PV power, and cold tank conditions.

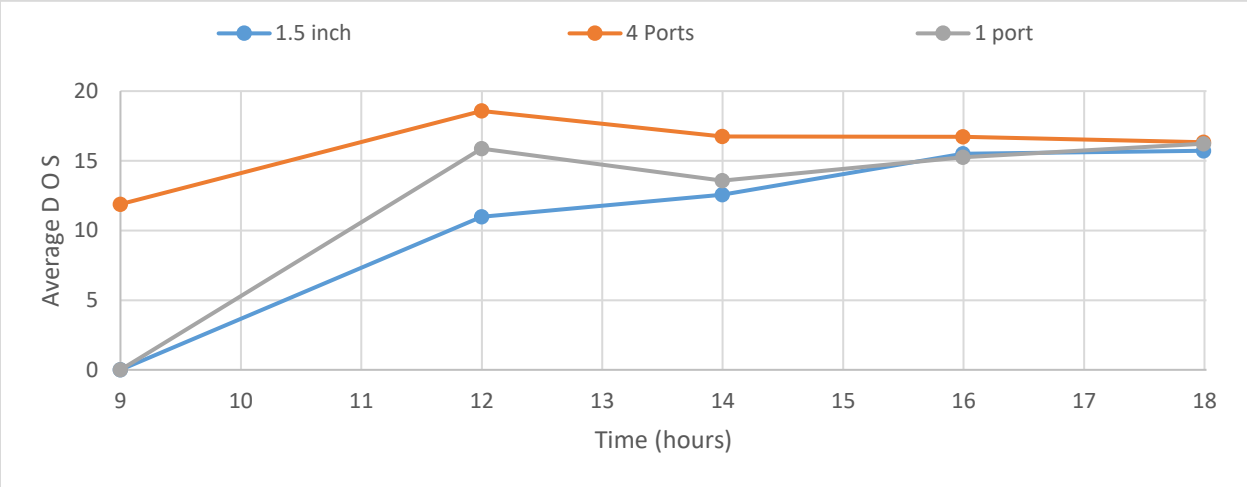


Figure 6-109 Average DOS of three inlet devices, high average PV power, and cold tank conditions.

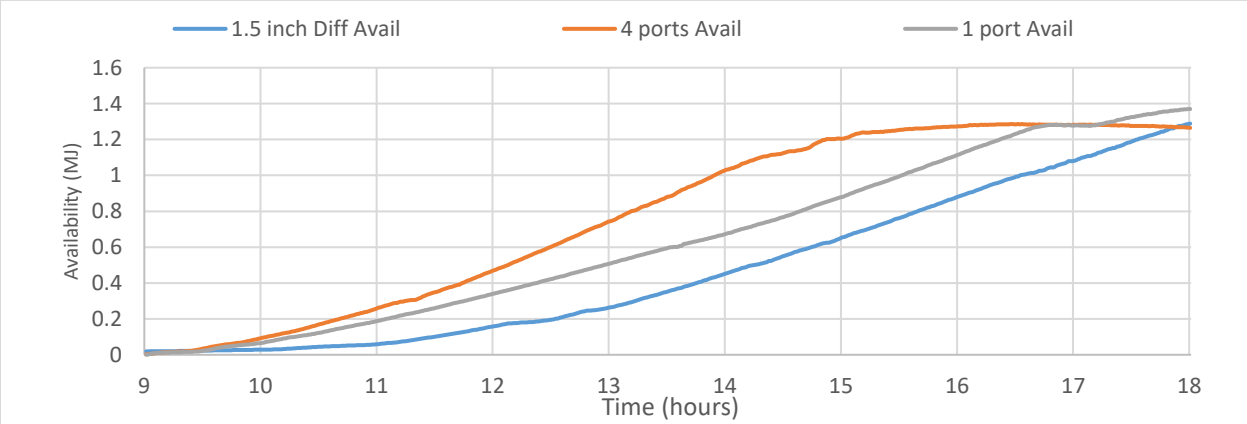


Figure 6-110 Availability for three inlet devices in high average PV power and cold tank conditions.

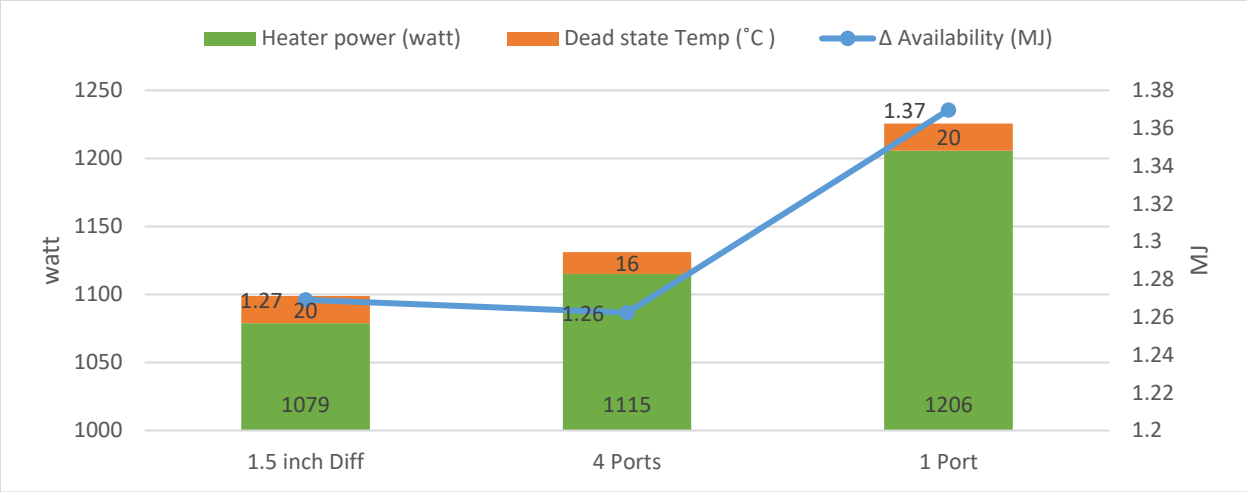


Figure 6-111 Availability change for three inlet devices in high average PV power and cold tank conditions.

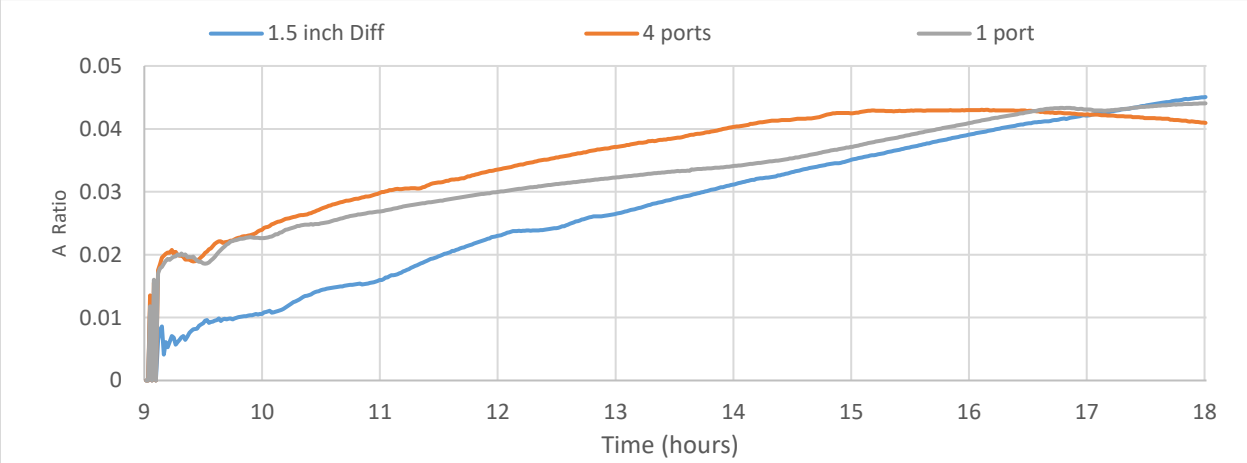


Figure 6-112 Availability ratios for three inlet devices in high average PV power and cold tank conditions.

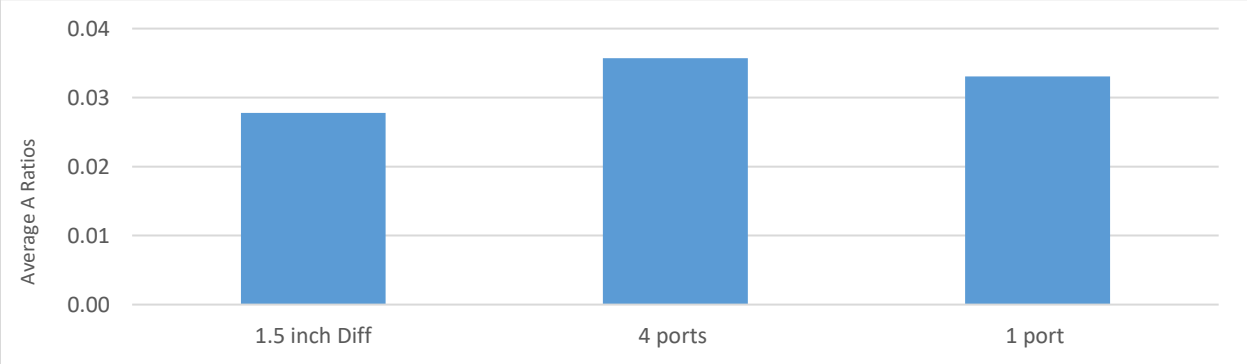


Figure 6-113 Average availability ratio for three inlet devices in high average PV power and cold tank conditions.

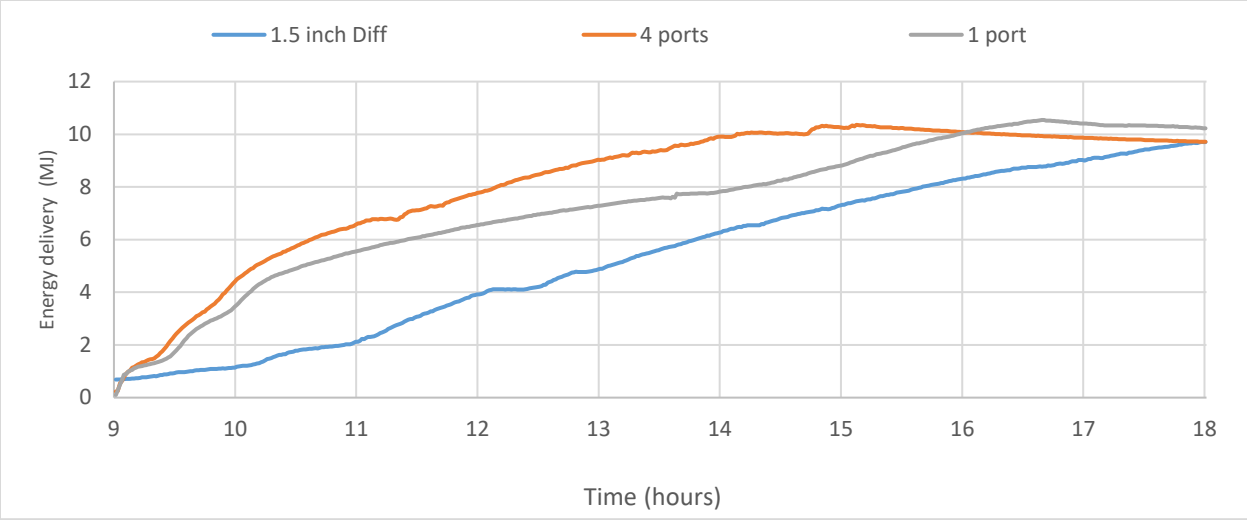


Figure 6-114 Energy delivery for three inlet devices in high average PV power and cold tank conditions.

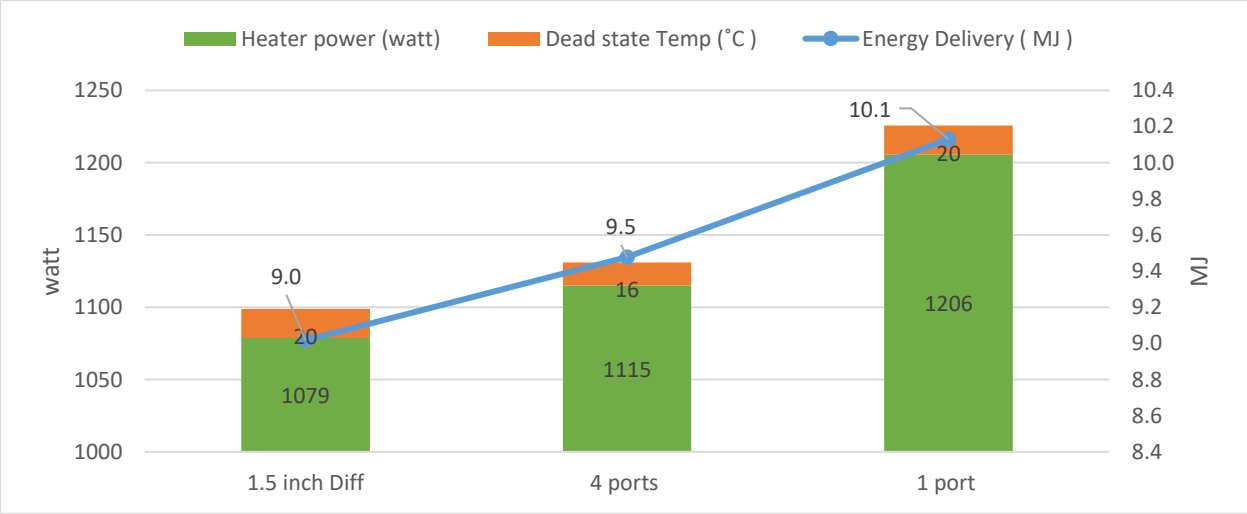


Figure 6-115 Energy delivery, high PV power, and dead-state temperature of the three devices in cold tank conditions.

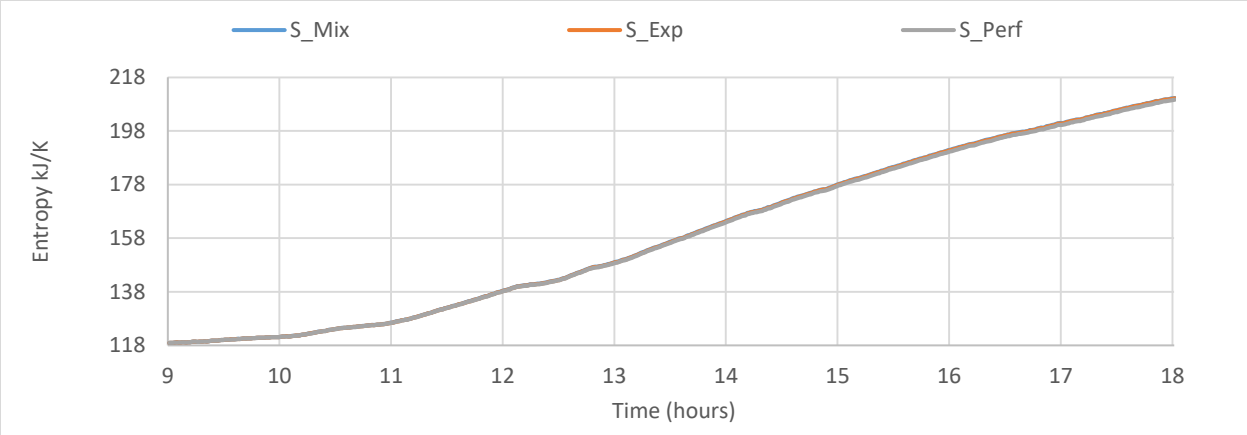


Figure 6-116a Entropy of 1.5-inch diffuser for three inlet devices in high average PV power and cold tank conditions.

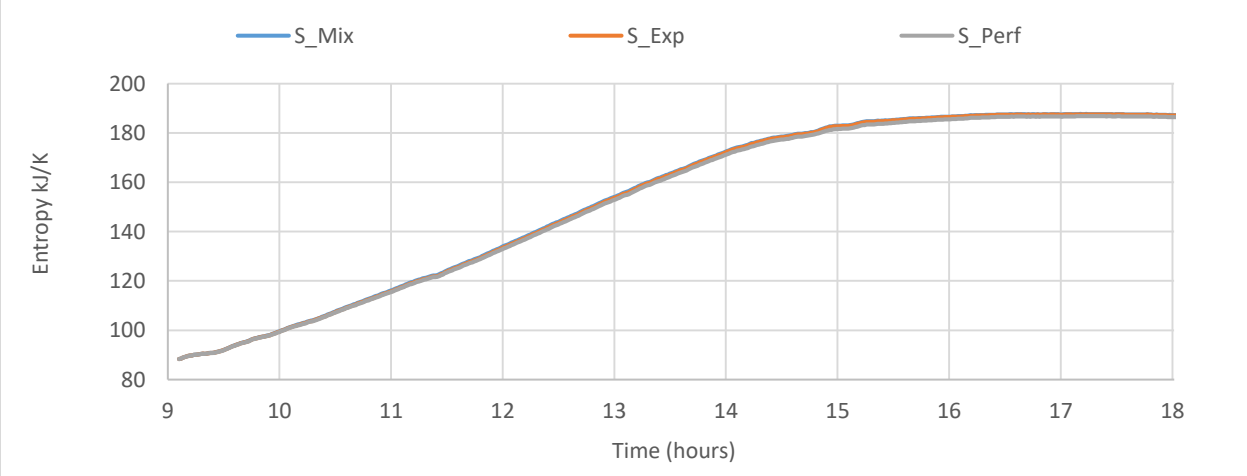


Figure 6-116b Entropy of four ports manifold for three inlet devices in high average PV power and cold tank conditions.

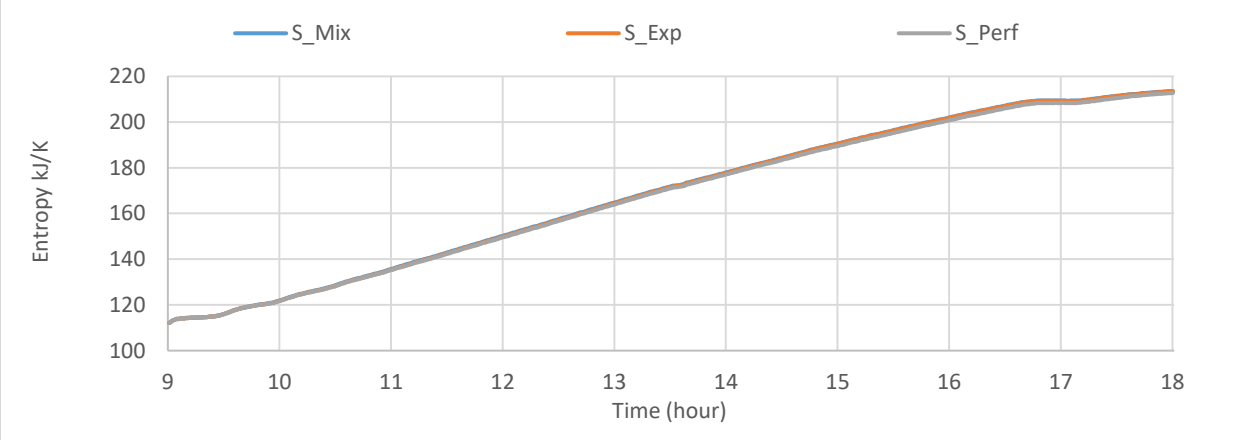


Figure 6-116c Entropy of one port copper tube for three inlet devices in high average PV power and cold tank conditions.

Figure 6-116 Entropy inside the DHW Tank of three hot water inlet devices

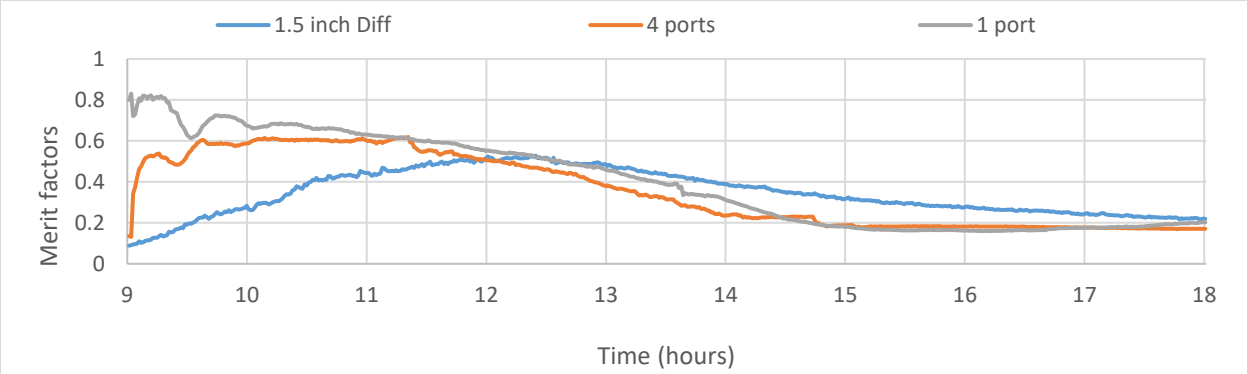


Figure 6-117 Merit factor for three hot water inlet devices in high average PV power, and cold tank conditions.

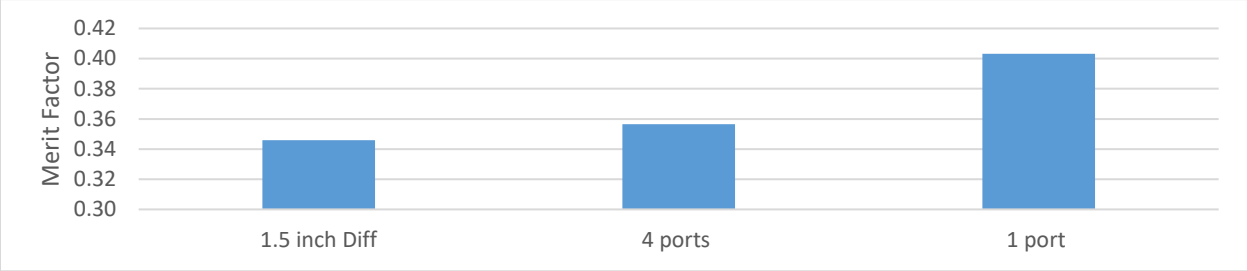


Figure 6-118 Merit factor for three hot water inlet devices at the end of the test in cold tank conditions.

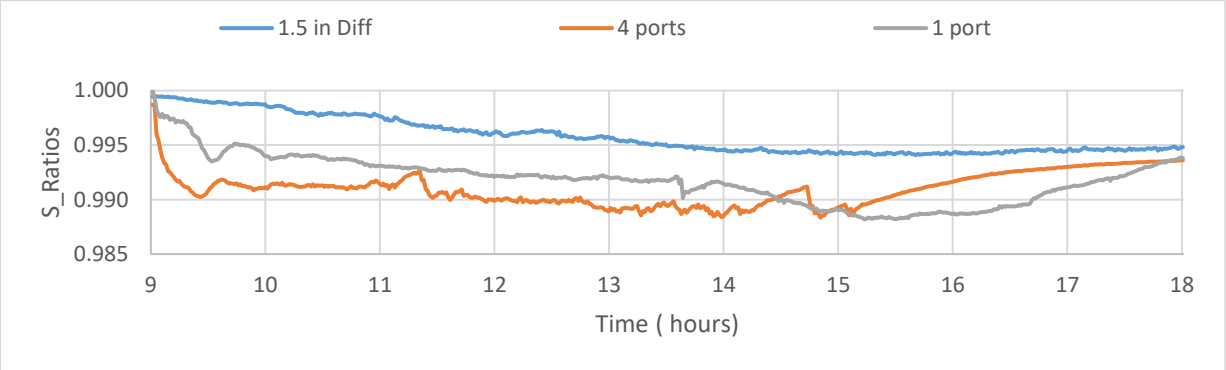


Figure 6-119 Entropy ratios of three inlet devices in high average PV power and cold tank conditions.

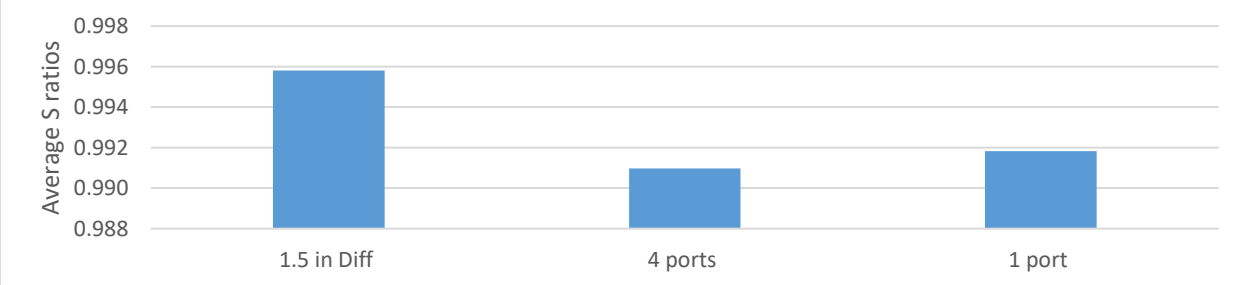


Figure 6-120 Entropy ratios of three inlet devices in high average PV power and cold tank conditions.

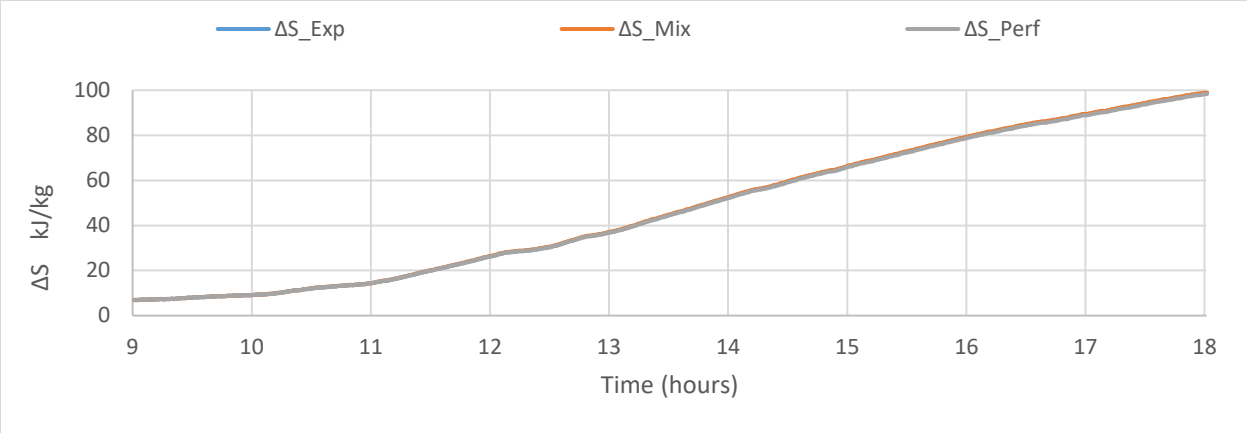


Figure 6-121a Entropy difference of 1.5-inch diffuser in high average PV power and cold tank conditions.

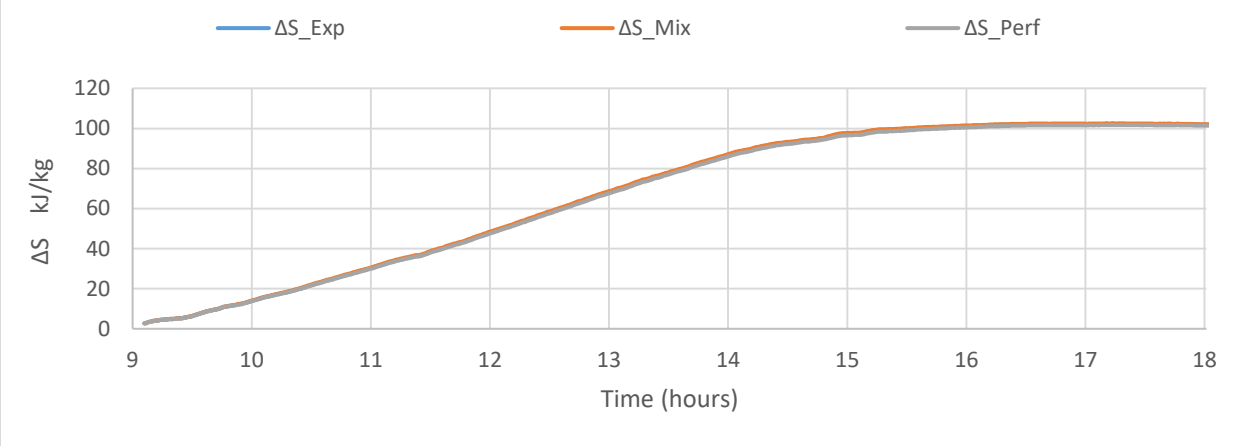


Figure 6-121b Entropy difference of four ports manifold in high average PV power and cold tank conditions

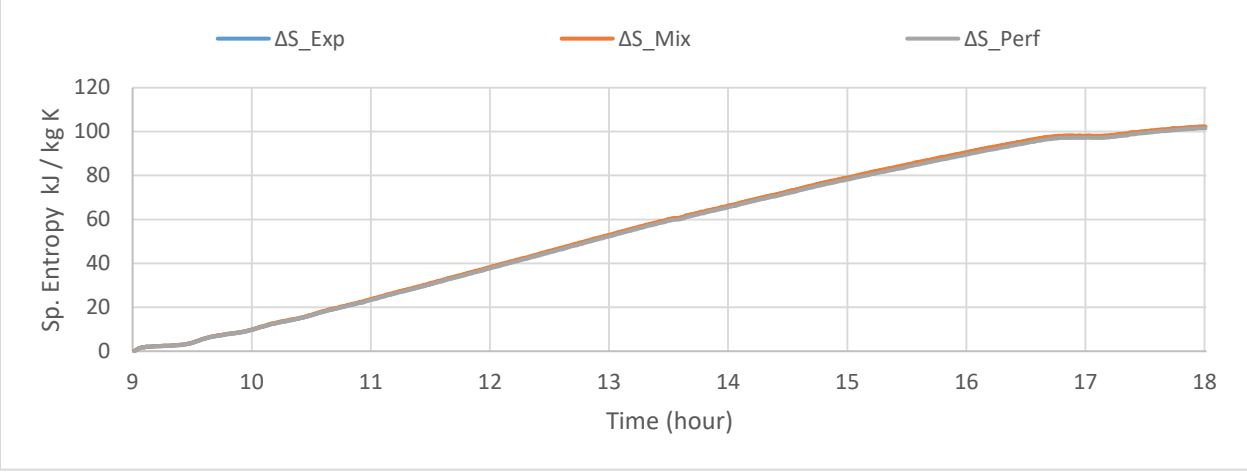


Figure 6-121c Entropy difference of one port copper tube in high average PV power and cold tank conditions

Figure 6-121 Entropy difference inside the DHW Tank of three hot water inlet devices

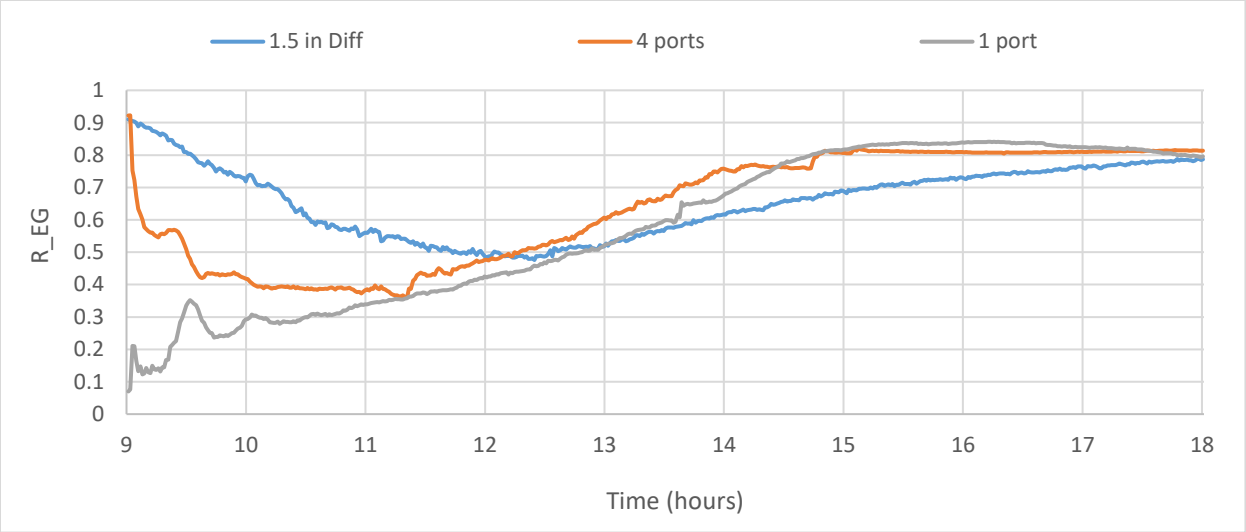


Figure 6-122 Internal entropy generation of inlet devices in high average PV power and cold tank conditions.

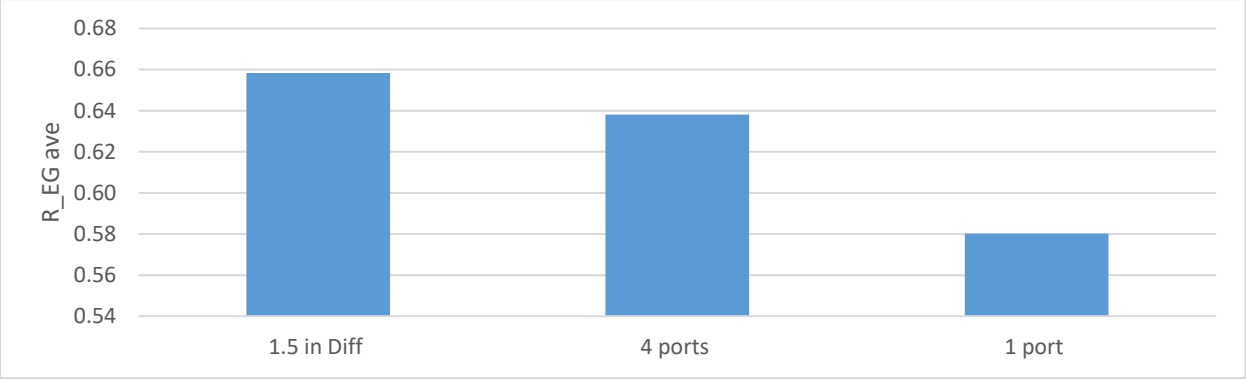


Figure 6-123 Average internal entropy generation of three inlet devices in high average PV power and cold tank conditions

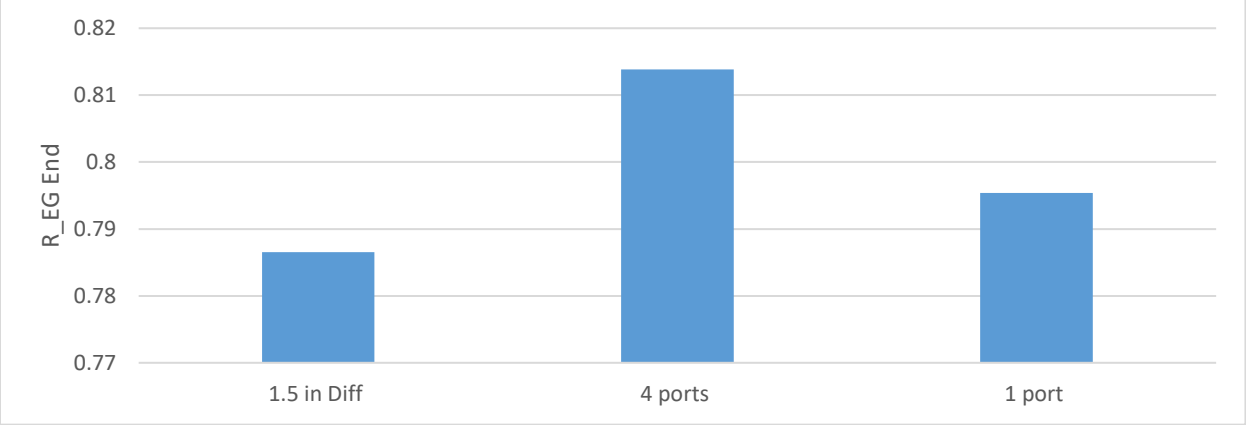


Figure 6-124 Internal entropy generation of three inlet devices at the end in high average PV power and cold tank conditions

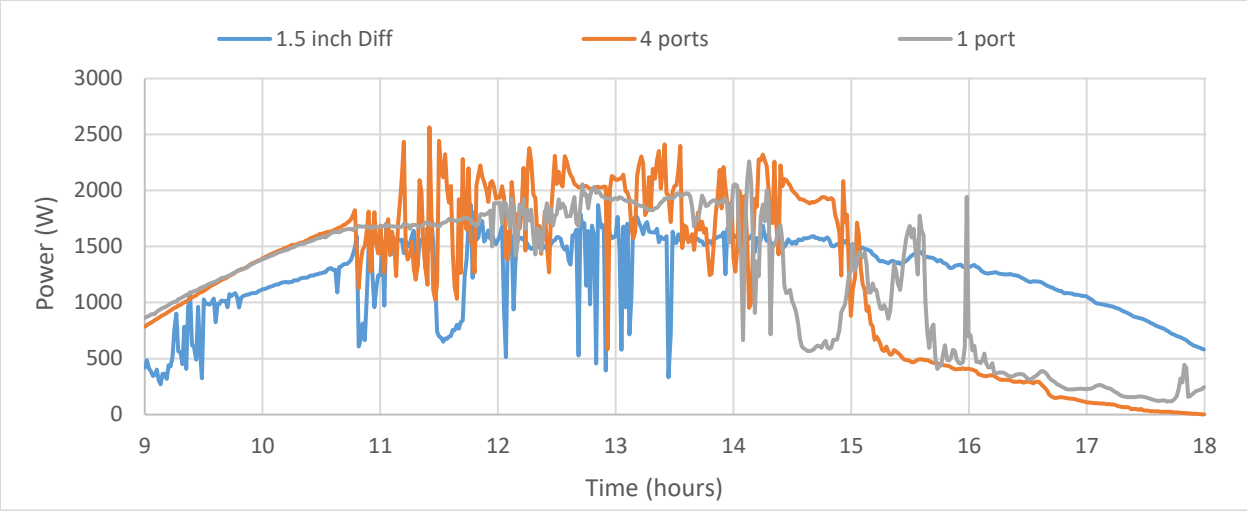


Figure 6-125 High PV power heater during three hot water inlet device tests for hot tank conditions.

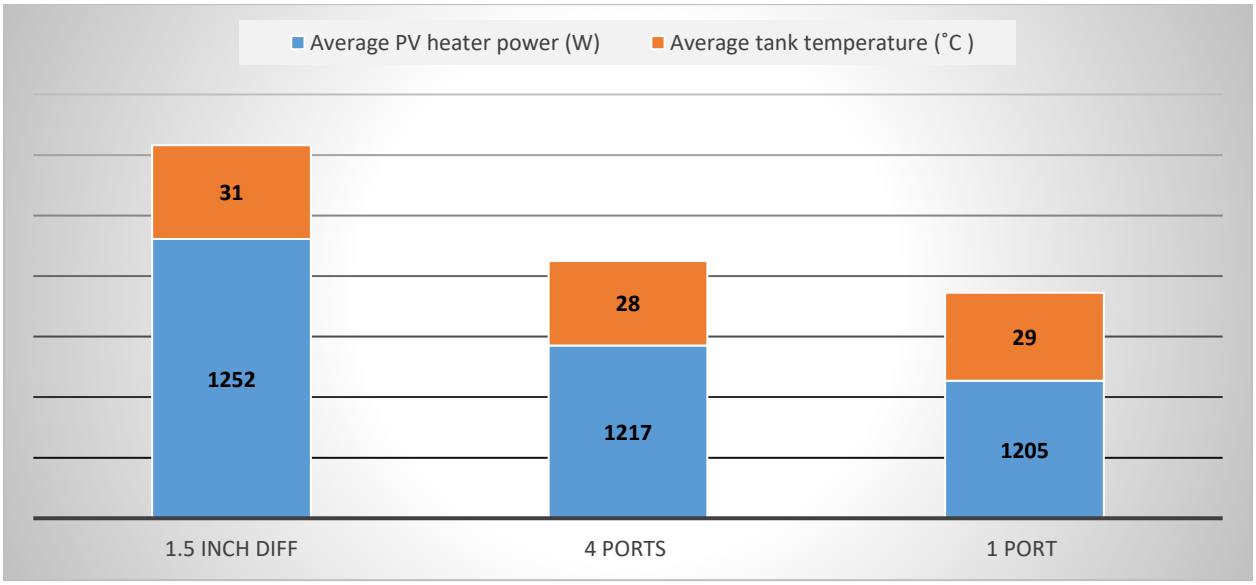


Figure 6-126 High average PV power and hot tank condition tests.

Table 6-11 Temperature Change Rate of the three tank Top Layers for High Average PV power and Hot Tank Condition

| 1.5 inch diffuser | 4 ports | 1 port |
|---|---|---|
| ˚C/h | ˚C/h | ˚C/h |
| 2.3 | 3.7 | 3.3 |

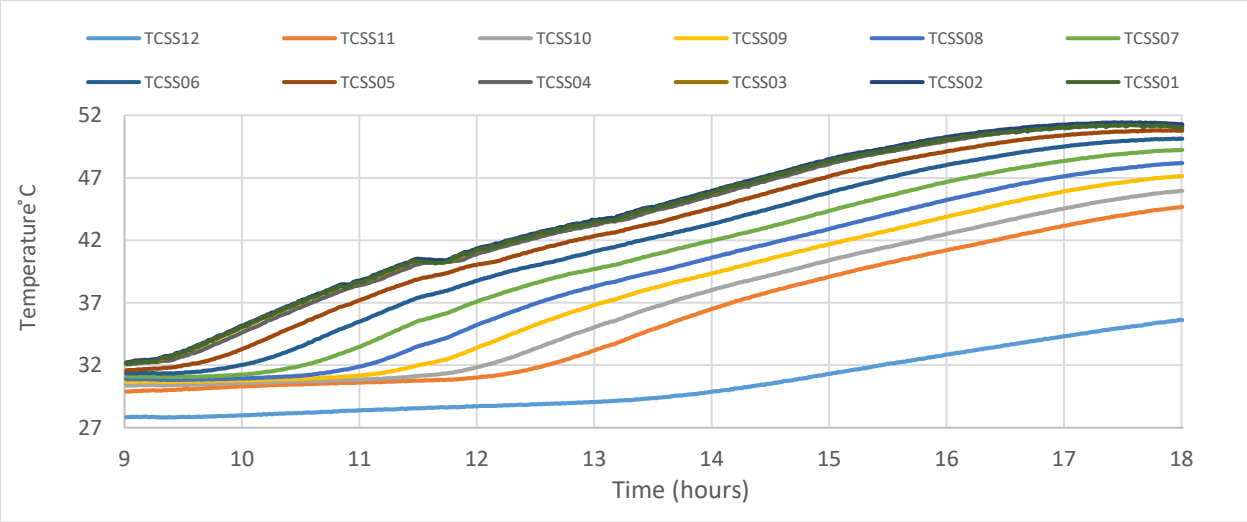


Figure 6-127a Graph showing 1.5-inch diffuser inlet device, high average PV power, and hot tank conditions.

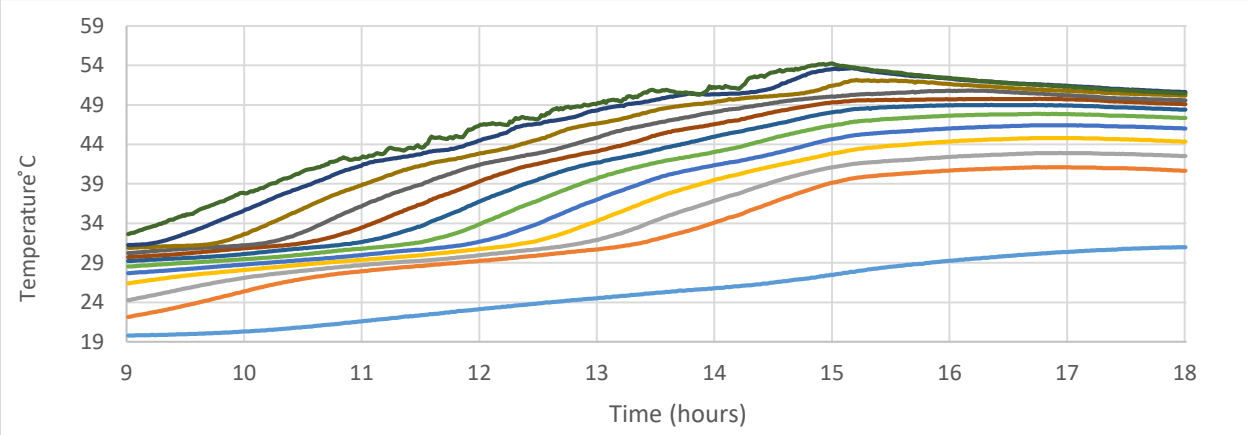


Figure 6-127b Graph showing four-port manifold inlet device, high average PV power, and hot tank conditions.

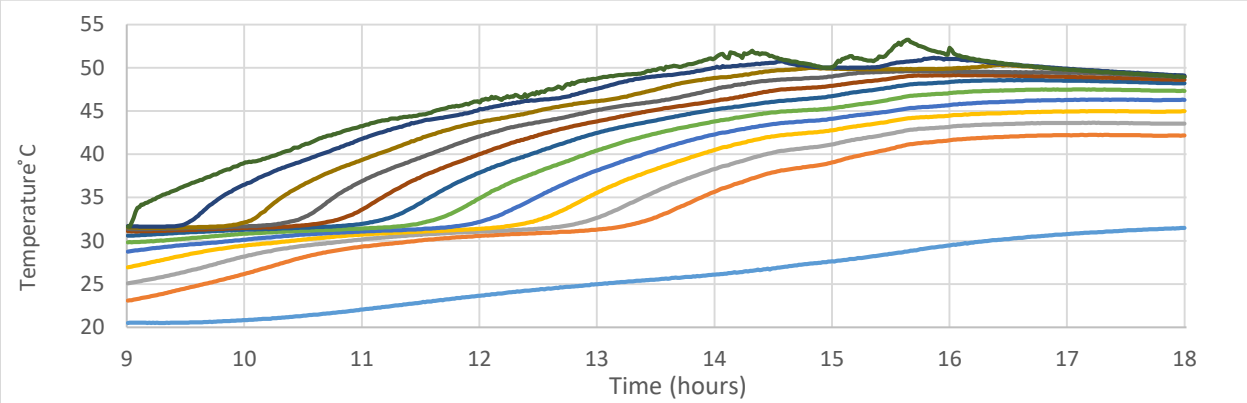


Figure 6-127c Graph showing one-port tube inlet device, high average PV power, and hot tank conditions.

Figure 6-127 Temperature distribution inside DHW tanks using three hot water inlet devices.

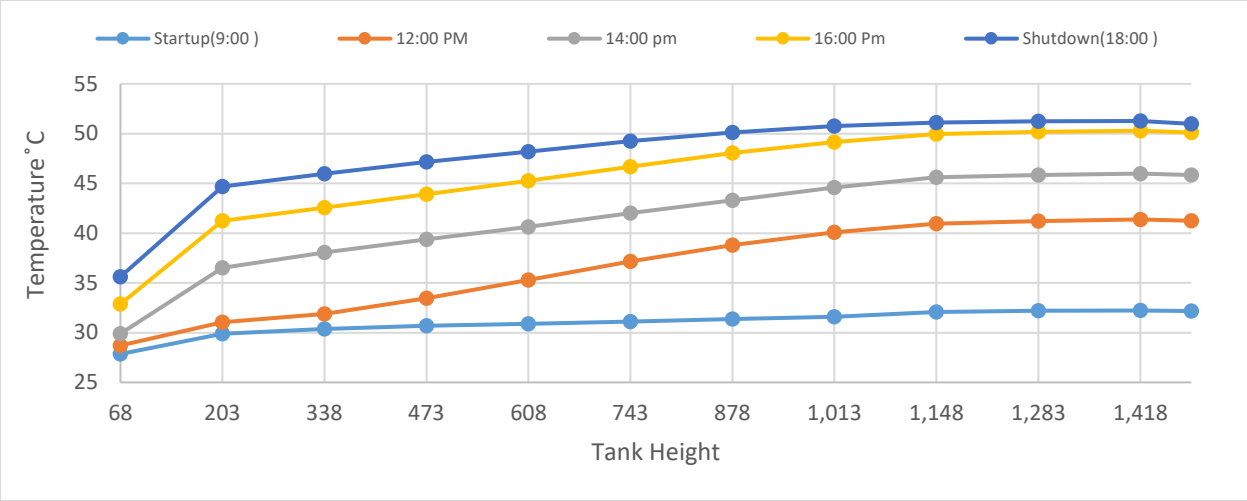


Figure 6-128a Graph showing 1.5-inch diffuser inlet device, high average PV power, and hot tank conditions.

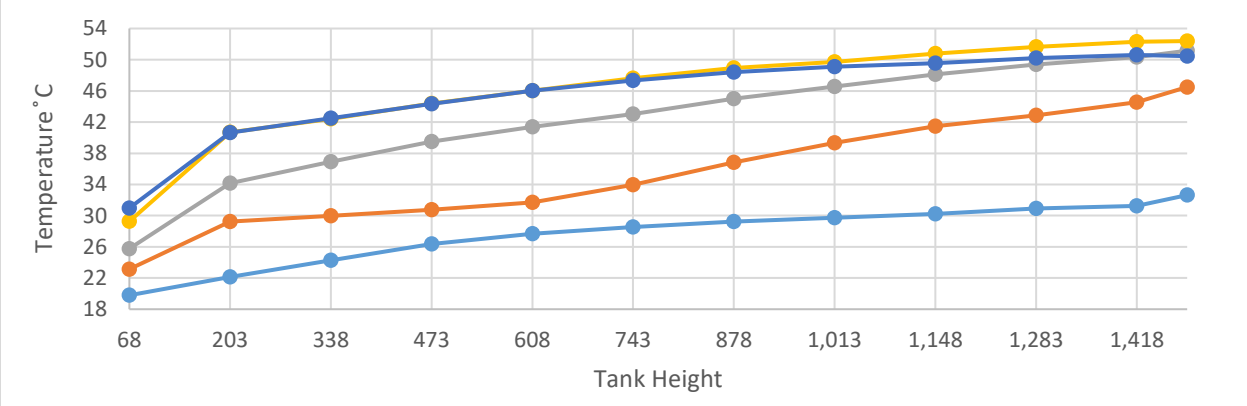


Figure 6-128b Graph showing four-port manifold inlet device, high average PV power, and hot tank conditions.

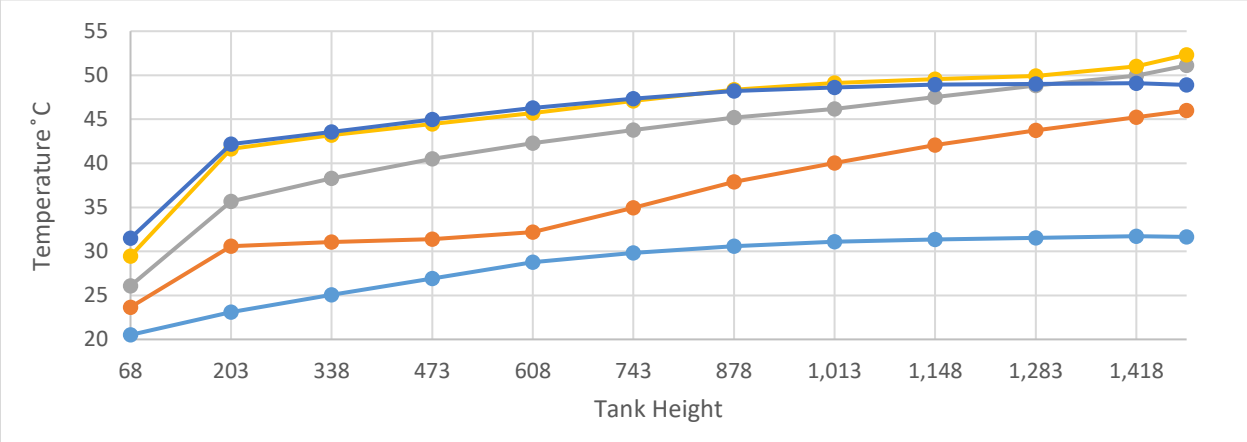


Figure 6-128c Graph showing one-port copper inlet device, high average PV power, and hot tank conditions.

Figure 6-128 Temperature distribution inside DHW tanks using hot water inlet devices.

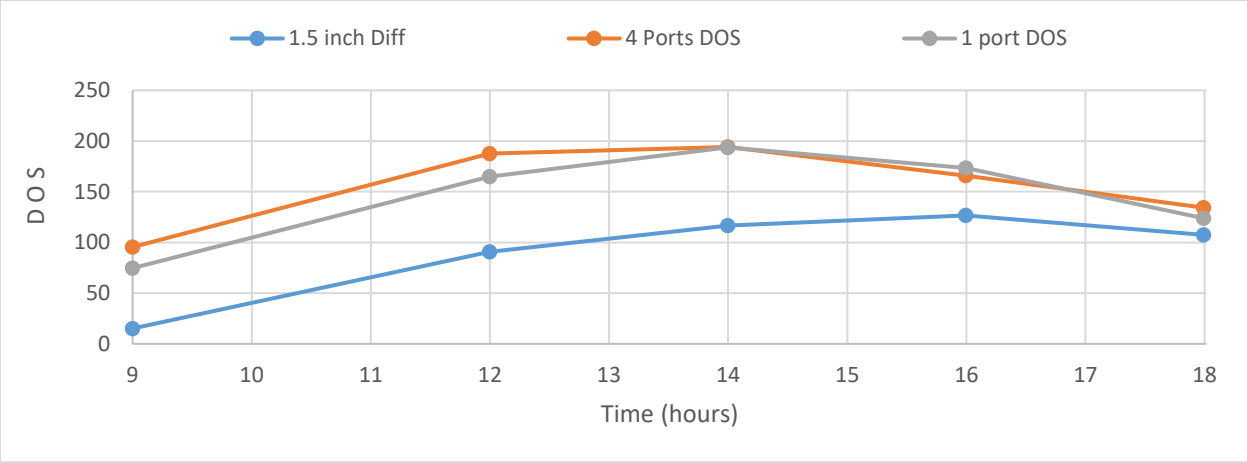


Figure 6-129 Degree of stratification of three hot water inlet devices, high average PV power, and hot tank conditions.

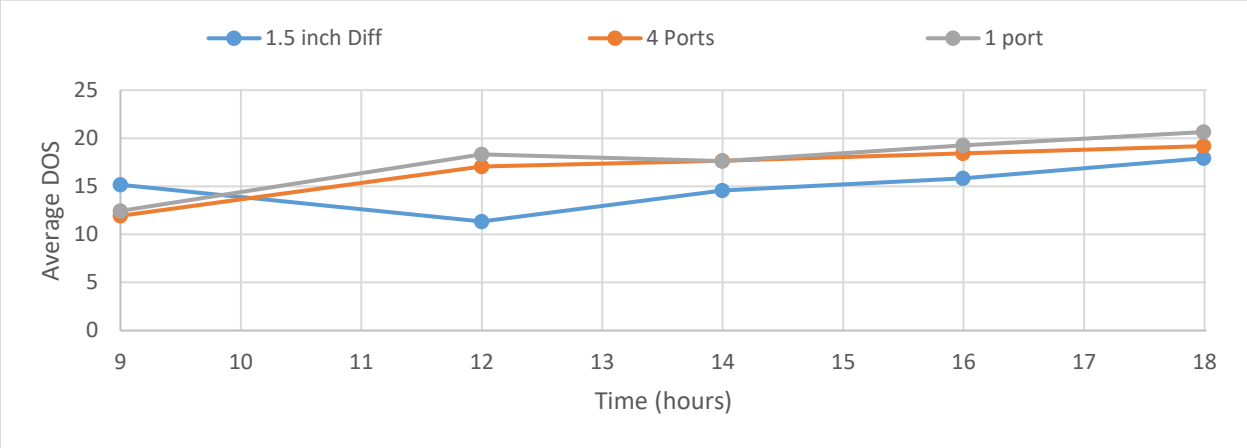


Figure 6-130 Average DOS of three inlet devices, high average PV power, and hot tank conditions.

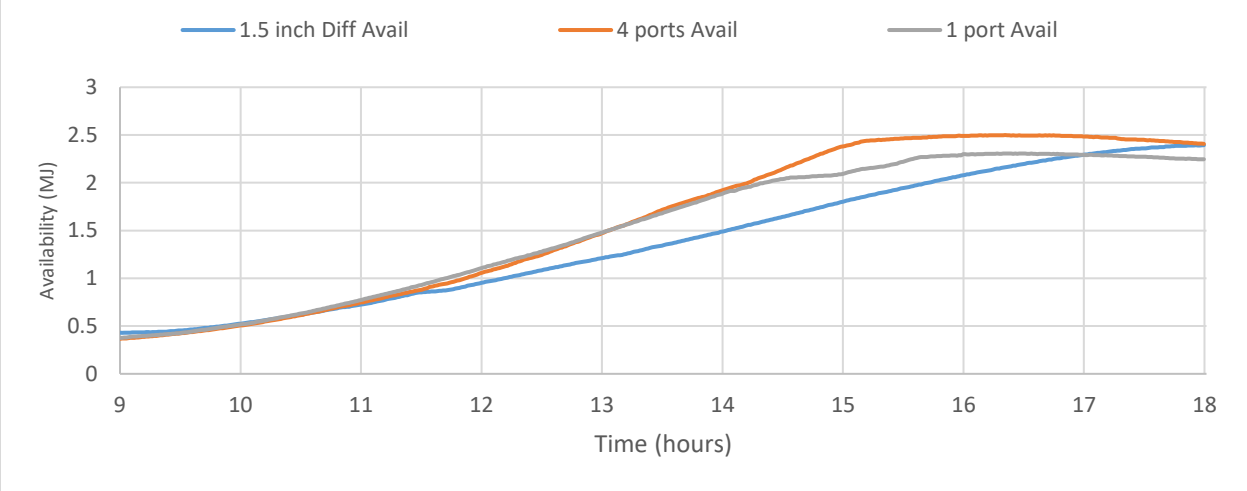


Figure 6-131 Availability for three inlet devices in high average PV power and hot tank conditions.

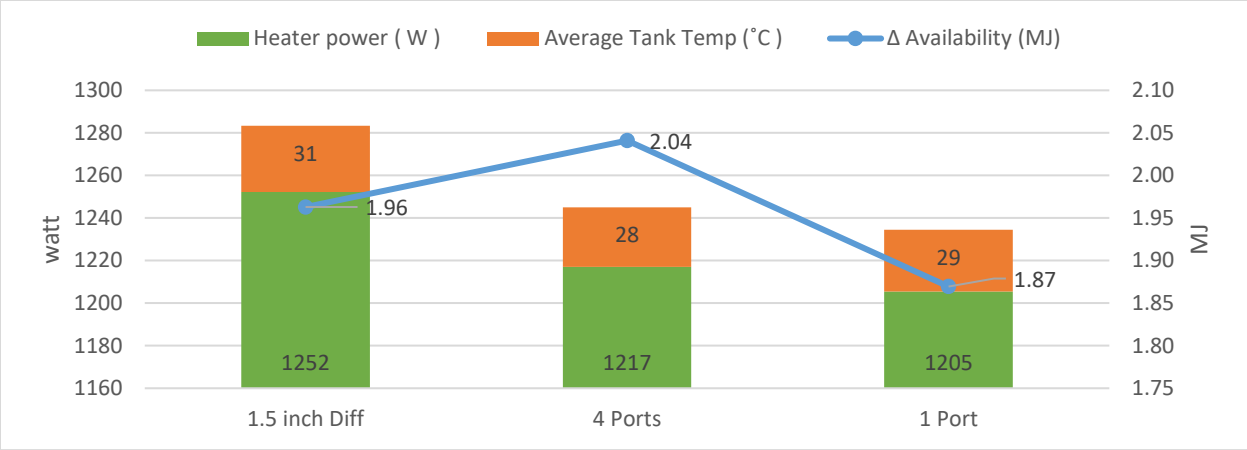


Figure 6-132 Availability change for three inlet devices in high average PV power and hot tank conditions.

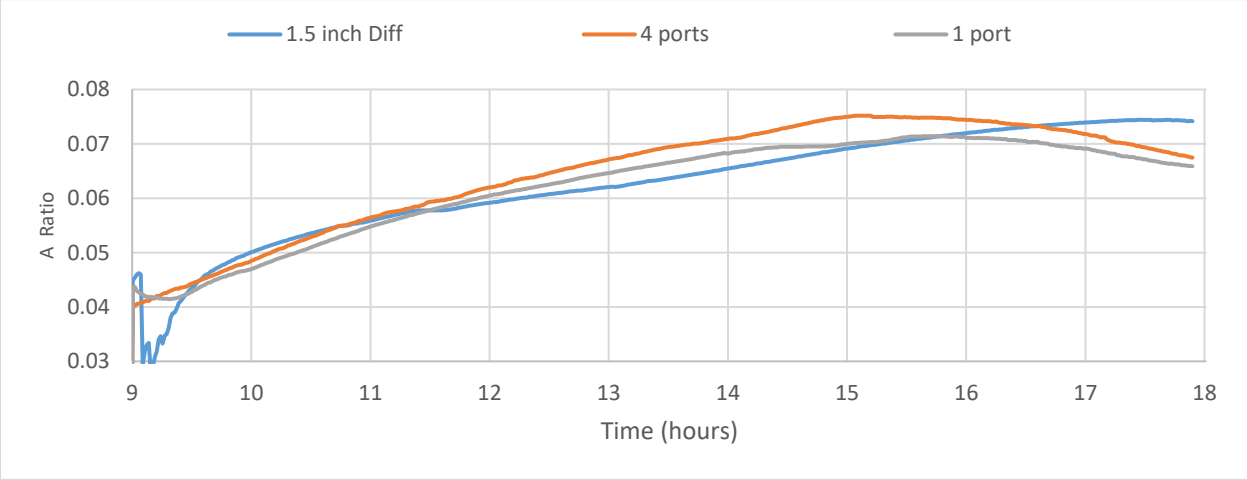


Figure 6-133 Availability ratios for three inlet devices in high average PV power and hot tank conditions.

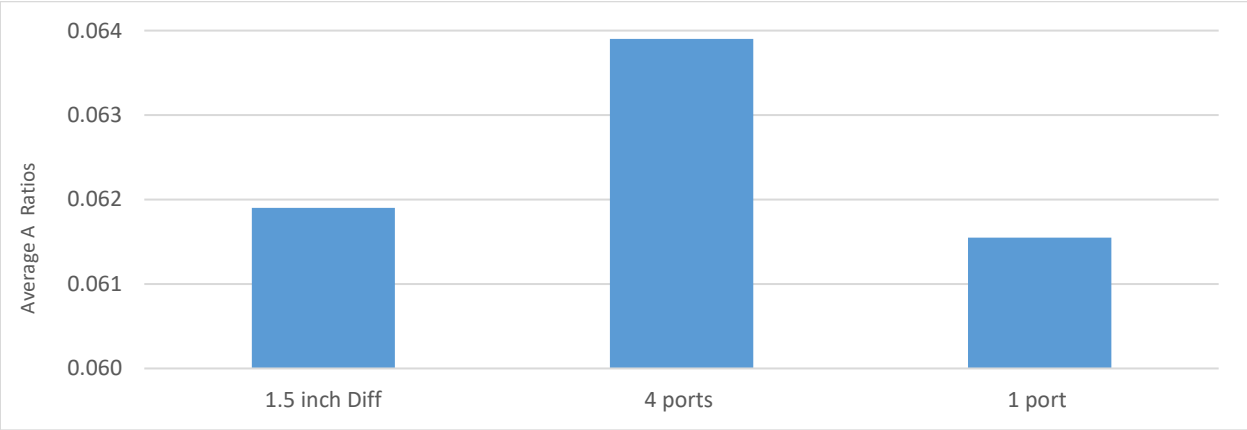


Figure 6-134 Average availability ratio for three inlet devices in high average PV power and hot tank conditions.

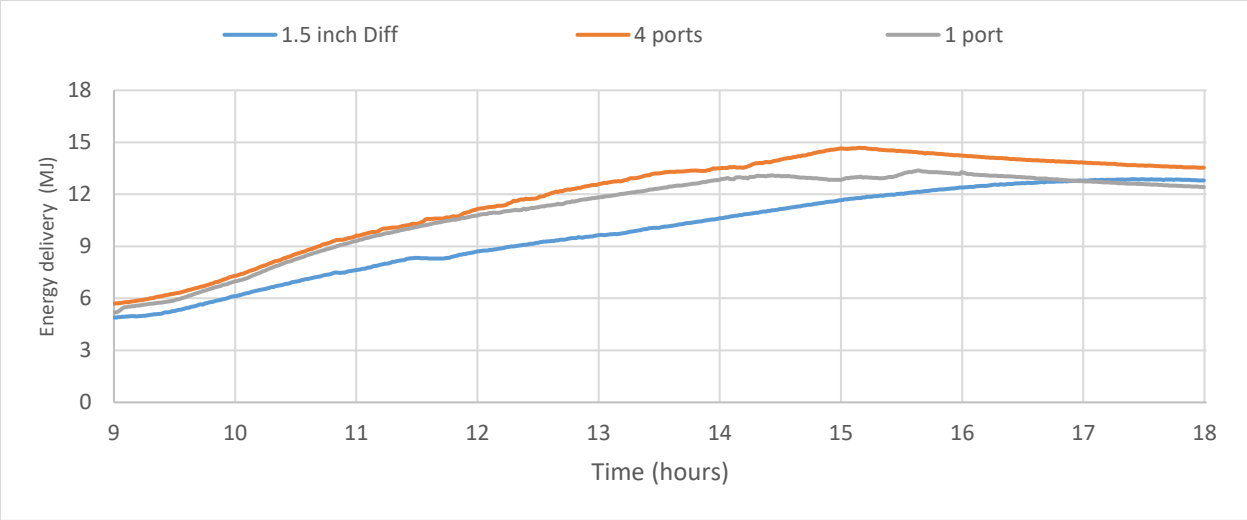


Figure 6-135 Energy delivery for three inlet devices in high average PV power and hot tank conditions.

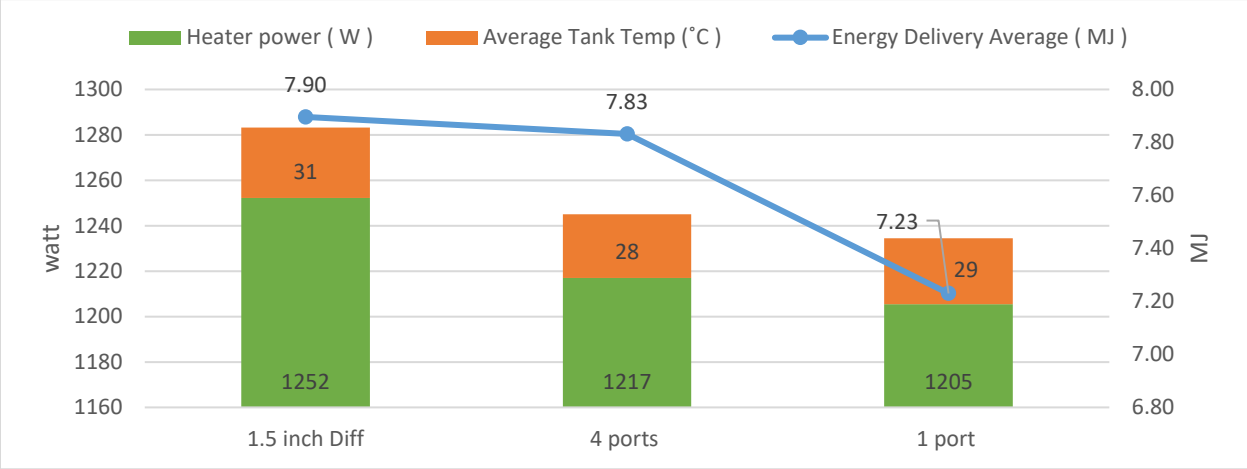


Figure 6-136 Energy delivery, high PV power, and dead-state temperature of the three devices in hot tank conditions.

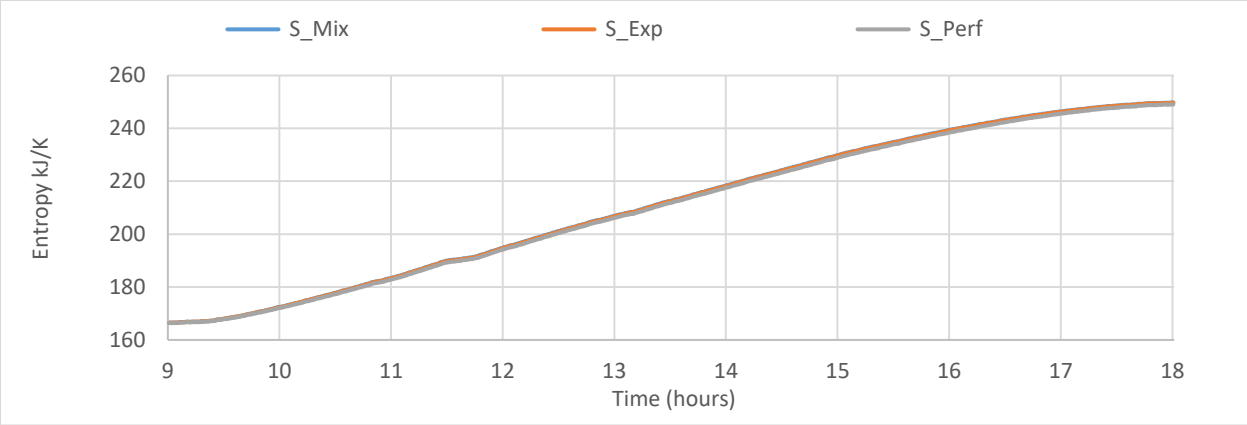


Figure 6-137a Entropy of 1.5-inch diffuser for three inlet devices in high average PV power and hot tank conditions.

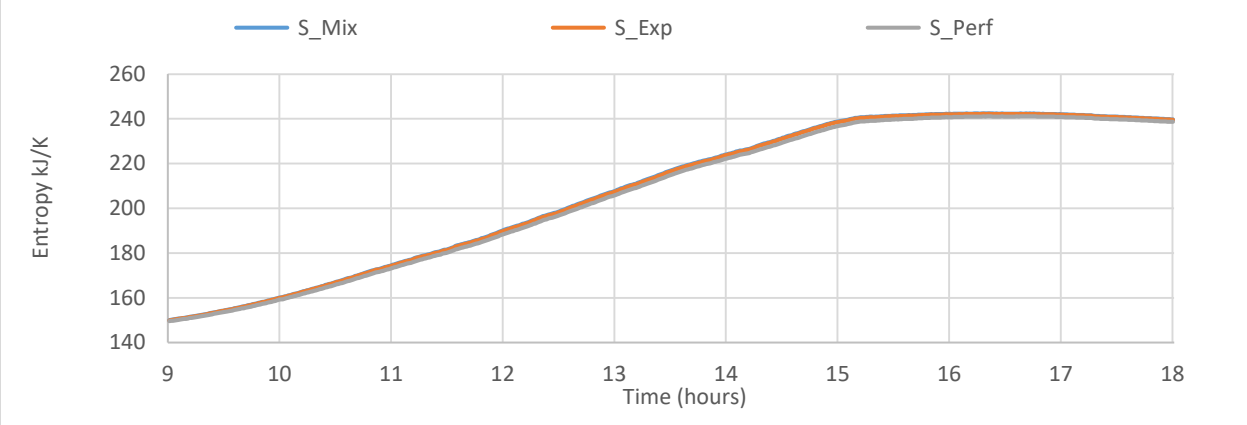


Figure 6-137b Entropy of four ports manifold for three inlet devices in high average PV power and hot tank conditions.

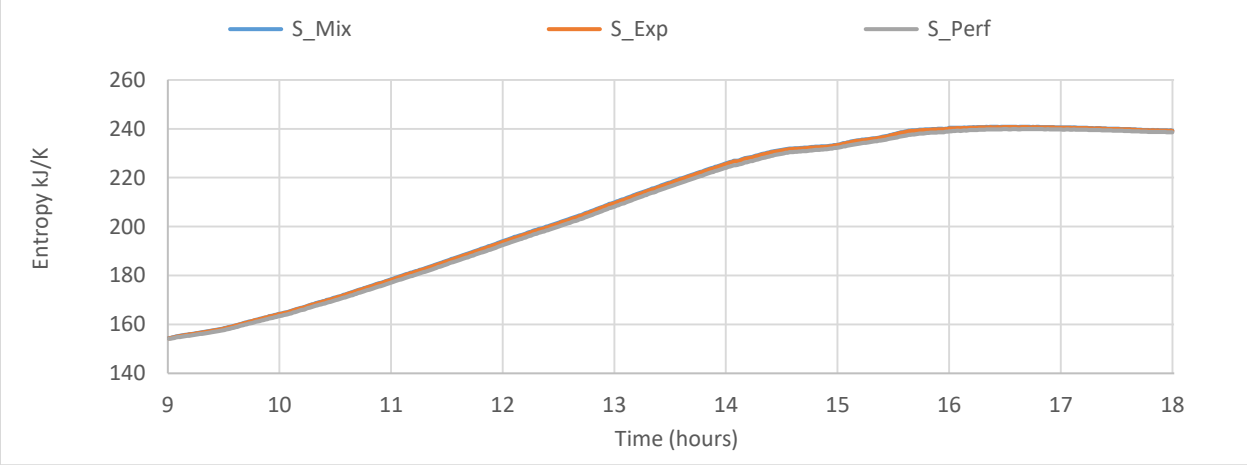


Figure 6-137c Entropy of one port copper tube for three inlet devices in high average PV power and hot tank conditions.

Figure 6-137 Entropy inside the DHW Tank of three hot water inlet devices

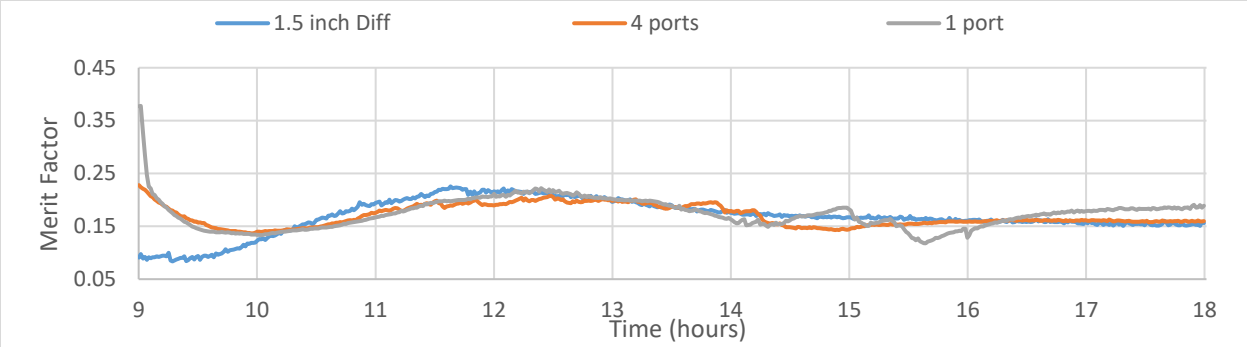


Figure 6-138 Merit factor for three hot water inlet devices in high average PV power, and hot tank conditions.

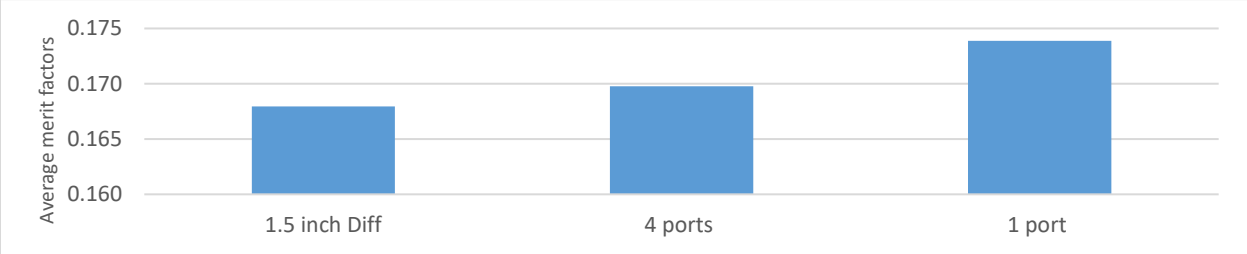


Figure 6-139 Merit factor for three hot water inlet devices at the end of the test in hot tank conditions.

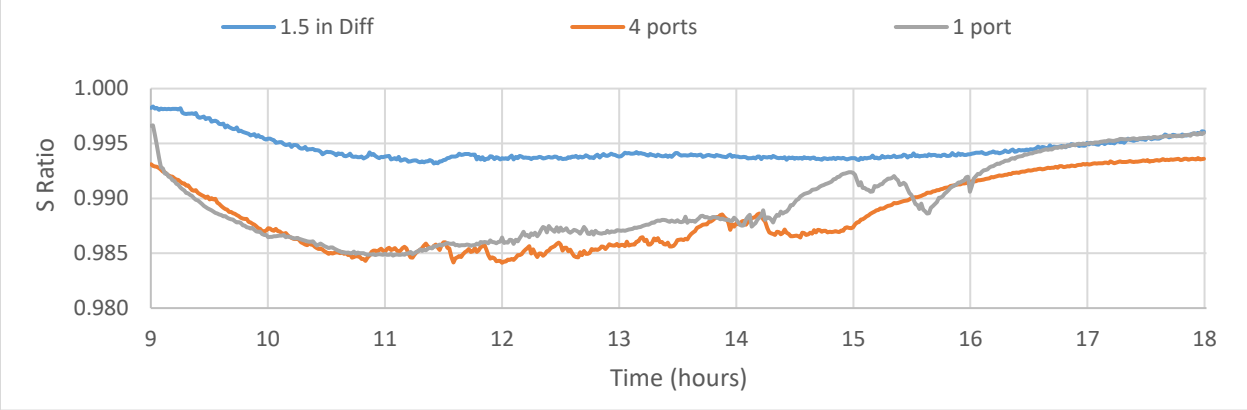


Figure 6-140 Entropy ratios of three inlet devices in high average PV power and hot tank conditions.

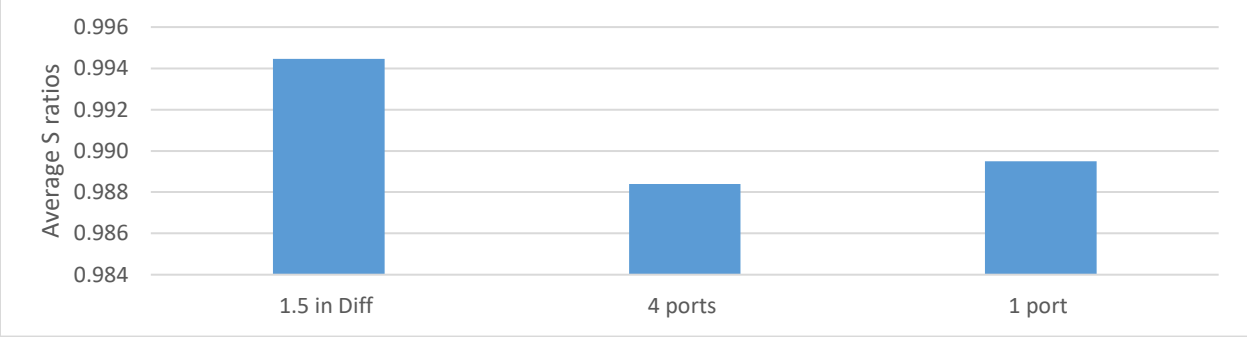


Figure 6-141 Entropy ratios of three inlet devices in high average PV power and hot tank conditions.

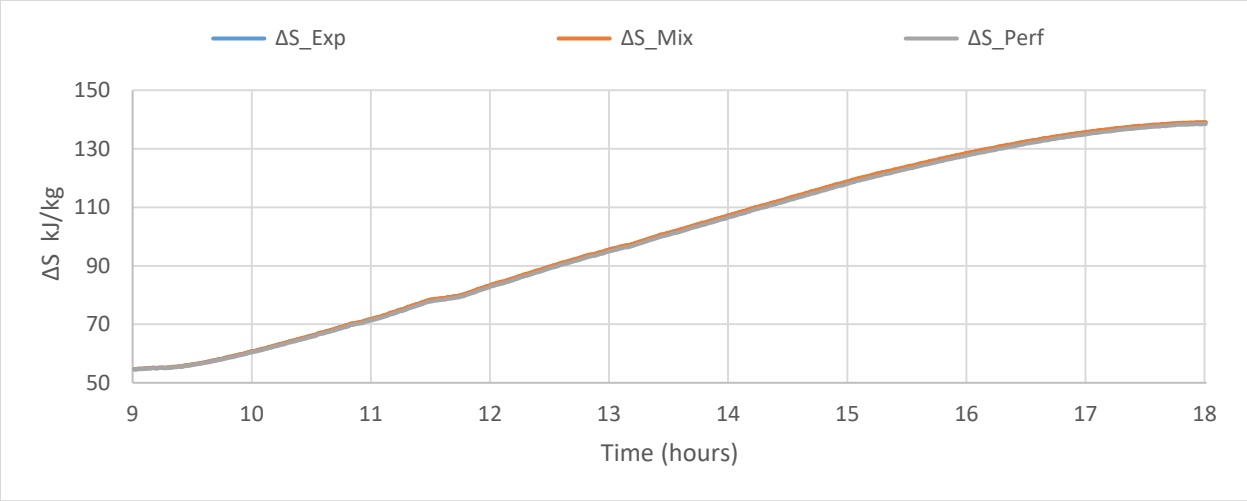


Figure 6-142a Entropy difference of 1.5-inch diffuser in high average PV power and hot tank conditions.

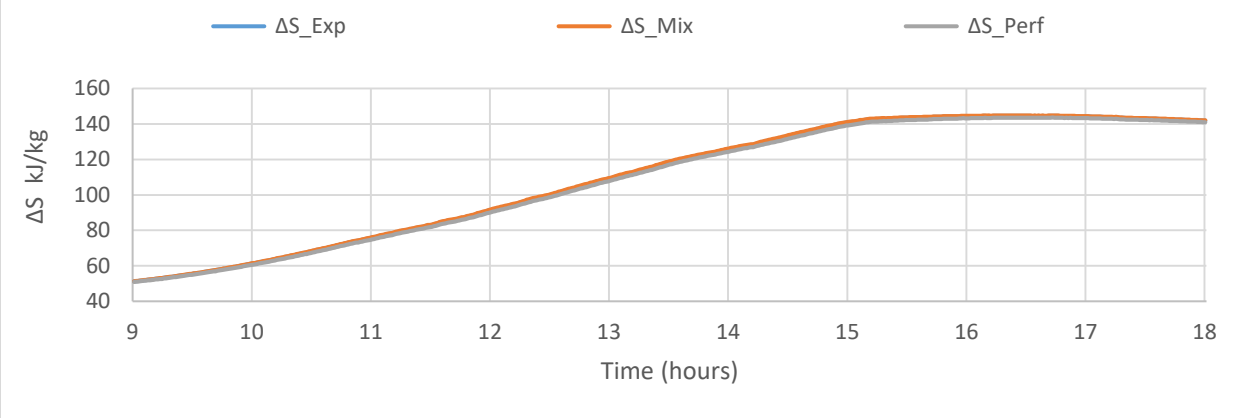


Figure 6-142b Entropy difference of four ports manifold in high average PV power and hot tank conditions

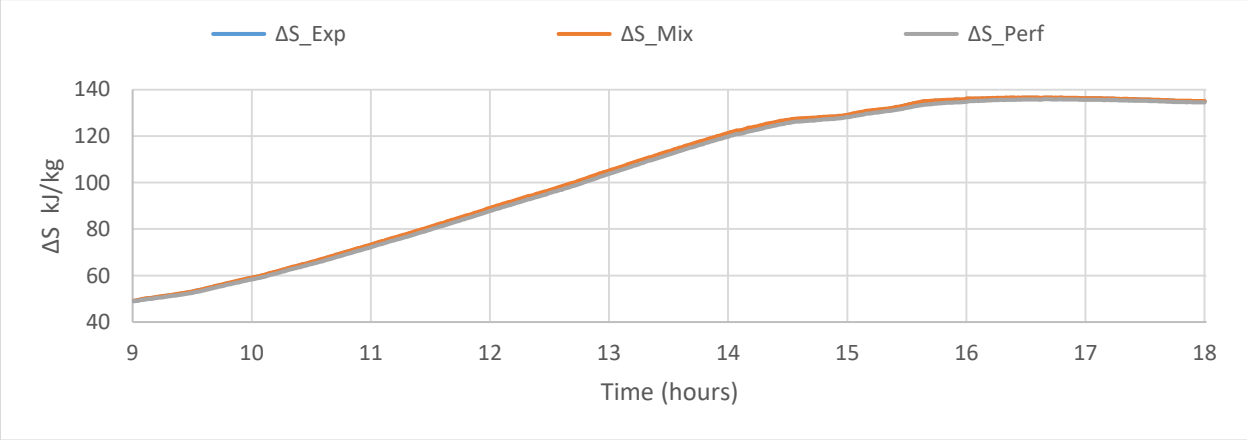


Figure 6-142c Entropy difference of one port copper tube in high average PV power and hot tank conditions

Figure 6-142 Entropy difference inside the DHW Tank of three hot water inlet devices

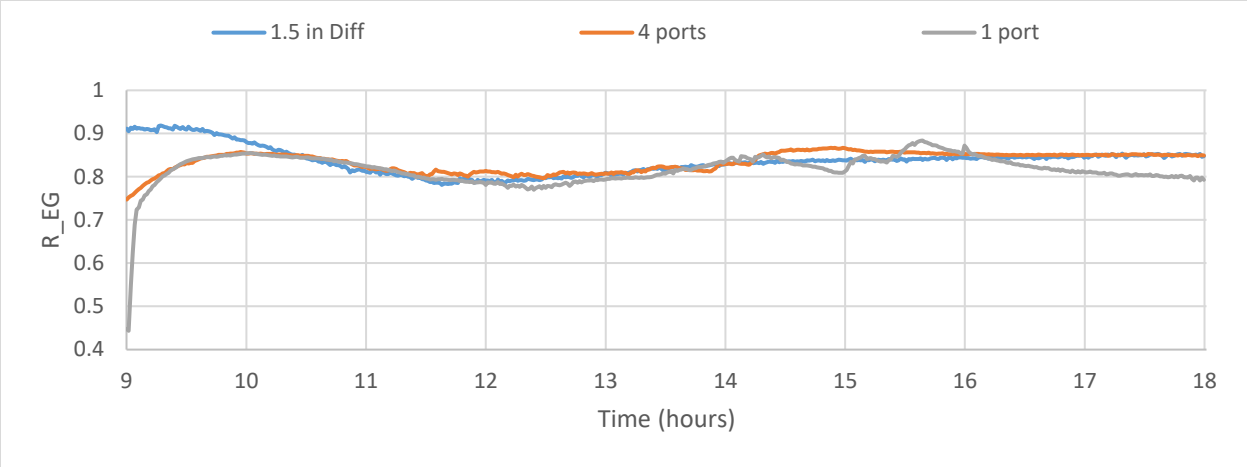


Figure 6-143 Internal entropy generation of inlet devices in high average PV power and hot tank conditions.

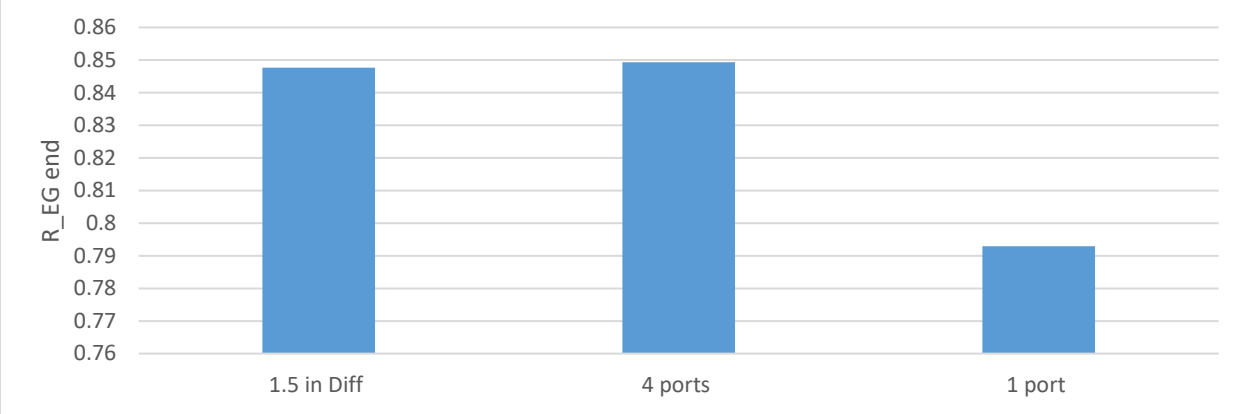


Figure 6-144 Average internal entropy generation of three inlet devices in high average PV power and hot tank conditions

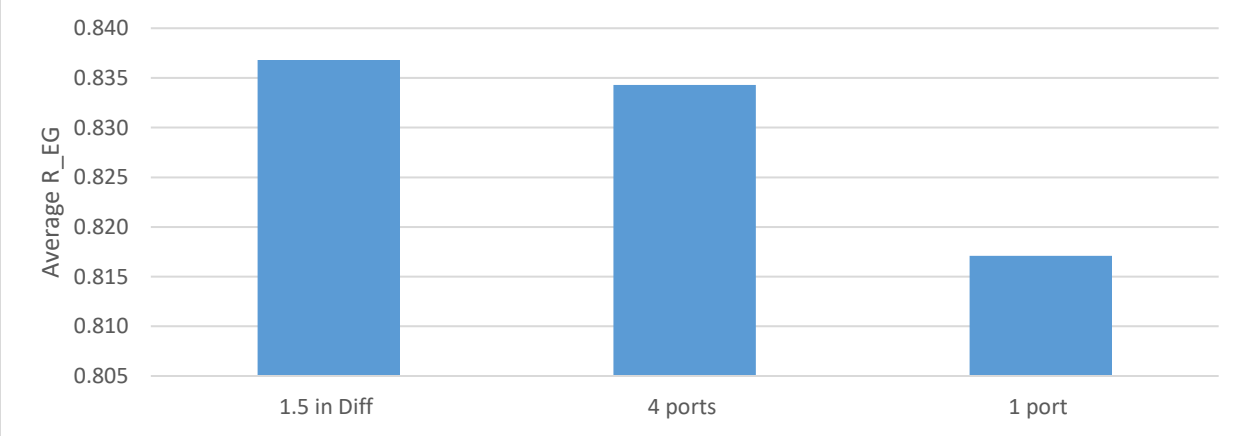


Figure 6-145 Internal entropy generation of three inlet devices at the end in high average PV power and hot tank conditions

# Appendix B

Regression Equation to calculate the properties

1. Density

$$\rho = 1000 + 10.2 \times 10^{-3} T - 5679 \times 10^{-6} T^2 + 13 \times 10^{-6} T^3$$

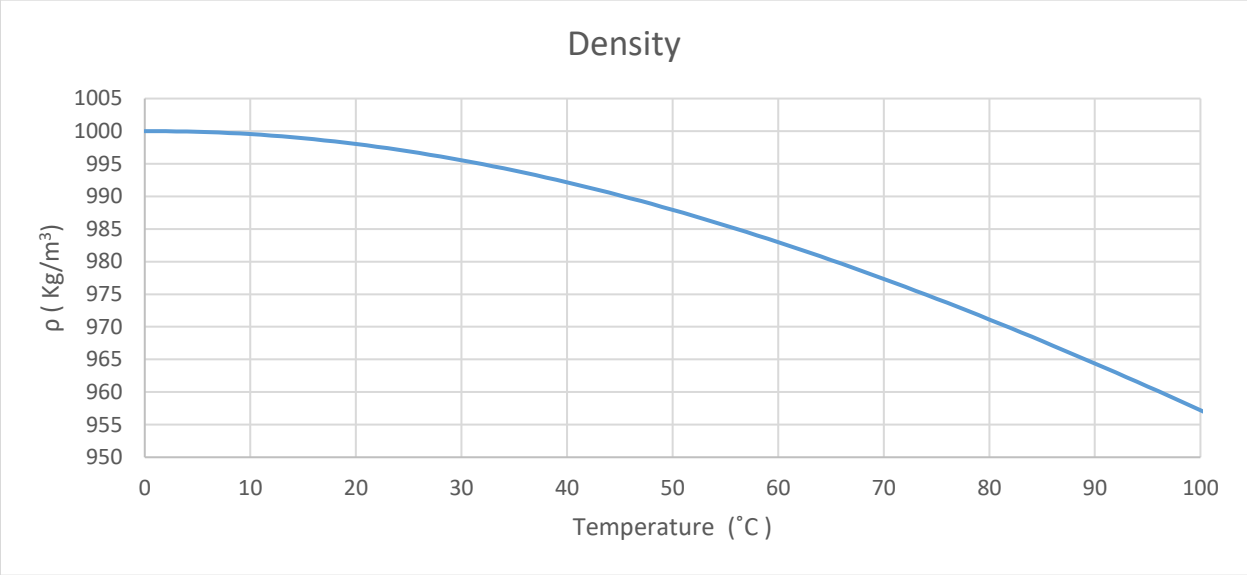


2. Entropy

$$S = 6 \times 10^{-8} - 3 \times 10^{-5} T^2 + 1.0154 \times T - 8 \times 10^{-5}$$

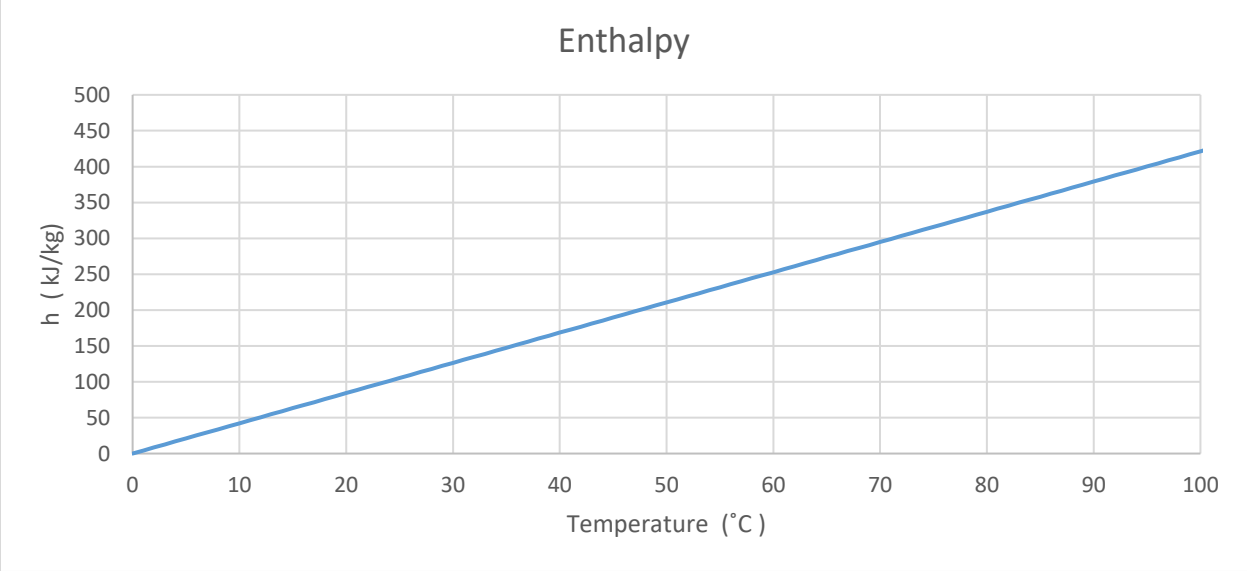

3. Enthalpy

$$h = 4.2126\,T - 9 \times 10^{-4}\,T^2 - 8 \times 10^{-6}\,T^3 - 10^{-5}\,T^4 - 0.0227$$

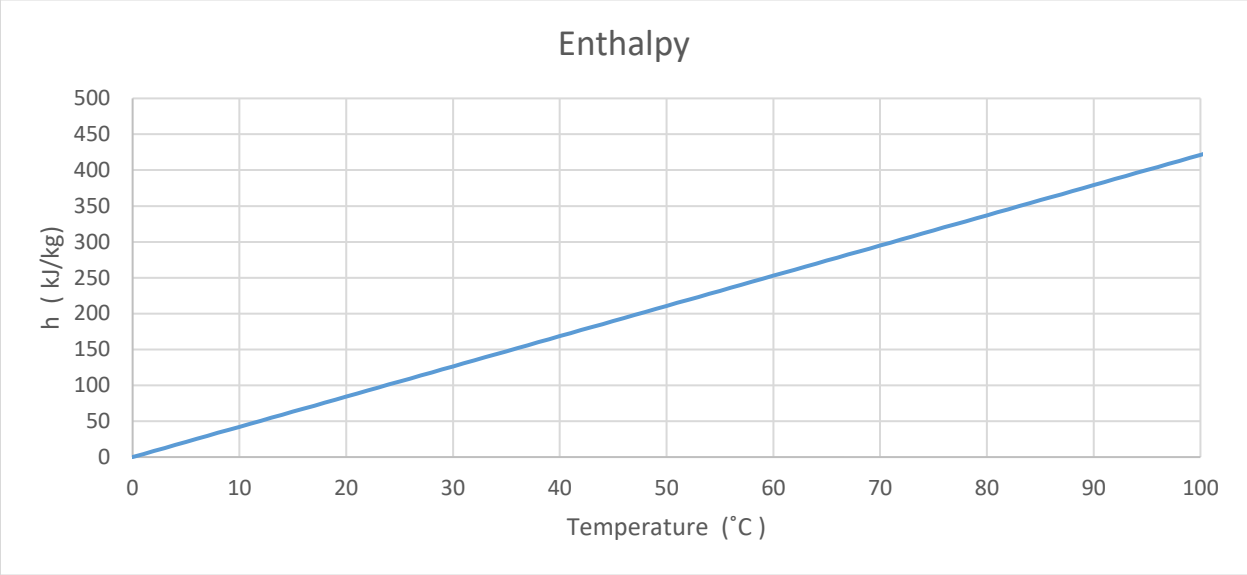


4. Specific heat

$$Cp = 4215 - 2.77\,T + 7.046 \times 10^{-2}\,T^2 - 7.132 \times 10^{-4}\,T^3 - 2.898 \times 10^{-6}\,T^4$$

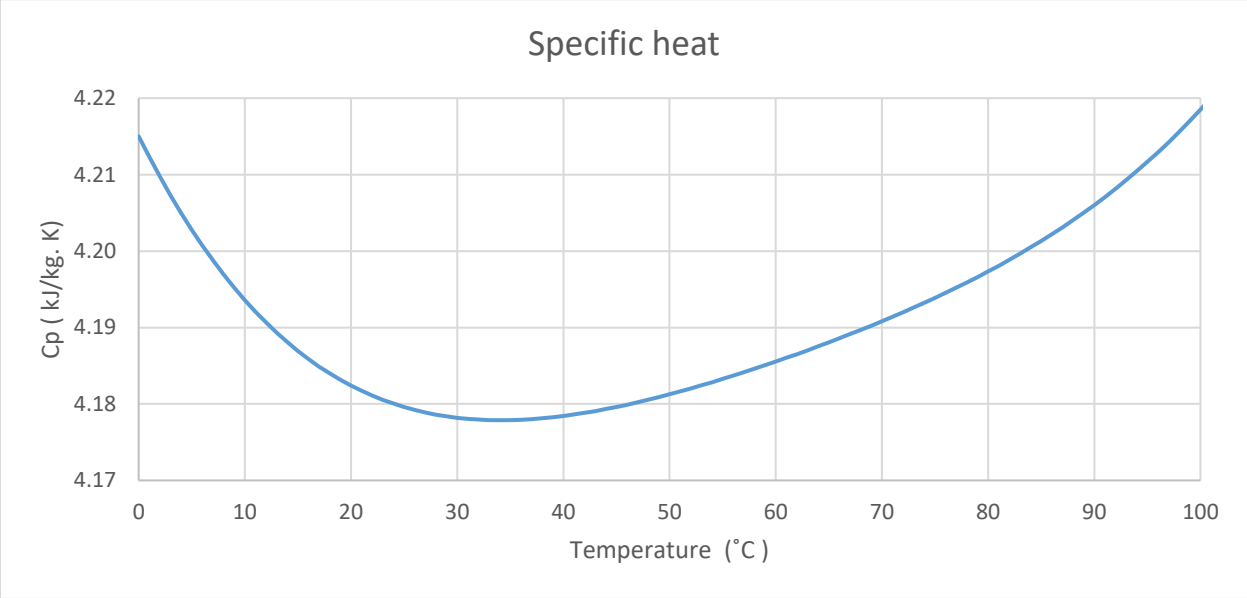

# Appendix C

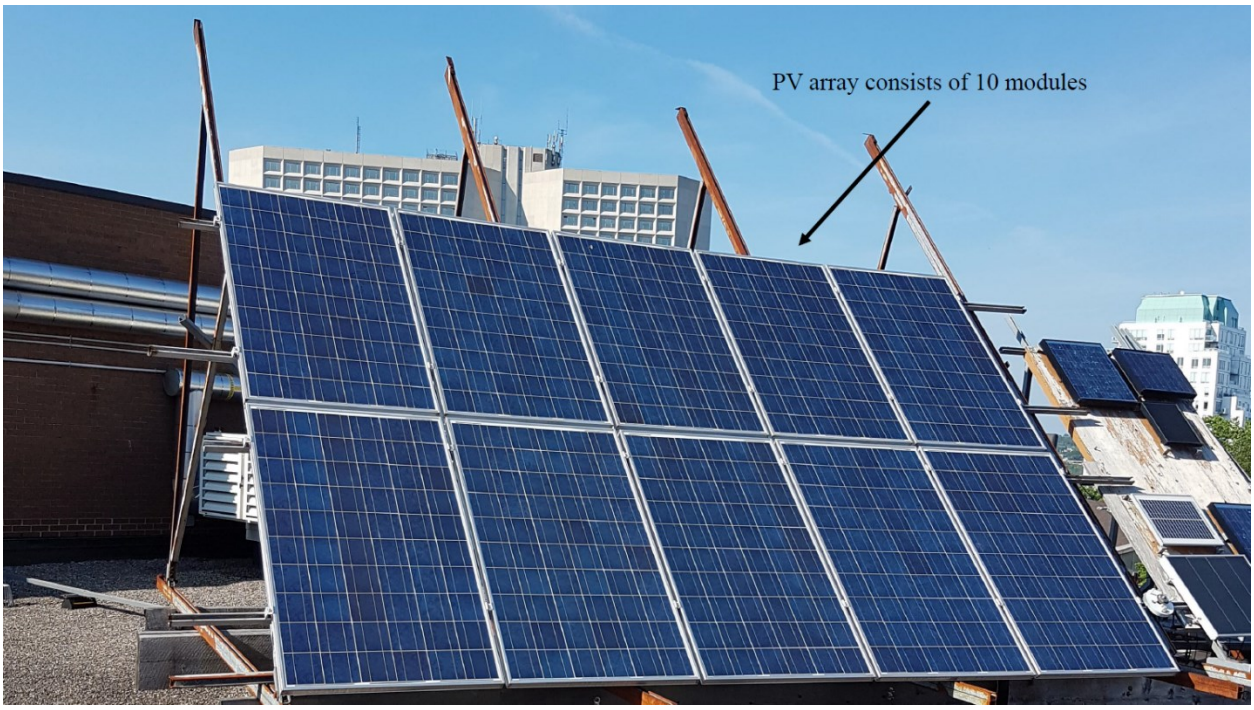


PV Modules

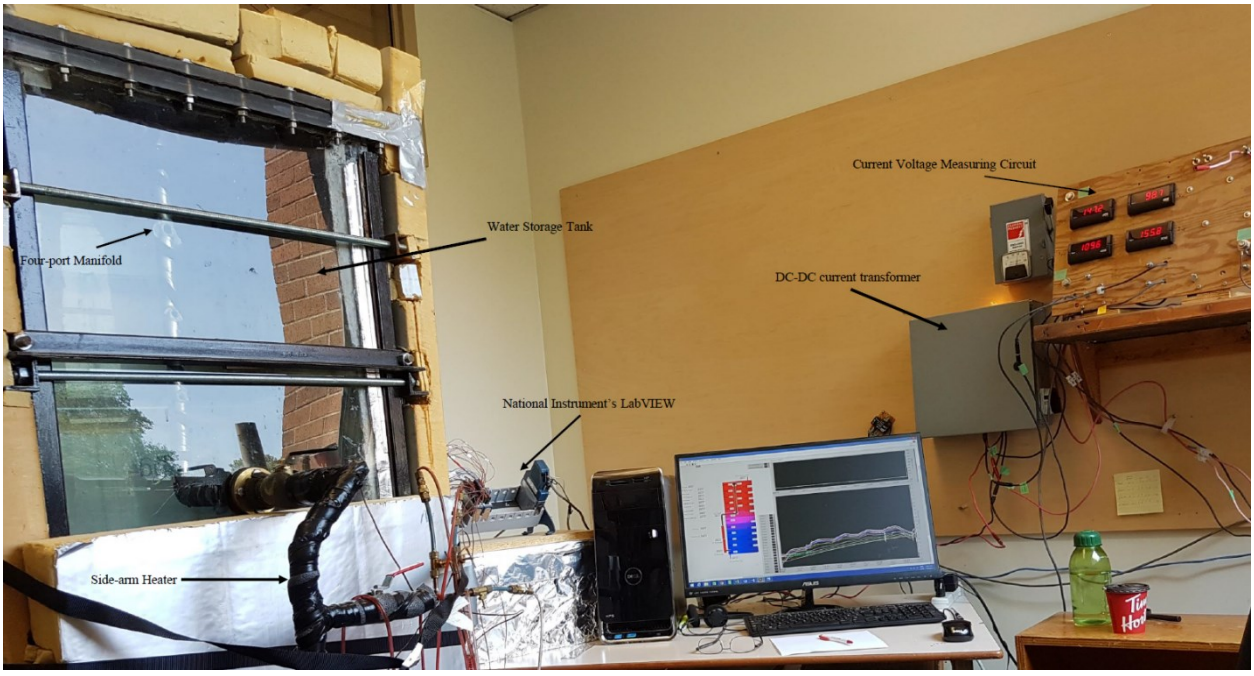


Experimental Setup

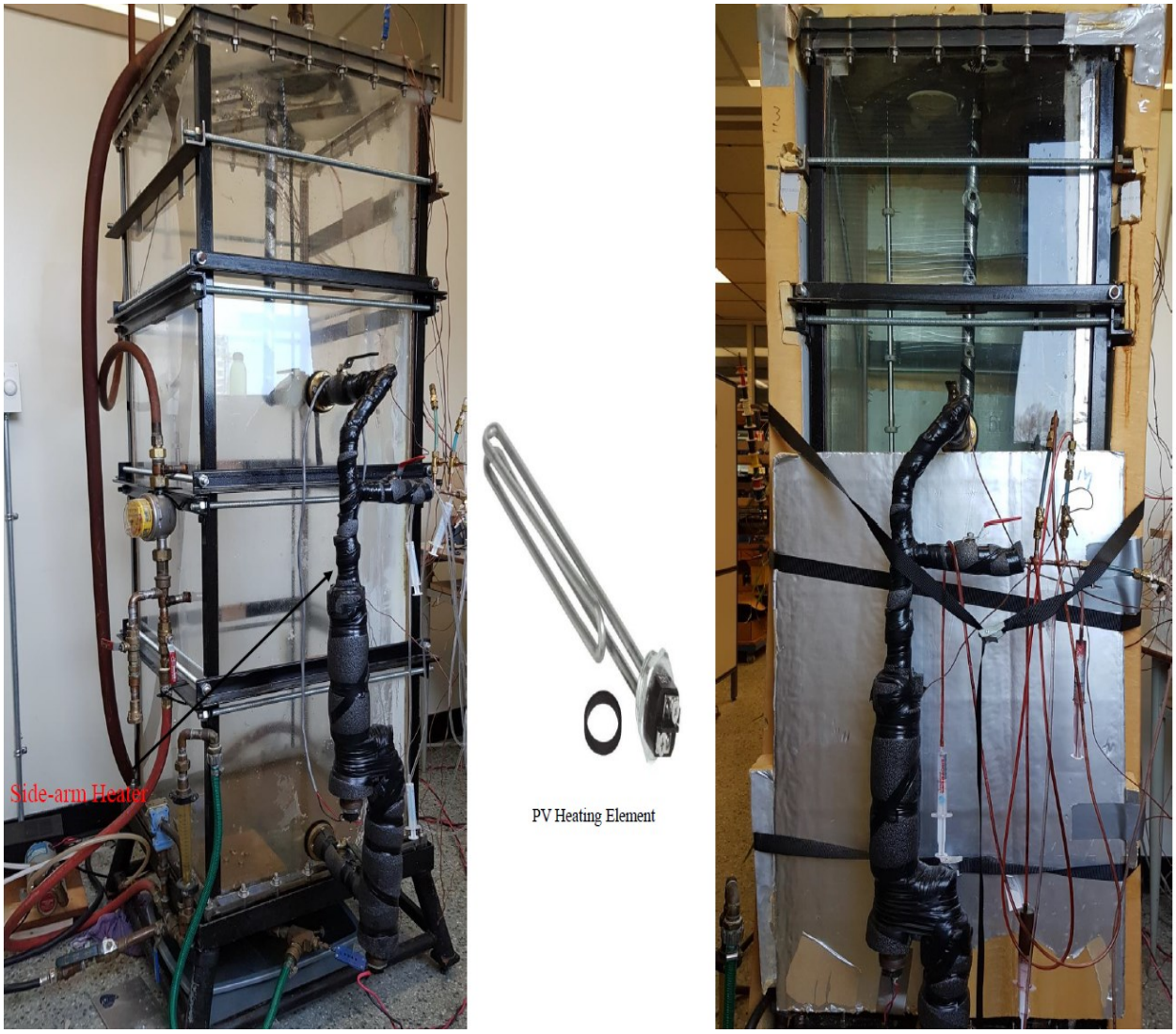


Water Storage Tank and the side-arm heater

# Appendix D

SHARP

solar electricity

## 235 WATT

**MULTI-PURPOSE MODULE**

**ND-235QCJ**

### MULTI-PURPOSE 235 WATT MODULE FROM THE WORLD'S TRUSTED SOURCE FOR SOLAR.

Using breakthrough technology, made possible by nearly 50 years of proprietary research and development, Sharp's ND-235QCJ solar module incorporates an advanced surface texturing process to increase light absorption and improve efficiency. Common applications include commercial and residential grid-tied roof systems as well as ground mounted arrays. Designed to withstand rigorous operating conditions, this module offers high power output per square foot of solar array.

This module is ideal for large commercial applications, demonstrating financial astuteness and environmental stewardship.

**ENGINEERING EXCELLENCE**
High module efficiency for an outstanding balance of size and weight to power and performance.

**5% POSITIVE POWER TOLERANCE**
Count on Sharp to deliver all the watts you pay for with a positive-only power tolerance of +5%.

**RELIABLE**
25-year limited warranty on power output and 10-year limited warranty on materials or workmanship.

**HIGH PERFORMANCE**
This module uses an advanced surface texturing process to increase light absorption and improve efficiency.

Sharp multi-purpose modules offer industry-leading performance for a variety of applications.

Tempered glass, EVA lamination and weatherproof backskin provide long-life and enhanced cell performance.

**SHARP: THE NAME TO TRUST**

When you choose Sharp, you get more than well-engineered products. You also get Sharp's proven reliability, outstanding customer service and the assurance of both our 10-year warranty on materials or workmanship as well as the 25-year limited warranty on power output. With over 50 years experience in solar and over 4.3 GW of installed capacity, Sharp has a proven legacy as a trusted name in solar.

**BECOME POWERFUL**

# 235 WATT

## ND-235QCJ

**Module output cables: 12 AWG PV Wire** (per UL Subject 4703)

### ELECTRICAL CHARACTERISTICS

| | |
|---|---|
| Maximum Power (Pmax)* | 235 W |
| Tolerance of Pmax | +5%/-0% |
| PTC Rating | 211.8 W |
| Type of Cell | Polycrystalline silicon |
| Cell Configuration | 60 in series |
| Open Circuit Voltage (Voc) | 37.2 V |
| Maximum Power Voltage (Vpm) | 29.3 V |
| Short Circuit Current (Isc) | 8.60 A |
| Maximum Power Current (Ipm) | 8.02 A |
| Module Efficiency (%) | 14.4% |
| Maximum System (DC) Voltage | 600 V (UL)/1000V (IEC) |
| Series Fuse Rating | 15 A |
| NOCT | 47.5°C |
| Temperature Coefficient (Pmax) | -0.485%/°C |
| Temperature Coefficient (Voc) | -0.36%/°C |
| Temperature Coefficient (Isc) | 0.053%/°C |

*Illumination of 1 kW/m² (1 sun) at spectral distribution of AM 1.5 (ASTM E892 global spectral irradiance) at a cell temperature of 25°C.

### MECHANICAL CHARACTERISTICS

| | |
|---|---|
| Dimensions (A x B x C to the right) | 39.1" x 64.6" x 1.8"/994 x 1640 x 46 mm |
| Cable Length (G) | 43.3"/1100 mm |
| Output Interconnect Cable | 12 AWG with *SMK Locking Connector |
| Hail Impact Resistance | 1" (25 mm) at 52 mph (23 m/s) |
| Weight | 41.9 lbs / 19.0 kg |
| Max Load | 50 psf (2400 Pascals) |
| Operating Temperature (cell) | -40 to 194°F / -40 to 90°C |

*Intertek recognized for mating with MC-4 connectors (part numbers PV-KST4; PV-KBT4)

### CERTIFICATIONS

UL 1703, ULC/ORD-C1703, IEC 61215, IEC 61730, CEC, FSEC

### WARRANTY

25-year limited warranty on power output
Contact Sharp for complete warranty information

### DIMENSIONS

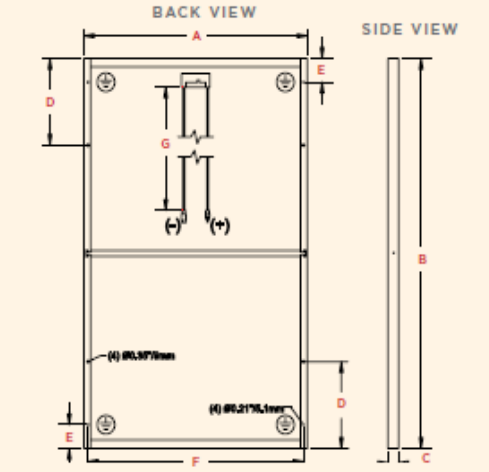


| A | B | C | D | E |
|---|---|---|---|---|
| 39.1"/994 mm | 64.6"/1640 mm | 1.8"/46 mm | 14.4"/365 mm | 3.9"/100 mm |

| F | G |
|---|---|
| 37.7"/958 mm | 43.3"/1100 mm |

Contact Sharp for tolerance specifications

### ISO QUALITY & ENVIRONMENTAL MANAGEMENT

Sharp solar modules are manufactured in ISO 9001:2000 AND ISO 14001:2004 certified facilities.

### "BUY AMERICAN"

Sharp solar modules are manufactured in the United States and Japan, and qualify as "American" goods under the "Buy American" clause of the American Recovery and Reinvestment Act (ARRA).



SHARP

SHARP ELECTRONICS CORPORATION
5700 NW Pacific Rim Boulevard, Camas, WA 98607
1-800-SOLAR-06 • Email: sharpsolar@sharpusa.com
www.sharpusa.com/solar



Printed in U.S.A. on recycled paper. 12F-108°PC-08-12

# NI 9213

## 16-Channel Thermocouple Module


- Built-in CJC (cold-junction compensation)
- High-speed mode for up to 1,200 S/s (aggregate)
- 250 Vrms channel-to-earth ground safety isolation
- 24-bit ADC for up to 0.02 °C measurement sensitivity

| Input Characteristics | |
|---|---|
| Number of channels | 16 thermocouple channels, 1 internal autozero channel, 1 internal cold-junction compensation channel |
| ADC resolution | 24 bits |
| Type of ADC | Delta-Sigma |
| Sampling mode | Scanned |
| Voltage measurement range | ±78.125 mV |
| Temperature measurement ranges | Works over temperature ranges defined by NIST (J, K, T, E, N, B, R, S thermocouple types) |

| Temperature Measurement Accuracy | |
|---|---|
| Measurement sensitivity [4] | |
| High-resolution mode | |
| Types J, K, T, E, N | <0.02 °C |
| Types B, R, S | <0.15 °C |
| High-speed mode | |
| Types J, K, T, E | <0.25 °C |

# NI 9209

## 16 AI Differential/32 AI Single-Ended, ±10 V, 24 Bit, 500 S/s Aggregate


- DSUB connectivity
- 50 Hz/60 Hz noise rejection
- 60 VDC, CAT I, channel-to-earth isolation

The NI 9209 voltage input C Series module features 16 differential channels or 32 single-ended channels of ±10 V input with built-in 50/60 Hz rejection for noise rejection. Designed with industrial systems in mind, the NI 9209 has high-channel density to reduce the number of modules needed.

**Table 1.** Accuracy

| Calibrated Measurement Conditions | Percent of Reading (Gain Error) | Percent of Range[1] (Offset Error) |
|---|---|---|
| Maximum (-40 °C to 70 °C) | ±0.46% | ±0.011% |
| Typical (25 °C ±5 °C) | ±0.06% | ±0.003% |
| Input range | | |
| Minimum | ±10.2 V | |
| Typical | ±10.4 V | |

# Split-Core DC Voltage Current Transducer

## Hall Effect Current Sensor

## HCT-0010-XXX, ±4 Vdc Output

### 10mm Opening With Ratings Up to 50 Amps


### Description:

Magnelab's HCT-0010-XXX split-core current transducer "senses" DC current up to 50 amps passing through the center conductor. Split-core transformers are ideal for installation on existing electrical wiring by snapping around the conductor. The HCT-0010-XXX has a self-locking mechanism.

### Features:

- Rated input up to 50 Amps DC
- Output of ±4 Vdc at rated current
- Accuracy 1% at rated current
- System Voltage: DC 500 V , AC 1500 V/1min. withstand
- UL recognized IEC 61010-1, CE, and RoHS Compliant
- Lead length 15" ±0.50"
- Power Suply ±15 V (25mA)
- Offset voltage ±30mV max
- Noise level less than 20mVp-p
- di/dt response 3u sec (typ.) at Full scale
- Operating temperture -25℃ to 75℃
- Temperature Impact: ±0.2% / ℃

| PART NUMBER AND RATING | | SATURATION CURRENT |
|---|---|---|
| HCT-0010-005 | 5 Amp | 7.5 AT |
| HCT-0010-010 | 10 Amp | 15 AT |
| HCT-0010-020 | 20 Amp | 30 AT |
| HCT-0010-025 | 25 Amp | 37.5 AT |
| HCT-0010-050 | 50 Amp | 75 AT |

| DIMENSION | INCH | MM |
|---|---|---|
| A | 1.60 | 40.50 |
| B | 0.91 | 23.10 |
| C | 0.93 | 23.70 |
| D | 1.05 | 26.60 |
| E | 0.58 | 14.70 |

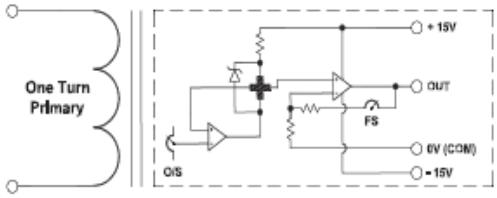


SCHEMATIC

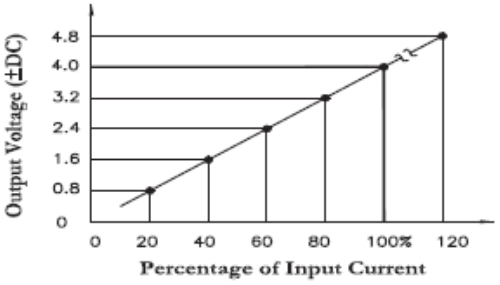


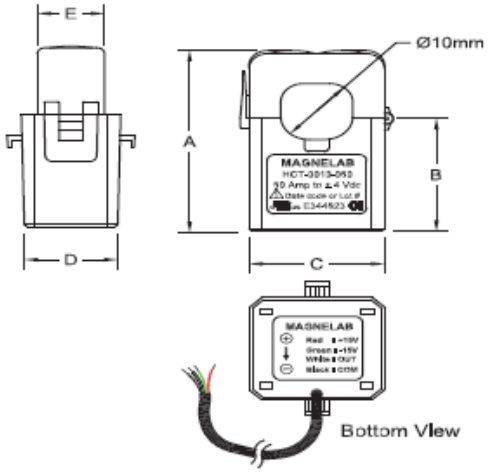


cULus CE RoHS2 ISO 9001:2008

# Appendix E

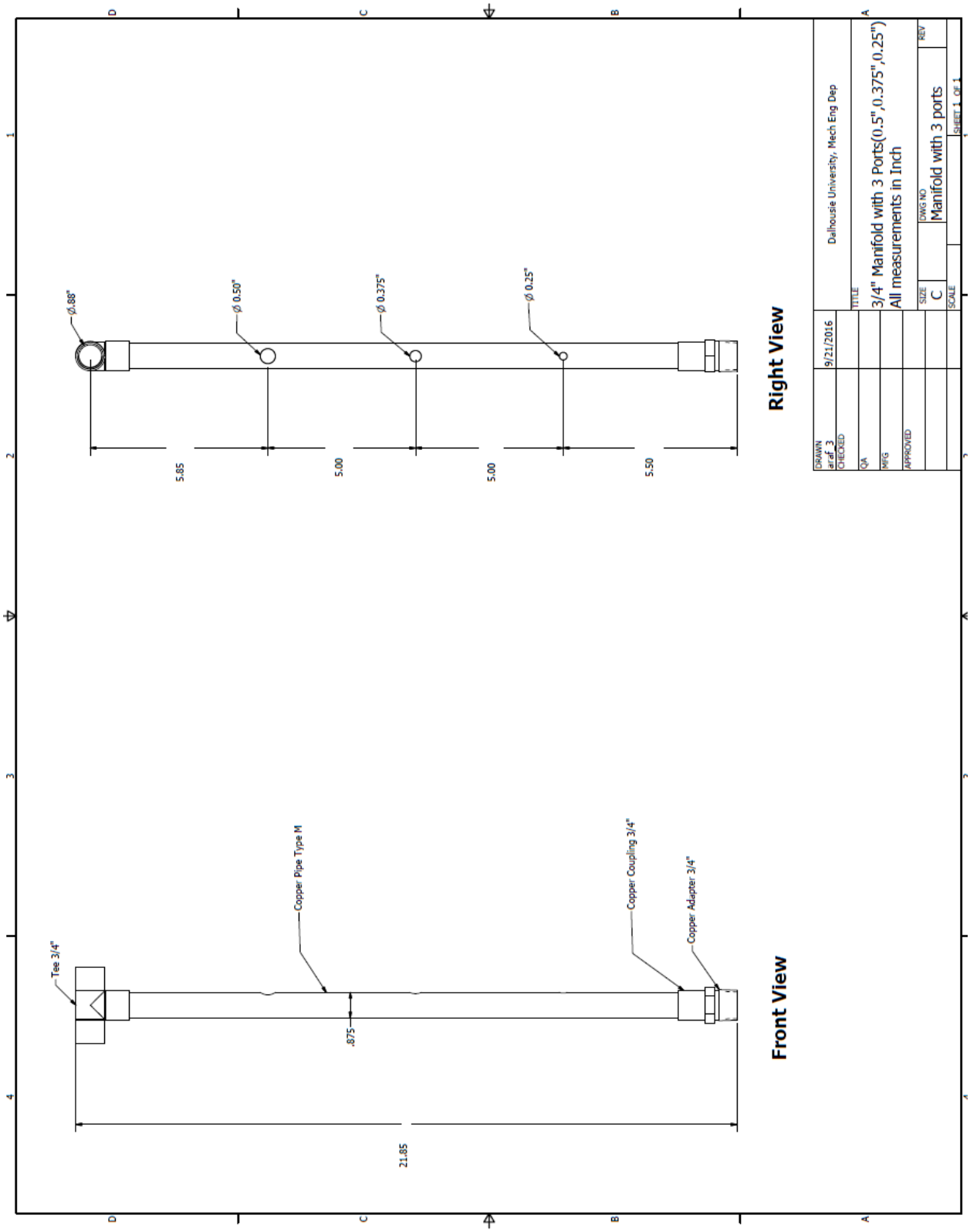
Right View
Ø.88"
Ø 0.50"
Ø 0.375"
Ø 0.25"
5.85
5.00
5.00
5.50
Front View
Tee 3/4"
Copper Pipe Type M
Copper Coupling 3/4"
Copper Adapter 3/4"
.875
21.85
DRAWN
afaf_3
9/21/2016
CHECKED
QA
MFG
APPROVED
Dalhousie University, Mech Eng Dep
TITLE
3/4" Manifold with 3 Ports(0.5",0.375",0.25")
All measurements in Inch
SIZE
C
DWG NO
Manifold with 3 ports
REV
SCALE
SHEET 1 OF 1

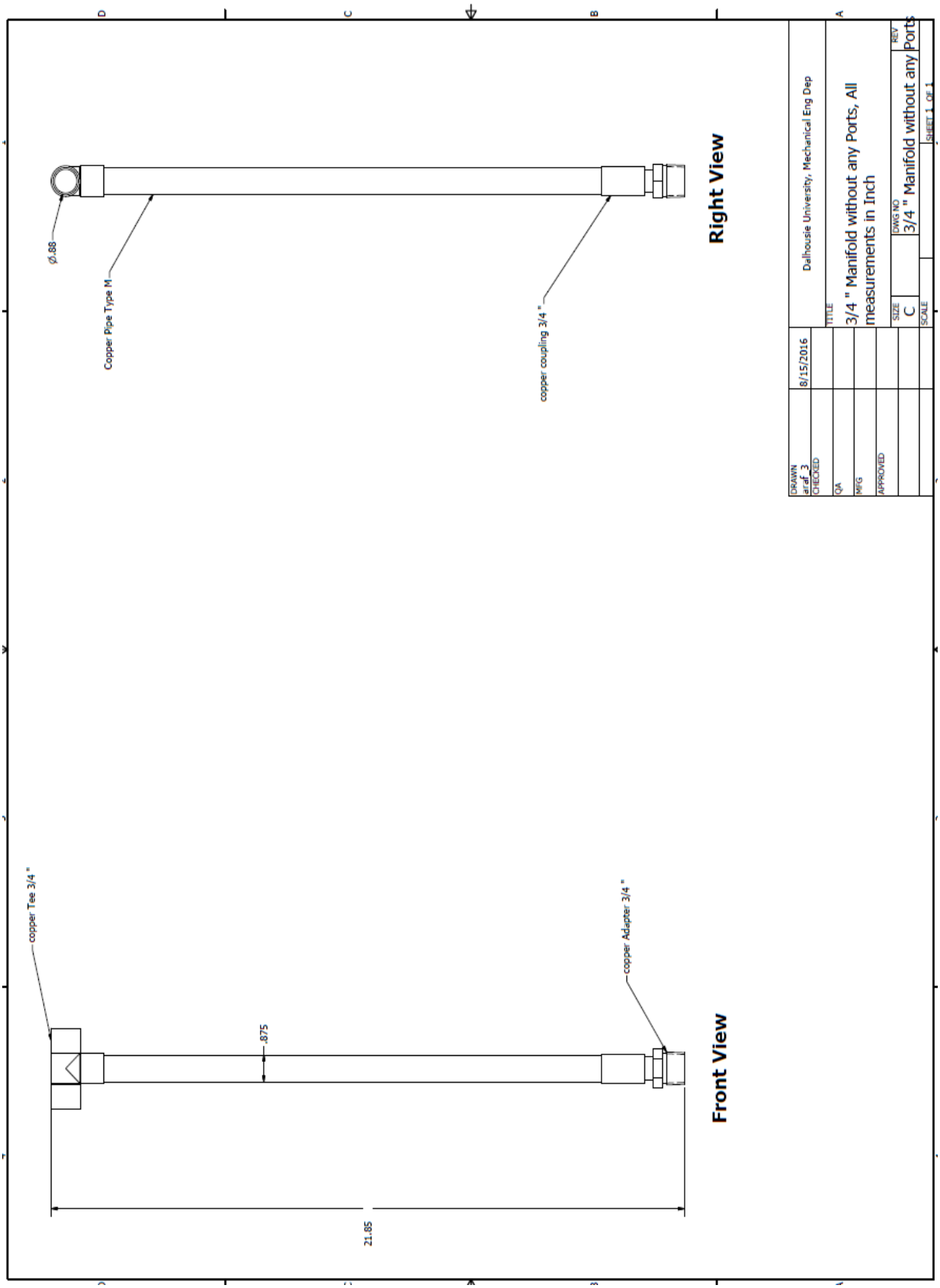
Right View
Ø.88
Copper Pipe Type M
copper coupling 3/4 "
Front View
copper Tee 3/4 "
.875
copper Adapter 3/4 "
21.85
Dalhousie University, Mechanical Eng Dep
DRAWN
araf_3
CHECKED
QA
MFG
APPROVED
8/15/2016
TITLE
3/4 " Manifold without any Ports, All measurements in Inch
SIZE
C
DWG NO
3/4 " Manifold without any Ports
REV
SCALE
SHEET 1 OF 1

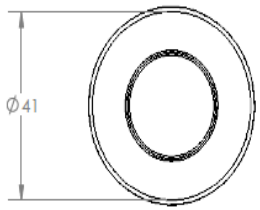


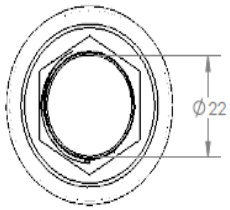


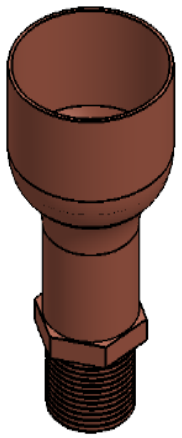

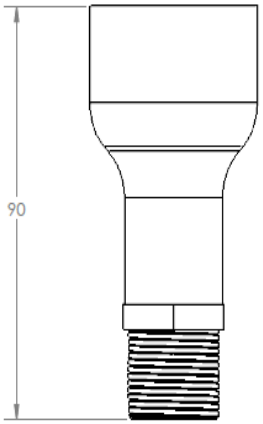


| | | | | | |
|---|---|---|---|---|---|
| | | UNLESS OTHERWISE SPECIFIED: | | NAME | DATE |
| | | DIMENSIONS ARE IN INCHES<br>TOLERANCES:<br>FRACTIONAL ±<br>ANGULAR: MACH ± BEND ±<br>TWO PLACE DECIMAL ±<br>THREE PLACE DECIMAL ± | DRAWN | | |
| | | | CHECKED | | |
| | | | ENG APPR. | | |
| | | | MFG APPR. | | |
| | | INTERPRET GEOMETRIC TOLERANCING PER: | Q.A. | | |
| | | MATERIAL | COMMENTS: | | |
| NEXT ASSY | USED ON | FINISH | | | |
| APPLICATION | | DO NOT SCALE DRAWING | All measurements in "mm". | | |

TITLE:

SIZE: A | DWG. NO.: Assemble | REV: Araf

SCALE: 1:1 | WEIGHT: | SHEET 1 OF 1

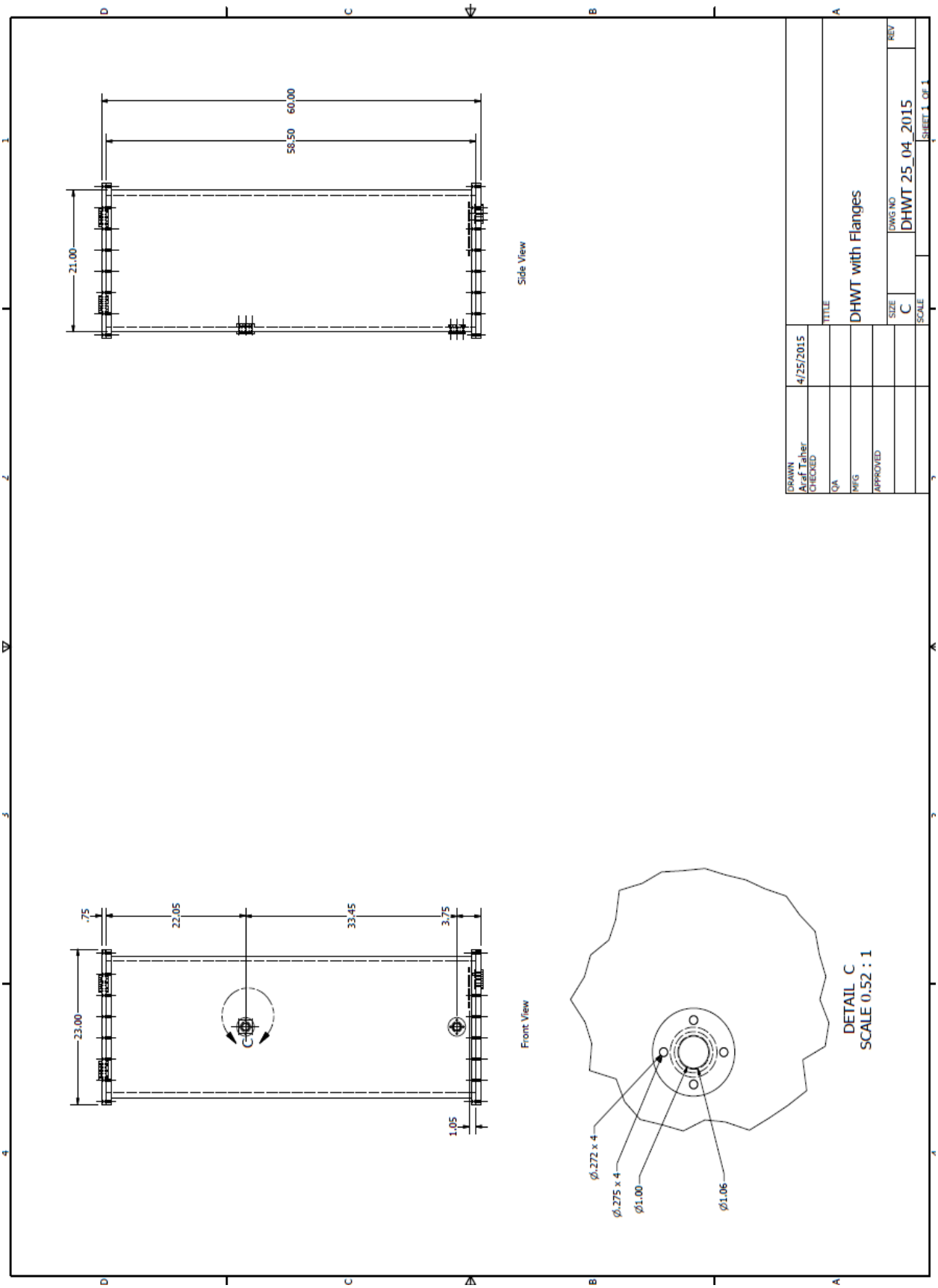
60.00
58.50
21.00
Side View
.75
22.05
33.45
3.75
23.00
1.05
Front View
Ø.272 x 4
Ø.275 x 4
Ø1.00
Ø1.06
DETAIL C
SCALE 0.52 : 1
DRAWN
Araf Taher
4/25/2015
CHECKED
QA
MFG
APPROVED
TITLE
DHWT with Flanges
SIZE
C
DWG NO
DHWT 25_04_2015
REV
SCALE
SHEET 1 OF 1

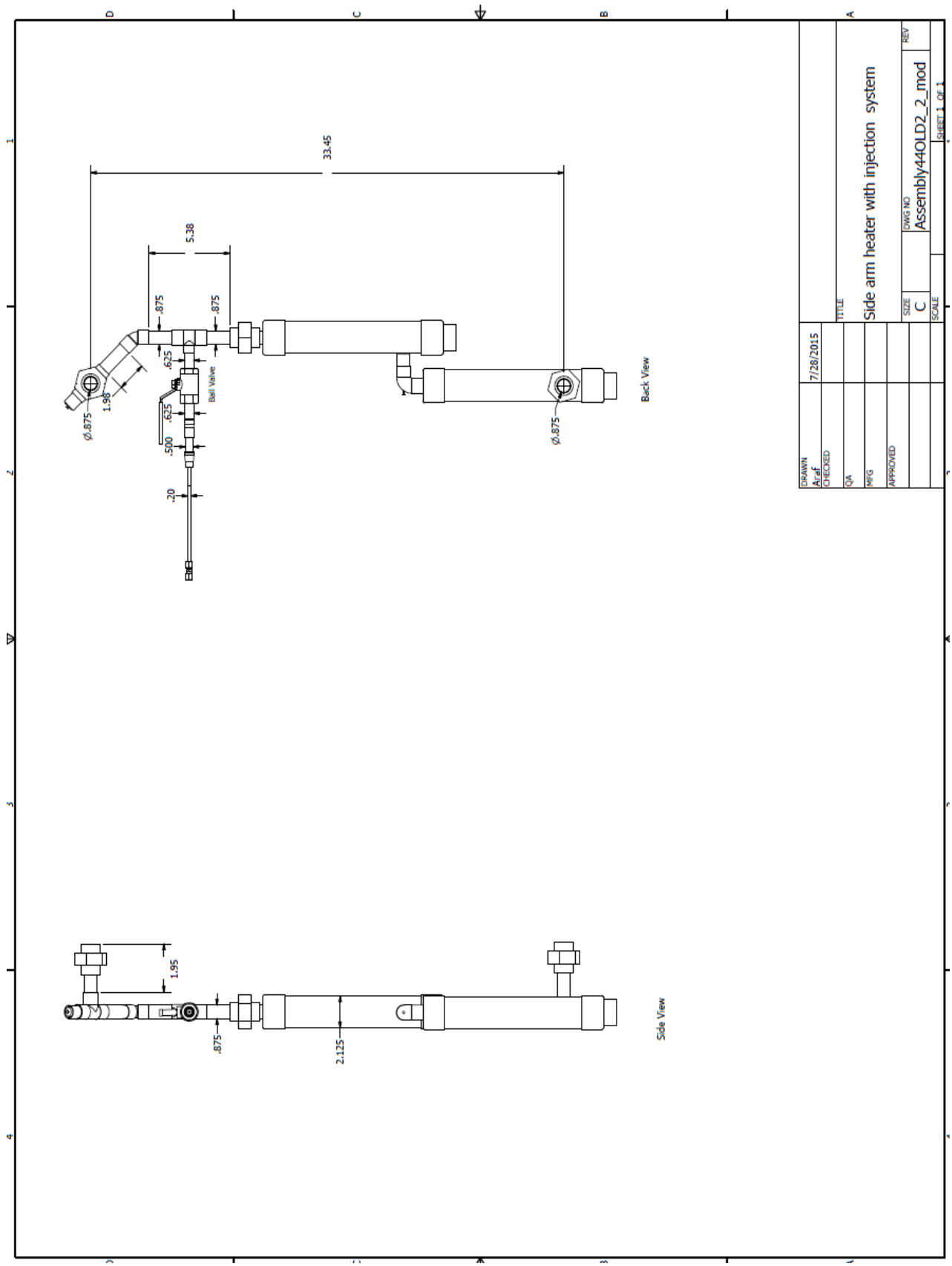
33.45
5.38
.875
.875
.625
.625
.500
.20
1.98
Ø.875
Ball Valve
Ø.875
Back View
1.95
.875
2.125
Side View
DRAWN
Aref
7/28/2015
CHECKED
QA
MFG
APPROVED
TITLE
Side arm heater with injection system
SIZE
C
DWG NO
Assembly44OLD2_2_mod
REV
SCALE
SHEET 1 OF 1

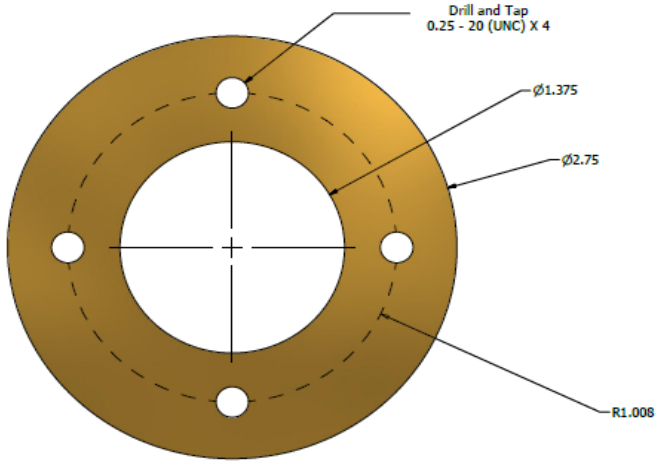


Front View

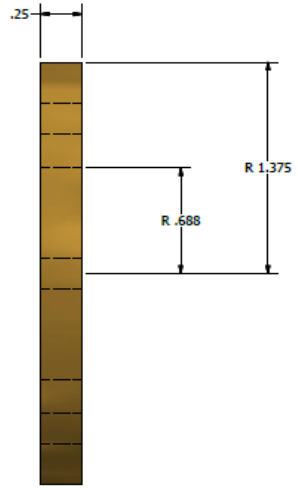


Side View

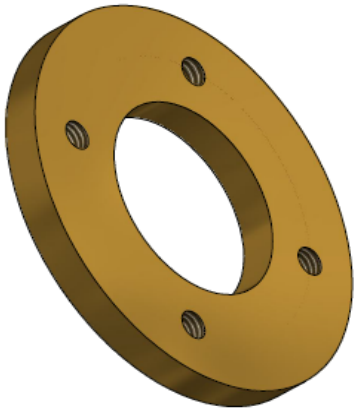

Iso Bottom Left

| | | | |
|---|---|---|---|
| DRAWN Araf Taher | 5/4/2015 | | |
| CHECKED Dr Allen | | TITLE | In side flange ( Material: Brass ) |
| QA | | | |
| MFG | | | |
| APPROVED | | SIZE C | DWG NO In side flange |
| | | SCALE | SHEET 1 OF 1 |

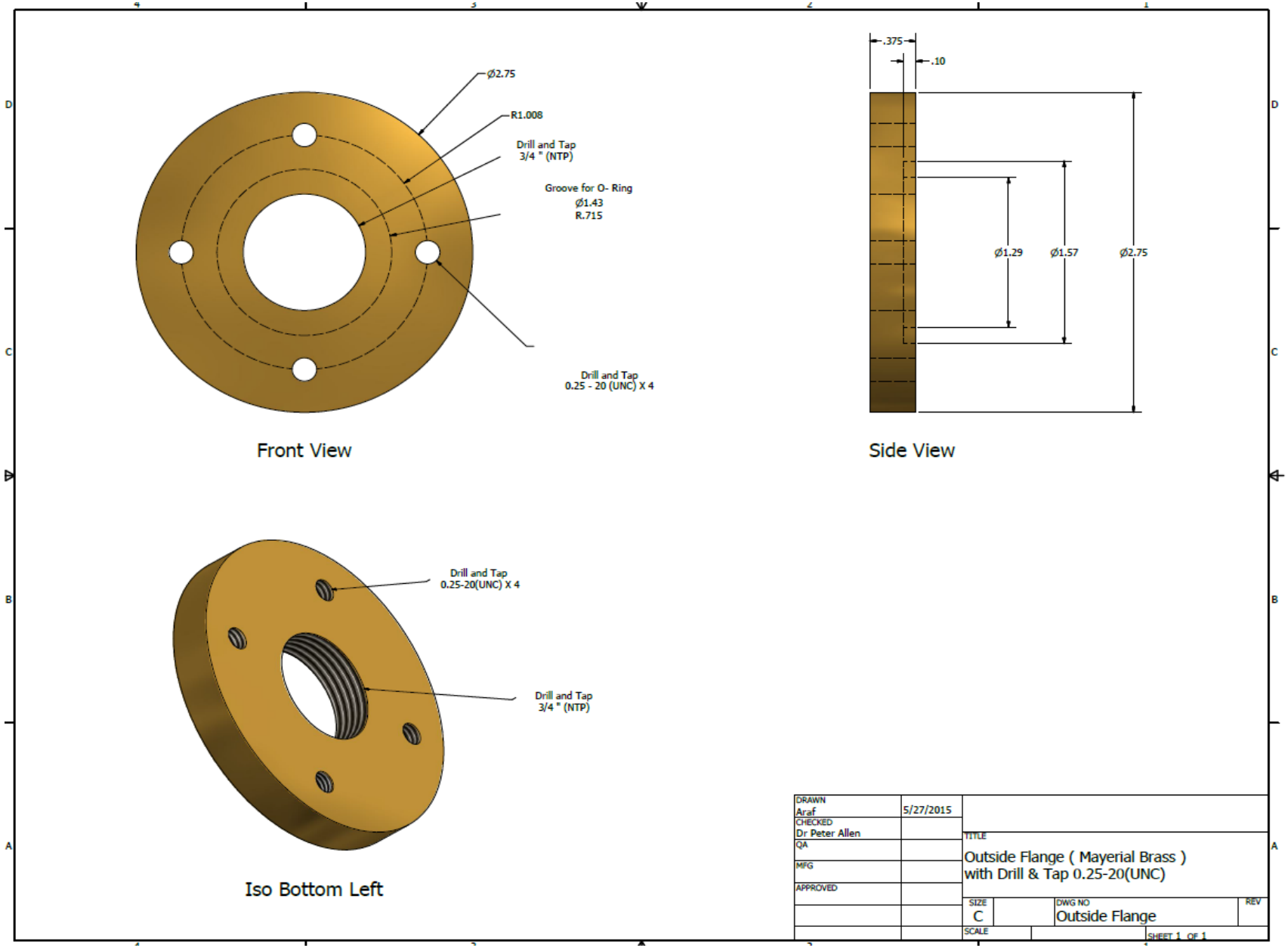
Ø2.75
R1.008
Drill and Tap
3/4 " (NTP)
Groove for O- Ring
Ø1.43
R.715
Drill and Tap
0.25 - 20 (UNC) X 4
Front View
.375
.10
Ø1.29
Ø1.57
Ø2.75
Side View
Drill and Tap
0.25-20(UNC) X 4
Drill and Tap
3/4 " (NTP)
Iso Bottom Left
DRAWN
Araf
5/27/2015
CHECKED
Dr Peter Allen
QA
MFG
APPROVED
TITLE
Outside Flange ( Mayerial Brass )
with Drill & Tap 0.25-20(UNC)
SIZE
C
DWG NO
Outside Flange
REV
SCALE
SHEET 1 OF 1